Johannes Gutenberg-Universität Mainz

Fachbereich 10 – Biologie

# Exploring transcriptomic regulation of the developing brain through integrative bioinformatics and deep learning approaches

**DISSERTATION**

zur Erlangung des Grades

Doktor der Naturwissenschaften

am Fachbereich Biologie

der Johannes Gutenberg-Universität Mainz

Stephan Weißbach

geb. am 17.03.1994 in Groß-Gerau

Mainz, 2024

**Dekan:** Prof. Dr. Eckhard Thines

**1. Berichterstatter**:

**2. Berichterstatter**:

**Tag der mündlichen Prüfung**: 21.01.2025

## Statutory Declaration

I herewith declare that I have composed the present thesis myself and without the use of any other than the cited sources and aids. Sentences or parts of sentences quoted literally are marked as such; other references with regards to the statement and scope are indicated by full details of the publications concerned. The thesis in the same or similar form has not been submitted to any examination body and has not been published.

Place, Date: _____ Signature: _____

# Acknowledgments

## Abstract

The mammalian brain is a remarkably complex organ whose development relies on precise molecular and cellular processes. One of the most sophisticated brain structures is the cerebral cortex. Many proteins and microRNAs play distinct roles in the posttranscriptional regulation of corticogenesis. Mutations in RNA-binding proteins and miRNAs are linked to neurodevelopmental disorders, highlighting their crucial role in central nervous system development.

This doctoral thesis investigates posttranscriptional mechanisms that shape brain development, focusing on alternative splicing and microRNA regulation. Premature overexpression of the RNA binding protein *Rbfox2* during murine corticogenesis caused migration and differentiation defects through an altered splicing pattern, likely antagonizing PTBP2's splicing program. In this study, it was further shown that the neuronal progenitor cell-specific miR-92a-3p repressed *Rbfox2* both *in vitro* and *in vivo*, revealing a novel regulatory relationship between miRNAs and splicing factors during neural development.

Furthermore, analysis of miRNAs during embryonic corticogenesis revealed clusters of coregulated miRNAs with overlapping target sets. Luciferase assays showed that such cotargeting of miRNAs enhances the repression effect on shared target mRNAs. This finding suggests a complex regulatory network where multiple miRNAs cooperatively fine-tune gene expression during brain development.

To support future research, two computational tools were developed: a web portal (www.cortexa-rna.com) providing access to neocortex/hippocampus RNA-sequencing datasets, improving the accessibility of transcriptomic data to the broader scientific community. Additionally, I implemented a deep learning framework for denoising functional imaging recordings. This computational tool enables the validation of molecular changes in synaptic function at single synapse resolution, bridging the gap between molecular alterations (including splicing-induced changes) and their functional consequences in neurons.

# Zusammenfassung

Das Gehirn von Säugetieren ist ein komplexes Organ, dessen Entwicklung von präzisen molekularen und zellulären Prozessen abhängt. Eine der komplexesten Gehirnstrukturen ist der Kortex. Mehrere Proteine und microRNAs spielen bei der posttranskriptionellen Regulierung der Kortikogenese eine besondere Rolle. Mutationen in RNA-bindenden Proteinen und microRNAs werden mit neurologischen Entwicklungsstörungen in Verbindung gebracht, was ihre entscheidende Rolle bei der Entwicklung des zentralen Nervensystems unterstreicht.

Diese Doktorarbeit untersuchte posttranskriptionale Mechanismen, welche die Entwicklung des Gehirns beeinflussen, und fokussiert sich dabei auf alternatives Spleißen und die Regulierung von microRNAs. Die vorzeitige Überexpression des RNA-bindenden Proteins *Rbfox2* während der Kortikogenese bei Mäusen verursachte Migrations- und Differenzierungsdefekte durch ein verändertes Spleißmuster, das wahrscheinlich das Spleißprogramm von PTBP2 antagonisiert. Diese Studie konnte außerdem zeigen, dass die für neuronale Vorläuferzellen spezifische miR-92a-3p *Rbfox2* sowohl *in vitro* als auch *in vivo* unterdrückt, was eine neuartige regulatorische Beziehung zwischen miRNAs und Spleißfaktoren während der neuralen Entwicklung aufzeigt.

Darüber hinaus ergab die Analyse der miRNAs während der embryonalen Kortikogenese Cluster koregulierter miRNAs mit sich überschneidenden Zielgruppen. Luziferase-Assays konnten zeigen, dass eine solche gemeinsame Ausrichtung von miRNAs die Unterdrückungswirkung auf gemeinsame Ziel-mRNAs verstärkt. Dieses Ergebnis deutet auf ein komplexes regulatorisches Netzwerk hin, in dem mehrere miRNAs die Genexpression während der Gehirnentwicklung gemeinsam feinabstimmen.

Zur Unterstützung künftiger Forschung wurden zwei Tools entwickelt: ein Webportal (www.cortexa-rna.com), das Zugang zu RNA-Sequenzierungsdatensätzen von Neokortex und Hippocampus bietet und die Zugänglichkeit transkriptomischer Daten für eine breitere wissenschaftliche Gemeinschaft verbessert. Darüber hinaus habe ich einen Deep-Learning-Framework für die Unterdrückung von Rauschen in funktionellen Mikroskopieaufnahmen implementiert. Dieses Tool ermöglicht die Validierung von

durch Spleißen induzierten Veränderungen der synaptischen Funktion und ermöglicht somit in einzelnen Synapsen molekularen Veränderungen auf ihre funktionellen Konsequenzen hin zu untersuchen.

# Table of Contents

# Abbreviations

| | |
|---|---|
| 3’-UTR | 3' untranslated region |
| AS | alternative splicing |
| APA | alternative polyadenylation |
| CP | cortical plate |
| FACS | fluorescence-activated cell-sorting |
| IPC | intermediate progenitor cell |
| IZ | intermediate zone |
| LASR | large assembly of splicing regulators |
| m6A | N6-methyladenosine |
| MBNL | Muscleblind Like Splicing Regulator |
| miRNA | microRNA |
| mRNA | messenger RNA |
| MZ | marginal zone |
| NMD | nonsense-mediated decay |
| PCA | principal component analysis |
| PTBP | polypyrimidine tract binding protein |
| RBFOX | RNA-binding Fox-1 homologs |
| RBP | RNA-binding protein |
| RGC | radial glial cell |
| RRM | RNA recognition motif |
| SVZ | subventricular zone |
| TPD43 | TAR DNA-binding protein 43 |
| VGGC | Voltage-gated calcium channels |
| VZ | ventricular zone |

| | |
|---|---|
| WES | whole exome sequencing |
| XPO5 | Exportin 5 |

# List of Figures

# List of Tables

# 1 Introduction

Brain development is a complex process that begins during early embryogenesis and continues well into adulthood. Forming specialized brain regions involves the precise orchestration of cell proliferation, migration, and differentiation into diverse neural cell types. Among brain regions, the cerebral cortex has emerged as one of the most evolutionarily advanced structures, responsible for higher-order processing and cognitive capabilities[1]. The cerebral cortex forms the outermost layer of the cerebral hemispheres and harbors a wide variety of specialized cells ranging from auxiliary cells (e.g., glial cells) to highly specialized neurons. It controls cognitive functions such as thought and language in mammals, enabling complex behavior. The neocortex, which represents the largest and most evolutionarily advanced component of the cerebral cortex[2], is structured in six layers composed of different neurons. Most neurons are excitatory, pyramidal-projection neurons (75-85 %). The remaining 15-25 % can be attributed to inhibitory GABAergic interneurons. The composition of inhibitory and excitatory neurons in the cerebral cortex differs among mammalian species[3].

In *Mus musculus*, a widely used model organism for investigating mammalian physiology and development (**Figure 1**), corticogenesis is initiated mid-gastrulation between embryonic days 9 and 10 (E9–E10)[4]. In this early phase, the pool of neural progenitor cells (NPCs) in the form of neuroepithelial cells expands through symmetric divisions. Gradually, neuroepithelial cells transform into radial glial cells (RGCs), the main type of NPC. Most RGCs are attached to the ventricular surface and are multipotent cells. Thus, they can differentiate into different types of neural cells, e.g., neurons, astrocytes, or oligodendrocytes, by asymmetric divisions. In asymmetric divisions, a radial glial cell divides to produce two distinct daughter cells: one that retains the properties of the parent cell (self-renewal) and another that becomes a more differentiated cell type[5]. The fate of the differentiating daughter cell is determined by the precise temporal competence of the parent cell and the influence of various intrinsic and extrinsic factors at the time of division[4]. Once generated, newborn neurons migrate radially from the ventricular zone toward the cortical plate, using the basal processes of radial glial cells as scaffolds[5]. This migration occurs in an inside-out pattern, with earlier-born neurons forming the deeper layers of the cortex and later-born neurons migrating past them to form the upper layers. This process results in the formation of

the characteristic six-layered structure of the mammalian neocortex, with each layer containing neurons with distinct molecular identities and functional properties[6].

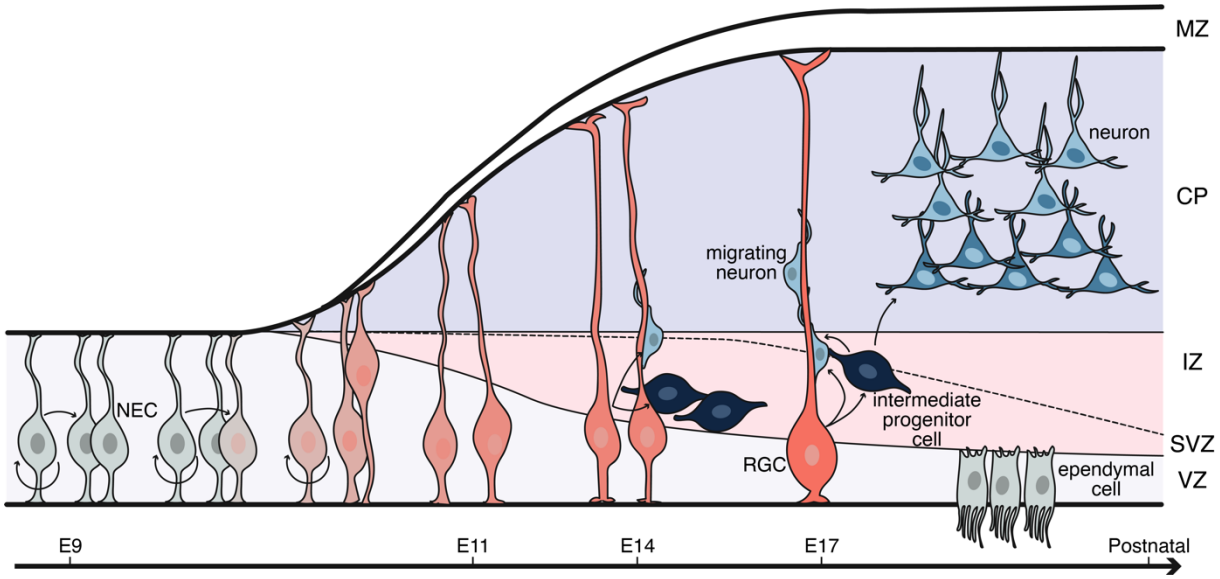


**Figure 1** Spatiotemporal progression of murine cerebral cortex development inspired by Koo et al., 2023[4]. The schematic illustration depicts the key stages and cell types involved in the development of the mouse cerebral cortex from early embryonic day 9 (E9) through postnatal stages. The figure shows the transformation of the neuroepithelium into a complex, layered structure. E9 - E11: Neuroepithelial cells (NECs) in the ventricular zone (VZ). At E11 - E14, NECs transform into radial glial cells (RGCs), which span from the VZ to the pial surface. E14 - E17: RGCs produce neurons directly or via intermediate progenitor cells (IPCs) in the subventricular zone (SVZ). Neurons migrate along RGC processes. E17-Postnatal: Cortical layers form in an inside-out pattern, creating a mature structure: the VZ, SVZ, intermediate zone (IZ), cortical plate (CP), and marginal zone (MZ).

Underlying these complex processes of asymmetric division, fate determination, and neuronal migration is a regulatory framework that extends beyond transcriptional control. During cortical development, extensive changes occur in the posttranscriptional landscape (**Figure 2**), playing a crucial role in shaping the neurogenic process. These modifications go beyond mere gene expression and involve complex regulatory mechanisms that fine-tune the production, processing, and stability of RNA molecules. Among the most prominent posttranscriptional regulatory mechanisms that are studied in the context of CNS development are alternative splicing and gene translation suppression through microRNA (miRNA) binding (**Figure 2**)[7,8]. Recent technological advancements, such as direct RNA sequencing, most prominently using nanopore technology, have shed light on additional regulatory mechanisms that are gaining increasing attention in the research community. These

include dynamic changes in 3' untranslated region (3'-UTR) length through alternative polyadenylation, which can significantly impact RNA stability[9]. Furthermore, various RNA modifications have emerged as important factors in posttranscriptional regulation (**Figure 2**). These mechanisms provide an extra layer of control over gene expression, allowing for fine-tuned regulation of cellular processes during development[10].

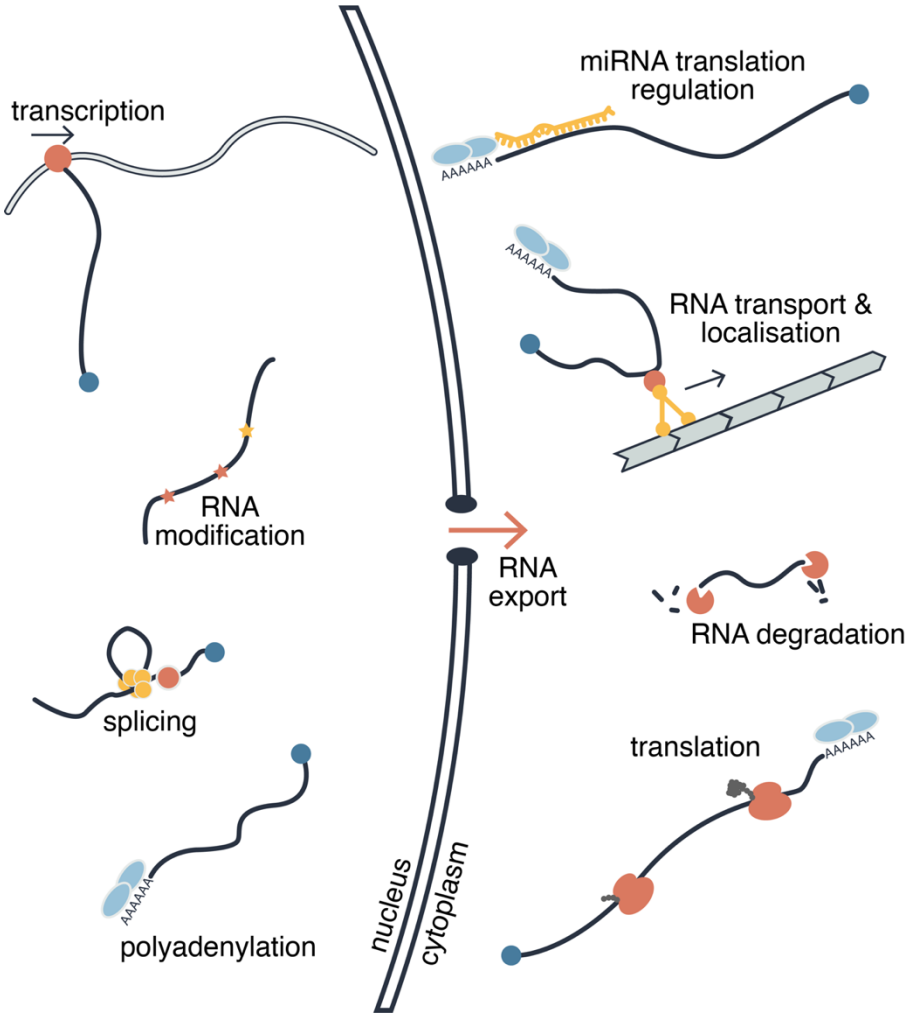


**Figure 2** Key mechanisms of RNA regulation. The schematic shows RNA processing steps from transcription through nuclear export to cytoplasmic events including miRNA-mediated regulation, transport, translation, and degradation. Nuclear processes include RNA modification, splicing, and polyadenylation. The nuclear membrane (vertical line) separates nuclear and cytoplasmic events.

## 1.1 Alternative splicing

Although the genome of the mouse has approximately 22,000 protein-coding genes[11] that are shared among all cells, the mammalian brain exhibits a remarkable

transcriptomic diversity. As described by the Allen Brain Institute[12], as many as 388 transcriptomic cell types have been characterized in the cortex and hippocampus. This diversity is achieved partly by the process of alternative splicing (AS). Nearly every multi-exon gene in mammals undergoes alternative splicing[13]. Failures in alternative splicing can be linked to several neurological developmental disorders, highlighting its relevance for proper brain development[14].

After a gene is transcribed into premature mRNA, the introns are removed from the sequence, and the exons are joined together into the mature mRNA[15]. The process of constitutive splicing is catalyzed by a large ribonucleotide complex called the spliceosome. The spliceosome assembles over introns or exons, respectively, and thus recognizes the boundaries of an exon[16]. Alternative splicing is a deviation from constitutive splicing, and therefore, individual exons of a gene may be included or excluded from the mature messenger RNA (mRNA)[17]. Exons are joined in different combinations, leading to differing mRNA transcripts (**Figure 3**). Proteins translated from alternatively spliced mRNAs usually exhibit differences in their amino acid sequence and, often, in their biological functions and structure[17].

Moreover, alternative splicing not only shapes protein diversity but also exerts regulatory control over gene expression. By the inclusion of short exons that introduce a premature stop codon, so-called poison exons, the mRNA is degraded through the process of nonsense-mediated decay. Notably, one-third of all annotated transcripts include a premature stop codon[18], highlighting the prevalence of this regulatory mechanism.

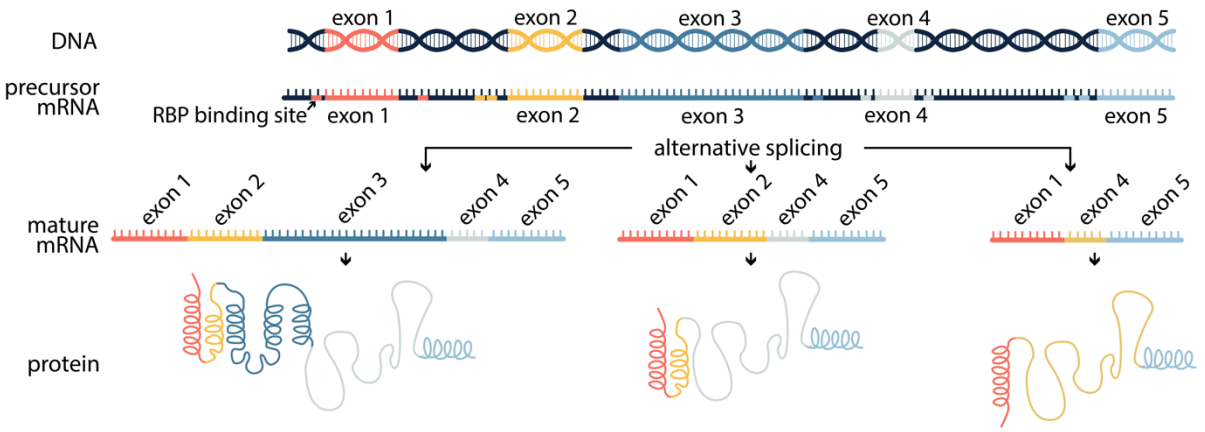


**Figure 3** Simplified schematic of the process of alternative splicing. The gene, consisting of exons and introns, is read from the DNA into mRNA (transcription). In proximity to the exons, specific RBP binding sites (short sequences recognized by the

RBP) are present. RBPs regulate the process of alternative splicing, which is the alternative use of exons. Finally, the alternatively spliced mature mRNAs are processed into proteins with different structures (through translation). RBP: RNA binding protein.

There are different alternative splicing events known; in this thesis, the definition used within the rMATS software will be used (**Figure 4**)[19]. Thus, alternative splicing events include skipping exons (often referred to as cassette exons), mutually exclusive exons, intron retention, A5' alternative splice sites, and A3' alternative splice sites, as depicted in **Figure 4**. Skipping exons are the most common alternative splicing event, accounting for 73.2 % of all annotated splicing events in mm39. A mutually exclusive exon is an event with a group of two exons in which exactly one is spliced in, while the other is spliced out. Retained intron alternative splicing involves the inclusion of an intronic sequence in the mature mRNA. Finally, there are alternative A5' and A3' splice sites that lead to exons of varying length.

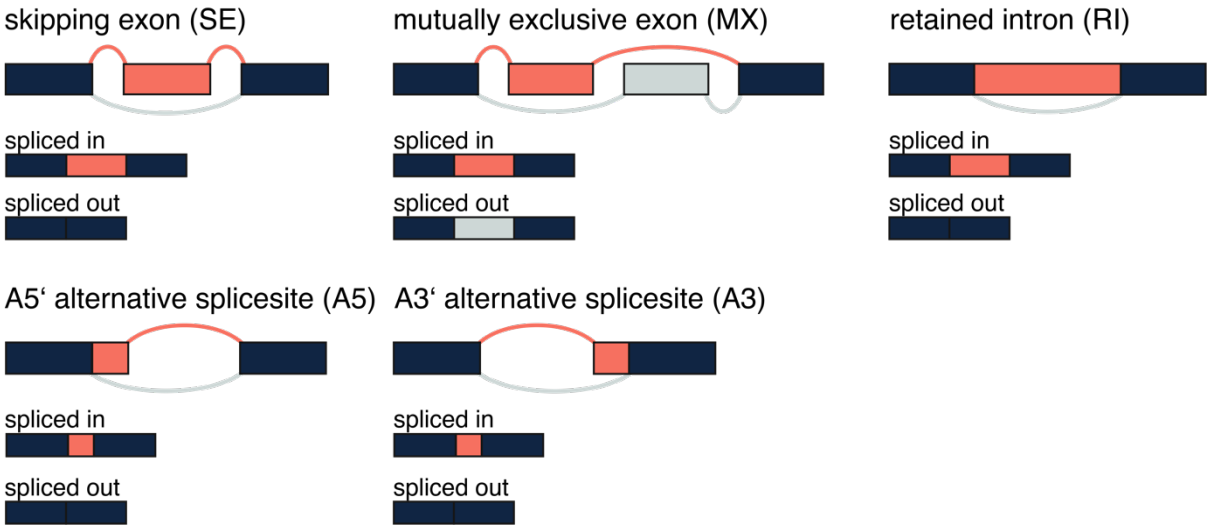


**Figure 4** Different types of splicing events: skipping of exons, mutually exclusive exons, retained introns, alternative A5' splice sites, and alternative A3' splice sites.

### 1.1.1 Alternative splicing is guided by RNA-binding proteins

The assembly of the spliceosome can be altered by auxiliary proteins that bind to pre-mRNAs, so-called RNA binding proteins. RBPs are a diverse set of proteins that possess preferred binding motifs located in intronic or exonic mRNA sequences (**Figure 3**)[16]. The class of RBPs comprises over 2,000 known proteins that can interact with RNA in various ways[20]. Many RBPs induce splicing changes upon binding to their

binding motif(s) on pre-mRNAs. The binding motifs of RBPs are relatively short, e.g., the four nucleotide sequence YCAY[1] to which NOVA2 binds[21]. These short sequences are referred to as RNA recognition motifs (RRMs). In general, RBPs regulate between 200 and 1,000 exons[8]. Despite the conserved RRMs shared by paralogous RBPs within families, such as the RBFOX family, there is notable redundancy in their functions. The RBFOX family, for instance, comprises three paralogs with a common (U)GCAUG RRM, exhibiting significant overlap in their target sets[22]. Intriguingly, these paralogs display distinct expression patterns across various developmental stages, tissues, and cell types (**Figure 5**)[8,23]. The reasons for this redundancy remain poorly understood.

Many RNA-binding proteins exert position-dependent splicing changes, where upstream binding relative to a regulated exon leads to repression and downstream binding to the inclusion of the exon. This position-dependent effect has been reported for multiple RBPs involved in cortical development, such as RBFOX[22,24], NOVA[25], and MBNL[26]. However, a notable exception is the PTBP family, whose member proteins mostly bind upstream of regulated exons[27] and cause exon repression.

### 1.1.2 Alternative splicing in developing and mature tissues

Several splicing changes are required for key processes during embryonic brain development, such as cell proliferation[7], neuronal differentiation[28], and neuronal migration[21,29], among others. Moreover, cell-type-specific transcripts have a vast impact on the functionality of the resulting proteins, as exemplified by the vSNARE protein VAMP1, which is specifically expressed in inhibitory neurons. Its expression is regulated by the RNA-binding protein RBFOX1, and disruption of this regulation leads to decreased inhibitory synaptic transmission, highlighting the importance of neuron-specific transcript regulation[30]. Splicing switches are mainly driven by regulatory RBPs, and they must occur with high temporal precision[8]. The expression of RBPs is, therefore, tightly controlled and specific to developmental stages (**Figure 5**a left and middle, **Figure 5**b) and cell types (**Figure 5**a right, **Figure 5**c)[8,23,31]. For instance, several RNA-binding proteins are sequentially expressed, especially during cortical

[1] Y represents a pyrimidine (cytosine or uracil)

development (**Figure 5**a left and middle). Interestingly, the reduced representation of global expression of RBPs related to alternative splicing in two-dimensional space reveals a bell-shaped trajectory which is typically observed for multiple brain developmental processes (**Figure 5**b). Though the transition from pre- to post-natal stages accounts for the highest amount of variance, P0 emerges as an inflection point in this developmental trajectory indicating a shift in the expression direction of RBPs postnatally compared to embryonic stages.

Alternative splicing also plays an important role in adult cells and neurons[13,29,32,33] and mature cortical and hippocampal cells differ based on the expression signature of RBPs (**Figure 5**c). While excitatory neurons cluster together, the group of inhibitory neurons is more diverse. *Vip*- and *Parvalbumin*-positive inhibitory neurons are distinct from all other neuronal subtypes, revealing a more complex splicing-associated protein composition for inhibitory compared to excitatory neurons. Consequently, the presence or absence of distinct RBPs can mediate cell-type specific alternative splicing[34].

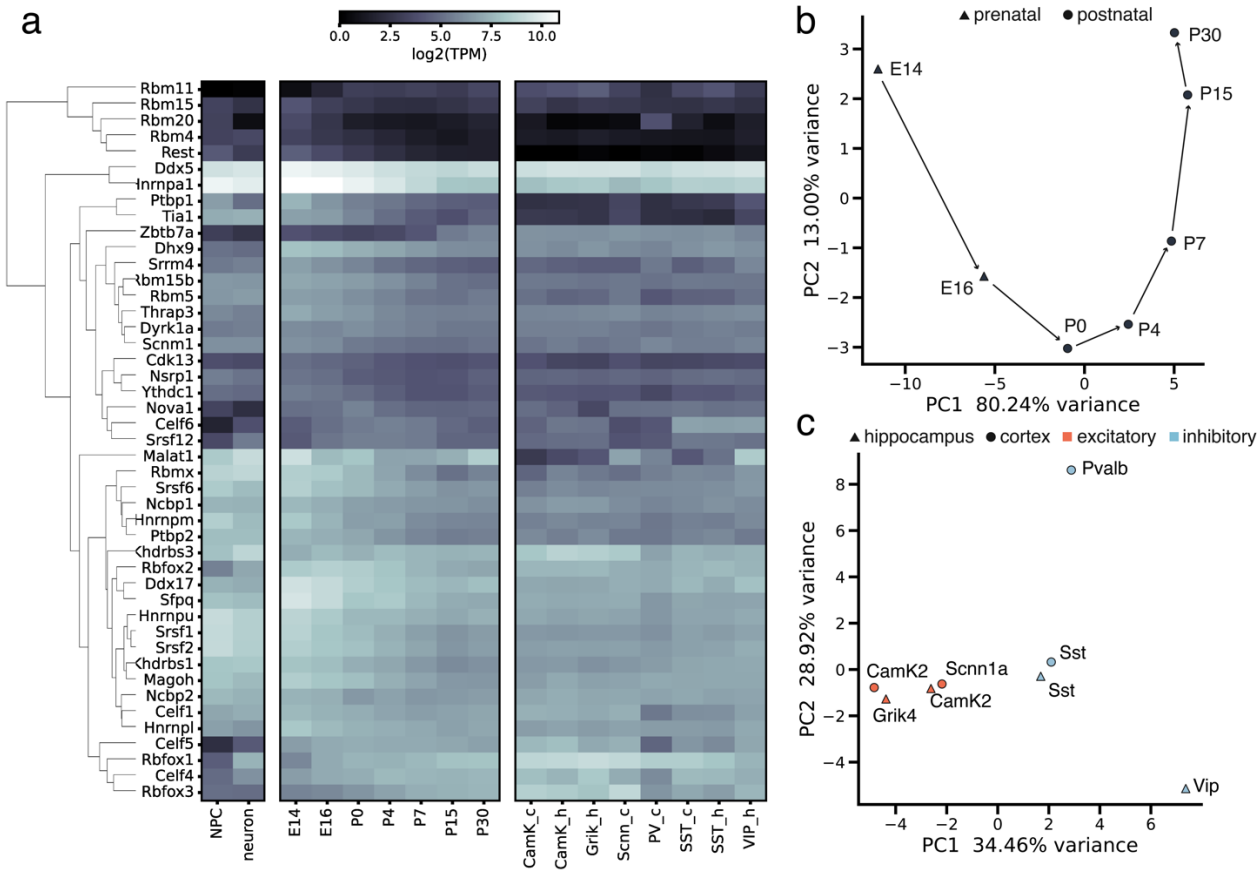


**Figure 5** Differentially expressed alternative splicing-associated genes during cortical development. Genes associated with the GO term **alternative mRNA splicing via the spliceosome** (GO:0000380) were selected and further filtered for base expression > 100 and differential regulation between E14 and P0, resulting in a

list of 43 genes. Due to their known involvement in cortical development, *Rbfox2*[35] and *Ptbp2*[27] were manually added to this list. **a** Heatmap depicting the log2 transformed transcripts per million (TPM) expression values for the differentially expressed splicing-associated proteins during cortical development. Original data from left to right: FACS-sorted NPCs and neurons of the cerebral cortex[31], Developmental data of the cerebral cortex[36], FACS-sorted neuronal cells in the cortex and hippocampus[23]. Processed data were obtained from the web portal Cortexa[37]. **b** Principal component analysis based on the expression values of the selected genes involved in splicing during development. The variance is mainly captured by PC1 (~80 %). The direction of development is indicated by arrows. **c** Principal component analysis for the selected genes in the mature cortex and hippocampus for specific neuronal cell types. Excitatory and inhibitory neurons are separated by PC1, which accounts for a majority of the variance (~34 %). PC2 separates *Vip*-positive neurons from other inhibitory neurons.

Global splicing changes that occur during development and the differences between distinct neuronal subtypes can be represented using principal component analysis[8,37,38]. This integrative data analysis method reveals that alternative splicing gradually changes throughout the development of the cerebral cortex. Typically, the main axis of variation is encompassed by principal component 1, which captures the changes in the splicing pattern of embryonic day 14 to postnatal day 30 (**Figure 6**). The inferred developmental trajectory shows a typical bell shape, peaking at the day of birth of (P0) as previously observed[8,37,38]. Intriguingly, splicing patterns remain robust to batch effects even when data from fluorescence-activated cell-sorted (FACS) mature neurons[23] are integrated. In contrast, gene expression studies[39] are particularly affected by biases from different sequencers and bioinformatic pipelines[40].

Distinct splicing patterns are also attributable to different types of differentiated cells in the brain (**Figure 6**). CamK2-positive, Grik4-positive, and Scnn1a-positive excitatory neurons form a tight cluster that is closely located to P30 bulk cortical samples in reduced dimensional space. Inhibitory neurons form a less homogenous cluster whose global splicing pattern differs from the remaining samples. Strikingly, although these cells were extracted from the hippocampus or cerebral cortex, inhibitory neurons do not develop within these structures but migrate from three distinct regions of the subpallium: the medial and caudal ganglionic eminences and the preoptic area[41].

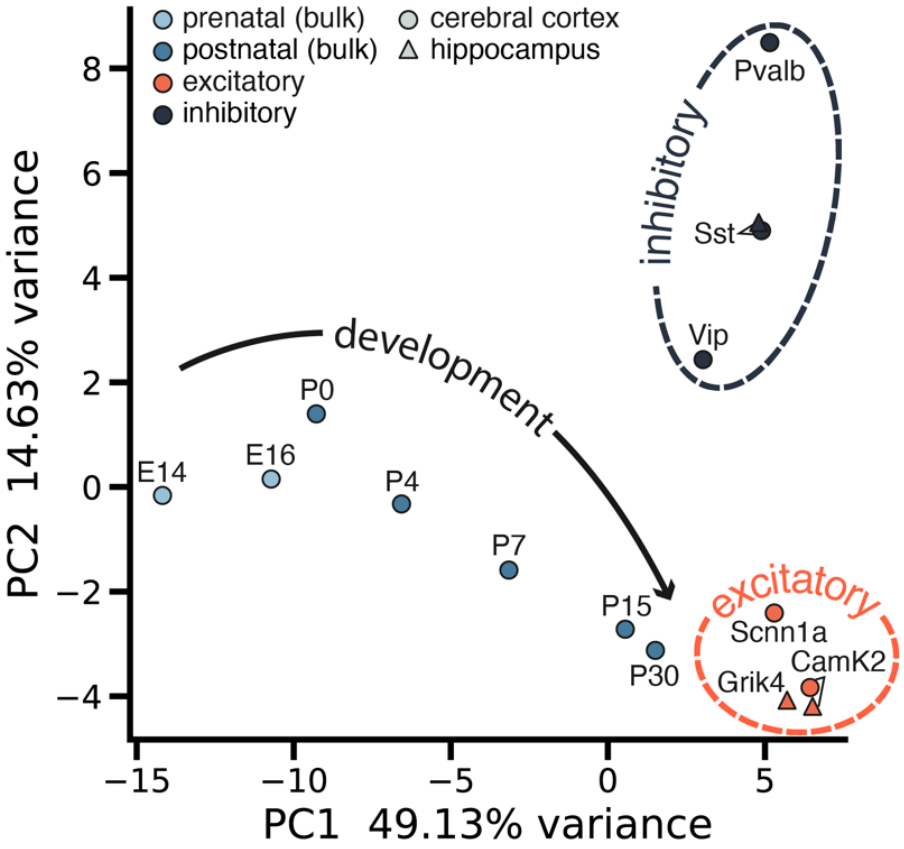


**Figure 6** Principal component analysis of skipping exon events in the developing cortex and distinct neuronal cell types in the adult cortex and hippocampus. The developmental data are separated from left (E14) to right (P30) along the first principal component and show a bell-shaped curve with a peak at birth (P0). The different excitatory cell types (all mature cells) in the cortex and hippocampus are grouped into one small cluster (marked with an orange, dashed circle), while the inhibitory neurons form a looser cluster (marked with a blue, dashed ellipse). Data were analyzed and obtained from the web portal Cortexa[37].

### 1.1.3 Regulation of RNA binding proteins

Due to their ubiquitous relevance in developing and mature tissues, RBPs themselves are tightly regulated[42] via several fail-safe mechanisms to ensure correct splicing activities[43]. RBPs often have an autoregulatory feedback mechanism in which overexpression leads to changes in the splicing of their mRNAs and results in the production of fewer functional proteins. For example, the inclusion of a poison exon leads to the presence of premature stop codons and subsequently triggers nonsense-mediated decay (NMD)[18,44]. Moreover, the induction of NMD is also a common mechanism through which RBPs can regulate other members of their family. A

prominent example is the PTBP family. Polypyrimidine tract binding protein 1 (PTBP1) binds to the pre-mRNA of *Ptbp2,* which results in the skipping of exon 10 with a frameshift mutation and a premature stop codon in exon 11. The premature stop codon marks the spliced mRNA for NMD; therefore, the expression of *Ptbp1* and *Ptbp2* is mutually exclusive[45].

Several non-autoregulatory mechanisms also play a crucial role in the posttranscriptional control of the expression levels of RBPs. For instance, microRNAs typically act as fine-tuners of gene expression[46,47]. However, they have been reported to exert strong repressive effects on some RNA-binding proteins such as PTBP1 during cortical development. PTBP1 is a known repressor of neuronal differentiation due to its ability to induce non-neuronal splicing. It is widely expressed in non-neuronal tissues and absent in neurons[48]. Makeyev and colleagues previously showed that miR-124-3p strongly repressed *Ptbp1* and the miRNA's expression in a neuroblastoma cell line was sufficient to induce neuronal differentiation. Normally, this process requires serum starvation or retinoic acid treatment[45]. This example of strong microRNA repression highlights the relevance of the interplay between RBP-dependent alternative splicing and miRNA regulation during cortical development.

### 1.1.4 RBFOX

The RNA-binding Fox-1 homologs (RBFOX) represent a prominent family of RNA-binding proteins. RBFOX1 was the first discovered paralog and was originally named Ataxin 2-binding protein because of its interaction with *Ataxin 2*[49]. The name Rbfox was derived from an orthologous gene in *C. elegans*, *fox-1*, that is involved in the sex-determination process of the species[50,51].

The number of paralogs within the RBFOX family varies between different species. For example, less complex animals, such as the invertebrate *Drosophila melanogaster,* rely on a single RBFOX protein. Mammals are known to have three RBFOX paralogs, namely, RBFOX1 (FOX1 or A2B1), RBFOX2 (FOX-2 or RBM9), and RBFOX3 (FOX-3, HRNBP3, or NeuN). All three RBFOX members share a highly conserved RNA recognition motif with very high sequence similarity[52], they regulate largely overlapping target sets[22], and have high sequence similarity (**Figure 7**c)[36,52].

The origin of multiple redundant RBFOX paralogs lies in sequence duplication and subsequent labor division and specification (**Figure 7**b)[50]. Therefore, *Rbfox1-3* are expressed in a tissue-, cell type-, and time-specific manner (**Figure 7**b, d). RBFOX1 is expressed in the brain, heart, and skeletal muscle. RBFOX2 is more ubiquitously expressed throughout multiple organs and tissues, such as in the nervous system, heart, and ovary. RBFOX3, which is also often used as a specific neuronal nuclear marker, is predominantly expressed in neurons (**Figure 7**b)[53]. *Rbfox2* is up-regulated in the transition from neuronal progenitor cells to neurons[38]. During the development of the cerebral cortex, this is comparable with peak expression at E16 (**Figure 7**d). *Rbfox1* and *Rbofx3* are also expressed in the neocortex; however, their expression peaks at a much later developmental stage - P30 (**Figure 7**d, middle).

In mature neurons (P30 or older), *Rbfox1* and *Rbfox3* show distinct expression patterns between glutamatergic and GABAergic neurons (**Figure 7**d, right). Nevertheless, their depletion does not contribute to a shift toward a GABAergic splicing pattern, contrary to other differentially expressed RBPs, such as *Mbnl1/2* or *Khdrbs3*[54]. This might be due to the compensatory effect that is at least apparent for RBFOX1 and RBFOX2[29,32,38]. An array of known regulatory mechanisms controls the abundance and effectiveness of RBFOX proteins in the cell (**Figure 7**e). *Rbfox1* and *Rbfox2* possess a highly conserved binding motif close to their singular RRM, and binding of an RBFOX protein induces partial exclusion of the RRM. The resulting RBFOXΔRRM has a significantly reduced binding affinity[55]. RBFOX3 can include a poison exon in *Rbfox2*, leading to subsequent degradation via the NMD pathway[56], a mechanism that could play a crucial role in neurons due to the pan-neuronal presence of RBFOX3. Additionally, all *Rbfox* paralogs are subject to miRNA regulation. The translation of *Rbfox1/3* is inhibited by miR-129-5p[57], and *Rbfox2* is regulated by miR-92a-3p[38]. However, potentially, more microRNAs target *Rbfox*. For example, TargetScan version 7.2 predicts 35 additional miRNAs to target the 3'-UTR of *Rbfox2* that are expressed in the embryonic neocortex[38,47,58]. Specifically, for *Rbfox2*, excess levels can be sequestered by SNORD116, to which the protein binds without initiating any splicing changes[52]. These manifold regulatory mechanisms highlight the importance of the precise amount of RBFOX in cells. Therefore, it is unsurprising that mutations in RBFOX are implicated in several neuronal and cardiac disorders. RBFOX1 has been identified as an autism spectrum disorder risk gene[59] and is associated with idiopathic

generalized epilepsy[60]. RBFOX2 is highly expressed in diabetic hearts. However, the RBFOX2ΔRRM is the most abundant form, which subsequently leads to impaired splicing[61]. Mutations in *Rbfox2* were enriched in a large patient cohort with congenital heart disease[62]. In a knockout study of *Rbfox3*, reduced splicing of RBFOX3 was shown to be linked with epilepsy[63].

Due to their prominent function in mediating alternative splicing, all three RBFOX proteins preferably bind to the (U)GCAUG sequence located within the intronic regions of mRNA and exert a position-dependent splicing effect (**Figure 7**a). In general, binding upstream to a regulated exon promotes exon skipping, while downstream binding is associated with exon inclusion[64]. The RBFOX motif is further found to be enriched in intronic regions flanking alternatively spliced exons for known RBFOX expression sites (**Figure 7**b), e.g. the heart, skeletal muscle, and cerebellum[65].

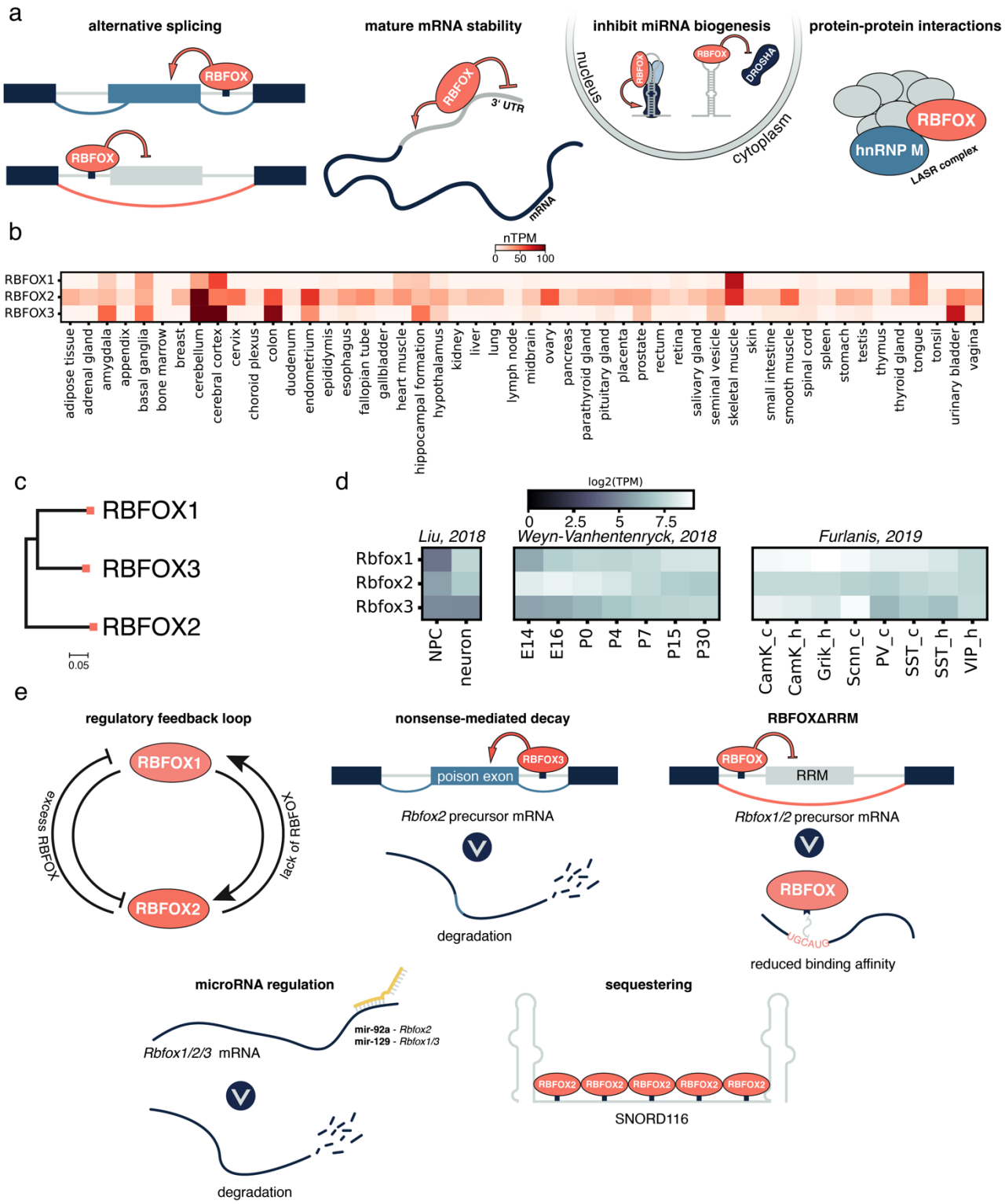


**Figure 7 a** Schematic representation of RBFOX protein functions: alternative splicing regulation, mature mRNA stability control, inhibition of miRNA biogenesis, and protein-protein interactions. **b** Heatmap showing expression levels of RBFOX1, RBFOX2, and RBFOX3 across various human tissues and cell types. Data from human protein atlas[66] **c** Phylogenetic analysis of RBFOX paralogs in *Mus musculus*. The canonical protein sequences were obtained from UniProt and aligned using the Clusta algorithm. Afterward, the phylogenetic tree was constructed using the neighbor-joining method within the MegaX software[67]. **d** Expression pattern of *Rbfox1-3* in NPCs/neurons (E14)[68], throughout

development (E14-P30) in the neocortex[8], and in mature neocortical/hippocampal neurons sorted according to marker genes[23]. Data were obtained from the web portal Cortexa[37]. **e** Regulatory mechanisms ensuring precise RBFOX levels: regulatory feedback loop of RBFOX1 and RBFOX2, RBFOX3 induced NMD of *Rbfox2*, splicing of the RRM to reduce the binding affinity of RBFOX, miRNA suppression, and sequestering.

Although solo RBFOX binding is sufficient to initiate alternative splicing, RBFOX can also be part of the large assembly of splicing regulators (LASRs), multiprotein complexes that are bound by protein-protein interactions. Here, RBFOX can indirectly alter splicing activity through interactions with hnRNPM or it can bind with the entire complex to its preferred (U)GCAUG motif[69].

In addition to its canonical function in alternative splicing, RBFOX is also involved in other transcriptional regulatory processes[50]. RBFOX2 can recognize and bind to its motif located in the terminal loop of pri-miRNA and subsequently block processing by Drosha within the nucleus. The binding of RBFOX2 results in a significant reduction in the expression of miR-20b and miR-107 *in vivo* and *in vitro*, while the absence of RBFOX2 significantly increases the abundance of these two microRNAs. Furthermore, many other predicted target miRNAs of RBFOX have not been identified[70]. In addition, RBFOX3 can enhance the processing of pri-miRNAs via the Drosha complex[71]. RBFOX can also be located outside the nucleus in the cytoplasm[72], but to date, there have been no reports on whether RBFOX also binds pre-miRNA in the cytoplasm and thus potentially regulates pre-miRNA.

A known function of cytoplasmic RBFOX is the regulation of mRNA stability in the cytoplasm. It has been reported that RBFOX1 binds to the 3'-UTR, consequently blocking the binding of miRNA and enhancing mRNA stability[73]. However, the opposite effect has also been described in *Drosophila melanogaster,* where binding in the 3'-UTR was associated with modestly decreased mRNA stability[74]. Additionally, RBFOX2 acts as a transcriptional repressor[75]; but upon *Rbfox2* overexpression, only a few changes in gene expression have been observed compared to those under control conditions[38].

## 1.2 MicroRNA regulation

MicroRNA regulation of gene expression is a ubiquitous phenomenon in higher eukaryotes[76]. miRNAs are a class of small RNAs that have a length of ~22 nt[77], comprising a diverse class of regulators in *Mus musculus* and other mammals, showing distinct temporal and cell type-specific expression patterns in the developing and mature neocortex[47,78]. miRNAs bind in the cytoplasm to the 3'-UTR of mRNAs and subsequently initiate rapid degradation[79]. Therefore, miRNAs are generally fast posttranscriptional repressors of gene translation.

### 1.2.1 Biogenesis of microRNAs

Despite the existence of noncanonical miRNA pathways (see Shang et al., 2023 for review[76]), most miRNAs are processed through the canonical pathway (**Figure 8**). Knockout of *DROSHA*, *DICER*, and *XPO5*, members of the canonical miRNA biogenesis pathway, resulted in 96.5 %, 96 %, and 29 %[2], respectively, of the miRNAs being reduced to ≤ 0.1-fold levels[80], highlighting the prevalence of the canonical pathway. MicroRNAs are transcribed from a few intergenic but mostly intragenic regions (introns or rarely exons) in DNA[81] and form the well-recognized hairpin structure. First, a complex of the RNase III Drosha and two DGCRPs crops the hairpin base of the pri-miRNA. The resulting pre-miRNA is exported through Exportin 5 into the cytoplasm[82]. Here, another essential RNase III of the miRNA pathway, Dicer, cleaves the pre-miRNA close to the terminal loop. Thereafter, the miRNA consists of two strands, one encoding the mature miRNA and the other being the passenger miRNA (miRNA*). The miRNA forms a complex with the Argonaute protein, and together, they bind to the target mRNA. The mRNA is recognized by the seed sequence of the miRNA (6–8 nt long sequence).

[2] 75.5 % of miRNA were decreased by ≤ 0.5-fold upon *XPO5* knock-out

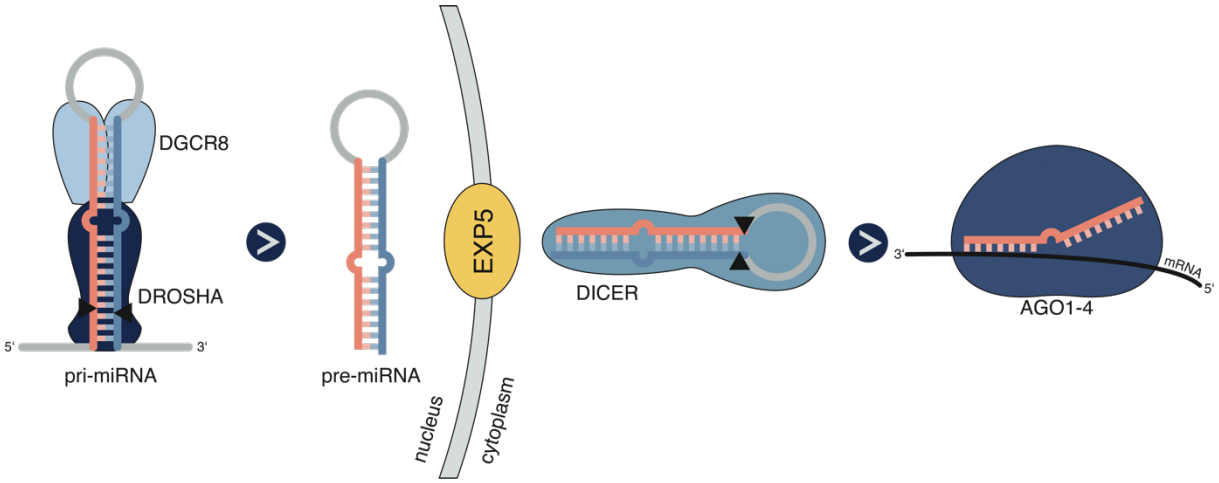


**Figure 8** Canonical miRNA biogenesis pathway. The pri-miRNA is cleaved by a protein complex consisting of Drosha and two DGCRB proteins. The resulting pre-miRNA is exported through Exportin 5 into the cytoplasm. Dicer removes the loop, and subsequently, the mature miRNA can bind together with Agonaute 1-4 to the target mRNA's UTR. Figure modeled after Shang et al., 2023[76].

This gives three possible 6-mers (positions 1 - 6, 2 - 7 and 3 - 8), two 7-mers (positions 1 - 7 and 2 - 8), and one 8-mer (position 1 - 8) for binding to the target mRNA. Moreover, in animals, mismatches in the binding sequence are frequently observed, expanding the set of predicted targets even further. However, many of the predicted targets remain unaffected by the presence of a miRNA, while other unpredicted mRNAs are regulated by this miRNA[83]. One common issue in target prediction is the short seed sequence (6 - 8 nt) that is recognized by the miRNA in the 3'-UTR of the mRNA. In large genomic sequences, seed matches can often be found by chance. Therefore, some target prediction databases consider only conserved sequences (e.g., the widely popular TargetScan[58]) and can eliminate many false positives with this strategy[84]. In addition to the canonical target sites, i.e. those that contain the matching sequence within their 3'-UTR, there are functional noncanonical target sites. Hence, the exact mechanisms of miRNA target identification remain only partly understood.

### 1.2.2 Regulatory effect of microRNAs

Although the regulatory effect is often described as weak, regulation by microRNAs is crucial during brain development and maintenance of mature tissue[7,47,85]. This was proven in a series of experiments in which essential proteins of the microRNA biogenesis pathway were knocked out, which is often complicated by lethality. However, successful knockouts of *Drosha*[80,86], *Dgcr8*[87,88], *Dicer1*[80,80,89–93],

*Exportin5*[80,89], and *Argonaute*[94] have been reported. The consequences depend on the time point of knockout and range from severe developmental impairment to lethality[92]. Excitatory neurons in the hippocampus lacking Dicer *in vivo* have drastically altered dendritic branching, dendritic spine length, apoptosis, and axonal pathfinding[91]. However, early knockout of *Dicer1* is lethal until approximately embryonic day 8[90].

miRNA regulation of gene expression mostly involves fine-tuning rather than strong repression[85], but some miRNAs exert a strong silencing effect on their targets[28]. When targeting dosage-sensitive genes (e.g. RNA binding proteins or transcription factors), the downstream effects of miRNA-binding can be significant[83]. For example, the expression of miR-124-3p can lead to complete silencing of its target *Ptbp1*[28] with subsequent strong alterations in splicing patterns (see section 1.1.3 – Regulation of RNA binding proteins).

MicroRNAs play pivotal roles in cortical development as indicated by significantly altered expression patterns at different developmental stages[47]. In particular, some miRNAs orchestrate corticogenesis (**Figure 9** a, b) by targeting developmentally relevant genes[7].

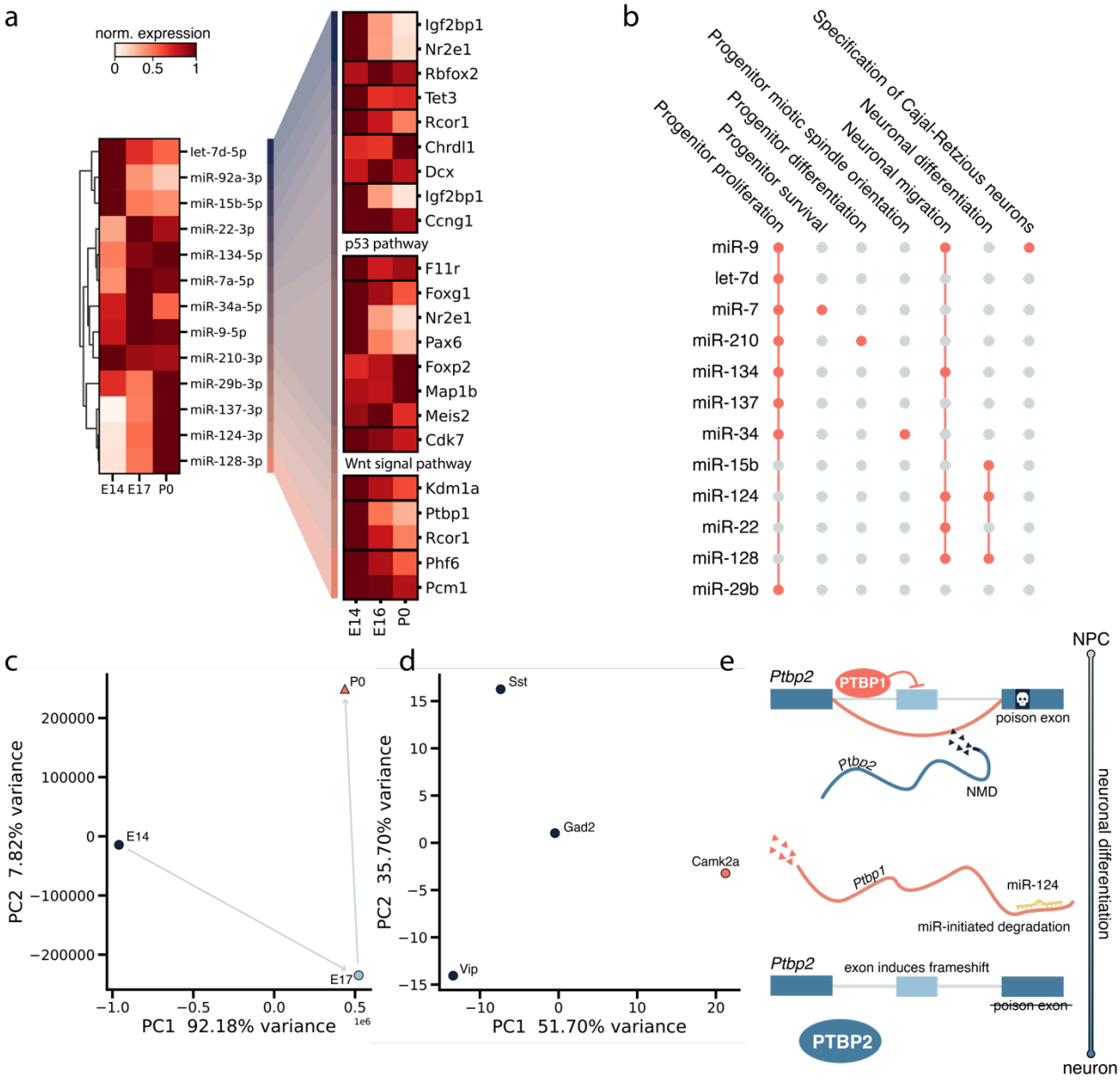


**Figure 9** Regulatory effect of microRNAs during cortical development **a** Heatmap on the left shows the expression of known relevant miRNAs during the development of the neocortex[7] and miR-92a[38] at time points E14, E17, and P0[47]; the heatmap on the right shows the expression of validated developmentally important miRNA targets[8]. Expression was normalized to the maximum value for E14, E16/E17, and P0 of the respective miRNA/gene. **b** Developmental GO terms of the targets regulated by the respective miRNAs, according to Lennox et al., 2018[7]. **c** Principal component analysis of microRNA expression during neocortical development[38]. The main variance is encoded on PC1 (92.18 %), and E14 is separated from the two later stages, E17 and P0. **d** Principal component analysis of cell-specific miRNA expression in the neocortex for the inhibitory neurons Sst, Vip, pan-inhibitory Gad2-positive neurons, and excitatory Camk2a neurons[78]. **e** Schematic representation of the PTBP1/PTBP2 switch during neural differentiation. PTBP1 induces the inclusion of a poison exon into the pre-mRNA of *Ptbp2,* and the resulting mRNA is subsequently degraded by NMD. By the expression of miR-124-3p, *Ptbp1* is degraded, and thus, the poison exon in *Ptbp2* is not included[45]. Therefore, the expression of PTBP1 and PTBP2 is mutually exclusive[65].

### 1.2.3 Regulation of the microRNA biogenesis pathway

Precise regulation of miRNAs is important for maintaining adequate expression levels. This is achieved through multiple mechanisms in the miRNA-biogenesis pathway (**Figure 10**). The microprocessor complex, which contains at least Drosha and DGCR8, is engaged in a complex regulatory circuit. DGCR8 stabilizes Drosha through protein-protein interactions (**Figure 10**a). Moreover, Drosha can reduce the stability of *Dgcr8* mRNA by cleavage and thereby suppress the expression of DGCR8 (**Figure 10**b). A reduced level of DGCR8 decreases the stability of Drosha itself and, thus the protein level[95,96]. This cross-regulatory loop is thought to prevent harmful effects within the cell.

Furthermore, the microprocessing complex is regulated by multiple protein modifications. Drosha's stability is enhanced, and its degradation is inhibited by acetylation[97] and binding of TAR DNA-binding protein 43 (TDP43)[98] (**Figure 10**c), a known neuronal activity response factor[99]. Thus, this is a potential mechanism of miRNA-mediated neuronal plasticity. The other essential part of the microprocessing complex, DGCR8, is also subject to protein modifications. Deacetylation of DGCR8 by histone deacetylase 1 leads to increased affinity for pri-miRNAs (**Figure 10**c)[100]. Herbert et al. showed that the stability of DGCR8 increases significantly when DGCR8 is phosphorylated by ERK/MAPKs, thereby responding to extracellular cues (**Figure 10**c)[101]. Interestingly, DGCR8 is also regulated in an activity-dependent manner. Phosphorated MEPC2 sequesters DGCR8 and blocks it from forming a microprocessing complex with Drosha (**Figure 10**c). Upon neuronal stimulation, however, MEPC2 is dephosphorylated, releasing DGCR8 to process pri-miRNA in cooperation with Drosha[102].

Pre-miRNAs are exported from the nucleus to the cytoplasm by Exportin 5 (XPO5). XPO5 is also involved in *Dicer* expression; thus, the overexpression of pre-miRNA leads to decreased levels of DICER in the cytoplasm and subsequently to less mature miRNA due to a lack of pre-miRNA processing capacity (**Figure 10**f)[89].

The expression of *Dicer* is regulated through a homeostatic feedback loop involving the miRNA let-7 (**Figure 10**d, e). Pre-let-7 is processed to let-7, like other miRNAs, by Dicer. Intriguingly, the binding of let-7 leads to miRNA-dependent degradation of *Dicer* mRNA and a reduction in Dicer protein expression. Since let-7 is processed through

the canonical miRNA biogenesis pathway, which requires Dicer, let-7 levels also decrease. Therefore, *Dicer* is not posttranscriptionally repressed, and protein level increases[103].

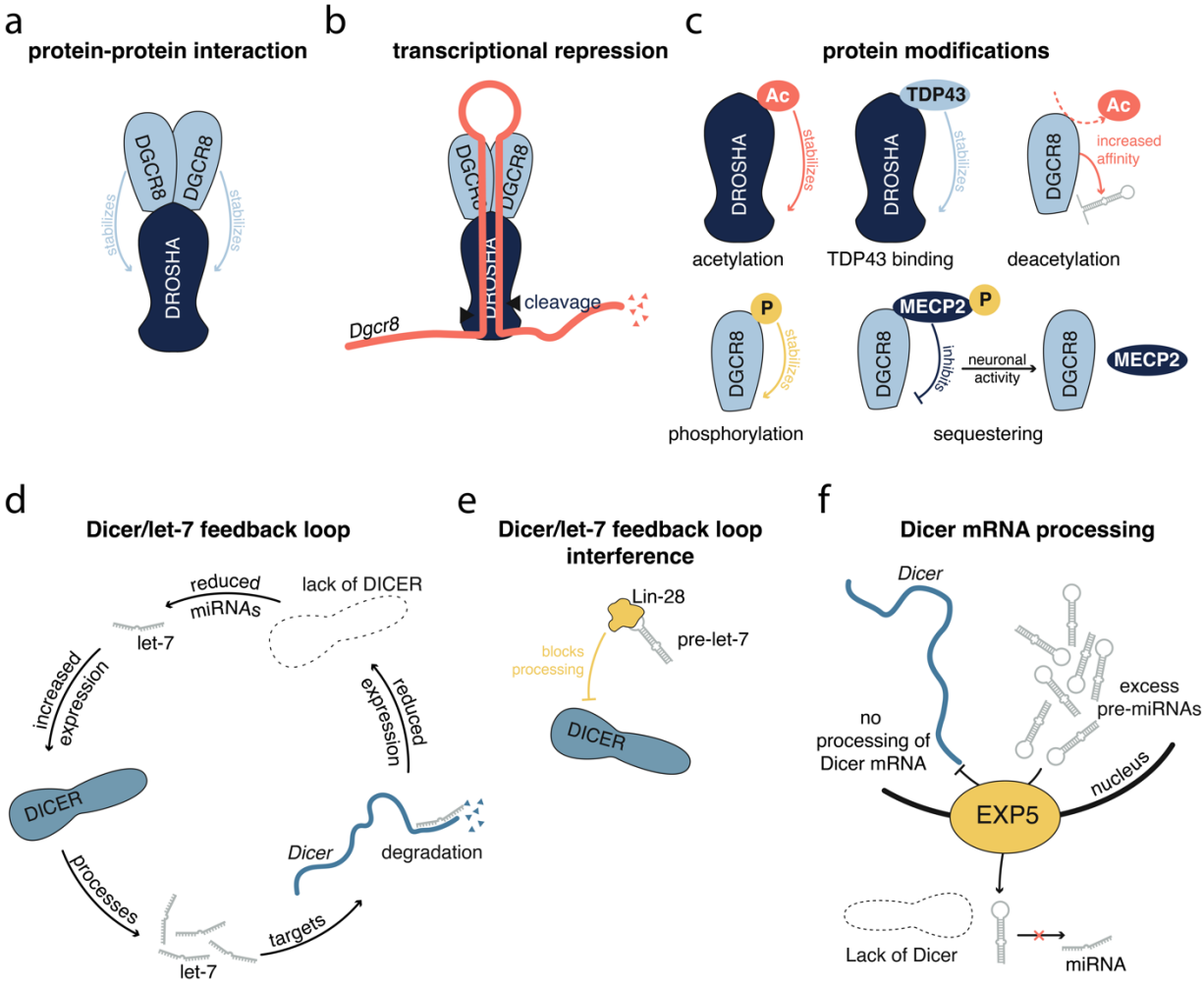


**Figure 10** Regulatory mechanisms of microRNA biogenesis and processing **a** Protein-Protein interaction: DGCR8 forms a complex with Drosha in the microprocessor. **b** Transcriptional repression: The DGCR8-DROSHA complex binds to and cleaves *Dgcr8* mRNA, regulating its expression. **c** Protein modifications: Posttranslational modifications of DGCR8, including acetylation, TDP43 binding, and deacetylation. Phosphorylation of DGCR8 leads to sequestration by MECP2, affecting neuronal activity. **d** Dicer/let-7 feedback loop: lack of Dicer leads to reduced miRNAs and increased let-7 expression. Let-7 targets Dicer mRNA, creating a regulatory feedback loop. **e** Dicer/let-7 feedback loop interference: Lin-28 blocks the processing of pre-let-7, interfering with the feedback mechanism. **f** Dicer mRNA processing: Exp5 inhibits Dicer mRNA processing, resulting in accumulation of excess pre-miRNAs in the nucleus and reduced mature miRNA production.

## 1.3 Other posttranscriptional regulatory mechanisms

In addition to regulation through alternative splicing and microRNAs, other important mechanisms modulate gene expression. Although these are not within the scope of the thesis, they are briefly introduced here.

### 1.3.1 RNA modifications

RNA modifications are chemical changes to RNA molecules that can affect their stability, function, and interactions. Over 170 types of RNA modifications have been identified since the discovery of pseudouridine in the 1950s[104], with the abundant N6-methyladenosine (m6A) being one of the most studied[105]. They were often neglected in the past due to low abundance and technical limitations in detection. Recently, RNA modifications have gained increasing interest, also in the context of cortical development[104]. Advancements in high-throughput sequencing and mass spectrometry have allowed a more comprehensive and accurate profiling of RNA modifications. Direct RNA sequencing, particularly nanopore sequencing, has recently emerged as a promising method for detecting RNA modifications. Nanopore sequencing relies on changes in the electric current measured in the nanopore that are attributable to chemical alterations in RNA molecules. While these alterations make basecalling challenging, they also provide an opportunity for direct and comprehensive RNA modification detection[106–108]. Consequently, it is now becoming possible to directly identify modifications such as m6A[109,110] or pseudouridine[111,112] simultaneously with standard RNA-seq experiments.

These recent technical advancements in detection methods have led to a greater appreciation of the critical roles RNA modifications play in regulating complex biological processes. For example, studies have revealed that m6A is dynamically regulated in the brain, influencing mRNA stability and neuronal plasticity[113].

### 1.3.2 RNA localization

Cellular organization depends on the ability of the cell to localize its constituents, i.e., DNA, RNA, and proteins, to precise regions to carry out their functions. Specifically, mRNA was initially expected to be rarely transported to distal sites of the cell; however, it has become clear that mRNA is subject to localization regulation[114]. This represents

a significant expansion of the central dogma of biology, which postulates that mRNA simply transfers information from DNA to protein. The transport of mRNA to different subcellular compartments regulates the local proteome.

Transporting mRNA to the location where it is needed can offer several advantages, such as energy efficiency due to reduced cost of protein transport, and quick response to internal or external stimuli through repeated translation of the same transcript. This is particularly relevant in neurons, where neurites (axons and dendrites) can extend several hundred micrometers away from the cell body (in extreme cases up to several 100 centimeters) and thus require local protein translation. In rat hippocampal neurons, approximately 50 % of transcripts were found to be enriched in dendrites compared to the soma[115], demonstrating the capability of neurons for local protein homeostasis. Subsequently, all relevant components for synthesis of cytosolic proteins (tRNA, mRNA, miRNA, translation factors, RISC, and ribosomes) have been detected within synaptic areas[116,117].

In general, there are three mechanisms for RNA localization described:

1. **Local protection of mRNA from degradation**: In synapses, RNA-binding proteins can shield transcripts from degrading enzymes, allowing for longer persistence and local translation. This mechanism is crucial in synapses because local protein synthesis allows for rapid, spatially specific responses to synaptic stimulation, i.e., synaptic tuning[118].
2. **Diffusion and anchoring**: mRNA can diffuse throughout the cell and be anchored at specific locations, such as synapses, through interactions with local cytoskeletal elements or specialized anchoring proteins[119].
3. **Active transport**: mRNA can be actively transported to specific subcellular locations through direct or indirect interactions with cytoskeletal elements and motor proteins such as kinesins and dyneins[119]. RNA granules, containing mRNAs bound to specialized RBPs like Staufen, play a key role in this transport and localization process[120,121].

Central to the active transport mechanism are cis-acting elements, often found in the 3'-UTR of the mRNA. These RNA sequences act as "zip codes" that direct mRNA to particular subcellular locations and are recognized by RBPs, facilitating the mRNA's transport and localization[122]. To prevent premature translation, mRNAs

are often transported and maintained in a translationally repressed state and activated by synaptic stimuli[118].

### 1.3.3 Polyadenylation

Polyadenylation is an essential process in the biogenesis of mRNA. This posttranscriptional modification involves the addition of a poly(A) tail to the 3' end of mRNA, significantly influencing its stability, localization, and translation efficiency[123]. A primary function of the poly(A) tail is to protect mRNA from degradation, with longer tails generally associated with increased mRNA stability.

The poly(A) tail is generated directly after transcription by the non-templated addition of adenosines to the mRNA 3′-end, a process catalyzed by nuclear poly(A)-polymerases. The initial length of poly(A) tails generated by this process has been estimated to be around 250 nucleotides *in vitro*, consistent with the typical length observed in mammals. After nuclear export, poly(A) length is dynamically regulated by the interplay of 3′-to-5′ degradation through exoribonucleases, poly(A) tail stabilization via poly(A) tail binding proteins, and elongation by cytoplasmic poly(A)-polymerases[9].

As poly(A) tails are shortened throughout the lifetime of the mRNA, deadenylation is one of the main factors determining the mRNA half-life[124]. While it has been shown that the poly(A) tail has a regulatory role, it is still not fully understood whether a specific length allows for specific regulatory outcomes. A minimal poly(A) tail is needed to prevent quick degradation, yet hyperadenylated RNAs are marked for fast RNA degradation in the nucleus[125].

Beyond tail length regulation, alternative polyadenylation (APA) adds another layer of complexity to gene expression control. While polyadenylation typically occurs at the 3'-UTR, alternative polyadenylation sites can exist within introns or coding regions. This phenomenon produces different mRNA isoforms from a single gene, each potentially having distinct characteristics. These isoforms may possess altered 3'-UTRs, which can significantly impact the mRNA's stability, localization, and translation efficiency. In some instances, APA can even result in the generation of altered protein products, further expanding the diversity of gene expression outcomes[126].

## 1.4 Scope and outline of the thesis

The following thesis comprises five studies that demonstrate how integrative bioinformatics and deep learning techniques can be leveraged to study the role of posttranscriptional regulation during cortical development. A summary of the main findings of each study is provided below.

- **Study 1: Premature upregulation of miR-92a's target RBFOX2 hijacks PTBP splicing and impairs cortical neuronal differentiation.** This study focused on elucidating the role of RBFOX2 in mediating alternative splicing changes that occur during corticogenesis. Premature overexpression of *Rbfox2* in mouse embryos at E14 was associated with impaired neuronal differentiation and migration and a mixed neuron- and NPC-like splicing pattern. Furthermore, we identified a set of significantly included cassette exons that are otherwise repressed by PTBP2 at this developmental time point. The antagonistic splicing relationship between these two RNA-binding proteins highlights the importance of precise temporal expression of alternative splicing factors in the developing brain. Consequently, we identified miRNA 92a-3p-mediated silencing as an important posttranscriptional mechanism to ensure appropriately low expression levels of *Rbfox2* in NPCs.
- **Study 2: Stage-specific expression patterns and co-targeting relationships among miRNAs in the developing mouse cerebral cortex.** miRNAs play an important role in the development of the neocortex. They act as posttranscriptional repressors by binding to the 3'-UTR of their target mRNA, thereby inhibiting translation or initiating degradation. Through miRNA-seq at three key time points during corticogenesis (E14, E17, and P0) and in NPCs and *in vitro* differentiated neurons, we identified microRNAs that regulate genes involved in crucial developmental processes such as stem cell maintenance, cell fate commitment, neuronal differentiation, and alternative splicing. A weighted co-expression network analysis revealed several microRNAs acting as hubs at early and late embryonic brain developmental stages. Moreover, using a custom statistical pipeline, we constructed an interaction network of miRNAs sharing more targets than expected by chance. Using luciferase

assays, we showed that the cooperative binding of two miRNAs to the same target could increase the repressive effect compared to individual miRNAs.

- **Study 3: Cortexa: a comprehensive resource for studying gene expression and alternative splicing in the murine brain.** Cortexa is a web portal designed to facilitate the analysis of RNA-sequencing datasets focusing on gene expression and alternative splicing in the mouse cerebral cortex and hippocampus. Gene expression and alternative splicing significantly change during cortical development, and both processes differ between distinct cell types in the adult brain. We reanalyzed three transcriptomic datasets (longitudinal development, neuronal cell-type specific, and NPC/neuronal datasets) concerning gene expression and alternative splicing and integrated them into the cortexa web portal (www.cortexa-rna.com). Furthermore, we implemented SplicePCA as an integrative method for studying global alternative splicing patterns. Cortexa provides a valuable resource accessible to a broad range of scientists, as it includes understandable visualizations as well as global and single-gene level representations of gene expression and alternative splicing. Users, furthermore, have the option to integrate their data and compare them with the data sets already available in cortexa.
- **Study 4: More than a pore: How voltage-gated calcium channels act on different levels of neuronal communication regulation.** Voltage-gated calcium channels (VGGC) are key regulators of calcium influx into the cell. They are activated upon depolarization of the membrane, and the subsequent increase in cellular calcium leads to the fusion of vesicles and neurotransmitter release into the synaptic cleft. Since VGCCs are multi-subunit structures composed of alpha, beta, gamma, and alpha-2-delta subunits, they exhibit many functions beyond the conductance of $Ca^{2+}$. Thus, alternative splicing of VGCCs is a primary mode of modifying their molecular interactions and downstream signaling capabilities. Here, we analyzed ribosome-associated transcripts and specifically focused on alternative splicing between various cell types in the neocortex and hippocampus. This revealed distinct VGCC splicing patterns across the neuronal populations, with parvalbumin-positive interneurons exhibiting a particularly unique splicing pattern.

- **Study 5: Denoising functional imaging data for neurobiology.** Posttranscriptional regulation often results in subtle changes in neuronal function, which can be read at synaptic connections between neurons. Noise in imaging data can further obscure these minute alterations, particularly in techniques like glutamate imaging that aim to capture fast events of transmitter release. This study introduces Neuroimage Denoiser, a U-Net-based deep learning model specifically designed to reduce noise in microscopic recordings of fast synaptic events. The framework effectively preserves signal amplitudes while significantly improving the signal-to-noise ratios, enabling more accurate detection and analysis of synaptic responses. Neuroimage Denoiser can be applied to recordings with different acquisition rates and sensors without retraining, making it a versatile tool for various experimental setups. This approach enhances the ability to study complex synaptic structures, spontaneous activity, and synaptic plasticity at high temporal and spatial resolutions. Thus, it is a flexible tool for studying synaptic alterations induced by posttranscriptional regulation, such as the alternative splicing of calcium channels. The tool is open-source and available on GitHub (https://github.com/s-weissbach/neuroimage_denoiser).

# 2 Scientific publications

## 2.1 Premature upregulation of miR-92a's target RBFOX2 hijacks PTBP splicing and impairs cortical neuronal differentiation.

Authors: **Stephan Weißbach**, Hristo Todorov, Laura Schlichtholz, Sophia Mühlbauer, Lea Zografidou, Azza Soliman, Sarah Lor-Zade, Dewi Hartwich, Dennis Strand, Susanne Strand, Tanja Vogel, Martin Heine, Susanne Gerber, Jennifer Winter

This article is available as a preprint in *biorXiv* (doi: https://doi.org/10.1101/2024.09.20.614071) and is under revision at *Nucleic Acids Research*.

My contributions to this article are listed in 6.1 Contribution to individual publications.

# Premature upregulation of miR-92a's target RBFOX2 hijacks PTBP splicing and impairs cortical neuronal differentiation.

Stephan Weißbach[1,2], Hristo Todorov[2,3], Laura Schlichtholz[2], Sophia Mühlbauer[2], Lea Zografidou[2], Azza Soliman[2], Sarah Lor-Zade[2], Dewi Hartwich[2], Dennis Strand[4], Susanne Strand[4], Tanja Vogel[5], Martin Heine[1], Susanne Gerber[2], Jennifer Winter[2,*]

[1] Institute of Developmental Biology and Neurobiology (iDN), Johannes Gutenberg-University, 55128 Mainz, Germany

[2] Institute of Human Genetics, University Medical Center, Johannes Gutenberg-University, 55131 Mainz, Germany

[3] Current affiliation: Institute of Immunology, University Medical Center, Johannes Gutenberg-University, 55131 Mainz, Germany

[4] Department of Internal Medicine, University Medical Center, Johannes Gutenberg-University, 55131 Mainz, Germany

[5] Institute of Anatomy and Cell Biology, Department of Molecular Embryology, Medical Faculty, Albert-Ludwigs-University Freiburg, 79104 Freiburg, Germany

[*] Corresponding author: jewinter@uni-mainz.de

## Abstract

RBFOX2 is an RNA-binding protein crucial for alternative splicing regulation and implicated in several neurodevelopmental disorders. Here, we show that while RBFOX2 is present only at low levels in neural progenitor cells (NPCs), it is upregulated in differentiating neurons of the mouse embryonic neocortex. *In-utero*-electroporation-induced overexpression resulted in a cellular phenotype characterized by impaired neuronal migration and differentiation. Genome-wide analysis at E15.5 revealed numerous alternative splicing events associated with a mixed NPC- and neuron-like splicing pattern and a significant deviation from the normal splicing developmental trajectory. Remarkably, premature *Rbfox2* overexpression induced the inclusion of validated target exons that are otherwise repressed by PTBP2, indicating an antagonistic splicing relationship between these two RNA-binding proteins and highlighting the necessity for strict temporal regulation of their expression during embryonic brain development. Consequently, we showed that the NPC-specific miRNA 92a-3p reduced the expression levels of *Rbfox2 in vitro*. Furthermore, silencing miR-92a-3p *in vivo* in the embryonic neocortex led to a significant increase in *Rbfox2* levels. Our results therefore demonstrate that RBFOX2 is a crucial player in the NPC-to-neuron splicing switch. Furthermore, we present a novel post-transcriptional mechanism for controlling RBFOX2 levels during early neuronal differentiation via miR-92a-3p silencing.

## Introduction

Despite the presence of only approximately 22,000 protein-coding genes[1], the murine neocortex, and hippocampus exhibit a considerable diversity of neurons, amounting to 388 transcriptomic cell types, as reported by the Allen Brain Consortium[2]. A key factor enabling this diversity and complexity is alternative splicing (AS), a tightly regulated process that governs the production of multiple mRNA isoforms from a single gene. Intriguingly, nearly every multi-exon gene in the human genome can undergo alternative splicing, generating numerous protein isoforms with distinct structural and

functional properties[3]. This vast molecular diversity expands the proteome's complexity without necessitating a proportional increase in the genome's size. Within the nervous system, AS is a pervasive phenomenon, with various neural genes subject to this regulation[4]. Overall, AS has a higher prevalence across different species and is more conserved in the brain compared to other tissues[5,6].

Specifically, numerous changes in the splicing landscape occur in the developing brain with high temporal precision[4,7]. Among the processes that require correct splicing are neuronal migration, neuronal differentiation[8], axonogenesis[9], and synaptogenesis[10,11]. Notably, the significance of correct splicing is not confined to the developing brain alone. In the adult brain, different neuronal types exhibit distinct splicing patterns, further underscoring the importance of alternative splicing in maintaining the brain's functional diversity[11,12].

During embryonic development, neural stem cell differentiation requires precise extensive AS switches to create neuron-specific splicing patterns. Many of these splicing events alter key protein domains, particularly in proteins of the cytoskeleton[8]. Various RNA binding proteins (RBPs) regulate the transition from neural stem and progenitor cells to neurons by altering the splicing pattern of target genes, therefore their temporal expression needs to be strictly regulated. Here, microRNAs (miRNAs) that suppress gene expression post-transcriptionally by binding to the 3' untranslated region of target mRNAs[13–16], represent one important mechanism for mediating stage and cell-type specific levels of RBPs For instance, PTBP1 is expressed only in neural stem and progenitor cells, however, it is strongly repressed by miR-124-3p in neurons[17]. In contrast, other prominent RBPs, including NOVA, PTBP2, MBNL2, and RBFOX are predominant in neurons. These RBPs act in both synergistic (e.g. NOVA and RBFOX) and antagonistic relationships (e.g. PTBP1/2 and RBFOX)[18,4,8].

The RBFOX-family consists of three paralogs, namely, RBFOX1 (FOX-1 or A2B1), RBFOX2 (FOX-2 or RBM9) and RBFOX3 (FOX-3, HRNBP3, or NeuN). The association of mutations in human *RBFOX1* and *RBFOX2* with intellectual disability, autism, and other neurodevelopmental disorders, as well as the specific neurological phenotypes observed in *Rbfox* knockout mice, highlight the important functions of these proteins during neurodevelopment[19–26]. All RBFOX-proteins have a single, highly conserved RNA recognition motif (RRM) that binds to the target sequence (U)GCAUG harbored in the premature mRNA and initiates position-dependent splicing. RBFOX binding in the intronic region upstream of an alternatively spliced exon promotes its exclusion from the mature mRNA whereas downstream binding leads to inclusion[27]. Moreover, in humans, all RBFOX-proteins share the position-dependent splicing mechanism and the RRM which is identical in RBFOX1 and RBFOX2 and almost identical in RBFOX3. Therefore, the RBFOX family can act in a functionally redundant manner[28]. However, the temporal expression patterns of these proteins diverge significantly, exhibiting variations across different tissues and cell types[2,12]. In the developing brain, RBFOX proteins are either lowly expressed or not present in neural stem cells, but they are highly expressed in neurons which is in agreement with their role in promoting neuronal differentiation. Studies aiming at identifying splicing changes during neural stem cell differentiation have compared alternative exon usage between NPCs and neurons by RNA-sequencing[8,29]. While these studies have identified numerous splicing changes that are presumably driven by RBFOX binding, the exact role of RBFOX during neuronal differentiation in the embryonic brain has not been elucidated yet.

In the current study, we identified extensive AS changes upon premature *Rbfox2* overexpression (*Rbfox2*-OE) in the embryonic neocortex, specifically related to genes that are important for neuronal differentiation and localization. Remarkably, we observed a mixed neuronal and NPC-like splicing pattern that significantly deviated from the normal cortical splicing trajectory. In line with this, *Rbfox2* overexpression increased the percentage of neural stem and progenitor cells and blocked differentiation into neurons on the cellular level. Since a precise and tight control of RBFOX2 is essential for proper neuronal differentiation in the embryonic neocortex, we investigated if miRNAs might repress *Rbfox2* expression in NPCs. Indeed, we observed that the NPC-specific miR-92a led to reduced RBFOX2 levels. Conversely, miR-92a silencing in the embryonic neocortex was associated with a concomitant increase in *Rbfox2* expression.

## Results

### RBFOX2 is predominantly expressed in neurons

The RBFOX protein family exhibits distinct temporal expression patterns, varying also by cell type. For instance, RBFOX1 and RBFOX3 are expressed in mature neurons and exclusively in the cortical plate in the embryonic cerebral cortex[30] RBFOX2 shows early expression in Purkinje cells in the cerebellum[31]. To elucidate the composition of RBFOX proteins in the mouse embryonic cerebral cortex, we co-stained sections for RBFOX1 and RBFOX2. This confirmed RBFOX2's presence was not limited to the neuron-specific cortical plate, but it was also expressed in the intermediate and ventricular (VZ)/subventricular (SVZ) zones (Figure 1a). In contrast, RBFOX1 expression was restricted to the cortical plate/subplate. While this broader expression pattern of RBFOX2 compared to RBFOX1 was evident, not all cells in the cerebral cortex showed positive RBFOX2 staining. Especially in the VZ/SVZ where radial glia cells and basal progenitors reside at this developmental stage, the majority of cells were RBFOX2 negative (Figure 1a). This prompted us to investigate the temporal expression of RBFOX2 using an *in vitro* neuronal differentiation model. Here, we observed low *Rbfox2* mRNA expression in radial glia-like cells and early neural progenitor cells (NPCs). However, *Rbfox2* expression increased significantly during neuronal differentiation, peaking in late NPCs and young neurons (Figure 1b). Likewise, *Rbfox2* was only weakly expressed in NPCs derived from the embryonic cerebral cortex while it was strongly upregulated in cortical neurons at both RNA and protein levels (Figure 1c, d).

To further corroborate these data, we analyzed RBFOX2 expression in the embryonic cerebral cortex *in vivo* by immunostaining. To this end, we made use of a transgenic mouse model (HES5::GFP) expressing GFP exclusively in Notch-signaling neural progenitor cells. In agreement with the *in vitro* data, RBFOX2 expression was restricted to $GFP^-$ cells, that were presumably in a more differentiated state compared to HES5 positive NPCs (Figure 1e). Co-stainings with the basal progenitor marker TBR2 (EOMES) confirmed the absence of RBFOX2 from neural progenitor cells. Only cells with a low TBR2 expression exhibited low RBFOX2 expression, suggesting that these cells were currently differentiating into neurons (Figure 1f). In contrast, RBFOX2 was highly expressed in newborn neurons in all zones as revealed by co-staining with the early neuron marker β-III-Tubulin (TUBB3) (Figure 1g). In summary, RBFOX2 was weakly expressed in neural stem and progenitor cells and highly upregulated during neuronal differentiation, highlighting its potential role in mediating the neuron-specific splicing switch.

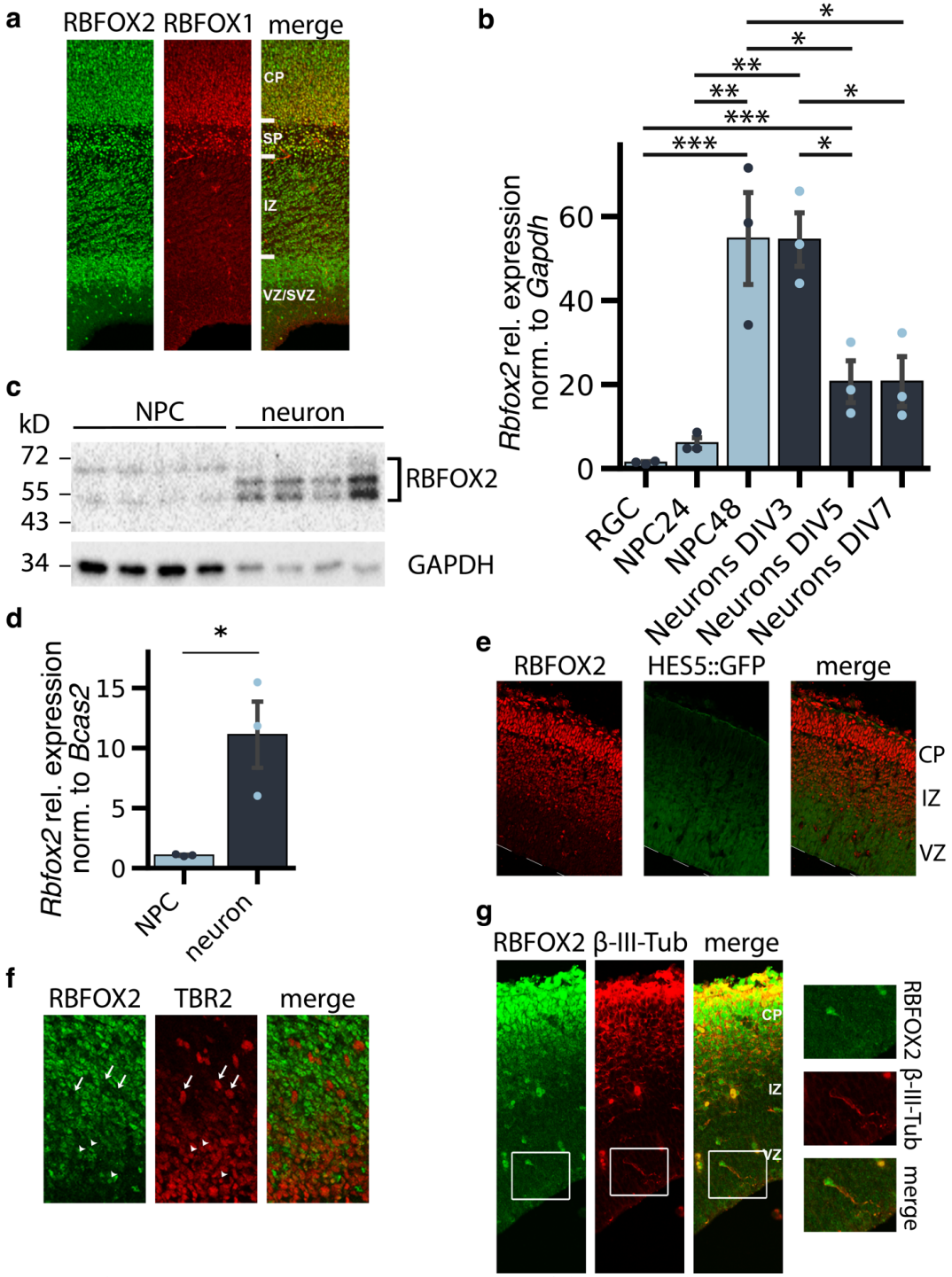


*Figure 1 Rbfox2 expression was upregulated in newborn neurons. a) Cryosections of E17.5 cerebral cortex were co-stained with antibodies against RBFOX1 and RBFOX2. Expression of RBFOX1 was restricted to the cortical plate/subplate whereas RBFOX2 was additionally expressed in cells of the ventricular zone (VZ)/subventricular zone (SVZ) and intermediate zone (IZ). b) To determine the expression of Rbfox2 during neuronal differentiation, embryonic stem cells were differentiated into radial glia cells (RGCs), NPCs, and neurons and subjected to RT-qPCR with Rbfox2-specific primers. Rbfox2 expression increased strongly in late NPCs and early neurons and*

*decreased again in late neurons. c) Western blot analysis with RBFOX2-specific antibodies illustrates the increase in RBFOX2 expression in neurons compared to NPCs. Note that due to alternative splicing, several RBFOX2 isoforms exist which differ between NPCs and neurons. d) RT-qPCR showed increased Rbfox2 expression in neurons compared to NPCs. e) Cryosections of the E14.5 cerebral cortex derived from HES5::GFP transgenic mice were immunostained with RBFOX2 antibodies. RBFOX2 was predominantly expressed in differentiating GFP$^-$ cells. f and g) Cryosections of the E17.5 cerebral cortex were co-immunostained for RBFOX2 and the basal progenitor marker TBR2 (f) or RBFOX2 and the newborn-neuron marker β-III-Tubulin (g). RBFOX2 was expressed in β-III-Tubulin+ neurons and absent from TBR2$^+$ basal progenitors. *p<0.05, **p<0.01, ***p<0.001, ANOVA followed by Tukey's post-hoc test in b, t-test in d.*

## Premature *Rbfox2* overexpression disrupts the splicing landscape of the developing cortex

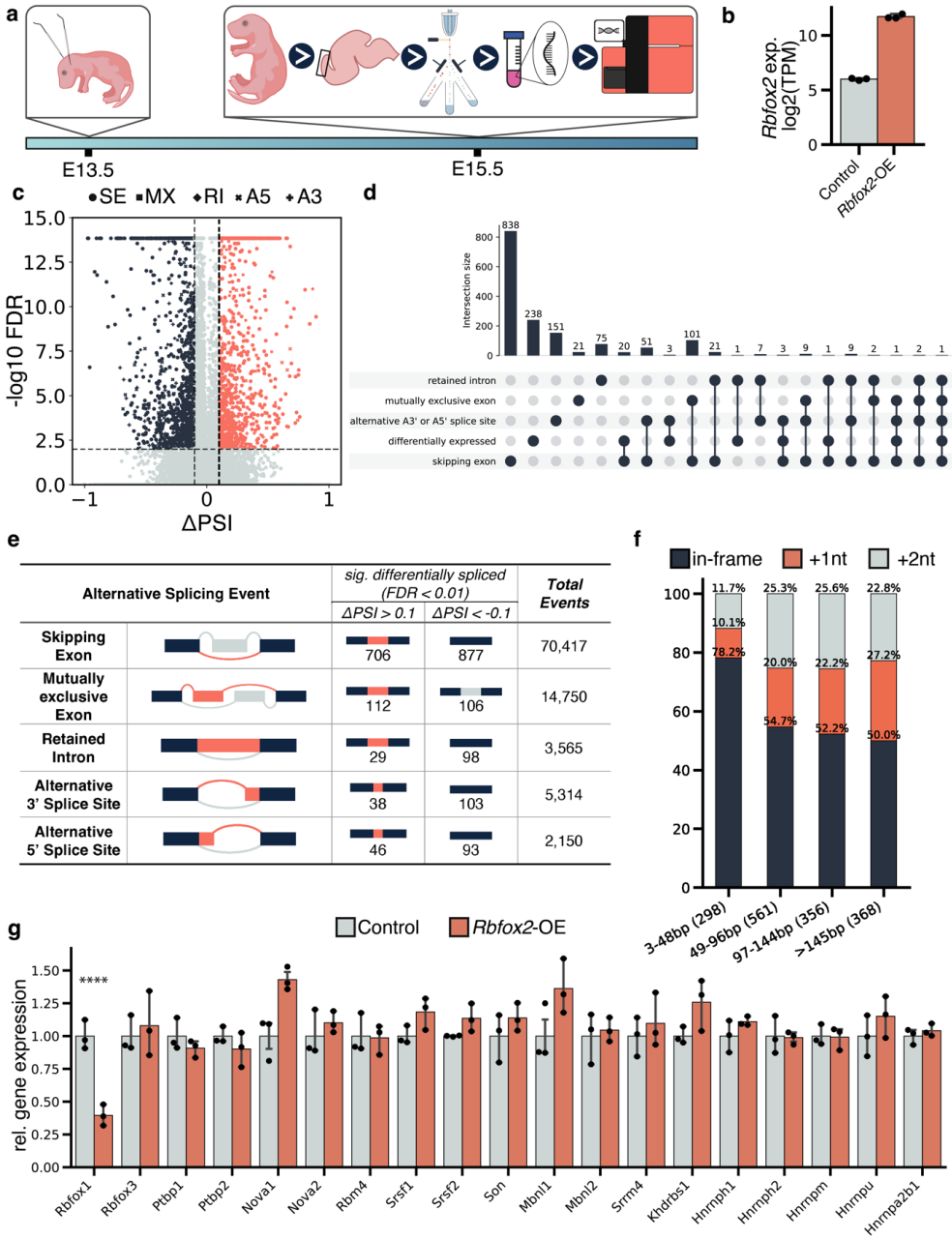


*Figure 2 Rbfox2 overexpression changed the splicing pattern of the developing cortex. a) Experimental timeline, Rbfox2 overexpression was induced in embryonic mouse neocortex at E13.5 by in-utero electroporation, and bulk RNA-sequencing was performed at E15.5 b) The electroporation of Rbfox2 constructs increased the mRNA abundance of Rbfox2 in the cortex significantly c) The volcano plot visualizes alternative splicing events. The x-axis shows delta percentage spliced in (ΔPSI), and the y-axis shows -log10 false discovery rate (FDR) values. Significantly spliced-in events are in orange, spliced-out events are in blue, and non-significant events are in grey. Shapes denote event types: circles for skipping exons, squares for mutually exclusive exons (MX), diamonds for retained introns (RI), and crosses for alternative A5 and A3 splice sites. d) UpSet plot depicts the overlap between 1) Differentially expressed genes, 2) Genes with significant alternatively spliced skipping exon events, 3) Genes*

*with significant alternatively spliced mutually exclusive exon events, and 4) Genes with other splice events, including retained intron, A3', and A5' splice sites. e) The table provides an overview of significant alternative splicing events, totaling 2,208 events. Significance was defined as FDR < 0.01 and either ΔPSI > 0.1 or ΔPSI < -0.1. f) Frequency of induced frameshifts due to alternative splicing for different exon lengths. g) Normalized gene expression levels of key splicing factors important in the CNS, upon Rbfox2 overexpression compared to control. Values for each gene are normalized to the mean of the control group. Data are shown as mean ± standard error of the mean *** p<0.001, ****p<0.0001, Wald test from DESeq2 in g.*

To study RBFOX2's impact on splicing during embryonic corticogenesis, we used *in-utero* electroporation to overexpress *Rbfox2* in the mouse cerebral cortex at E13.5 and subsequently performed RNA-sequencing at E15.5 (Figure 2a). As expected, *in utero* electroporation resulted in a significant increase in *Rbfox2* gene expression ($p_{adj}$ < 0.0001, log2fold = 5.754, Figure 2b). Furthermore, we detected 268 differentially expressed genes (Supplementary Figure S1a, Supplementary Data 1) and substantial changes in the alternative splicing landscape upon *Rbfox2* overexpression compared to control samples (Figure 2c). However, most alternatively spliced genes did not show altered expression levels. Only 30 genes were alternatively spliced and differentially expressed at the same time (Figure 2d) with *Snhg5*, a lncRNA, having all five types of analyzed splicing events. 17 genes were alternatively spliced and upregulated, while the remaining 13 were downregulated. While frameshifts induced by alternative splicing can result in early stop codons and nonsense-mediated decay (Figure 2f), we did not find significant changes in gene expression related to this phenomenon in our data.

Overall, we detected 2,208 significant alternative splicing events (Figure 2e, Supplementary Figure S2) between the *Rbfox2*-OE and control samples using a stringent threshold of FDR < 0.01 and |ΔPSI| > 0.1. Skipped exons (or cassette exons) represented ~71% of these events. Changes in splicing could mostly be attributed directly to RBFOX2 and not to altered expression of other known splice factors relevant during cortical development (Figure 2g). In line with this, we observed a significant overlap between skipping exon events in our data with *Rbfox* triple knock-out (t*Rbfox*-KO) samples[32] (fold enrichment ≈ 9.833, p-value < 0.0001; Supplementary Figure 3b, Supplementary Data 2). Importantly, inclusion levels of cassette exons present in both data sets were strongly negatively correlated (R = -0.6624, p < 0.0001) indicating that *Rbfox2*-OE induced the opposite splicing regulation compared to t*Rbfox*-KO. (Supplementary Figure 3a). The strong *Rbfox2*-OE induced a significant reduction in the expression level of *Rbfox1* ($p_{adj}$ < 0.0001, log2fold = -1.342). However, the expression of *Rbfox3* was unaltered ($p_{adj}$ ≈ 0.98, log2fold = 0.121) compared to the control group. Remarkably, genes that were alternatively spliced in our analysis were significantly enriched for high-confidence neurodevelopmental disorder (NDD) genes[33] (224 out of 1317 genes, fold enrichment ≈ 1.358, p < 2e-07, Supplementary Data 6, Supplementary Figure S4).

Alternative splicing is a key mediator for the development of proper neuronal functioning. Over 20,000 splicing events have been reported throughout cortical development[34]. To gain a perspective on the splicing pattern induced upon *Rbfox2*-OE, we integrated the previously published RNA-sequencing data from Weyn-Vanhentenryck et al. obtained at different developmental stages of wildtype mouse cerebral cortex (E14.5 to P30)[34] as well as RNA-sequencing from FACS-sorted NPCs and neurons[29]. The hierarchical clustering of splicing events that were significant both in our data and in the previous studies, revealed that our control group clustered with the FACS-sorted neurons as well as with the E14.5 and E16.5 cortical samples. In contrast, the *Rbfox2*-OE group did not closely cluster with any of the embryonic

223 samples or NPCs/neurons pointing to an abnormal splicing pattern (Supplementary
224 Figure S2).
225 To further investigate the impact of *Rbfox2*-OE on the splicing landscape during
226 neurogenesis, we applied a principal component analysis (PCA). We observed a bell-
227 shaped trajectory indicative of the expected splicing changes throughout embryonic
228 and postnatal cortical development (Figure 3a). Remarkably, the influence of batch
229 effects between the different studies was negligible, contrary to differential gene
230 expression analyses where batch effects are often prominent[35,36]. *Rbfox2*-OE resulted
231 in a substantial deviation from this expected developmental trajectory. Specifically, on
232 the first principal component (PC1), *Rbfox2*-OE exhibited a shift towards the splicing
233 pattern associated with mature neurons, while on the second principal component
234 (PC2), the shift was towards undifferentiated NPCs. To identify the main splicing
235 events that explained the observed splicing pattern, we calculated the loadings of the
236 original variables included in the PCA on both PC1 and PC2 (Figure 3b). This analysis
237 revealed numerous genes that are highly relevant for neuronal development.
238 Interestingly, some genes with the highest loadings were associated with
239 neurodevelopmental diseases. For instance, *Shank1* and *Dlgap4* are related to autism
240 spectrum disorder[37,38], whereas *Dlg2* has been linked with schizophrenia[39].
241 To gain insight into the biological processes regulated by the genes that were
242 correlated with each principal component, we performed a gene set enrichment
243 analysis (GSEA) of gene ontology (GO) terms. The loadings of the alternative splicing
244 events on each principal component were used as effect sizes in the GSEA (Figure
245 3c). PC1 was associated with higher-level GO terms such as “regulation of
246 transportation”, “animal organ development”, and “central nervous system
247 development”. This association is plausible given that PC1 represented 55.61% of the
248 variability and separated the samples from early embryonic stage E14.5 to the
249 prepubescent stage P30. During this broad period, manifold biological processes
250 occur, shaping the development of the central nervous system. The higher-level GO
251 terms reflected this complexity as descriptors for the wide-ranging changes captured
252 by PC1. More specifically, transport and localization were significantly enriched for
253 PC1. Interestingly, some splicing events with high PC1 loadings were associated with
254 multiple enriched GO terms. For instance, *Cadps*, a calcium-dependent segregation
255 activator, that was associated with 7 GO terms (Supplementary Data 3), was previously
256 reported to be differentially spliced upon *Rbfox2*-knockout[23]. This gene was also
257 among the top correlated genes of PC1 (Figure 3b, left). Another important gene
258 associated with 6 GO terms was *Ap2a1*. While PTBP2 was previously reported to
259 induce exon skipping in *Ap2a1* (chr7:44,552,885-44,552,951, Supplementary Figure
260 S5a) during brain development[40], *Rbfox2*-OE led to the opposite effect of exon
261 inclusion (FDR < 0.0001, ΔPSI = 0.297) in our data.
262 Moreover, neuron differentiation was among the significant terms associated with PC2,
263 where the *Rbfox2*-OE samples were more similar to an NPC splicing pattern. When
264 analyzing the splicing events that significantly contributed to this GO term, we identified
265 several developmentally relevant genes. For instance, *Clasp2*, a protein involved in
266 microtubule dynamics, is known to play a role in neuronal migration and axonal growth
267 during cortical development[41]. We detected an alternatively spliced exon in *Clasp2*
268 (chr9:113,691,503-113,691,530, Supplementary Figure S5b) that showed a
269 significantly higher inclusion in the *Rbfox2* overexpression group (FDR < 0.0001, ΔPSI
270 = 0.118). Interestingly, we observed a similar increase of the same exon when

analyzing the splicing changes between NPCs and neurons (FDR < 0.01, ΔPSI = 0.118).

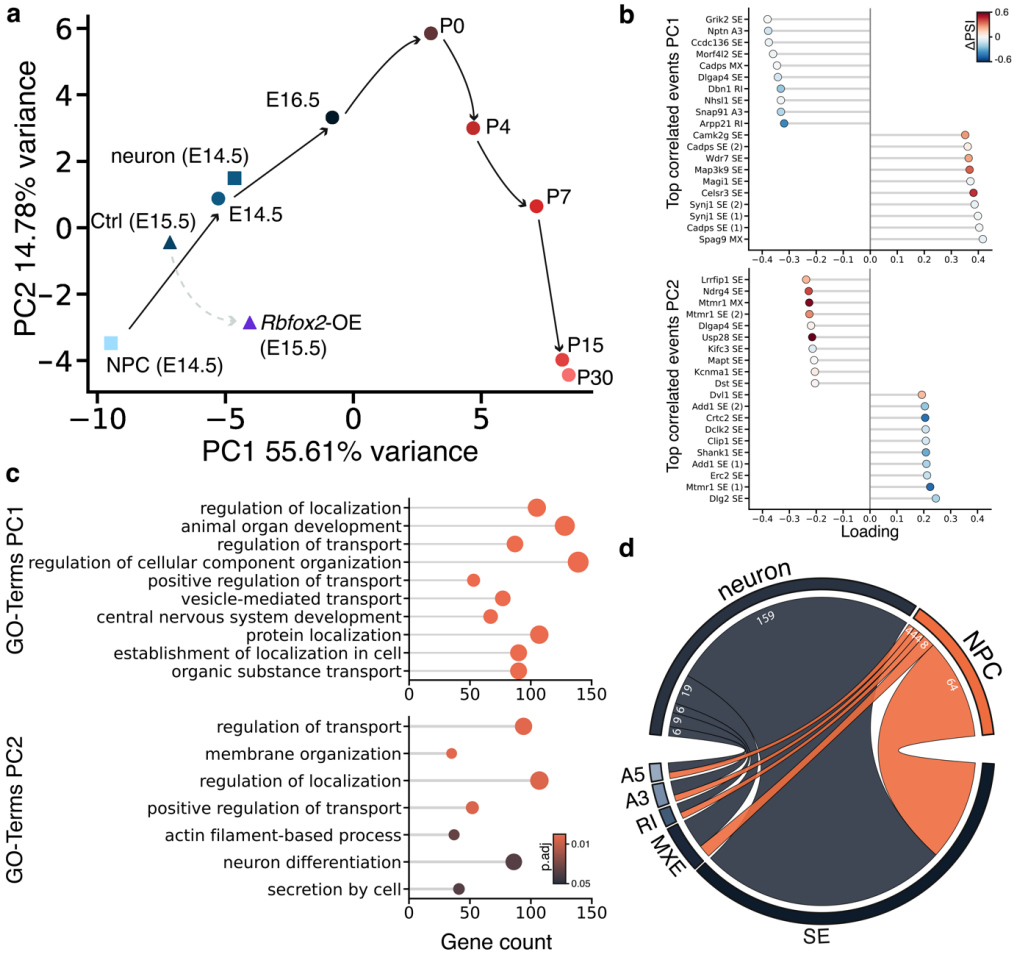


*Figure 3 Developmental regulation of alternative splicing by RBFOX2. a) Principal Component Analysis (PCA) of splicing patterns using SplicePCA[42] across embryonic and postnatal brain development. Blue color dots represent embryonic and red dots denote postnatal stages. Shapes indicate the source of the data used. Circles correspond to E14.5 to P30 samples from Weyn-Vanhentenryck et al.[34], squares represent NPC and neuron samples from Liu et al. [43]. Rbfox2 overexpression (OE) samples (triangle shape) noticeably deviate from the expected developmental trajectory. b) Loading analysis for PC1 and PC2, highlighting the top 10 positively and top 10 negatively correlated splicing events for each PC. Color gradient represents the ΔPSI values for Rbfox2-OE compared to control samples c) Gene Set Enrichment Analysis (GSEA) performed on splicing events for PC1 and PC2 using loadings on each component as effect sizes. D) Chord plot showing the association between significant splicing events in Rbfox2-OE vs. control samples compared with splicing events in neurons vs. NPCs obtained using the data from Liu et al. [43].*

The observed mixed phenotype upon *Rbfox2*-OE was not only characterized by the deviation from the expected developmental trajectory but also by the type of splicing events. When comparing the significant splicing events upon *Rbfox2*-OE with those of neurons vs. NPCs from the Liu et al. data[43], we found an overlap of 283 significant events. Strikingly, 70% of the events corresponded to a neuron-like splicing and 30% of events represent NPC-like splicing patterns (Figure 3d). Several of the overlapping genes have been reported previously to undergo alternative splicing during important developmental processes associated with NPC proliferation, radial migration of neurons, and neuronal differentiation[8]. Genes with a neuron-like splicing included

*Clasp2*, *Dctn1*, *Kif2a*, *Mast2*, and *Tpm1*. In contrast, *Add1*, *Clip1*, *Clasp1*, *Dync1i2*, *Gphn*, and *Macf1* were spliced in an NPC-like way (Supplementary Data 4).

## RBFOX2 misexpression impairs neuronal differentiation in the embryonic neocortex

After ascertaining the dramatic effect of *Rbfox2* overexpression on the splicing landscape of the developing neocortex, next, we investigated whether this translates into changes in neuronal differentiation and/or migration at the cellular level. Therefore, we electroporated *Rbfox2* constructs into the E13.5 neocortex and analyzed brain sections two days later by immunostaining experiments. We detected significantly more RBFOX2-OE cells in VZ and lIZ. Conversely, we observed significantly fewer RBFOX2-overexpressing cells in the uIZ and the CP (Figure 4a). In line with the observed phenotype of cells detaching from the ventricular surface and subsequently failing to migrate to the cortical plate and accumulating in the lIZ, *Rbfox2-OE* induced alternative splicing of two key constituents of the Reelin pathway which plays an important role during cortical development by guiding neurons to the correct position in the CP[44]. Specifically, an exon of *Lrp8* encoding the murine-specific eighth LDL receptor type A (chr4:107,705,477-107,705,600, Supplementary Figure S5f) was abnormally included (FDR < 0.0001, ΔPSI = 0.275). Expression of this exon was previously linked to neuronal migration[45]. Additionally, the exon (chr19:27,217,244-27,217,370, Supplementary Figure S5g) of *Vldlr* encoding the calcium-binding EGF domain was repressed following *Rbfox2*-OE (FDR < 0.0001, ΔPSI = -0.201). Repression of the EGF domain alters the binding affinity to ligands modulating the sensitivity of the receptor and its interacting ligands[46]. Moreover, RBFOX2 could synergistically act with NOVA2 which is known to induce alternative splicing changes in *Dab1*. DAB1 constitutes a switch within the Reelin pathway that is required for neuronal migration[47,48].

To investigate the impact of *Rbfox2* misexpression on neuronal differentiation, we performed immunostainings with antibodies against the marker genes PAX6 (radial glia cells), TBR2 (basal progenitors), and SATB2 (neurons). This revealed a significant differentiation defect in the *Rbfox2* overexpressing neocortex. In particular, the percentage of $PAX6^+$ radial glial cells and $TBR2^+$ basal progenitors was significantly increased compared to the control group (Figure 4b,c) whereas the percentage of $SATB2^+$ neurons was reduced (Figure 4d). This indicates that a correct and fine-tuned expression of RBFOX2 is essential for proper neuronal differentiation in the embryonic neocortex.

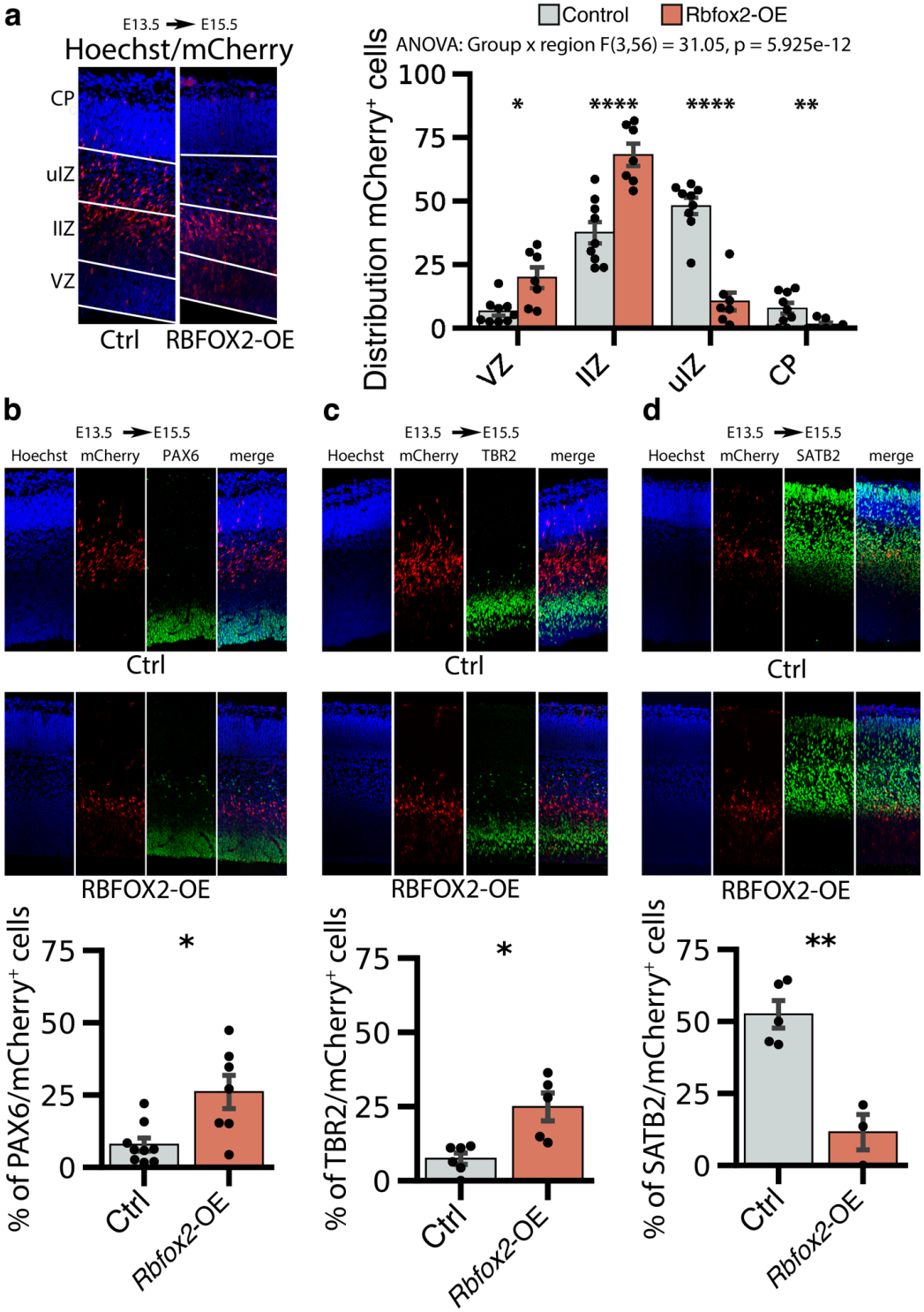


*Figure 4 Rbfox2 mis-expression disrupts neuronal* differentiation in the neocortex. *Rbfox2 expression constructs were co-electroporated* with *pCAG-mCherry at E13.5. The electroporated brains were analyzed 48 hours later.* a) Distribution of the electroporated mCherry+ cells in the embryonic neocortex. b-d) Cryosections of the electroporated brains were immunostained for markers (green) for radial glia cells (b; PAX6), basal progenitors (c; TBR2) and

neurons (d; SATB2). Bar plots show mean values ± standard error of the mean. * p<0.05, ** p<0.01, **** p<0.0001, two-way ANOVA followed by pairwise comparison of model means in a; * p<0.05, ** p<0.01, unpaired t-test in b-d.

## RBFOX2 canonical and non-canonical motifs are enriched around alternatively spliced exons

Previous studies have shown that RBFOX1, RBFOX2, and RBFOX3 preferably bind to the conserved sequence (U)GCAUG[49,50]. RBFOX's effect is position-dependent – an upstream intronic binding leads to exon repression, while downstream intronic binding enhances exon inclusion (Figure 5b)[51]. Therefore, we expected to find the canonical motif to be enriched at either location according to the type of alternative splicing events. We screened for all possible pentameric motifs in the 150 nt intronic region directly flanking alternatively spliced cassette exons, accounting for their occurrence in three distinct categories: significantly spliced-in (inclusion), significantly skipped (repression), and unregulated exons (background). To mitigate bias from motifs with higher genome-wide occurrence, we adjusted motif counts of significant splicing events by subtracting background counts and subsequently converted these to z-scores (see Methods).

As expected, the canonical RBFOX motif was enriched downstream of included exons and upstream of repressed exons (Figure 5a). The motif GCAUG was associated with the strongest enrichment, both for upstream binding & exon repression (z-score: 6.8) and downstream binding & exon inclusion (z-score: 9.4). Moreover, shifted motifs such as UGCAU and CAUGC were also enriched and had a high correlation with GCAUG ($r > 0.8$; Supplementary Figure S6). Subsequently, we analyzed the position of the canonical GCAUG for exon inclusion and repression events (Figure 5c). We discovered motifs that promote exon skipping, located both within ~100 nt upstream of the alternatively spliced exon and on the exon itself. Exon inclusion was related to GCAUG occurrence within ~150 nt downstream of the exon. These findings are in line with previous reports on the position-dependent splicing activity of RBFOX2[52,53].

However, we found additional motifs known to be bound by other splicing factors. For instance, UGCUU (z-score 4.9, downstream & exon inclusion) is the preferred motif of muscleblind-like splicing regulator 1 (MBNL1). MBNL1 and RBFOX2 have been found to act synergistically in pluripotent stem cell differentiation[54] and mesenchymal-specific splicing[55]. The relative abundance of MBNL1's motif UGCUU around alternatively spliced exons was only weakly correlated with the abundance of the GCAUG motif (r=0.27), therefore both motifs were likely not in close proximity to each other (Supplementary Figure S6).

Surprisingly, we also detected highly enriched poly CU-motifs upstream of included exons, although these are not primary binding sites for RBFOX2. The PTB proteins are known to preferentially bind to these polypyrimidine-rich intronic sequences[56] and to initiate exon exclusion upon binding[57]. Interestingly, these PTBP motifs were enriched upstream of significantly included exons in our data.

To differentiate motifs that are merely abundant around RBFOX2-regulated exons, we analyzed publicly available RBP-RNA interaction data (iClip)[52]. Most of the enriched motifs around alternatively spliced exons upon *Rbfox2*-OE were also confirmed to be bound by RBFOX2 in the iClip data (Figure 5d), specifically the known canonical RBFOX motifs showed high positive z-scores for both data sets. Overall, there was a high correlation between the abundance of motifs around alternatively spliced exons and their presence in iClip peaks (Figure 5e).

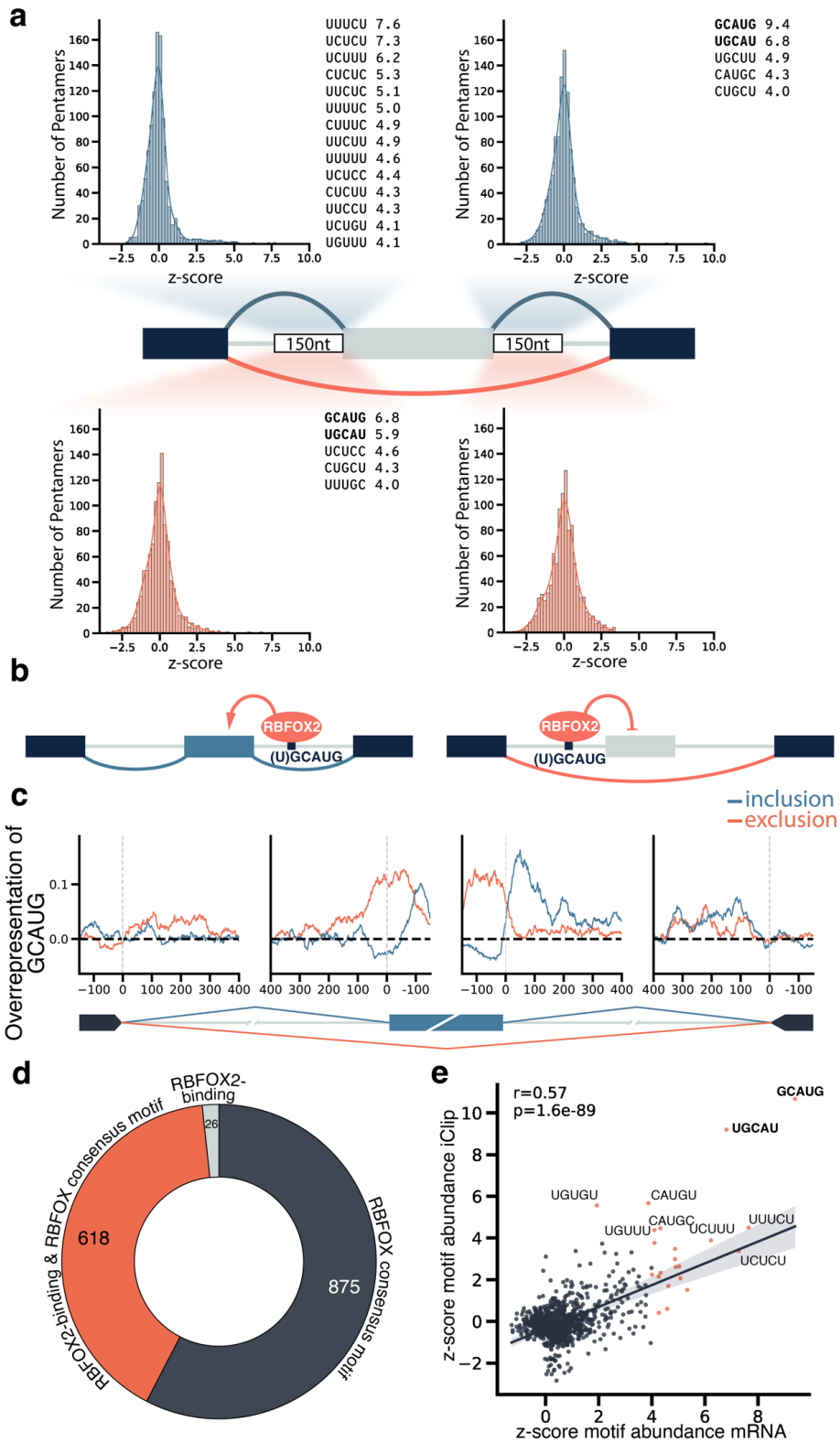

*Figure 5 RBFOX2 binding motifs are enriched in the vicinity of alternatively spliced exons. a) Histogram with the frequency of enriched pentameric motifs around alternatively spliced exons in Rbfox2 overexpression (OE) samples versus control. Blue color denotes motifs associated with exon inclusion, while orange represents motifs linked to exon skipping. Known RBFOX2 motifs are indicated with bold font b) Schematic representation of the position-dependent splicing of skipping exons by RBFOX2. c) Relative abundance of the RBFOX2-motif GCAUG in the vicinity of alternatively spliced exons and their flanking exons d) Analysis of alternatively spliced cassette exons reveals that 96% either host an RBFOX motif in the flanking intronic sequence or are bound by RBFOX, as confirmed by iClip data[52]. e) Correlation for the position-dependent prevalence of motifs enriched upstream or downstream of alternatively spliced exons in Rbfox2-OE vs. control comparison and in iClip data[52]. Motifs with high correlation are likely recognized by the same splicing factor.*

## RBFOX2 and PTBP antagonistically shape the transition from NPCs to neurons

The occurrence of the PTBP motifs upstream of significantly spliced-in exons upon *Rbfox2* overexpression hints at antagonistic splicing activities of RBFOX2 and PTBP (Figure 6a). Previous studies have indicated that PTBPs bind to pyrimidine-rich sequences located approximately up to 100 nt upstream of alternatively spliced exons[9,53]. Accordingly, we observed a prominent UCUCU peak in the ~100 nt intronic sequences upstream of exon inclusion events (Figure 6b). Notably, in experiments involving human brain tissue, cell lines, and the mouse cerebral cortex, the upstream occurrence of the PTBP motif was robustly correlated with exon inclusion events. In contrast, in other tissue types, the upstream enrichment of the PTBP motif was associated with exon-skipping[8,53].

These results raise the question of why a potential upstream PTBP binding leads to exon inclusion rather than the expected exclusion in cells of the nervous system.

We thus hypothesized that simultaneous downstream binding of RBFOX2 might antagonistically overrule the splicing outcome of PTBP and therefore favor exon inclusion. This process could contribute to guiding the transition from immature to mature neuronal splicing. Moreover, PTBP1 and PTBP2 are among the high-confidence protein interaction partners of RBFOX2 (Figure 6c). To investigate whether PTBP and RBFOX2 have antagonistic splicing targets, we first examined all significant cassette exon inclusion events (FDR < 0.01, ΔPSI > 0.1) for the co-occurrence of RBFOX and PTBP motifs. We screened for PTBP-motifs upstream and RBFOX-motifs downstream of alternatively spliced exons and for direct RNA-protein binding sites by reanalyzing iClip data from Vuong et al. for PTBP1[40] and PTBP2[40] and Jangi et al. for RBFOX2[52]. Roughly 45% of the significant inclusion events (320) had the combination of RBFOX-motif downstream with a PTBP-motif upstream, the majority of these were also highly conserved (Supplementary Figure S7). The cassette exons that were significantly included rarely contained only an RBFOX motif (3) or its binding site (0). The majority of included exons, making up 77.48% (547) of the alternatively spliced exons, harbored either a downstream RBFOX-motif and/or an RBFOX-binding site and simultaneously an upstream PTBP-motif or a PTBP-binding site (Figure 6d). While previous studies have indeed highlighted an interaction between RBFOX and PTBP1 specifically[8,58–61], the co-regulation of these RBPs may be less relevant in the context of neurodevelopment, as PTBP1 is primarily expressed in non-neuronal cells[17]. Thus, we only focused on PTBP2 in our further analyses.

To corroborate the RBFOX2/PTBP2 antagonistic splicing regulation of cassette exons, we re-analyzed wildtype and *Ptbp2*-KO data of P1 mouse neocortices[40]. We detected 707 significantly alternatively spliced exons in *Ptbp2*-KO (429 included, 187 excluded), with 128 events shared with *Rbfox2*-OE. This represented a 5.241-fold enrichment compared to the expected overlap ($p < 0.0001$, Supplementary Figure 8a). Given the

434 proposed antagonistic relationship between both RBPs, we expected *Ptbp2* knockout
435 to induce similar splicing changes as *Rbfox2* overexpression. Indeed, the majority of
436 shared target exons were spliced in the same direction (85.2%, Supplementary Figure
437 8c). Furthermore, we observed a moderate positive correlation between exon inclusion
438 levels in *Ptbp2*-KO and *Rbfox2*-OE samples ($R = 0.2993$, $p < 0.001$, Supplementary
439 Figure 8b). To further investigate the neurodevelopmental relevance of antagonistic
440 splicing, we analyzed the splicing pattern in our data of 230 PTBP2-repressed exons
441 that were reported to be relevant specifically in the context of neocortical
442 development[40]. *Rbfox2*-OE induced alternative splicing in 67 of these PTBP2 targets.
443 Importantly, the majority of the 67 significant events showed exon inclusion (55) and
444 not exon repression in the *Rbfox2*-OE group (Figure 6e, Supplementary Data 5).
445 Among the antagonistically spliced genes was *Ncam1,* encoding for a cell adhesion
446 protein*,* that showed an abnormal early exon inclusion (FDR < 0.0001, ΔPSI = 0.148)
447 in the *Rbfox2*-OE condition which led to an increased presence of the exon18
448 (chr9:49,418,152-49,418,953, Supplementary Figure S5c) producing the NCAM-180
449 isoform. Interestingly, the production of alternative isoforms of NCAM occurs during
450 cortical development between E16.5 and P0. In contrast, NCAM140 and NCAM180
451 are the predominant isoforms for neurons, unlike NPCs that express NCAM120 and
452 NCAM140[62].
453 Another PTBP2-excluded[40] and RBFOX2-included cassette exon event was identified
454 in *Kif21b* (chr1:136,101,209-136,101,389, Supplementary Figure S5d). KIF21B is an
455 important regulator of microtubule dynamics. The overexpression of *Rbfox2* induced a
456 highly significant inclusion event (FDR < 0.0001, ΔPSI = 0.305).

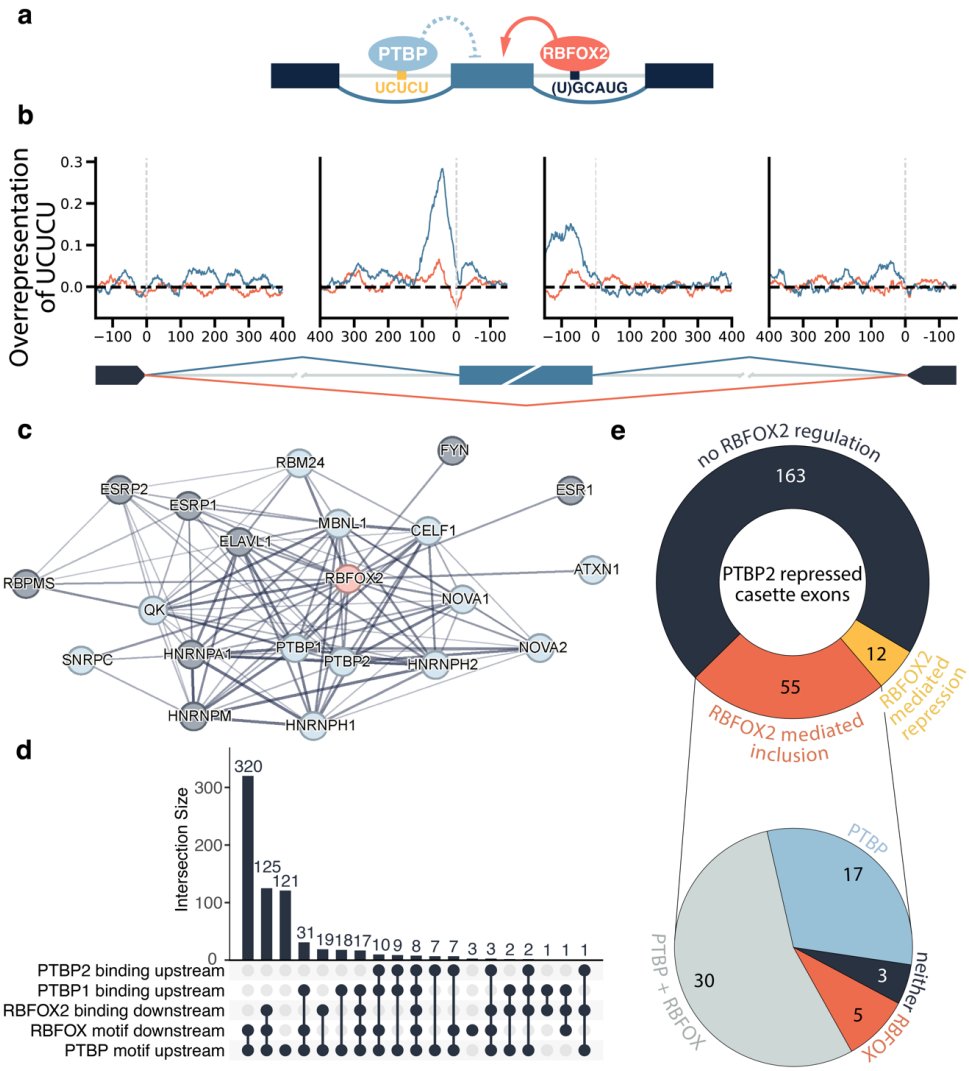


*Figure 6 RBFOX and PTBP regulate common targets a) Schematic representation of antagonistic splicing regulation between RBFOX2 and PTBP b) Relative abundance of the PTBP motif UCUCU in the vicinity of alternatively spliced exons in Rbfox2-OE vs. control and their flanking exons. Blue lines indicate exon inclusion and red lines correspond to exon skipping events c) StringDB protein-protein interaction network showing RBFOX2 (orange) and its interaction partners. High-confidence partners are highlighted in light blue d) UpSet plot showing the overlap of the presence of RBFOX or PTBP motifs in the flanking intronic sequences of alternatively spliced cassette exons (400 nt) as well as direct RBFOX2 and PTBP2 binding interactions as indicated by the presence of peaks obtained from iClip data[40,52] e) Analysis of developmentally regulated cassette exons suppressed by PTBP2 and the overlap with significantly alternatively spliced exons upon Rbfox2-OE. The donut-shaped circle represents 230 neurodevelopmentally relevant PTBP2-repressed cassette exon events[40]. Colors indicate regulation of these exons upon Rbfox2-OE, blue: unregulated, orange: inclusion, yellow: repression. The lower circle summarizes the presence of conserved binding motifs for RBFOX2 and/or PTBP2 for the exons that are regulated in opposite direction by PTBP2 (repression) and RBFOX2 (inclusion).*

Furthermore, exonN (chrX:73,284,421-73,284,478) of the *Flna* transcript was significantly included (FDR < 0.05, ΔPSI = 0.213) upon *Rbfox2*-OE (Supplementary Figure S5e). ExonN was specifically repressed in NPCs and included in neurons (FDR < 0.0001, ΔPSI = 0.4) and the exon inclusion was strongly elevated from E14.5 to E16.5 (FDR < 0.0001, ΔPSI = 0.4205). The iClip[40,52] data also confirmed protein

binding for RBFOX2, PTBP1, and PTBP2 in flanking sequences of exonN. *Flna* is an important regulator of neuronal migration[63] and its splicing by PTBP1 in NPCs is associated with shaping the NPC-to-neuron transition during cortical development[8,40]. Taken together, our data strongly suggest that RBFOX2 and PTBP2 have antagonistic roles in controlling alternative splicing, specifically affecting transcripts implicated in neuronal differentiation during cortical development. We identified that a significant portion of alternatively spliced cassette exons are excluded upon PTBP2- but included upon RBFOX2-binding in this developmental context.

## miR-92a-3p regulates the expression of *Rbfox2*

As we ascertained, NPCs exhibit substantially different splicing patterns compared to neurons (Supplementary Figure S2)[8,43]. Since RBFOX and PTB proteins seemingly regulated antagonistically an overlapping set of developmentally relevant splice targets, we hypothesized that a cell-type, spatially divergent, and time-specific expression of these splice factors would be necessary for normal cortical development. Indeed, *Ptbp1* and *Ptbp2* transcription peaked at E14.5, but contrary to *Ptbp2,* the *Ptbp1* mRNA abundance decreased in the following developmental stages (Figure 7a, right box). Moreover, *Ptbp1* expression is decreased significantly during the transition from NPCs to neurons (Figure 7a, left box) in accordance with previous reports[40,56,64]. *Ptbp1* repression is mediated via miR-124-3p, which is a highly specific neuronal miRNA (Figure 7c)[17,65]. Furthermore, miR-124-3p becomes significantly up-regulated in the transition between E14 and E17 of cortical development (Figure 7c)[65].

In contrast to *Ptbp1* and *Ptbp2*, *Rbfox2* expression was nearly absent in NPCs and increased significantly in neurons (Figure 1a-b, Figure 7a). In a previous study, we identified 36 miRNAs that were expressed in the embryonic cerebral cortex and predicted to target the 3' untranslated region (3' UTR) of *Rbfox2.* By further inspecting these miRNAs, we observed that most of them were upregulated at E14 followed by a significant reduction of expression levels at the subsequent developmental stages E17 and P0 (Supplementary Figure S9)[65]. This prompted us to hypothesize that miRNAs might mediate the low expression levels of *Rbfox2* in NPCs. Specifically, miR-92a-3p was identified as a hub microRNA at E14 during cortical development[65] and it has a predicted binding site in the 3' UTR of *Rbfox2.* Furthermore, the expression of miR-92a-3p was higher in NPCs compared to neurons and decreased gradually from E14 to P0 (Figure 7c). Together this data suggests that miRNA-92a-3p might contribute to silencing *Rbfox2* in NPCs at early developmental stages.

To follow up on this hypothesis, we performed a luciferase assay using a fragment of the 3' UTR of *Rbfox2* which contained the miR-92a-3p binding site downstream of the *Renilla* luciferase gene. Co-transfection of this reporter plasmid into HEK293 cells together with a miR-92a-3p mimic or a control revealed a reduced luciferase activity of more than two-fold in cells transfected with miR-92a-3p compared to the control. This finding confirmed the gene silencing effect of miR-92a-3p on *Rbfox2* ($p < 0.01$, Figure 7d). To investigate the mir-92a-3p-mediated suppression of *Rbfox2 in vivo,* we electroplated mouse embryos at E14.5 with a miR-92a-3p-silencing construct. Expression of miR-92a-3p was reduced more than 10-fold compared to control samples ($p < 0.0001$, Figure 7e). Following miR-92a-3p reduction, we observed a significantly increased *Rbfox2* expression at E16.5 in the miR-92a knock-down samples compared to the control ($p < 0.01$, fold change = 1.571; Figure 7e). To further corroborate these results, we overexpressed miR-92a-3p in an N2A cell culture. This resulted in a significant increase of miR-92a-3p abundance, as measured by RT-qPCR

($p < 0.05$, fold change = 2.442; Figure 7f). Importantly, both the mRNA expression ($p < 0.05$, fold change = 0.748 relative to control; Figure 7f) and the protein levels of RBFOX2 ($p < 0.05$, fold change = 0.707 relative to control; Figure 7g,h) were reduced significantly upon miR-92a-3p-overexpression.

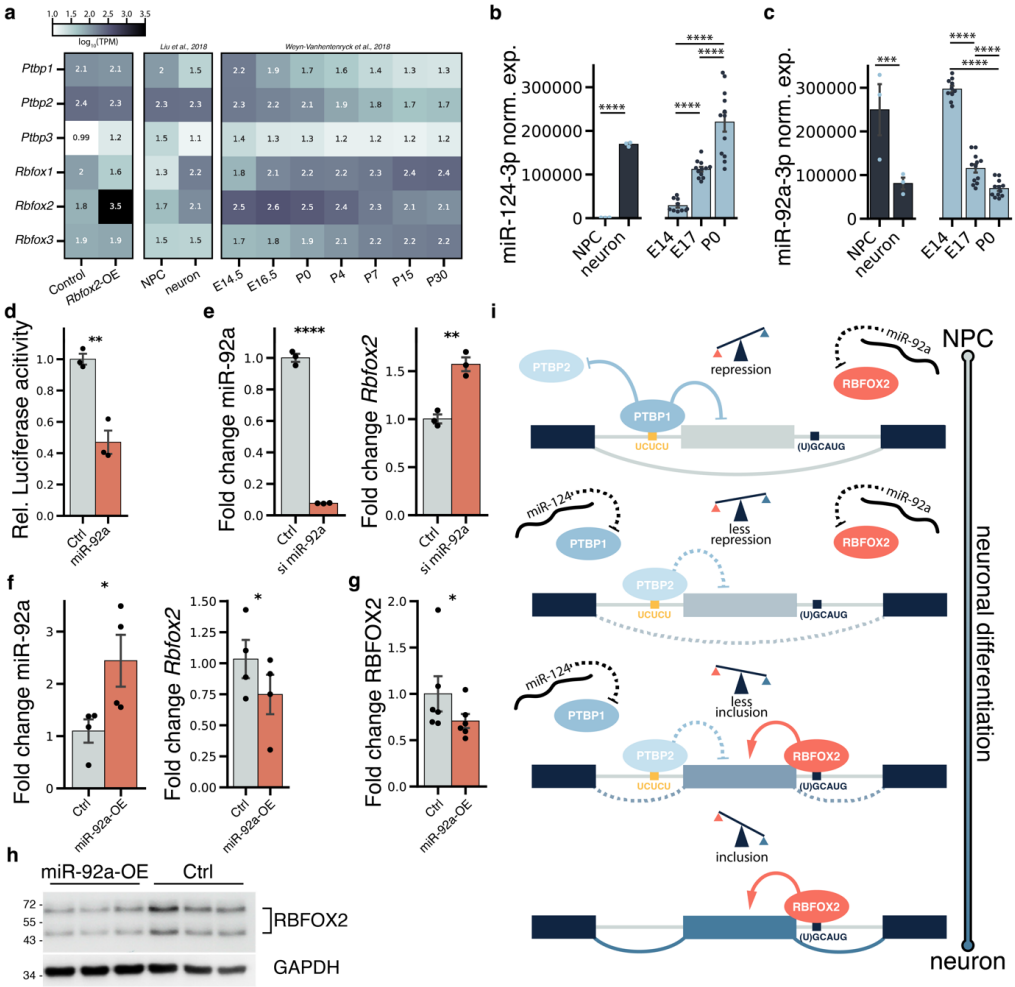


*Figure 7 a) Heatmap showing the gene expression of the RBFOX and PTBP protein families in our study, as well as in NPCs and neurons from Liu et al. [43] and E14.5 to P30 cortical samples obtained from Weyn-Vanhentenryck et al.[34].Values correspond to log10-transformed transcripts per million (TPM). b) Expression of mir-124-3p known to repress Ptbp1 c) Expression of mir-92a-3p predicted to target Rbfox2. Data on miRNA expression shown in b and c were obtained from Todorov et al.[65]d) Luciferase activity in lysates of HEK293 cells transfected with plasmids containing 3' UTR fragments of Rbfox2 and miR-92a. Fold change of luciferase activity was obtained by calculating the ratio of Renilla luciferase and firefly luciferase activity and then normalizing to the mean of the control. e) In vivo knock-down of miR-92a resulted in a more than 10-fold reduction in miR-92a-3p abundance (left side), and subsequently, Rbfox2 was 1.5-fold enriched (right side). f) Overexpression of miR-92a-3p in N2A cells led to >2-fold enrichment of miR-92a-3p (left side) and subsequently to a decreased abundance of Rbfox2 (right side), as measured by RT-qPCR. h) Overexpression of mir-92a-3p in N2A cells reduced the RBFOX2 protein level significantly. g) Representative image of the western blot for miR-92a overexpression in N2A cells. h) Schematic representation of the proposed splicing mechanism for the transition of immature NPC to mature neurons. Data are shown as mean ± standard error of the mean. *p<0.05, ** p<0.01, *** p<0.001, ****p<0.0001, Wald z-test from DESeq2 in b,c; paired t-test or paired Wilcoxon test in d-g.*

## Discussion

RBFOX2 is a crucial component of the complex regulatory network that orchestrates cerebral cortical development. We revealed that misexpression leads to a global disruption of the alternative splicing landscape with a significant overrepresentation of high-confidence NDD risk genes. Consequently, aberrant RBFOX2 splicing activities could produce target gene isoforms that lead to impaired brain development and disorders of the central nervous system in humans[66,67]. For instance, a mutation in *RBFOX2* has been detected previously in a patient with hypoplastic left heart syndrome and NDD[21]. Surprisingly, however, limited research has been conducted on the clinical significance of RBFOX2 as most studies focus on RBFOX1. Mutations in *Rbfox1* have been consistently linked with autism spectrum disorder[68–71] and susceptibility to epilepsy[72–74]. Interestingly, *Rbfox1* knock-out resulted in higher seizure susceptibility[75], whereas overexpression was also linked with epilepsy and cortex malformation[76]. Furthermore, reduced cytoplasmic RBFOX1 levels in the prefrontal cortex of individuals with schizophrenia[24] decrease the stability of *Vamp1*, a schizophrenia-associated gene, in $PV^+$ interneurons[25]. This reduction impairs inhibitory drive from $PV^+$ interneurons, contributing to schizophrenia pathogenesis[77].

Though RBFOX1 and RBFOX2 have largely overlapping alternative splicing targets[49], the divergent expression patterns we observed here and in previous research indicate that both proteins have common but also distinct functions[23,75,78,79]. To disentangle the specific role of RBFOX2 in the developing brain, we employed an overexpression model instead of a knock-down strategy, as the members of the RBFOX family can compensate for the absence of one of their paralogues[23]. Interestingly, early *Rbfox2*-OE caused a premature detachment and migration of neural cells to the IIZ but not further (Figure 4a). This was accompanied by significant splicing events in key components of the Reelin pathway[44,45] , which plays a crucial role in the migration and localization of cortical neurons and Purkinje cells in the cerebellum. Gehman and colleagues previously showed that the Reelin-binding *Lrp8* gene was alternatively spliced upon *Rbfox2* knock-out. Consequently, Purkinje cells failed to detach and therefore remained near their origin in the VZ[23]. Together with our results, this indicates an important role of RBFOX2 in the initiation and control of cell migration in different parts of the developing nervous system.

Apart from the altered migration, we also observed impaired neuronal differentiation of *Rbfox2*-overexpressing cells (Figure 4b-d). RBFOX2 was specifically upregulated in the transition from NPCs to newly differentiated neurons (Figure 1e), highlighting its role in neural differentiation. Accordingly, we detected a strong alternative splicing pattern in *Numb* which is a key player in asymmetrical neural stem cell division, determining the cell fate of progenitor cells and neurons[80]. Different isoforms of *Numb* can either promote neuronal differentiation or enhance cell proliferation[81], giving a possible explanation for the observed phenotype of decreased neuronal differentiation in our study.

Interestingly, *Rbfox2* expression negatively correlates with expression patterns of the PTBP family. In particular, PTBP1 is a key regulator of non-neuronal splicing in progenitor cells and its repression is required to induce the transition to neurons[17]. In contrast, PTBP2, which is reported to be a weaker repressor of alternatively spliced exons than PTBP1[57,82], is down-regulated by PTBP1 via poison exon inclusion leading to nonsense-mediated decay[17,52,64,83]. Remarkably, our data provided compelling evidence for an antagonistic splicing relationship between RBFOX2 and PTBP2.

595 Specifically, RBFOX2 and PTBP2 shared a set of targets that undergo alternative
596 splicing during cerebral cortical development (Figure 6d, e). Although PTBP2 typically
597 promotes the exclusion of these antagonistically spliced exons, RBFOX2 induced the
598 opposite effect of exon inclusion. Therefore, the premature overexpression in our
599 experimental set-up likely led to RBFOX2 overruling the splicing program of PTBP2
600 which could explain the aberrant cellular phenotype and altered splicing landscape we
601 observed. Indeed, several targets that are spliced antagonistically between RBFOX2
602 and PTBP2 play crucial roles, for example, in regulating neuronal differentiation
603 (*Flna*)[8], neurite outgrowth (*Ncam1*), and microtubule dynamics (*Kif21b*). Furthermore,
604 PTBP-recognized motifs are reportedly enriched upstream of alternatively spliced
605 exons that show high inclusion levels in the brain, heart, and skeletal muscles[53]. These
606 tissues are known expression sites of RBFOX2[84] with a concurrent low expression of
607 PTBP1[53]. Therefore, our results and existing reports highlight a complex antagonistic
608 interplay between these proteins in regulating neuronal differentiation[4,8]. Supporting
609 the concept of such dose-sensitive antagonistic interactions among RNA-binding
610 proteins, Ellis and colleagues recently reported that even a modest increase in RBFOX
611 expression levels was sufficient to alter splicing events dependent on another RBP,
612 MBNL1[85]. Furthermore, RBFOX-concentration-dependent splicing regulation has been
613 described in relation to binding to secondary motifs. Accordingly, high RBFOX2 protein
614 levels during neuronal differentiation can mediate exon inclusion through binding to
615 low-affinity motifs[86]. These findings illustrate how nuanced temporal and spatial RBP
616 expression levels enable cell- and developmental-stage specific gene regulation during
617 brain development.
618 Indeed, several post-transcriptional regulatory mechanisms controlling RBFOX levels
619 have been reported already. For instance, snoRNAs can act as sequestering sites for
620 excess RBFOX2 proteins[78]. Furthermore, RBFOX3 can splice poison exons into
621 *Rbfox2* leading to NMD[87]. Another potential layer of regulation is a putative *Rbfox1*-
622 and *Rbfox2*-specific feedback loop. Accordingly, we observed significantly reduced
623 levels of *Rbfox1* following the overexpression of *Rbfox2* (Figure 2g). Similarly, a knock-
624 out of *Rbfox1* was previously reported to lead to an increased level of RBFOX2[75] and
625 vice versa[23]. Furthermore, both RBFOX1 and RBFOX2 contain RBFOX binding sites
626 near a highly conserved 93-nucleotide exon encoding the second half of the RRM.
627 RBFOX binding leads to exon skipping, thereby resulting in a *Rbfox*ΔRRM isoform with
628 significantly reduced RNA binding affinity[88]. In line with this, the *Rbfox2* overexpression
629 in early-stage cortical cells in our study did not result in a complete splicing switch with
630 all regulated exons being either fully spliced in or spliced out.
631 miRNA binding to 3' UTRs represents another key post-transcriptional regulatory
632 mechanism for controlling gene expression and protein levels. In a study investigating
633 the expression patterns of miRNAs in the embryonic cerebral cortex, we recently
634 highlighted targeting of RNA binding proteins as one of the major processes through
635 which miRNAs impact brain development[65]. Similarly to the reported silencing of *Ptbp1*
636 in neurons via miR-124-3p[17], here we showed for the first time that the NPC hub
637 miRNA 92a-3p suppresses the expression of *Rbfox2* (Figure 7f-h). Conversely,
638 silencing miR-92a-3p in the embryonic neocortex led to a significant *Rbfox2*
639 upregulation (Figure 7e, i). In accordance with our results, miR-92a-3p was previously
640 reported to be enriched in intermediate progenitor cells in humans[89,90] and,
641 interestingly, differentially expressed in neurodevelopmental and mental disorders. For
642 instance, levels were elevated in blood[91] and serum[92] of patients with schizophrenia.
643 In contrast, miR-92a-3p was reported to be downregulated in individuals with

autism[93,94]. Given the overlapping splicing targets between RBFOX2 and its paralogue RBFOX1, whose mutations have been consistently implicated in such disorders, disruption of the miR-92a-3p/RBFOX2 axis represents an intriguing mechanism for the emergence of diseases of the central nervous system as well as a potential therapeutic target. In particular, future research should focus on elucidating the link between altered miR-92a-3p expression levels and aberrant splicing activities that contribute to disease pathogenesis.

Collectively, our results underscore the crucial role of RBFOX2 in the developing cerebral cortex and shed light on the complex interplay with the PTBP family. In our proposed model (Figure 7b), a miRNA-mediated gradual shift from high PTBP levels to a subsequent up-regulation of RBFOX2 shapes neuronal differentiation through a progressive splicing switch from exon exclusion to exon inclusion in commonly regulated targets.

## Methods

### Animals

Hes5::GFP mice have been described previously[95]**.** For *in utero* electroporation, timed mated c57BL6/JRj female mice were purchased on gestation day 12 from Janvier (Janvier Labs, Le Genest-Saint-Isle, France), a certified international breeder. Mice were housed in type II long filter top cages (Tecniplast, Buguggiate, Italy) and kept in a 12 h light/dark cycle in a temperature and humidity-controlled animal room (22 ± 2°C, 55 ± 5%). Water and food (ssniff M-Z Extrudat, ssniff, Soest, Germany) were supplied *ad libitum*. Mice were treated according to the protocols approved by the local authorities (Landesuntersuchungsamt Rheinland-Pfalz, license number 23 177-07/G 13-1-089).

### Constructs

HA-tagged full-length *Rbfox2* was cloned into the XhoI and BglII sites of the pCAGGS-mCherry vector using the following primer combinations: *Rbfox2* 1A full-length forward 5′-actgctcgaggccaccatgtacccatacgatgttccagattacgctgcggaaggcggccaggcg-3′, with *Rbfox2* reverse 5′-actgagatcttcacgtcacttcagtagg-3′. The miR-92a pre-miRNA including approximately 150 bp of flanking genomic sequence was cloned into the BamHI and EcoRI sites of the pcDNA3.1+ vector using the following primer combinations: miR-92 forward 5′-agtcggatcctttagcgttggaaagtggcc-3′ with miR-92a reverse 5′-agtcgaattctaagttgaggtgtgggtggg-3′. A fragment of the *Rbfox2* 3'UTR containing the miR-92a binding site was cloned into the XbaI site of the pGL3P vector using the following 5'-end phosphorylated oligonucleotides: Sense [Phos] 5′-CTAGACCCCAGTTCATGAGGCCTGGCTATTGCAATATTTACTAGTAGAGGACTC TATAGCT-3′, Antisense [Phos] 5′-CTAGAGCTATAGAGTCCTCTACTAGTAAAT ATTGCAATAGCCAGGCCTCATGAACTGGGGT-3′. Sense and Antisense oligos were annealed in annealing buffer (10mM Tris-HCL; pH 7.5; 0.1 M NaCl; 1 mM EDTA) and cloned into the XbaI site of the pGL3P vector.

### Cell Culture, transfections, and luciferase assays

N2A and HEK293 cells were cultured in Dulbecco´s Modified Eagle Medium (DMEM) with 10% fetal bovine serum as well as 1% Penicillin/Streptomycin. For Luciferase assays, HEK293 cells were seeded on 12-well plates at a density of 90,000 cells per well. Twenty-four hours later, the cells were transfected with 400 ng of the constructs

cloned into the pGL3P vector, 600 ng miRNA construct and 10 ng pRL-TK vector using the calcium phosphate method. After 48 hours, cells were lysed, and luciferase activity was measured with a CentroXS LB 960 luminometer (Berthold Technologies). N2A cells were transfected with Transfectin reagent (Biorad). The day before the experiment. For transfection, N2A cells were seeded at a density of 250,000 cells per well on 6-well plates. Twenty-four hours later, the cells were transfected with 4000 ng miRNA construct per well. The cells were lysed and processed for RT-qPCR and Westernblot analysis 48 hours after transfection.

## RT-qPCR and Western blot

Small RNAs were isolated using the miRNeasy Kit (Qiagen), and total RNA was isolated using the High Pure RNA isolation kit (Roche). TaqMan MicroRNA Assays (Applied Biosystems) were used for miRNA RT-qPCR experiments. The miRNA quantities are relative to U6 snRNA. Total RNA was reverse transcribed using the RevertAid First Strand cDNA Synthesis Kit (Fermentas, Sankt Leon Rot, Germany). For qPCR, SYBR Green Mix was used (TB Green Premix Ex Taq II (RR82WR, Takara)).

For Western blot analysis, the cells were lysed, and the proteins were resolved by electrophoresis on SDS acrylamide gels. After transferring the proteins to PVDF membranes, Western blot analyses were performed with antibodies specific for RBFOX2 (rabbit-Anti Rbm9; Bethyl Laboratories) and GAPDH (mouse-Anti GAPDH ab8245, Abcam). Quantification of the bands was performed with ImageJ and normalized to GAPDH band intensity.

## *In utero* Electroporation

For *in utero* electroporation, embryonic day E13.5 pregnant female mice were deeply anesthetized with isoflurane, and the uterine horns were exposed. For overexpression, control or *Rbfox2* expression vectors (4 $\mu$g/$\mu$l) were injected with either pCAG-mCherry or pCAG-eGFP (0.5 $\mu$g/$\mu$l) into the lateral ventricle of each embryo. For electroporation 5 pulses of 40 V for a pulse length of 50 ms at 950-ms intervals were applied (Nepagene, Japan). Subsequently, the uterine horns were returned to the abdominal cavity. After 48 h, the mice were sacrificed by cervical dislocation. The embryos were collected and sacrificed by decapitation. For immunostaining experiments, the brains were isolated, fixed in 4% paraformaldehyde, cryoprotected in 15% and 30% Sucrose solutions, embedded in Cryomatrix (Thermo Scientific), and cryosectioned into 20 $\mu$m-thick brain slices.

For RNA-sequencing, the brain's GFP$^+$ area was dissected and digested with trypsin. After stopping the digestion by adding 20% FBS in DMEM and washing with PBS, cells were resuspended in PBS and passed through a 100 $\mu$m filter to achieve a single-cell suspension. GFP$^+$ cells were then collected by fluorescent activated cell sorting (FACS).

## Immunostaining and Imaging

For immunostaining, brain cryosections were fixed in 4% paraformaldehyde (PFA) at room temperature (RT) for 10 minutes. After two washes with PBS, antigen retrieval was performed by incubating the slides in 10 mM sodium citrate with 0.5% Tween-20, pH 6, at 80°C for 20 minutes. Subsequently, the sections were blocked in PBS with

0.2% Tx-100 containing 2% sheep serum. The sections were then incubated with primary antibody (rabbit anti-RBM9 (Bethyl), mouse anti-RBFOX1 (MABE985, Merck/Millipore, Burlington, MA, USA), rabbit anti-beta III Tubulin (ab18207, Abcam), rabbit Anti-PAX6 (901301, Biolegends), chicken Anti TBR2 (ab34735, Millipore), rabbit Anti-SATB2 (ab34735, Abcam)) in blocking solution overnight at 4°C. The sections were washed three times in PBS 0.2% Tx-100 and incubated in blocking solution containing Alexa-488- or Alexa-594-conjugated secondary antibody (Invitrogen) for 3 hours at RT. After three washes in PBS, the sections were embedded in Fluoromount-G with DAPI (00-4959-52, Invitrogen).
The sections were viewed using a laser-scanning confocal microscope (LSM710), and images were acquired with the zen software (Zeiss, Oberkochen, Germany). The images were analyzed, and the cells were counted using ImageJ software[96].

## RNA-sequencing

NGS library prep was performed with Clontech SMARTer Ultra Low Input RNA Kit for cDNA generation, followed by NuGEN Ovation Ultralow v2 System for library preparation. Libraries were profiled in a DNA 1000 chip on a 2100 Bioanalyzer (Agilent Technologies) and quantified using the Qubit dsDNA HS Assay Kit, in a Qubit 4.0 Fluorometer (Invitrogen by Thermo Fisher Scientific). All six samples were pooled in equimolar ratio and sequenced on an Illumina NextSeq 500/550 device.

## RNA-sequencing analysis

The paired-end reads were trimmed using BBDuk (version 39.01)[97]. The trimmed reads were mapped to the Gencode reference genome of Mus musculus mm39 (released 19.10.2022) using STAR (version 2.7.10b)[98] and the count per gene and sample was determined using FeatureCounts provided by SubRead (version 2.0.6)[99].
We used DESeq2 (version 1.40.1)[100] in R (version 4.3.0)[101] to analyze differentially expressed genes with default settings. Since *Rbfox2* was heavily overexpressed, it was removed from the volcano plot for improved visualization. Genes with an adjusted p-value (Benjamini-Hochberg method) $< 0.05$ were considered to be differentially expressed.
rMATS (version 4.1.2)[102] with default settings was used to detect alternatively spliced genes between the *Rbfox2*-OE and control samples. We did not include novel splice events in our analysis. A splicing event with a false discovery rate (FDR) adjusted p-value $< 0.01$ and an inclusion level difference $|\Delta PSI| > 0.1$ was considered significant. Data processing was done with numpy (version 1.23.5)[103] and pandas (version 2.0.1)[104] in Python (version 3.10.12)[105].
Plots were generated if not specified otherwise with Matplotlib (version 3.7.1)[106] and seaborn (version 0.12.2)[107].
The overlap between significantly alternatively spliced genes and significantly differentially expressed genes was visualized in an UpSet plot (version 0.9.0)[108] using Python (version 3.10.12)[105]. Sashimiplots were created using rmats2sashimiplot within a Docker container using the image xinglab/rmats2sashimiplot. Due to its MISO backend, PSI values may differ from rMATS results.

## Analysis of publicly available transcriptomic data sets

We re-analyzed two publicly available data sets to further characterize the alternative splicing landscape during cortical development. The study by Weyn-Vanhentenryck et

al. contains RNA-sequencing of the mouse cortex from nine-time points (E14.5, E16.5, P0, P4, P30, 4 months, and 21 months). Sequencing files were downloaded from the NCBI Short Read Archive, accession number SRP055008. The study by Liu et al. contains RNA-sequencing from NPCs and neurons purified from mouse cortices at E15.5, sequencing files were obtained from the Gene Expression Omnibus, accession number GSE96950. Furthermore, we re-analyzed transcriptomic data from *Ptbp2* knockout mouse cortices at P1, obtained from the Gene Expression Omnibus (accession number GSE84803)[40], and triple knockout (*Rbfox*1/2/3) mouse embryonic stem cells, retrieved from the Short Read Archive (accession number SRP128054)[32]. The sequencing data were processed according to the protocol specified under the section "RNA-sequencing analysis". The developmental data from Weyn-Vanhentenryck et al. did not allow a pairwise statistical test with rMATS, therefore we conducted a pairwise Fisher's exact test in scipy (version 1.10.1)[109] for consecutive time points and corrected p-values for multiple comparisons by using Benjamini Hochberg's procedure with scipy (version 1.10.1)[109]. An event was considered significantly developmentally alternatively spliced when two successive time points had an adjusted p-value < 0.01 and |ΔPSI| > 0.1.

We used a Monte Carlo simulation to statistically assess the overlap of alternative splicing events (cassette exons) between *Rbfox2*-OE and either t*Rbfox*-KO[32] or *Ptbp2*-KO[40] conditions (see Monte Carlo simulation for details).

### Analysis of publicly available iClip data sets

To validate which significant splicing events could be attributable to direct RBFOX2 binding, we re-analyzed publicly available iClip data for RBFOX2 expressed in V6.5 mESCs. The data was downloaded from NCBI Gene Expression Omnibus, accession number GSE54794[52]. This dataset was supplemented by iClip data for PTBP1 and PTBP2, downloaded from the NCBI short read archive, accession number SRP080878[40].

The iClip data was analyzed in several steps. First, we extracted the unique molecular identifiers from the reads using UMI tools (version 1.1.4)[110] and trimmed the adapters with BBDuk (version 39.01)[97]. The trimmed reads were aligned to the reference genome mm39 from Gencode (released 19.10.2022) using STAR (version 2.7.10b)[98]. Following the alignment, we removed PCR duplicates by leveraging the unique molecular identifiers with UMI tools. Crosslinking sites were identified as peaks using Clipper[111], which was run within a Docker container based on the image brianyee/clipper:61d5456.

### Inferring the alternative splicing trajectory during cortical development

We used the SplicePCA tool[42] integrating our data set with the developmental data of Weyn-Vanhentenryck et al.[4] and Liu et al.[29] to analyze the effect of *Rbfox2*-overexpression on the alternative splicing pattern compared to normal cortical development. We selected events that did not have missing data for any sample and were significantly alternatively spliced in our data and the publicly available data. To investigate how splicing events are correlated with the principal components, we then computed the loading matrix A

$$qA = V\sqrt{L}$$

where V is the matrix of eigenvectors, L is a diagonal matrix with the corresponding eigenvalues and loadings correspond to correlations between the principal components and the original variables[112].

For each principal component, we then performed a gene set enrichment analysis (GSEA) using the clusterProfiler package (version 4.8.1)[113,114] in R v4.3.0[101] with the biological process ontology, miGSSize of 100, maxGSSize of 500, and an adjusted p-value cut-off of 0.05. The loadings for each gene on the respective principal component were used as input for the GSEA.

Inferring the direction of exon inclusion

We leveraged the NPC and neuron RNA-sequencing data from Liu et al.[29] to assess whether Rbfox2-OE is related to a mature (neuronal) or immature (NPC-specific) splicing pattern. By intersecting our significant alternative splicing results with the Liu et al. data set[43], we assigned the *Rbfox2*-OE splicing events to three categories: 1) Neuronal direction when the exon inclusion level of the respective gene was significantly higher in neurons than in NPCs in the Liu et al. data; 2) NPC direction when the inclusion level was significantly lower in neurons than in NPC; 3) non-regulated, when the inclusion level was not significantly altered, or the splicing event was not detected in the Liu et al. data set[43]. The results of this analysis were visualized with a chord diagram using the circlize package (version 0.4.15)[115] in R v4.3.0[101].

Motif enrichment analysis

We performed a *de novo* motif enrichment analysis to identify enriched motifs in the intronic regions located upstream and downstream of alternatively spliced exons. The intronic sequences around alternatively spliced exons (enriched and suppressed exons separately) and a set of background sequences that were not alternatively spliced (FDR > 0.8 and |ΔPSI| < 0.1) were loaded from the mm39 reference genome (Gencode released 19.10.2022) using pysam (version 0.21)[116].
All possible pentameric sequences and their occurrence in the up- and downstream intronic sequences were counted in a sliding window of 50 nt. For each motif, we then subtracted its occurrence in the respective background sequences. Next, motif frequencies were transformed to z-scores using scipy (version 1.10.1)[109]. A motif was considered to be enriched when it had a z-score > 4 ($p < 0.0001$, two-sided z-test).
The iClip peaks were used to validate these predicted motifs. We again screened for the occurrence of every possible pentameric sequence within the peaks of RBFOX2 and the control, subsequently subtracted the respective values, and performed z-scoring. Next, the z-scores of the iClip and RNA-Sequencing motif enrichment analysis were correlated using scipy (version 1.10.1)[109].

Motif co-occurrence analysis

The co-occurrence of motifs was analyzed similarly to the motif enrichment analysis. 400 nt of intronic sequence flanking the alternatively spliced exon or the exon itself was loaded with pysam (version 0.21.0)[116] and screened for the presence of a PTBP-associated CU-rich motifs (UCUCU, UUUCU, UCUUU, CUCUC, UCUCC, CUCUU, UUCCU)[117] with a z-score > 4 upstream and RBFOX2 canonical motif downstream (GCAUG, UGCAU, CAUGC). Moreover, we integrated confirmed binding sites from the iClip data for RBFOX2[52], PTBP1[40], and PTBP2[40]. We visualized this using an UpSet plot (version 0.9.0)[108] using Python (version 3.10.12)[105]. and only included overlapping sets with a minimum size of 1.
Further, we examined evolutionarily conserved motif occurrences around these exons by filtering for motifs with a phastcons 35-way[118] score > 0.8.

884

885 Motif localization map

886 Next, we mapped the localization of the enriched motifs identified in the previous
887 analysis on the alternatively spliced exon and the flanking exons. To the end, we
888 computed the motif density in a sliding window of 50 bp for all up- and downregulated
889 events and background (non-regulated events). Motif density corresponds to the
890 fraction of the 50 nt sliding window that is covered by the motif. The estimates were
891 corrected by subtracting the background density for each motif. This analysis was
892 limited to 150 nt of exonic and 400 nt of intronic sequences spanning up- and
893 downstream from the intron/exon boundaries.

894

895 STRING network analysis

896 Potential interaction partners of RBFOX2 were identified with STRING using all
897 potential interaction sources (version 12.0 beta)[119] , allowing 20 interacting proteins
898 and showing confidence as edges. Interactions with RBFOX2 with a confidence score
899 higher than 0.7 were considered high-confidence.

900

901 Statistical analysis of immunohistochemistry data

902 Two groups were compared statistically using a t-test or a Wilcoxon test when
903 assumptions of the parametric test were violated, and a data transformation did not
904 improve the model fit. More than two groups were analyzed using one-way or two-way
905 analysis of variance followed by Tukey's post hoc test or post hoc comparison of model
906 means. Data were transformed using a $\log_e$ or an arcsine square root transformation
907 when assumptions of normality and homogeneity of variance were violated. All p-
908 values are two-tailed and a p-value $< 0.05$ was considered statistically significant.
909 Statistical analysis was performed using R v4.2.2[101] or Python (version 3.10.12)[105]
910 using scipy (version 1.10.1)[109].

911

912 Overlap of alternatively spliced genes with NDD risk genes

913 Alternatively spliced genes were intersected with high-confidence NDD genes from the
914 GeneTrek database v33[33] to calculate the observed overlap. To obtain a null
915 distribution of the expected overlap, 1317 genes (equal to the total number of
916 alternatively spliced genes upon *Rbfox2*-OE) were randomly sampled from the
917 universe of genes with annotated splice events and the overlap with high-confidence
918 NDD genes and the p-value computed (see Monte Carlo Simulation section for details).

919

920 Monte Carlo Simulation

921 Monte Carlo simulations were performed to evaluate the statistical significance of
922 overlaps for various splicing events and genes. In each simulation, a number of genes
923 equal to the observed count of alternatively splicing events (t*Rbfox*-KO and *Ptbp2*-KO)
924 or genes (NDD risk genes) were randomly sampled from the universe of genes or
925 splicing events. The overlap with the gene set of interest (e.g., high-confidence NDD
926 genes) was then calculated. This process was repeated 100,000 times using a seed
927 of 42 to generate a null distribution of expected overlaps. The p-value was calculated
928 as

$$p = 2 * (1 - CDF(zscore))$$

using Python (version 3.10.12)[105], numpy (version 1.23.5)[103], and scipy (version 1.10.1)[109]. CDF corresponds to the cumulative distribution function of the normal distribution.

## Data availability

The RNA Sequencing data generated for this study are available on NCBI SRA (Sequence Read Archive) under the accession number PRJNA1013323.

## References

1. Breschi, A., Gingeras, T. R. & Guigó, R. Comparative transcriptomics in human and mouse. *Nat Rev Genet* **18**, 425–440 (2017).
2. Yao, Z. *et al.* A taxonomy of transcriptomic cell types across the isocortex and hippocampal formation. *Cell* **184**, 3222-3241.e26 (2021).
3. Jiang, W. & Chen, L. Alternative splicing: Human disease and quantitative analysis from high-throughput sequencing. *Computational and Structural Biotechnology Journal* **19**, 183–195 (2021).
4. Weyn-Vanhentenryck, S. M. *et al.* Precise temporal regulation of alternative splicing during neural development. *Nat Commun* **9**, 2189 (2018).
5. Raj, B. & Blencowe, B. J. Alternative Splicing in the Mammalian Nervous System: Recent Insights into Mechanisms and Functional Roles. *Neuron* **87**, 14–27 (2015).
6. Barbosa-Morais, N. L. *et al.* The Evolutionary Landscape of Alternative Splicing in Vertebrate Species. *Science* **338**, 1587–1593 (2012).
7. Silbereis, J. C., Pochareddy, S., Zhu, Y., Li, M. & Sestan, N. The Cellular and Molecular Landscapes of the Developing Human Central Nervous System. *Neuron* **89**, 248–268 (2016).
8. Zhang, X. *et al.* Cell-Type-Specific Alternative Splicing Governs Cell Fate in the Developing Cerebral Cortex. *Cell* **166**, 1147-1162.e15 (2016).
9. Zhang, M. *et al.* Axonogenesis Is Coordinated by Neuron-Specific Alternative Splicing Programming and Splicing Regulator PTBP2. *Neuron* **101**, 690-706.e10 (2019).
10. Lin, Y.-S. *et al.* Neuronal Splicing Regulator RBFOX3 (NeuN) Regulates Adult Hippocampal Neurogenesis and Synaptogenesis. *PLOS ONE* (2016).
11. Heck, J. *et al.* More than a pore: How voltage-gated calcium channels act on different levels of neuronal communication regulation. *Channels* **15**, 322–338 (2021).
12. Furlanis, E., Traunmüller, L., Fucile, G. & Scheiffele, P. Landscape of ribosome-engaged transcript isoforms reveals extensive neuronal-cell-class-specific alternative splicing programs. *Nat Neurosci* **22**, 1709–1717 (2019).
13. Cai, Y., Yu, X., Hu, S. & Yu, J. A Brief Review on the Mechanisms of miRNA Regulation. *Genomics, Proteomics & Bioinformatics* **7**, 147–154 (2009).

14. Diederichs, S. & Haber, D. A. Dual Role for Argonautes in MicroRNA Processing and Posttranscriptional Regulation of MicroRNA Expression. *Cell* **131**, 1097–1108 (2007).
15. Lee, R. C., Feinbaum, R. L. & Ambros, V. The C. elegans heterochronic gene lin-4 encodes small RNAs with antisense complementarity to lin-14. *Cell* **75**, 843–854 (1993).
16. Cho, K. H. T., Xu, B., Blenkiron, C. & Fraser, M. Emerging Roles of miRNAs in Brain Development and Perinatal Brain Injury. *Frontiers in Physiology* **10**, (2019).
17. Makeyev, E. V., Zhang, J., Carrasco, M. A. & Maniatis, T. The MicroRNA miR-124 Promotes Neuronal Differentiation by Triggering Brain-Specific Alternative Pre-mRNA Splicing. *Mol Cell* **27**, 435–448 (2007).
18. Fisher, E. & Feng, J. RNA splicing regulators play critical roles in neurogenesis. *WIREs RNA* **13**, e1728 (2022).
19. Bhalla, K. *et al.* The de novo chromosome 16 translocations of two patients with abnormal phenotypes (mental retardation and epilepsy) disrupt the A2BP1 gene. *J Hum Genet* **49**, 308–311 (2004).
20. Sebat, J. *et al.* Strong Association of De Novo Copy Number Mutations with Autism. *Science* **316**, 445–449 (2007).
21. Homsy, J. *et al.* De novo mutations in congenital heart disease with neurodevelopmental and other congenital anomalies. *Science* **350**, 1262–1266 (2015).
22. Verma, S. K. *et al.* Rbfox2 function in RNA metabolism is impaired in hypoplastic left heart syndrome patient hearts. *Sci Rep* **6**, 30896 (2016).
23. Gehman, L. T. *et al.* The splicing regulator Rbfox2 is required for both cerebellar development and mature motor function. *Genes Dev.* **26**, 445–460 (2012).
24. O'Leary, A. *et al.* Behavioural and functional evidence revealing the role of RBFOX1 variation in multiple psychiatric disorders and traits. *Mol Psychiatry* **27**, 4464–4473 (2022).
25. Vuong, C. K. *et al.* Rbfox1 Regulates Synaptic Transmission through the Inhibitory Neuron-Specific vSNARE Vamp1. *Neuron* **98**, 127-141.e7 (2018).
26. Wamsley, B. *et al.* Rbfox1 Mediates Cell-type-Specific Splicing in Cortical Interneurons. *Neuron* **100**, 846-859.e7 (2018).
27. Zhang, C. *et al.* Defining the regulatory network of the tissue-specific splicing factors Fox-1 and Fox-2. *Genes Dev.* **22**, 2550–2563 (2008).
28. Choi, S. *et al.* Rbfox family proteins make the homo- and hetero-oligomeric complexes. *Biochemical and Biophysical Research Communications* **495**, 1022–1027 (2018).
29. Liu, J., Geng, A., Wu, X., Lin, R.-J. & Lu, Q. Alternative RNA Splicing Associated With Mammalian Neuronal Differentiation. *Cerebral Cortex* **28**, 2810–2816 (2018).
30. Mullen, R. J., Buck, C. R. & Smith, A. M. NeuN, a neuronal specific nuclear protein in vertebratesxs. *Development* **116**, 201–211 (1992).
31. Gehman, L. T. *et al.* The splicing regulator Rbfox2 is required for both cerebellar development and mature motor function. *Genes Dev.* **26**, 445–460 (2012).

32. Jacko, M. *et al.* Rbfox Splicing Factors Promote Neuronal Maturation and Axon Initial Segment Assembly. *Neuron* **97**, 853-868.e6 (2018).
33. Leblond, C. S. *et al.* Operative list of genes associated with autism and neurodevelopmental disorders based on database review. *Mol Cell Neurosci* **113**, 103623 (2021).
34. Weyn-Vanhentenryck, S. M. *et al.* Precise temporal regulation of alternative splicing during neural development. *Nat Commun* **9**, 2189 (2018).
35. Leek, J. T. *et al.* Tackling the widespread and critical impact of batch effects in high-throughput data. *Nat Rev Genet* **11**, 733–739 (2010).
36. Weißbach, S. *et al.* Reliability of genomic variants across different next-generation sequencing platforms and bioinformatic processing pipelines. *BMC Genomics* (2021).
37. Qin, Y. *et al.* A recurrent SHANK1 mutation implicated in autism spectrum disorder causes autistic-like core behaviors in mice via downregulation of mGluR1-IP3R1-calcium signaling. *Mol Psychiatry* **27**, 2985–2998 (2022).
38. Schob, C. *et al.* Cognitive impairment and autistic-like behaviour in SAPAP4-deficient mice. *Transl Psychiatry* **9**, 1–19 (2019).
39. Sanders, B. *et al.* Transcriptional programs regulating neuronal differentiation are disrupted in DLG2 knockout human embryonic stem cells and enriched for schizophrenia and related disorders risk variants. *Nat Commun* **13**, 27 (2022).
40. Vuong, J. K. *et al.* PTBP1 and PTBP2 Serve Both Specific and Redundant Functions in Neuronal Pre-mRNA Splicing. *Cell Reports* **17**, 2766–2775 (2016).
41. Dillon, G. M. *et al.* CLASP2 Links Reelin to the Cytoskeleton during Neocortical Development. *Neuron* **93**, 1344-1358.e5 (2017).
42. Weißbach, S. *et al.* Cortexa: a comprehensive resource for studying gene expression and alternative splicing in the murine brain. *BMC Bioinformatics* **25**, 293 (2024).
43. Liu, J., Geng, A., Wu, X., Lin, R.-J. & Lu, Q. Alternative RNA Splicing Associated With Mammalian Neuronal Differentiation. *Cerebral Cortex* **28**, 2810–2816 (2018).
44. Tissir, F. & Goffinet, A. M. Reelin and brain development. *Nat Rev Neurosci* **4**, 496–505 (2003).
45. Gallo, C. M., Ho, A. & Beffert, U. ApoER2: Functional Tuning Through Splicing. *Frontiers in Molecular Neuroscience* **13**, (2020).
46. Reddy, S. S., Connor, T. E., Weeber, E. J. & Rebeck, W. Similarities and differences in structure, expression, and functions of VLDLR and ApoER2. *Molecular Neurodegeneration* **6**, 30 (2011).
47. Yano, M., Hayakawa-Yano, Y., Mele, A. & Darnell, R. B. Nova2 Regulates Neuronal Migration through an RNA Switch in Disabled-1 Signaling. *Neuron* **66**, 848–858 (2010).
48. Saito, Y. *et al.* Differential NOVA2-Mediated Splicing in Excitatory and Inhibitory Neurons Regulates Cortical Development and Cerebellar Function: Neuron. *Neuron* **101**, 707-720.E5 (2019).

49. Weyn-Vanhentenryck, S. M. *et al.* HITS-CLIP and Integrative Modeling Define the Rbfox Splicing-Regulatory Network Linked to Brain Development and Autism. *Cell Reports* **6**, 1139–1152 (2014).
50. Yeo, G. W. *et al.* An RNA code for the FOX2 splicing regulator revealed by mapping RNA-protein interactions in stem cells. *Nat Struct Mol Biol* **16**, 130–137 (2009).
51. Zhang, C. *et al.* Defining the regulatory network of the tissue-specific splicing factors Fox-1 and Fox-2. *Genes Dev.* **22**, 2550–2563 (2008).
52. Jangi, M., Boutz, P. L., Paul, P. & Sharp, P. A. Rbfox2 controls autoregulation in RNA-binding protein networks. *Genes Dev.* **28**, 637–651 (2014).
53. Castle, J. C. *et al.* Expression of 24,426 human alternative splicing events and predicted cis regulation in 48 tissues and cell lines. *Nat Genet* **40**, 1416–1425 (2008).
54. Venables, J. P. *et al.* MBNL1 and RBFOX2 cooperate to establish a splicing programme involved in pluripotent stem cell differentiation. *Nat Commun* **4**, 2480 (2013).
55. Venables, J. P. *et al.* RBFOX2 Is an Important Regulator of Mesenchymal Tissue-Specific Splicing in both Normal and Cancer Tissues. *Mol Cell Biol* **33**, 396–405 (2013).
56. Keppetipola, N., Sharma, S., Li, Q. & Black, D. L. Neuronal regulation of pre-mRNA splicing by polypyrimidine tract binding proteins, PTBP1 and PTBP2. *Crit Rev Biochem Mol Biol* **47**, 360–378 (2012).
57. Ling, J. P. *et al.* PTBP1 and PTBP2 Repress Nonconserved Cryptic Exons. *Cell Reports* **17**, 104–113 (2016).
58. Li, Y. I., Sanchez-Pulido, L., Haerty, W. & Ponting, C. P. RBFOX and PTBP1 proteins regulate the alternative splicing of micro-exons in human brain transcripts. *Genome Res* **25**, 1–13 (2015).
59. Underwood, J. G., Boutz, P. L., Dougherty, J. D., Stoilov, P. & Black, D. L. Homologues of the Caenorhabditis elegans Fox-1 Protein Are Neuronal Splicing Regulators in Mammals. *Molecular and Cellular Biology* **25**, 10005 (2005).
60. Jin, Y. *et al.* A vertebrate RNA-binding protein Fox-1 regulates tissue-specific splicing via the pentanucleotide GCAUG. *The EMBO Journal* **22**, 905–912 (2003).
61. Bak, M. *et al.* MAPP unravels frequent co-regulation of splicing and polyadenylation by RNA-binding proteins and their dysregulation in cancer. *Nat Commun* **15**, 4110 (2024).
62. Huang, R. *et al.* NCAM regulates temporal specification of neural progenitor cells via profilin2 during corticogenesis. *Journal of Cell Biology* **219**, e201902164 (2019).
63. Sarkisian, M. R., Bartley, C. M. & Rakic, P. Trouble making the first move: interpreting arrested neuronal migration in the cerebral cortex. *Trends in Neurosciences* **31**, 54–61 (2008).

64. Licatalosi, D. D. *et al.* Ptbp2 represses adult-specific splicing to regulate the generation of neuronal precursors in the embryonic brain. *Genes Dev.* **26**, 1626–1642 (2012).
65. Todorov, H. *et al.* Stage-specific expression patterns and co-targeting relationships among miRNAs in the developing mouse cerebral cortex. *Commun Biol* **7**, 1–14 (2024).
66. Yang, Y. *et al.* Single-cell long-read sequencing in human cerebral organoids uncovers cell-type-specific and autism-associated exons. *Cell Reports* **42**, (2023).
67. Chau, K. K. *et al.* Full-length isoform transcriptome of the developing human brain provides further insights into autism. *Cell Reports* **36**, (2021).
68. Turner, T. N. *et al.* Genome Sequencing of Autism-Affected Families Reveals Disruption of Putative Noncoding Regulatory DNA. *The American Journal of Human Genetics* **98**, 58–74 (2016).
69. Bacchelli, E. *et al.* An integrated analysis of rare CNV and exome variation in Autism Spectrum Disorder using the Infinium PsychArray. *Sci Rep* **10**, 3198 (2020).
70. Griswold, A. J. *et al.* Targeted massively parallel sequencing of autism spectrum disorder-associated genes in a case control cohort reveals rare loss-of-function risk variants. *Molecular Autism* **6**, 43 (2015).
71. Kanduri, C. *et al.* The landscape of copy number variations in Finnish families with autism spectrum disorders. *Autism Research* **9**, 9–16 (2016).
72. Fanciulli, M. *et al.* Copy number variations and susceptibility to lateral temporal epilepsy: A study of 21 pedigrees. *Epilepsia* **55**, 1651–1658 (2014).
73. Lal, D. *et al.* Rare exonic deletions of the RBFOX1 gene increase risk of idiopathic generalized epilepsy. *Epilepsia* **54**, 265–271 (2013).
74. Lal, D. *et al.* Extending the phenotypic spectrum of RBFOX1 deletions: Sporadic focal epilepsy. *Epilepsia* **56**, e129–e133 (2015).
75. Gehman, L. T. *et al.* The splicing regulator Rbfox1 (A2BP1) controls neuronal excitation in the mammalian brain. *Nat Genet* **43**, 706–711 (2011).
76. Wen, M. *et al.* Upregulation of RBFOX1 in the malformed cortex of patients with intractable epilepsy and in cultured rat neurons. *International Journal of Molecular Medicine* **35**, 597–606 (2015).
77. Chung, Y. *et al.* Altered Rbfox1-Vamp1 pathway and prefrontal cortical dysfunction in schizophrenia. *Mol Psychiatry* 1–10 (2024) doi:10.1038/s41380-024-02417-8.
78. Conboy, J. G. Developmental regulation of RNA processing by Rbfox proteins. *WIREs RNA* **8**, e1398 (2017).
79. Mukherjee, A. & Nongthomba, U. To RNA-binding and beyond: Emerging facets of the role of Rbfox proteins in development and disease. *WIREs RNA* **15**, e1813 (2023).
80. Cayouette, M. & Raff, M. Asymmetric segregation of Numb: a mechanism for neural specification from Drosophila to mammals. *Nat Neurosci* **5**, 1265–1269 (2002).

81. Gulino, A., Di Marcotullio, L. & Screpanti, I. The multiple functions of Numb. *Experimental Cell Research* **316**, 900–906 (2010).
82. Keppetipola, N. M. *et al.* Multiple determinants of splicing repression activity in the polypyrimidine tract binding proteins, PTBP1 and PTBP2. *RNA* **22**, 1172–1180 (2016).
83. Linares, A. J. *et al.* The splicing regulator PTBP1 controls the activity of the transcription factor Pbx1 during neuronal differentiation. *eLife* **4**, e09268 (2015).
84. Uhlén, M. *et al.* Tissue-based map of the human proteome. *Science* **347**, 1260419 (2015).
85. Ellis, J. A., Hale, M. A., Cleary, J. D., Wang, E. T. & Andrew Berglund, J. Alternative Splicing Outcomes Across an RNA-Binding Protein Concentration Gradient. *Journal of Molecular Biology* **435**, 168156 (2023).
86. Begg, B. E., Jens, M., Wang, P. Y., Minor, C. M. & Burge, C. B. Concentration-dependent splicing is enabled by Rbfox motifs of intermediate affinity. *Nat Struct Mol Biol* **27**, 901–912 (2020).
87. Dredge, B. K. & Jensen, K. B. NeuN/Rbfox3 Nuclear and Cytoplasmic Isoforms Differentially Regulate Alternative Splicing and Nonsense-Mediated Decay of Rbfox2. *PLOS ONE* **6**, e21585 (2011).
88. Damianov, A. & Black, D. L. Autoregulation of Fox protein expression to produce dominant negative splicing factors. *RNA* **16**, 405–416 (2010).
89. Nowakowski, T. J. *et al.* Regulation of cell-type-specific transcriptomes by microRNA networks during human brain development. *Nat Neurosci* **21**, 1784–1792 (2018).
90. Florio, M. *et al.* Human-specific gene ARHGAP11B promotes basal progenitor amplification and neocortex expansion. *Science* **347**, 1465–1470 (2015).
91. Ma, J. *et al.* Identification of miR-22-3p, miR-92a-3p, and miR-137 in peripheral blood as biomarker for schizophrenia. *Psychiatry Research* **265**, 70–76 (2018).
92. Shi, W. *et al.* Aberrant expression of serum miRNAs in schizophrenia. *Journal of Psychiatric Research* **46**, 198–204 (2012).
93. Talebizadeh, Z., Butler, M. G. & Theodoro, M. F. Feasibility and relevance of examining lymphoblastoid cell lines to study role of microRNAs in autism. *Autism Research* **1**, 240–250 (2008).
94. Huang, F. *et al.* Investigation of Gene Regulatory Networks Associated with Autism Spectrum Disorder Based on MiRNA Expression in China. *PLOS ONE* **10**, e0129052 (2015).
95. Basak, O. & Taylor, V. Identification of self-replicating multipotent progenitors in the embryonic nervous system by high Notch activity and Hes5 expression. *European Journal of Neuroscience* **25**, 1006–1022 (2007).
96. Schindelin, J. *et al.* Fiji: an open-source platform for biological-image analysis. *Nat Methods* **9**, 676–682 (2012).
97. BBMap. *SourceForge* https://sourceforge.net/projects/bbmap/ (2022).
98. Dobin, A. *et al.* STAR: ultrafast universal RNA-seq aligner. *Bioinformatics* **29**, 15–21 (2013).

99. Liao, Y., Smyth, G. K. & Shi, W. featureCounts: an efficient general purpose program for assigning sequence reads to genomic features. *Bioinformatics* **30**, 923–930 (2014).
100. Love, M. I., Huber, W. & Anders, S. Moderated estimation of fold change and dispersion for RNA-seq data with DESeq2. *Genome Biology* **15**, 550 (2014).
101. R Core Team. R: A language and environment for statistical computing. R Foundation for Statistical Computing (2022).
102. rMATS: Robust and flexible detection of differential alternative splicing from replicate RNA-Seq data | PNAS. https://www.pnas.org/doi/10.1073/pnas.1419161111.
103. Array programming with NumPy | Nature. https://www.nature.com/articles/s41586-020-2649-2.
104. team, T. pandas development. pandas-dev/pandas: Pandas. Zenodo https://doi.org/10.5281/zenodo.8092754 (2023).
105. The Python Language Reference — Python 3.10.12 documentation. https://docs.python.org/3.10/reference/.
106. Matplotlib: A 2D Graphics Environment | IEEE Journals & Magazine | IEEE Xplore. https://ieeexplore.ieee.org/document/4160265.
107. Waskom, M. L. seaborn: statistical data visualization. *Journal of Open Source Software* **6**, 3021 (2021).
108. Lex, A., Gehlenborg, N., Strobelt, H., Vuillemot, R. & Pfister, H. UpSet: Visualization of Intersecting Sets. *IEEE Transactions on Visualization and Computer Graphics* **20**, 1983–1992 (2014).
109. Virtanen, P. *et al.* SciPy 1.0: fundamental algorithms for scientific computing in Python. *Nat Methods* **17**, 261–272 (2020).
110. Smith, T., Heger, A. & Sudbery, I. UMI-tools: modeling sequencing errors in Unique Molecular Identifiers to improve quantification accuracy. *Genome Res.* **27**, 491–499 (2017).
111. Lovci, M. T. *et al.* Rbfox proteins regulate alternative mRNA splicing through evolutionarily conserved RNA bridges. *Nat Struct Mol Biol* **20**, 1434–1442 (2013).
112. Todorov, H., Fournier, D. & Gerber, S. Principal components analysis: theory and application to gene expression data analysis. *Genomics Comput Biol* **4**, 100041 (2018).
113. Wu, T. *et al.* clusterProfiler 4.0: A universal enrichment tool for interpreting omics data. *The Innovation* **2**, 100141 (2021).
114. Yu, Guangchuang, Wang, Li-Gen, & He, Qing-Yu. clusterProfiler: an R Package for Comparing Biological Themes Among Gene Clusters. *OMICS: A Journal of Integrative Biology* **16**, 284–287 (2012).
115. Gu, Z., Gu, L., Eils, R., Schlesner, M. & Brors, B. circlize implements and enhances circular visualization in R. *Bioinformatics* **30**, 2811–2812 (2014).
116. Pysam. pysam-developers (2023).

117. Llorian, M. *et al.* Position-dependent alternative splicing activity revealed by global profiling of alternative splicing events regulated by PTB. *Nature structural & molecular biology* **17**, 1114 (2010).
118. Siepel, A. *et al.* Evolutionarily conserved elements in vertebrate, insect, worm, and yeast genomes. *Genome Res.* **15**, 1034–1050 (2005).
119. Szklarczyk, Damian *et al.* STRING v11: protein–protein association networks with increased coverage, supporting functional discovery in genome-wide experimental datasets. *Nucleic Acids Research* **47**, (2019).

## Acknowledgments

S.W acknowledges financial support from the Emergent Algorithmic Intelligence Center of the Johannes Gutenberg University Mainz funded by the Carl-Zeiss-Stiftung. H.T. and S.G. acknowledge financial support from the Landesinitiative Rheinland-Pfalz and the Resilience, Adaptation, and Longevity (ReALity) initiative of the Johannes Gutenberg University of Mainz. J.W. acknowledges funding from the DFG (WI 3837/10-1).

## Author information

### Contributions

S.W. performed the bioinformatics analyses, interpreted and visualized the results. H.T. contributed to interpreting the results and performed statistical analyses. L.S. performed in-utero electroporation experiments and analyzed the data. L.Z. and S.M. performed immunostainings and analyzed the data. A.S. performed cell culture, RT-qPCR, and Western blot experiments. S.L.Z. performed Luciferase Assays. D.H. performed bioinformatics analyses. T.V. provided the *in vitro* neuronal differentiation model. DS and SS analyzed data and revised the manuscript. M.H. and S.G. provided supervision and organized funding. J.W. designed the research, supervised the study, and organized funding. S.W., H.T., and J.W. wrote the manuscript. All authors read and approved the final version of the manuscript.

## Ethics declarations

### Ethics approval

All animal experiments were performed in accordance with the regulations of the local authorities (Landesuntersuchungsamt Rheinland-Pfalz, license number 23 177-07/G 13-1-089).

### Competing interests

The authors declare no conflict of interest.

## Supplemental Figures

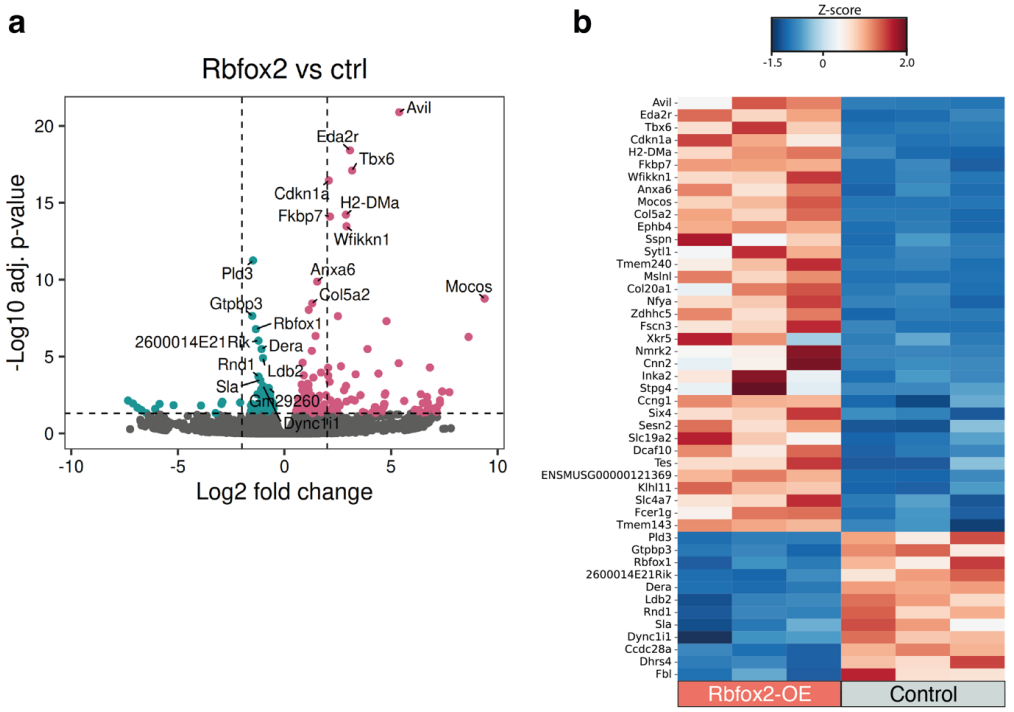


*Supplementary Figure 1 a) Volcano plot showing minimal alteration in differential gene expression upon Rbfox2-overexpression (Rbfox2-OE) in the embryonic neocortex compared to control samples b) Top 50 differentially expressed genes. Expression values are shown as z-scores.*

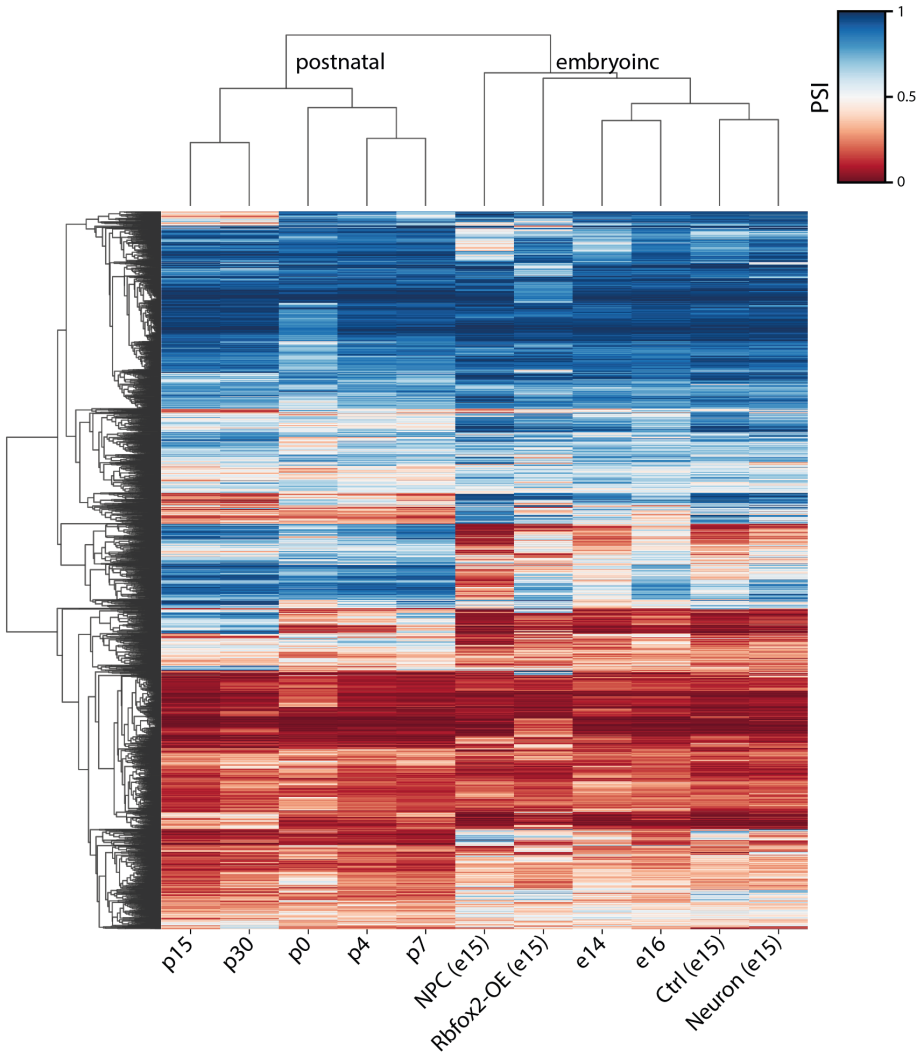


*Supplementary Figure 2 Developmentally regulated splicing events[1,2] hierarchically clustered using the percentage spliced-in (PSI) values. Embryonic and neuronal maturation stages cluster together. Clearly, Rbfox2-OE leads to an aberrant splicing pattern that does not cluster with samples from comparable developmental stages.*

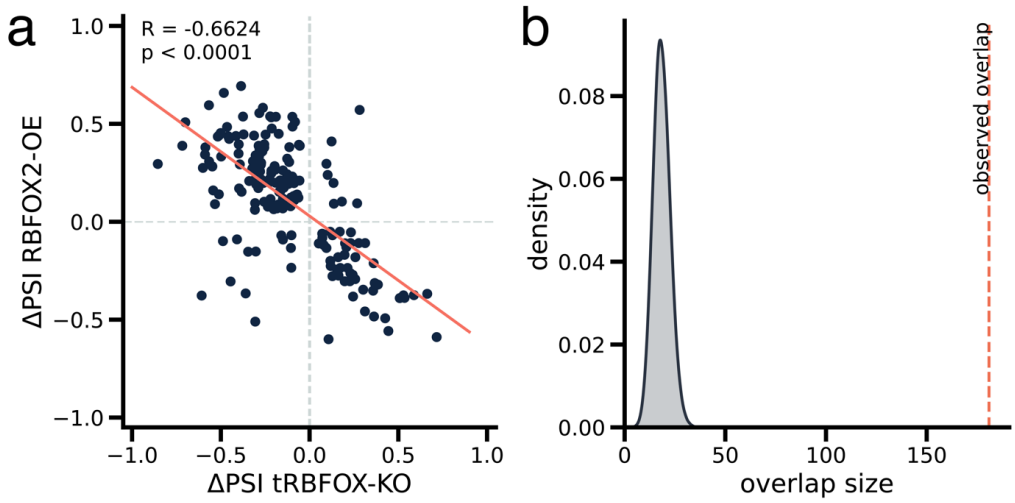


*Supplementary Figure 3 Comparison of splicing changes in Rbfox2 overexpression (OE) and Rbfox triple knockout (tKO) conditions in mouse embryonic stem cells (data from Jacko et al.)[3]. a) Correlation analysis of splicing changes (ΔPSI) between Rbfox2-OE and tRbfox-KO conditions. Each point represents a significant splicing event detected in both data sets. The x-axis shows ΔPSI values for tRBFOX-KO, while the y-axis shows ΔPSI values for Rbfox2-OE. A strong negative correlation (R = -0.6624, p < 0.0001) confirms the expected opposite splicing effects in OE versus KO conditions. b) Monte Carlo simulation results from 100,000 runs, showing the distribution of overlap sizes between Rbfox2-OE and tRBFOX-KO splicing events. The x-axis represents the overlap size, and the y-axis shows the density of occurrences. The observed overlap (indicated by the orange dashed line) is significantly larger than expected by chance (fold change ≈ 9.833, p < 0.0001).*

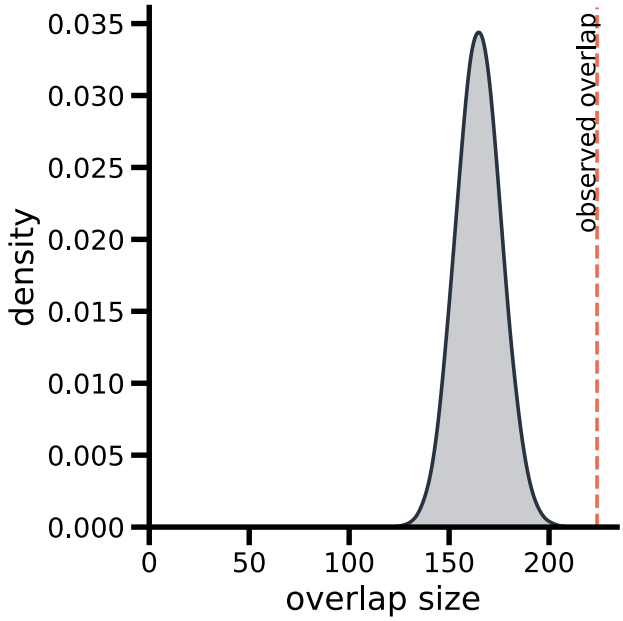


*Supplementary Figure 4 Monte Carlo simulation results from 100,000 runs, showing the overlap distribution between randomly selected genes and high-confidence neurodevelopmental disorder (NDD) genes[4]. The observed overlap between significantly alternatively spliced genes and NDD genes is significantly enriched (224 out of 1317 genes, fold change ≈ 1.358, p < 2e-07, Supplementary data 5))*

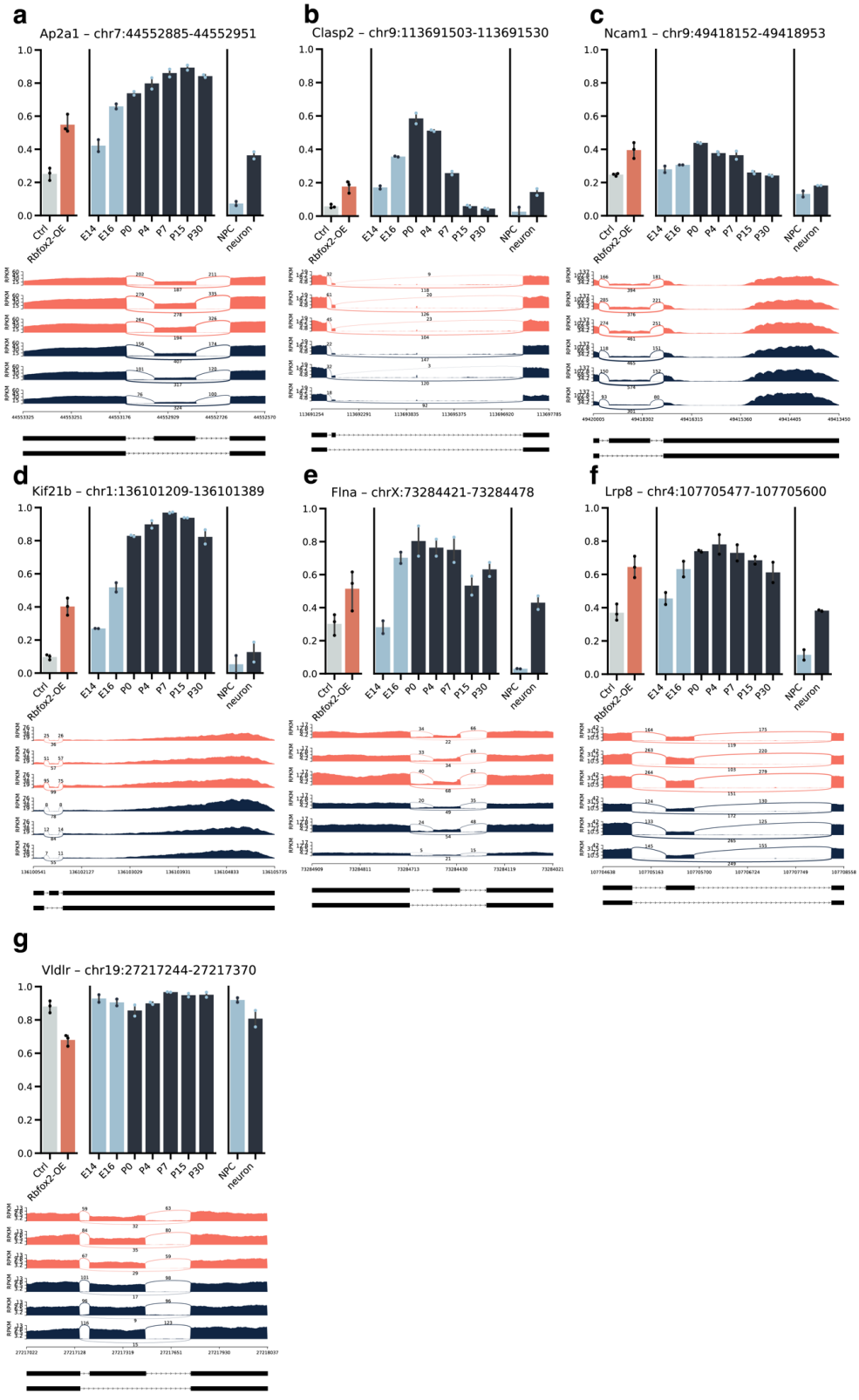
a
Ap2a1 – chr7:44552885-44552951
b
Clasp2 – chr9:113691503-113691530
c
Ncam1 – chr9:49418152-49418953
d
Kif21b – chr1:136101209-136101389
e
Flna – chrX:73284421-73284478
f
Lrp8 – chr4:107705477-107705600
g
Vldlr – chr19:27217244-27217370
Ctrl
Rbfox2-OE
E14
E16
P0
P4
P7
P15
P30
NPC
neuron
RPKM

*Supplementary Figure 5 Alternative splicing analysis of seven genes during development and upon Rbfox2 overexpression. (a-g) Each panel shows a different gene (Ap2a1, Clasp2, Ncam1, Kif21b, Flna, Lrp8, Vldlr) with bar graphs displaying percentage spliced-in (PSI) values across developmental stages and conditions (top), sashimi plots illustrating read coverage and junction reads (middle), and alternative isoforms from the GFF annotation file (bottom). Bar graphs include control, Rbfox2-OE, embryonic and postnatal stages, NPCs, and neurons. Sashimi plots show three replicates for two conditions (control: blue, Rbfox2-OE: orange).*

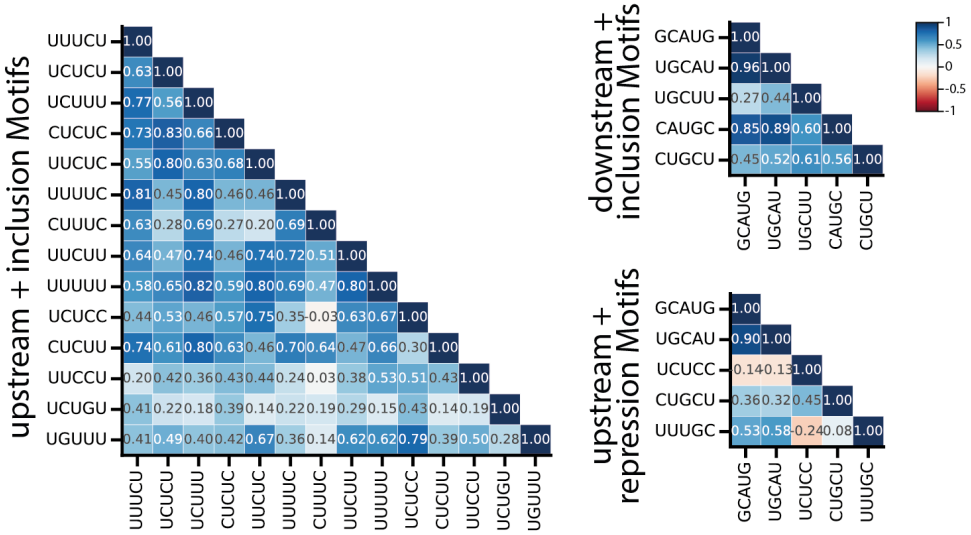


*Supplementary Figure 6 Correlation of motif occurrences for upstream inclusion events, downstream inclusion events, and downstream repression events of Rbfox2-overexpression samples compared to control.*

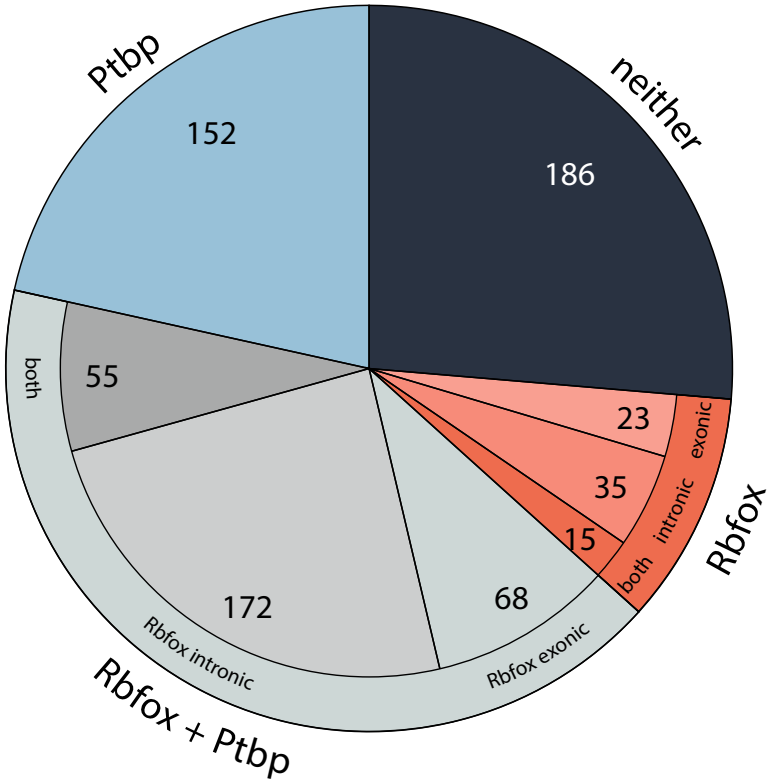


*Supplementary Figure 7 Analysis of significantly alternatively spliced cassette exons for conserved PTBP and RBFOX motifs.*

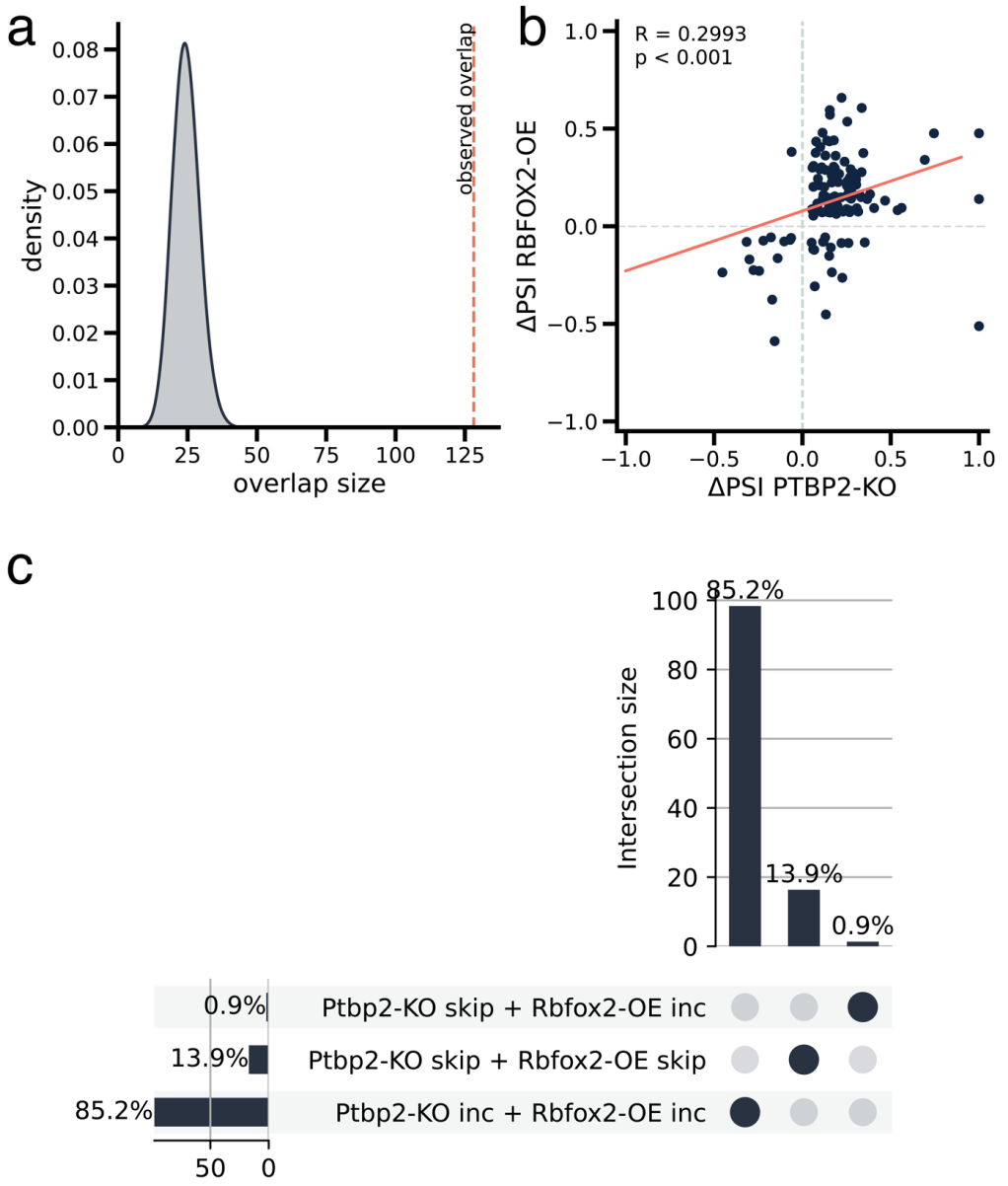


*Supplementary Figure 8 Comparison of splicing changes in Rbfox2-OE and Ptbp2-KO[5] conditions. a) Monte Carlo simulation results from 100,000 runs, showing the distribution of overlap sizes between randomly selected events and those affected by Rbfox2-OE and Ptbp2-KO. The x-axis represents the overlap size, and the y-axis shows the density of occurrences. The observed overlap (indicated by the red dashed line) is significantly larger than expected by chance, suggesting a substantial and non-random relationship between Rbfox2-OE and Ptbp2-KO splicing effects. b) Correlation analysis of splicing changes (ΔPSI) between Rbfox2-OE and Ptbp2-KO. Each point represents a splicing event. The x-axis shows ΔPSI values for Ptbp2-KO, while the y-axis shows ΔPSI values for Rbfox2-OE. A moderate, statistically significant positive correlation (R = 0.2993, p < 0.001) is observed, indicating a degree of similarity in splicing effects between the two conditions. c) Intersection analysis of splicing events affected by Ptbp2-KO and Rbfox2-OE. The upsetplot shows the percentages of cassette exons that are included (inc) or skipped (skip) in both conditions. The majority (85.2%) of events show increased inclusion in both Ptbp2-KO and Rbfox2-OE.*

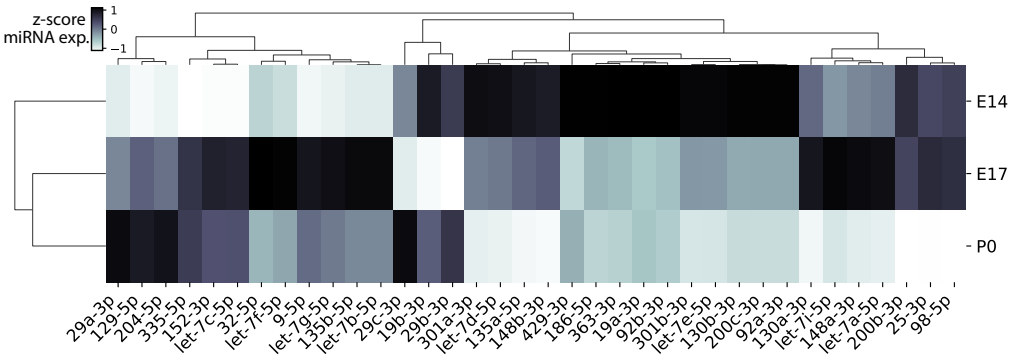


*Supplementary Figure 9 Heatmap showing the expression of miRNAs predicted to target Rbfox2. Normalized expression values are shown as z-scores. Data were obtained from Todorov et al.[6].*

**References**

1. Weyn-Vanhentenryck, S. M. *et al.* Precise temporal regulation of alternative splicing during neural development. *Nat Commun* **9**, 2189 (2018).

2. Liu, J., Geng, A., Wu, X., Lin, R.-J. & Lu, Q. Alternative RNA Splicing Associated With Mammalian Neuronal Differentiation. *Cerebral Cortex* **28**, 2810–2816 (2018).

3. Jacko, M. *et al.* Rbfox Splicing Factors Promote Neuronal Maturation and Axon Initial Segment Assembly. *Neuron* **97**, 853-868.e6 (2018).

4. Leblond, C. S. *et al.* Operative list of genes associated with autism and neurodevelopmental disorders based on database review. *Mol Cell Neurosci* **113**, 103623 (2021).

5. Vuong, J. K. *et al.* PTBP1 and PTBP2 Serve Both Specific and Redundant Functions in Neuronal Pre-mRNA Splicing. *Cell Reports* **17**, 2766–2775 (2016).

6. Todorov, H. *et al.* Stage-specific expression patterns and co-targeting relationships among miRNAs in the developing mouse cerebral cortex. *Commun Biol* **7**, 1–14 (2024).

## 2.2 Stage-specific expression patterns and co-targeting relationships among miRNAs in the developing mouse cerebral cortex.

Authors: Hristo Todorov, **Stephan Weißbach**, Laura Schlichtholz, Hanna Mueller, Dewi Hartwich, Susanne Gerber, Jennifer Winter

This article is published in *Communications Biology* (doi: https://doi.org/10.1038/s42003-024-07092-7).

My contributions to this article are listed in 6.1 Contribution to individual publications.

communications biology

Article

https://doi.org/10.1038/s42003-024-07092-7

# Stage-specific expression patterns and co-targeting relationships among miRNAs in the developing mouse cerebral cortex

Check for updates

Hristo Todorov[1], Stephan Weißbach[1,2], Laura Schlichtholz[1,3], Hanna Mueller[1], Dewi Hartwich[1], Susanne Gerber[1] ✉ & Jennifer Winter[1] ✉

microRNAs are crucial regulators of brain development, however, miRNA regulatory networks are not sufficiently well characterized. By performing small RNA-seq of the mouse embryonic cortex at E14, E17, and P0 as well as in neural progenitor cells and neurons, here we detected clusters of miRNAs that were co-regulated at distinct developmental stages. miRNAs such as miR-92a/b acted as hubs during early, and miR-124 and miR-137 during late neurogenesis. Notably, validated targets of P0 hub miRNAs were enriched for downregulated genes related to stem cell proliferation, negative regulation of neuronal differentiation and RNA splicing, among others, suggesting that miRNAs are particularly important for modulating transcriptional programs of crucial factors that guide the switch to neuronal differentiation. As most genes contain binding sites for more than one miRNA, we furthermore constructed a co-targeting network where numerous miRNAs shared more targets than expected by chance. Using luciferase reporter assays, we demonstrated that simultaneous binding of miRNA pairs to neurodevelopmentally relevant genes exerted an enhanced transcriptional silencing effect compared to single miRNAs. Taken together, we provide a comprehensive resource of miRNA longitudinal expression changes during murine corticogenesis. Furthermore, we highlight several potential mechanisms through which miRNA regulatory networks can shape embryonic brain development.

Mammalian brain development is an extraordinarily complex process where neural progenitor cells proliferate and give rise to all neuronal and glial cell types. Numerous transcriptional, post-transcriptional, and epigenetic mechanisms integrate with each other to control progenitor proliferation and self-renewal, differentiation, and lineage commitment as well as migration in a strictly spatio-temporal manner. One of the key regulators of these processes are microRNAs (miRNAs). In most cases, these small RNAs bind to their target mRNAs' 3'- untranslated region (3'UTR) to induce mRNA degradation or translational inhibition. In the canonical pathway, miRNA genes are transcribed into a pri-miRNA in the cell nucleus by PolII/III[1,2]. In subsequent processing steps, the pri-miRNA is cleaved into a hairpin pre-miRNA by the microprocessor complex Drosha-Dgcr8 and transported to the cytoplasm by Exportin-5[3–6]. In the cytoplasm, the pre-miRNA is bound and cleaved by a complex containing the RNase Dicer1 to form the mature miRNA duplex[7]. From this duplex, the functional strand is loaded into the RISC complex, guiding it to the 3′UTR's target site[8]. Mice carrying conditional *Dicer* gene deletions in the embryonic telencephalon have shown a variety of phenotypes in the cerebral cortex, such as reduced cell proliferation and impaired neuronal differentiation, increased apoptosis, defective cortical layering and microcephaly[9–14].

In the brain, 70% of all miRNAs are expressed, most of them in a highly cell-type- and developmental-time-specific manner[15]. Given that the total number of human miRNAs is estimated to be ~2300, at least 1600 different miRNAs may be expressed in the brain[16]. While this suggests that miRNA regulation is generally important for brain development and function, the specific functions of most miRNAs remain unknown. Single miRNAs are involved in some of these processes including, for example, cell proliferation (e.g., let-7, miR-124, miR-9), neuronal differentiation (e.g., let-7, miR-124, miR-9, miR-128) and migration (e.g., miR-9, miR-124, miR-379-410)[17,18]. Many of the functionally studied miRNAs are among the most highly expressed in the brain such as miR-9, miR-124 and let-7[17]. Most miRNAs

[1]Institute of Human Genetics, University Medical Center of the Johannes Gutenberg University Mainz, Mainz, Germany. [2]Institute of Developmental Biology and Neurobiology (iDN), Johannes Gutenberg University Mainz, Mainz, Germany. [3]Focus Program of Translational Neurosciences, University Medical Center Mainz, Mainz, Germany. ✉e-mail: sugerber@uni-mainz.de; jewinter@uni-mainz.de

https://doi.org/10.1038/s42003-024-07092-7 Article

typically have a relatively weak effect on their target genes[19,20]. Previous research has suggested that the regulatory potential of a given miRNA could be enhanced by cooperating with other miRNAs in co-targeting networks[21]. This hypothesis is supported by the fact that most 3'UTRs contain more than one miRNA binding site and most miRNAs have matching binding sites in up to several hundred 3'UTRs. A network of miRNAs co-operatively binding at distinct 3'UTR positions can potentially enhance target gene repression by additive or synergistic effects[22,23]. MiRNA binding at closely spaced binding sites (~15–35 nt) can further enhance the repressive effect[23–25]. We and others have previously identified mRNAs that are targeted by several miRNAs leading to a synergistic or additive repressive effect[19,20,26]. For example, miRNAs of the miR-379-410 cluster regulate neurogenesis by targeting multiple miRNA binding sites in the N-cadherin 3'UTR in an additive manner[19]. While this highlights the regulatory potential of such miRNA networks during brain development, their detailed composition and temporal dynamics remain poorly characterized. Using an unbiased bioinformatics approach to identify co-targeting networks in mouse tissues, Cherone and colleagues recently found that miRNAs enriched in the human prefrontal cortex had more co-targeting partners than those enriched in other tissues suggesting that miRNA co-targeting is especially important in the brain[20].

In the current study, we employed high-throughput small RNA sequencing of the mouse cerebral cortex to create a detailed map of miRNA expression patterns and their longitudinal dynamics at key developmental stages. Using miRNAs whose expression was significantly correlated with developmental time, we constructed a comprehensive co-targeting network in which miRNAs with higher expression levels were associated with significantly more co-targeting relationships. In luciferase assays, we validated the enhanced gene silencing effect of cooperative miRNA binding in a set of target genes involved in the regulation of nervous system development.

## Results

### Temporal dynamics of miRNA expression during cerebral cortex development

To study the expression patterns of miRNAs during mammalian corticogenesis, we performed small bulk RNA sequencing in both female and male mice at a progenitor-dominated developmental phase (embryonic day E14), at an intermediate time point (E17) and at birth (postnatal day P0) when neurons from all six layers of the neocortex have been born[27,28] (Fig. 1). Using stringent filtering criteria for expression levels (>10 CPM in at least five samples), we detected a total of 489 miRNAs with only 13 of those corresponding to novel miRNAs. In agreement with previous reports[17,29], miR-9, members of the let-7 family, miR-128, and miR-124 were among the top 20 most abundantly expressed miRNAs in the developing cerebral cortex (Supplementary Fig. 1). Principal component analysis (PCA) revealed a distinct separation of samples according to their developmental stage. However, E17 and P0 samples had a more similar global expression pattern to each other compared to E14 (Fig. 2a). Since we did not observe apparent differences related to sex, female and male samples were processed together in the subsequent analyses.

We detected the highest number of differentially expressed miRNAs at the E14 vs. P0 time points, where 169 miRNAs were up- and 172 were down-regulated (Fig. 2b–f, Supplementary data 1). However, the major transcriptional shift already occurred in the transition from E14 to E17, where ~57% of all detected miRNAs significantly changed their expression level (122 up- and 144 down-regulated miRNAs). In contrast, only 36% of all detected miRNAs were differentially expressed in E17 vs. P0 samples (82 upregulated and 93 downregulated miRNAs). Interestingly, a higher number of miRNAs were consistently downregulated at earlier developmental time-points in all pairwise comparisons (45 vs. 32 upregulated miRNAs, Fig. 2b, c, g).

To study the expression of miRNAs specifically during neurogenesis, we isolated NPCs from the cortices of mouse embryos at E14 and differentiated them in vitro into neurons. Small RNA sequencing of these cells

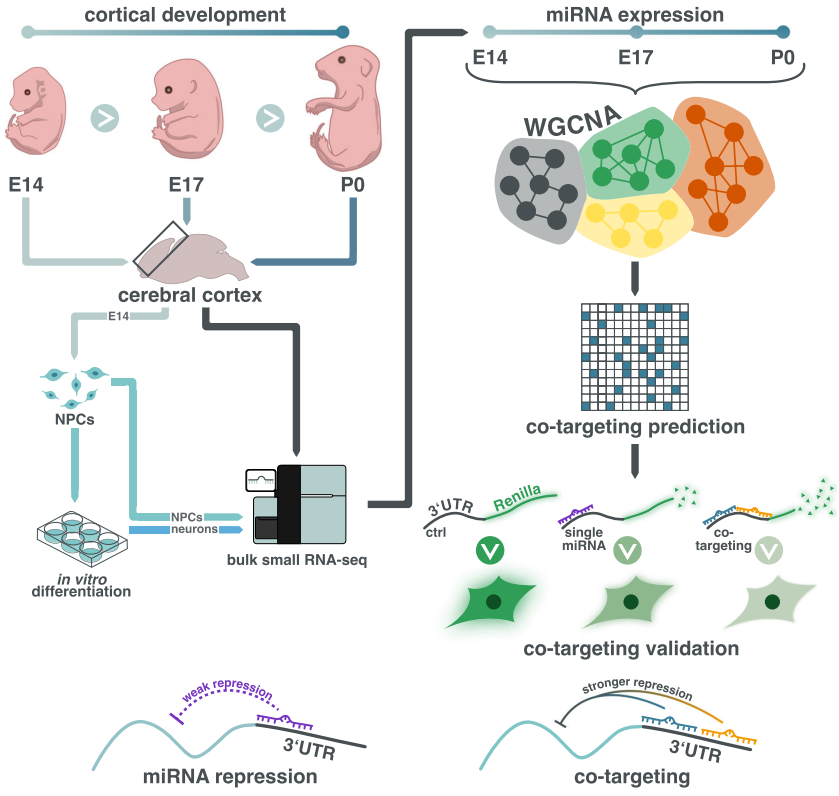


**Fig. 1 | Schematic representation of the study.** To investigate the expression patterns of miRNAs during cerebral cortical development in the mouse, we performed RNA-seq of bulk tissue at E14, E17 and P0 as well as in NPCs isolated from the cerebral cortex and differentiated into neurons. Subsequently, we employed weighted gene co-expression network analysis (WGCNA) to identify modules of co-expressed miRNAs. We then constructed a network of miRNAs sharing more target genes than expected by chance. Co-targeting relationships between selected miRNAs were validated using luciferase reporter assays, demonstrating enhanced gene silencing effect on neurodevelopmentally-relevant genes for combinations of miRNAs compared to individual miRNAs.

https://doi.org/10.1038/s42003-024-07092-7 **Article**

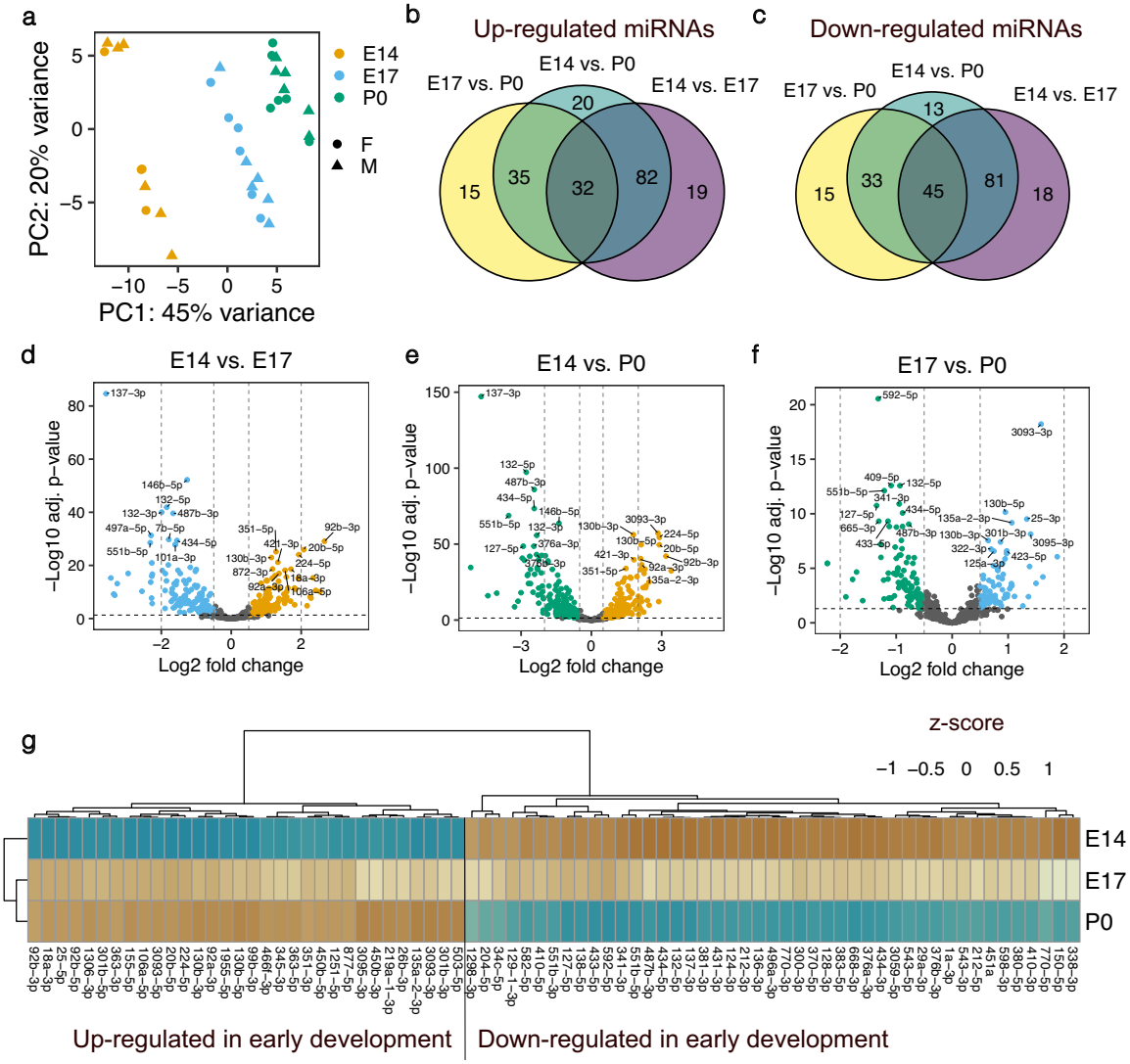


**Fig. 2 | Expression changes of miRNAs during mouse cerebral cortex development. a** Principal component analysis of bulk small RNA sequencing samples from the cerebral cortex of female and male mice at different developmental stages. $n = 4$ biological replicates for females at E14, $n = 6$ in all remaining groups. **b** Venn-diagram of upregulated miRNAs at earlier compared to later stages of cortical development. **c** Venn-diagram of downregulated miRNAs at earlier compared to later developmental stages. **d**–**f** Volcano plots of differentially expressed miRNAs. Positive log2 fold changes indicate miRNAs upregulated at earlier compared to later developmental stages in each pairwise comparison (E14 vs. E17, E14 vs. P0 and E17 vs. P0). **g** Heatmap of miRNAs differentially expressed in each pairwise comparison of different developmental stages. Mean expression values per developmental stage are shown as z-scores.

revealed 110 miRNAs that were upregulated and 113 miRNAs that were downregulated in NPCs compared to neurons, respectively. miR-124-3p and miR-369-3p were the most significantly upregulated miRNA in neurons, whereas miR-155-3p and miR-34b-3p were the most significantly upregulated miRNAs in NPCs (Supplementary Fig. 2a, d, Supplementary data 1). 66% of the upregulated (72 out of 110) and 65% of the downregulated (73 out of 113) miRNAs in NPCs vs. neurons were also differentially expressed in the comparison of bulk samples from E14 vs. P0, confirming the replicability of the expression patterns we observed (Supplementary Fig. 2b–d). Interestingly, these overlapping miRNAs corresponded to 43% of all upregulated and 42% of the downregulated miRNAs in E14 vs. P0, suggesting that a large proportion of the differentially regulated miRNAs might be attributable to the non-neuronal cells in the bulk samples. This observation is plausible, as gliogenesis takes place roughly between E17 and P0 of cortical development[28,30] therefore the bulk samples from P0 likely contained both neuronal and non-neuronal cell types. In agreement, several of the developmental-stage-dependent expression changes we observed align with previously reported roles of miRNAs in inhibiting or promoting gliogenesis. For instance, miR-106a-5p was upregulated at E14 compared to E17 and P0 (Fig. 2g). miR-106a was previously reported to suppress gliogenic differentiation of neural stem cells and induce neurogenic cell fate commitment[31], which fits well with the upregulation of expression during peak neurogenesis in our study. Furthermore, we observed an upregulation of the gliogenic miR-338[32] specifically at P0 but not in neurons compared to NPCs (Supplementary data 1), thus underscoring the potential role of this miRNA specifically in promoting differentiation of glia cells. As another example, miR-153 whose inhibition was shown to confer gliogenic competence to neural stem cells[33], was upregulated in neurons compared to NPCs in our analysis (Supplementary data 1).

https://doi.org/10.1038/s42003-024-07092-7 **Article**

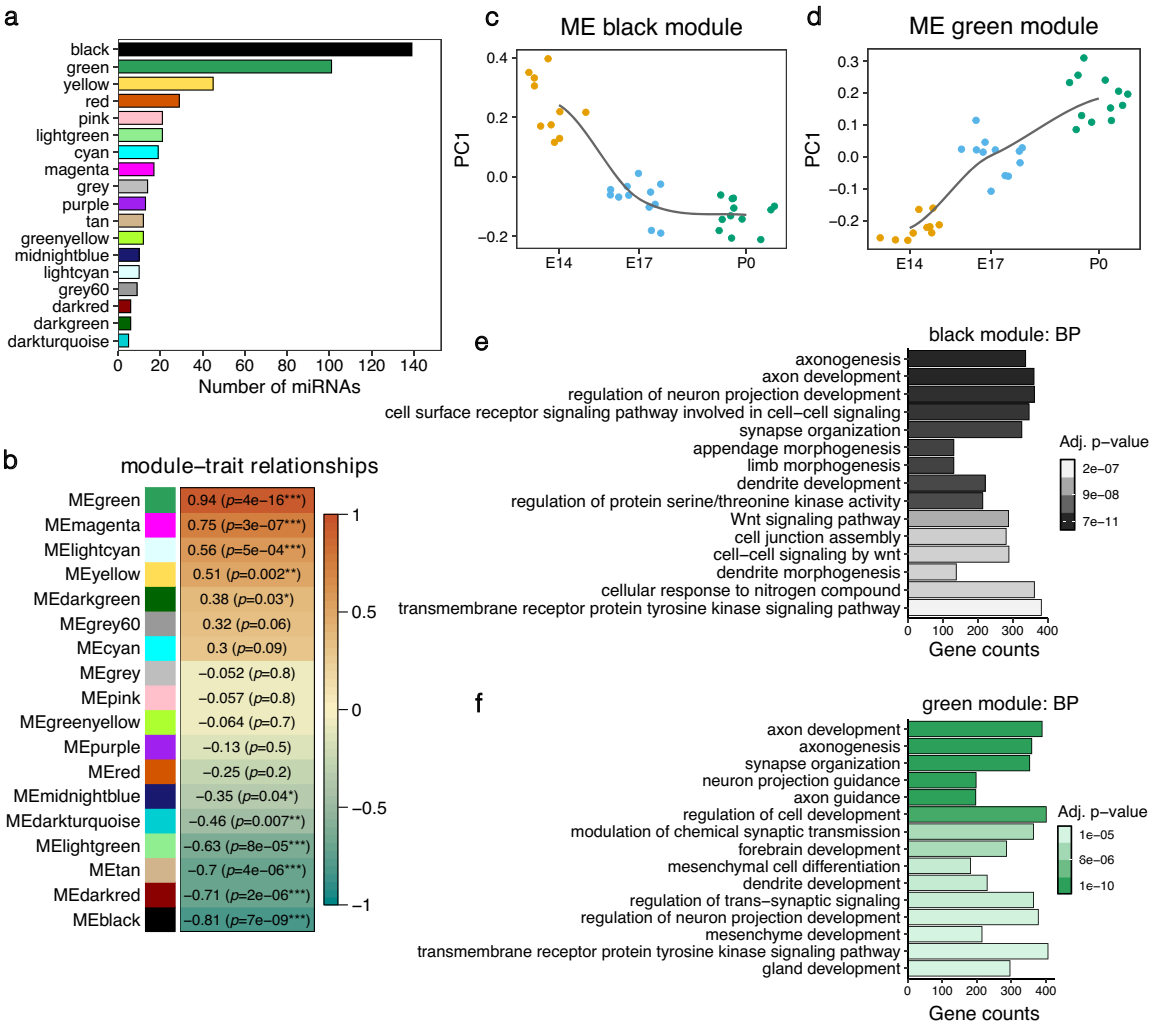


**Fig. 3 | Weighted miRNA co-expression analysis.** The co-expression network was derived using bulk small RNA-seq from mouse cerebral cortices at E14, E17 and P0. **a** Bar plot showing the number of miRNAs in each co-expression network module. **b** Pearson correlation between developmental stages of the mouse cerebral cortex (E14, E17 and P0) and the module eigengenes (ME). ***$p < 0.001$, **$p < 0.01$, *$p < 0.05$. **c**, **d** Module eigengene values at each developmental stage for the black and green module. $n = 10$ biological replicates at E14, $n = 12$ in all remaining groups. **e**, **f** Top 15 enriched GO terms for the biological process (BP) category for the gene targets of the black and green modules.

### Weighted gene co-expression gene network analysis identifies sets of co-regulated miRNAs during the development of the cerebral cortex

Next, we applied weighted gene co-expression network analysis (WGCNA) to construct networks of co-expressed miRNAs and better characterize their transcriptional dynamics along the cortical developmental trajectory (Fig. 1). We obtained 18 modules that were assigned to arbitrary colors (Fig. 3a, detailed information of the specific miRNAs included in each WGCNA module is included in Supplementary data 2). Module eigengenes (MEs) that correspond to the first dimension in a principal component analysis of the expression matrix of the corresponding WGCNA module, served as proxies for the characteristic transcriptomic signature of each module. Six MEs were significantly negatively correlated with the developmental time point indicating that the miRNAs in the respective modules showed overall reduced expression levels at later compared to earlier developmental stages (Fig. 3b). In contrast, four modules contained miRNAs whose eigengene expression significantly increased during brain development. The black module, which contained the highest number of miRNAs (139), had the strongest negative correlation with the developmental stage. The overall expression pattern captured by the ME, indicated that the black module contained miRNAs whose expression level peaked at E14 and dropped at E17, remaining stable afterwards (Fig. 3c). The green module was the second largest, containing 101 miRNAs with generally linearly increasing expression levels from E14 to P0 (Fig. 3d). Remarkably, although these two modules were regulated in opposite directions, they shared most of their targets (6244 common targets, corresponding to 79% of all black module and 72% of all green module targets, Supplementary Fig. 3c). Gene ontology analysis using the genes targeted by the miRNAs revealed that both the black and the green modules are involved in the regulation of key nervous system developmental processes such as axon development and guidance, neuron projection, dendrite development, and synapse organization (Fig. 3e, f, Supplementary data 3).

To identify key miRNAs at early and late embryonic brain developmental stages, we reconstructed the network structure of miRNAs within

https://doi.org/10.1038/s42003-024-07092-7 **Article**

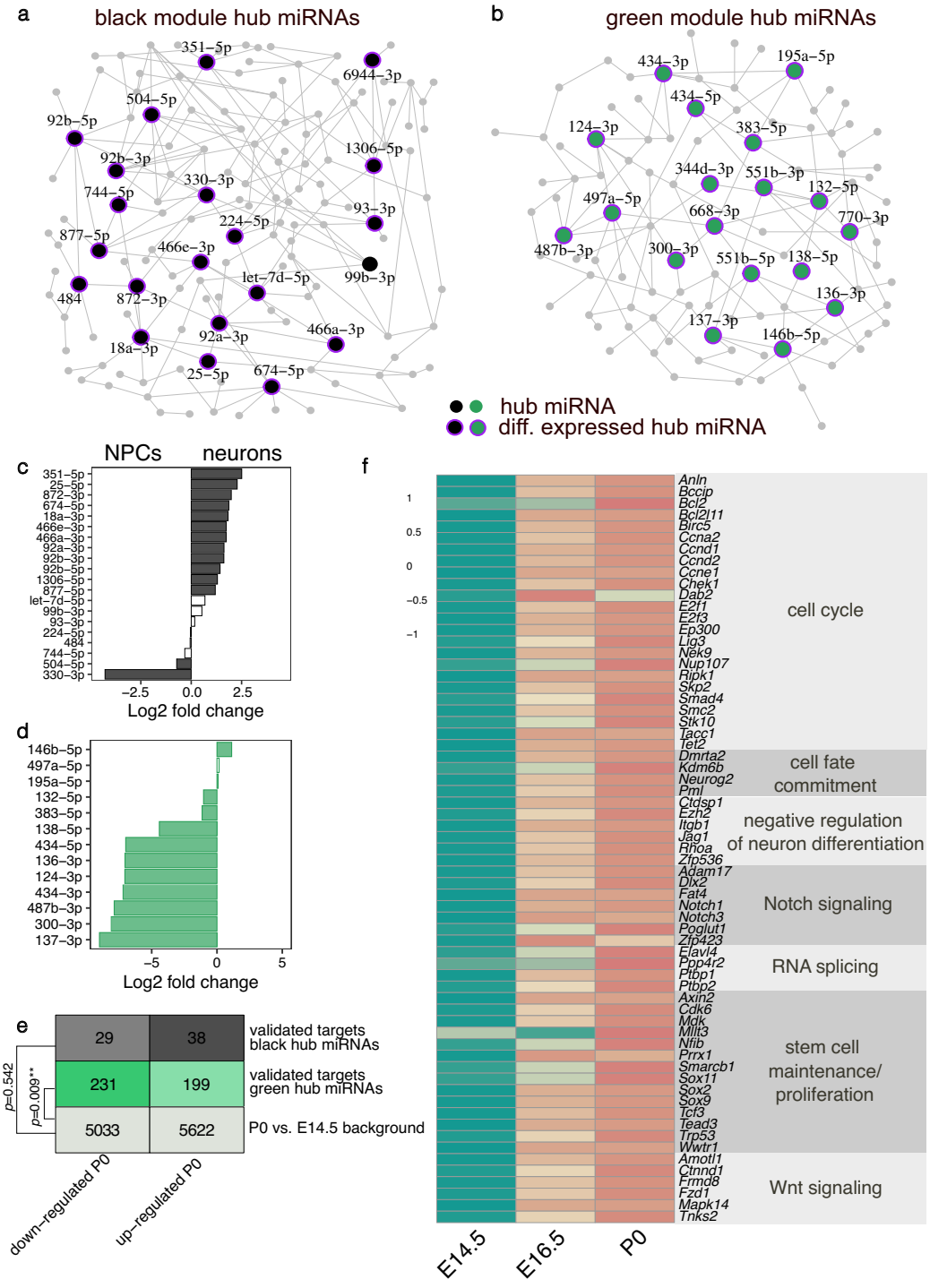


the black and green modules and identified key driver (hub) miRNAs as described previously[34,35]. The black module contained 21 hub miRNAs. 12 miRNAs were also upregulated in NPCs compared to neurons including members of the miR-92 family - miR-92a, miR-92b (Fig. 4c). Moreover, we detected 18 key driver miRNAs in the green module. Ten of these were also significantly upregulated in neurons compared to NPCs, including the neuron-specific miR-124 and miR-137 (Fig. 4d). This analysis confirmed the stage-specific regulation of a core set of miRNAs during embryonic cortical development.

Importantly, all hub miRNAs in the green module and all but one miRNA in the black module were significantly differentially regulated at E14 compared to the P0 developmental stage (Fig. 4a, b). Furthermore, hub

https://doi.org/10.1038/s42003-024-07092-7 **Article**

**Fig. 4 | Hub miRNAs in the black and green WGCNA modules.** Network plot showing the hub miRNAs in the black (**a**) and green (**b**) modules. Hub miRNAs are represented as bigger nodes. Purple halos around the nodes indicate miRNAs that are significantly differentially expressed between E14 and P0. Differential expression of hub miRNAs from the black (**c**) and green (**d**) module detected in the NPCs versus neurons analysis. Positive log2 fold changes indicate an upregulation in NPCs, negative values correspond to upregulation in neurons. White bars indicate non-significant fold changes. **e** Distribution of differentially expressed genes in the mouse cerebral cortex between E14.5 and P0. The overall number of genes as well as the number of these genes that are validated targets from miRNAs in the black and green module as obtained from miRTarBase are given. The comparison of the distribution of differentially expressed targets of the black or green module from the overall distribution of differentially expressed genes was performed with a Fisher's exact test. **f** Z-score transformed average expression of selected validated targets of miRNAs from the green module that are significantly upregulated at E14.5 compared to P0. The expression values in (**e**) and (**f**) were obtained from the bulk RNA-seq of the mouse cerebral cortex across development study by Weyn-Vanhentenryck et al.[37].

miRNAs in both the black and the green modules showed significantly stronger module membership and gene trait significance estimates compared to the remaining miRNAs in the respective module (Supplementary Fig. 3e–h), thereby confirming their importance. Here, module membership corresponds to the correlation between the miRNA's expression and the module eigengene. Furthermore, the gene trait significance represents the correlation between miRNA expression and the trait of interest, in our study —the developmental stage[36].

To gain an insight into the relevance of hub miRNAs in regulating target gene expression across development, we re-analyzed bulk RNA-seq data from the mouse cortex at E14.5, E16.5, and P0 from the study by Weyn-Vanhentenryck and colleagues[37]. We limited this analysis to the experimentally validated targets of the conserved hub miRNAs that we obtained from miRTarBase[38]. We did not observe a significant deviation in the differential expression of target genes of the black module when comparing P0 and E14.5 (Fig. 4e). This could likely be explained by the overall lower number of validated targets for conserved key driver miRNAs from the black module (Supplementary Fig. 3d). However, the number of downregulated targets of the green module's hub miRNAs was significantly higher compared to the overall background distribution of differentially expressed genes (Fig. 4e). The increased proportion of genes with a reduced expression at the time point when the green module's hub miRNAs that target them have their expression peak strongly suggests that these miRNAs are involved in repressing these targets' expression in vivo.

To gain insight into the biological processes that the downregulated targets of green module hub miRNAs are involved in, we performed a GO annotation analysis (Fig. 4f). Notably, many of these genes are associated with the cell cycle, stem cell maintenance and proliferation (e.g., the transcription factors *Sox2, Sox9* and *Sox11)*, cell fate commitment (e.g., *Neurog2)*, and negative regulation of neuronal differentiation. Furthermore, several targets are involved in activating the Notch signaling pathway (e.g., *Notch1, Notch3)* and negatively regulating the Wnt pathway. Important mediators of RNA splicing (e.g., the RNA binding proteins *Ptbp1* and *Ptbp2)* were also among the downregulated targets. Notably, the green module hub miR-124-3p is known to repress *Ptbp1* expression and thereby induce neuron-specific alternative splicing programs required for neuronal differentiation[39]. Therefore, these results indicate that miRNAs might be particularly important for the switch from undifferentiated NPCs to differentiated neurons by silencing the expression of key factors that promote stem cell maintenance, proliferation and non-neuronal splicing patterns.

### Prediction of miRNA co-targeting networks in the developing cerebral cortex

WGCNA revealed that clusters containing multiple miRNAs are co-expressed during cortical development. Furthermore, when looking at the predicted targets of the black and green modules, we observed that only ~30% were potentially targeted merely by a single miRNA. On average, each gene was associated with more than 3 miRNAs (Supplementary Fig. 3a, b). This apparent redundancy of simultaneously expressed miRNAs that putatively bind to overlapping sets of genes supports the previously proposed hypothesis that miRNAs might act together to co-operatively exert stronger gene silencing (Fig. 1). To construct a comprehensive co-targeting network of miRNAs in the developing cerebral cortex, we designed a statistical framework that allowed us to detect which miRNAs share significantly more targets than expected by chance. In this analysis, we included all miRNAs whose module eigengene was correlated significantly with developmental time in the WGCNA (Fig. 3b). Furthermore, we only considered conserved miRNAs with at least 300 conserved targets and distinct seed sequences[20]. miRNAs belonging to the same broad conserved family and thereby having identical seed sequences, were grouped together for the statistical testing. After applying these filtering criteria, we performed the co-targeting prediction with a set of 77 miRNA families corresponding to 106 individual miRNAs (Fig. 5a). We detected 1216 significant co-targeting pairs with an adjusted $p$-value < 0.05 (Fig. 6, Supplementary data 4) and each miRNA had on average 41 co-targeting relationships (Fig. 5b). Interestingly, the number of significant co-targeting relationships was positively correlated with the miRNA's average expression level (Fig. 5c). This finding implies that important miRNAs might need to be produced at higher amounts to facilitate their involvement in multiple cooperative gene silencing interactions in the co-targeting network. Importantly, hub miRNAs such as miR-92a/b from the black module as well as miR-124 and miR-137 from the green module were among the miRNAs with the highest expression level and highest number of co-targeting relationships (Fig. 5c) indicating that these miRNAs might be master regulators in both co-expression and multi-targeting networks. As expected, the length of the 3' UTR was positively correlated with the number of significant miRNA pairs targeting a gene (Fig. 5d). Interestingly, *Nova1*, was among the top 10 genes involved in the highest number of co-targeting associations. NOVA1 is a neuron-specific splice factor that is crucial for neuronal viability[40] and regulates the alternative splicing of genes involved in synapse formation[41]. In line with this, we detected a significant *Nova1* expression increase in cortical samples at P0 compared to E14.5 (log2 fold change = 0.84, adj. $p$-value < 0.0001) when re-analyzing the RNA-seq data from Weyn-Vanhentenryck et al.[37]. Thus, our findings further highlight the potential importance of miRNAs in regulating neurodevelopment by influencing the expression of crucial effectors of alternative splicing processes.

Remarkably, we detected the strongest co-targeting relationship between miR-137 and the miR-25/miR-363/miR-92 family, sharing 353 common gene targets (Fig. 5f). While miR-137 was upregulated at later developmental stages, all members of the miR-25/miR-363/miR-92 cluster were regulated in the opposite direction. This prominent association between hub miRNAs, that were not co-expressed, prompted us to investigate the distribution of intra-modular (between miRNAs from the same module) and inter-modular (miRNAs from different modules) co-targeting relationships for the black and green WGCNA modules. While we expected that relationships between co-expressed miRNAs might be enriched, we indeed observed a comparable distribution of intra- and inter-modular co-targeting pairs (Fig. 5e). These findings point to two distinct potential regulatory mechanisms justifying the need for miRNAs to share significantly more targets than expected by chance. On the one hand, miRNAs with common targets regulated in opposite directions during cortical development might arise from the need to facilitate target gene regulation at different time points or in distinct cell types. On the other hand, co-expressed miRNAs that regulate the same genes could cooperatively bind to their targets to exert a stronger repressive effect compared to single miRNAs.

https://doi.org/10.1038/s42003-024-07092-7 **Article**

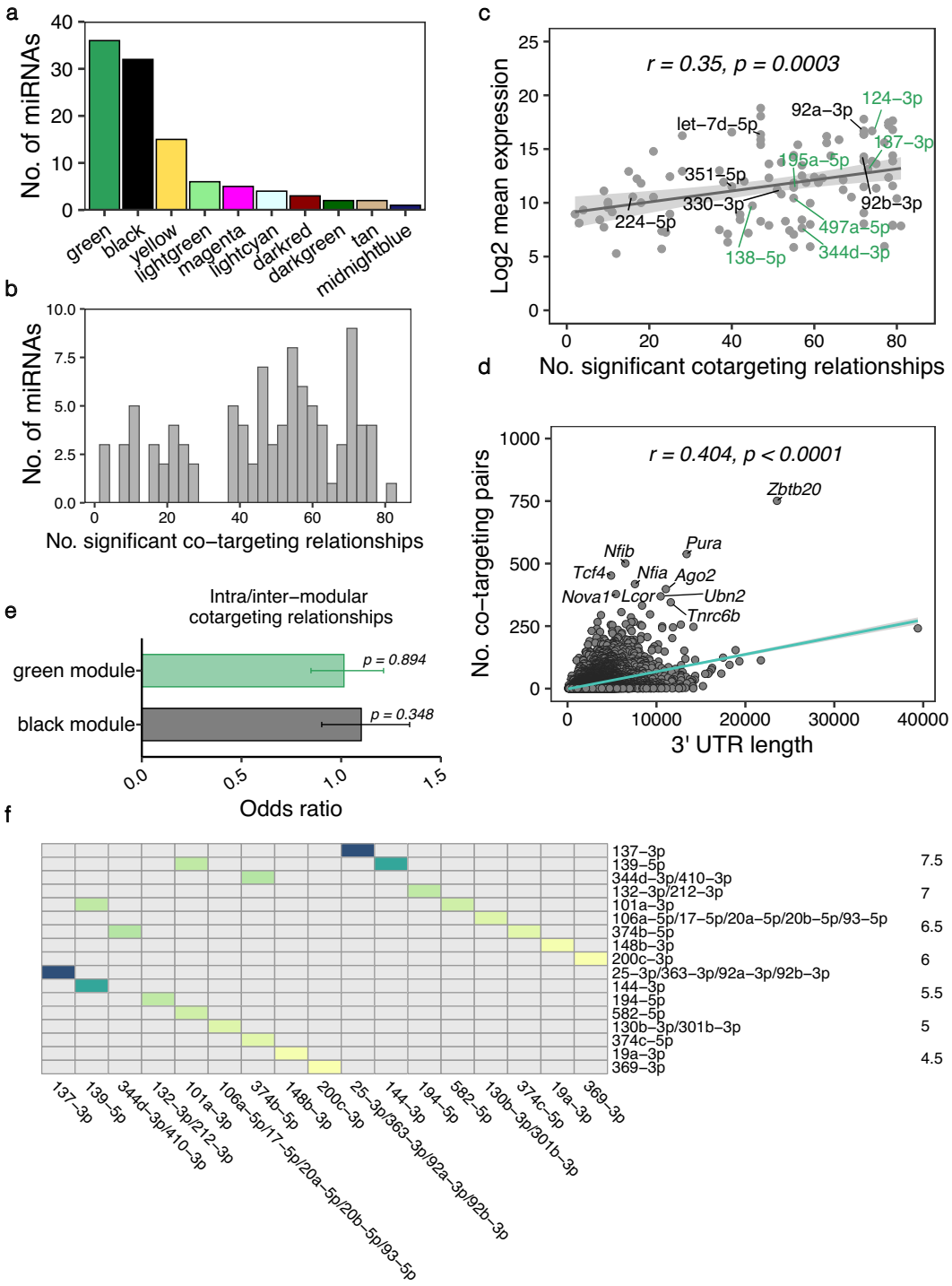


**Enhanced gene silencing effect by cooperative binding of co-expressed miRNAs**

To validate the hypothesis that co-expressed miRNAs bind co-operatively to their common targets to enhance their repressive effect, we employed luciferase reporter assays focusing on miRNAs that were upregulated during embryonic brain development. We performed a gene ontology term look-up of all targets and filtered potential candidate genes for terms including brain/forebrain development and (central) nervous system development. Then we looked for genes with two or more conserved binding sites in their 3' UTR for miRNAs upregulated during cortical development. Using this strategy, we compiled a list of 7 candidate target genes (*Neurod1, Apc, Dcx, Ndst1,*

https://doi.org/10.1038/s42003-024-07092-7 **Article**

**Fig. 5 | Features of the miRNA co-targeting network of the developing cerebral cortex.** The co-targeting network was constructed using miRNAs expressed in the mouse cerebral cortex at E14, E17 and P0. **a** Bar plot showing the number of miRNAs from each WGCNA module that were included in the co-targeting analysis after applying the filtering criteria. **b** Histogram of the number of miRNAs having a specific number of significant co-targeting relationships. **c** Scatter plot indicating the correlation between the number of co-targeting relationships with the log2-transformed miRNA's average expression level; *r* corresponds to Pearson's correlation coefficient. Labels indicate hub miRNAs from the WGCNA analysis of the black and green modules **d** Correlation between the 3' UTR length of target genes and the number of significant co-targeting miRNA pairs the genes are targeted by; *r* corresponds to Pearson's correlation coefficient. **e** Bar plot with the association of the number of intra-modular (between miRNAs of the same module) and inter-modular (involving miRNAs from different modules) co-targeting relationships. Odds ratios were obtained with a Fisher's exact test. Error bars indicate the 95% confidence interval. **f** Heatmap with the top 10 strongest co-targeting relationships between pairs of miRNAs/conserved miRNA families. Values indicate odds ratios as measures of association between the co-targeting pairs.

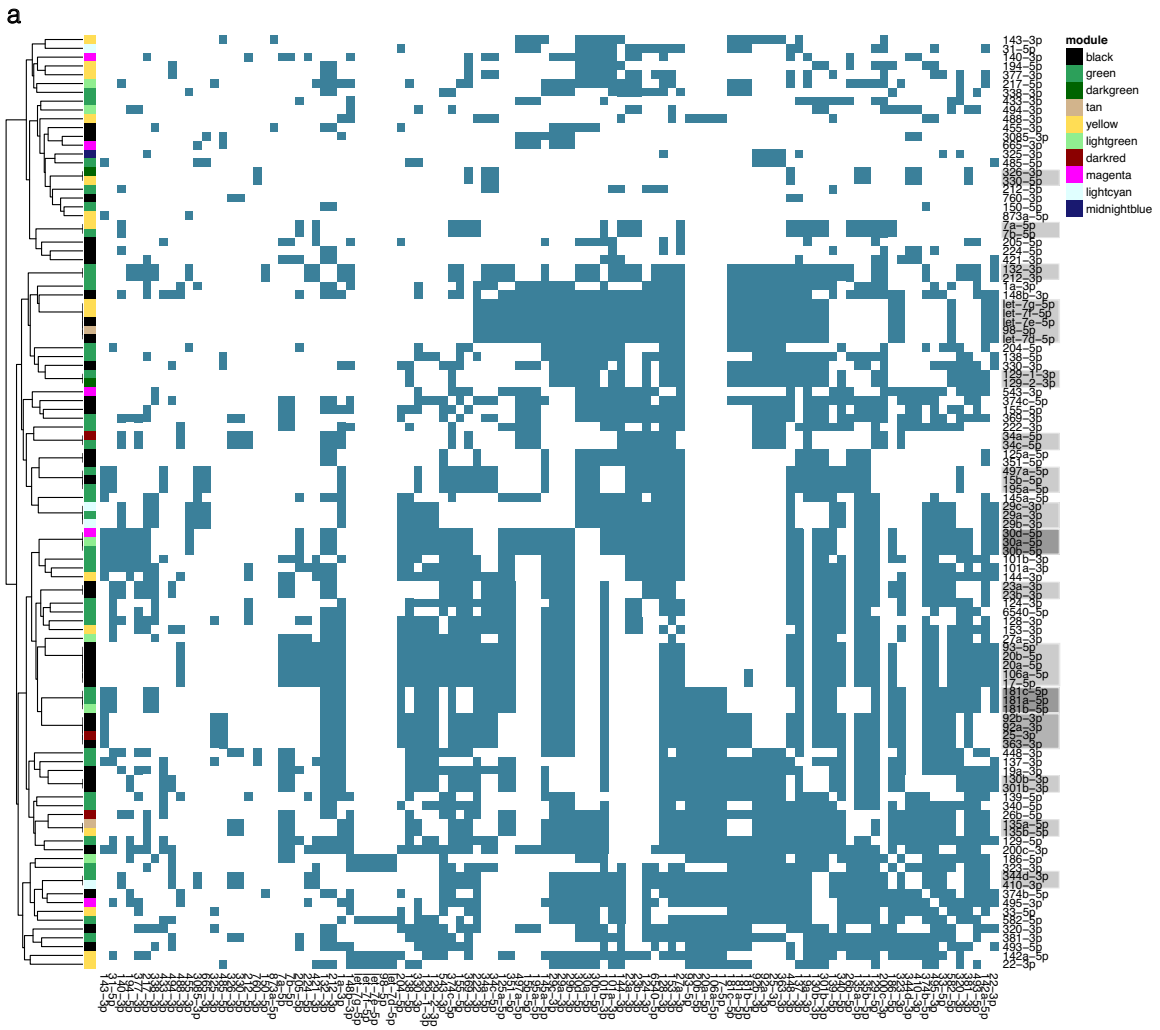


**Fig. 6 | Significant co-targeting miRNA pairs in the mouse cerebral cortex.** Colored squares on the heatmap indicate significant co-targeting relationships. miRNAs that belong to the same conserved family and therefore have identical co-targeting relationships to each other, are indicated with gray rectangles on the vertical axis of the heatmap.

*Zeb2, Src* and *Cxcl12*) and 5 miRNAs (miR-128-3p, miR-129-5p, miR-135b-5p, miR-137-3p and miR-153-3p).

First, we performed RT-qPCR analyses to validate the expression patterns that we observed in the bulk sequencing of the miRNAs selected for luciferase assays. All 5 miRNAs showed significantly increased expression levels in neurons compared to NPCs with mean relative quantification (RQ) values ranging from 2.9 to 3987 in the case of miR-135b-5p (Supplementary Fig. 4a–e). Furthermore, all miRNAs were associated with increased expression at later developmental stages in cortical tissue samples. The relative expression of miR-128-3p and miR-135b-5p significantly increased over all time points analyzed (Supplementary Fig. 4f, h). miR-137-3p and miR-153-3p were associated with a significantly higher expression levels at E17 and P0 compared to E14 (Supplementary Fig. 4 i, j). miR-129-5p was the only miRNA that showed a non-significant trend of higher expression at later developmental stages (Supplementary Fig. 4g).

Subsequently, for each luciferase reporter assay, we cloned the target gene's 3'UTR fragment containing the binding sites of the selected miRNAs, downstream of the synthetic *Renilla* luciferase gene into the psiCHECK™-2

https://doi.org/10.1038/s42003-024-07092-7 **Article**

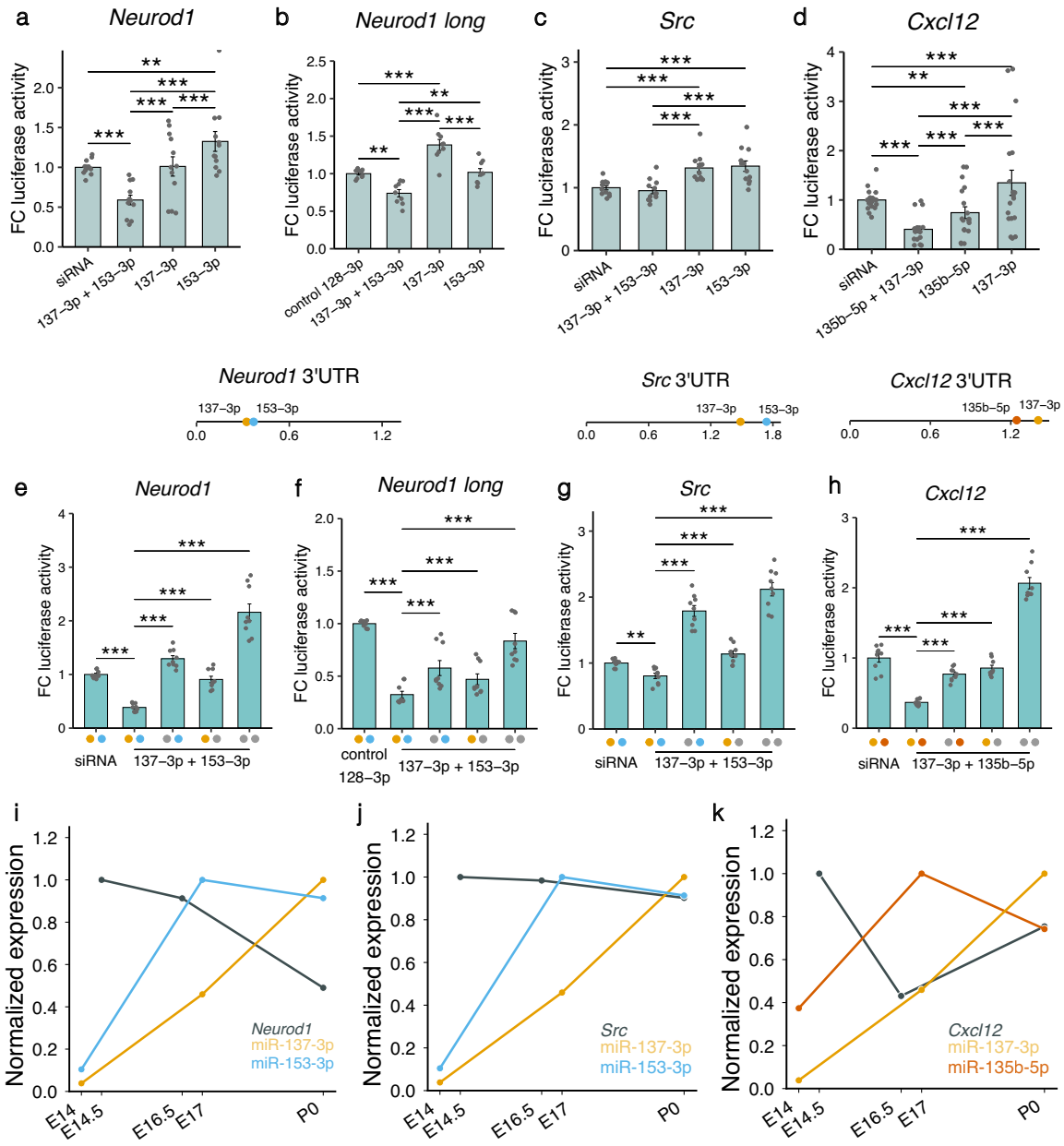


**Fig. 7 | Luciferase activity in lysates of HEK293 cells transfected with plasmids containing 3' UTR fragments of target genes. a–d** Lysates were co-transfected with different combinations of miRNA mimics. Fold change (FC) of luciferase activity was obtained by calculating the ratio of *Renilla* luciferase and firefly luciferase activity and then normalizing to the mean of the control siRNA or miRNA group. Locations of the binding sites in the 3' UTR of the respective gene are represented by colored dots. The length of the 3' UTRs is indicated in kbp. **e–h** Fold change of luciferase activity was measured after introducing point mutations in the binding sites of the miRNAs in the 3' UTR regions. Colored dots on the x-axis indicate that the binding site of the respective miRNA was intact, gray dots indicate a mutated binding site. **i–k** Expression of miRNAs and target genes during embryonic brain development. Expression values were normalized to a 0–1 range. miRNA expression was quantified by bulk RNA-seq of the mouse cerebral cortex at E14, E17 P0. Target gene expression values were measured at E14.5, E16.5 and P0 and were obtained from the bulk RNA-seq study of the mouse cerebral cortex at different developmental stages by Weyn-Vanhentenryck et al.[37]. Data are shown as mean ± standard error of the mean and individual values. $^{*}p < 0.05$, $^{**}p < 0.01$, $^{***}p < 0.001$, two-way analysis of variance followed by Tukey's post-hoc test. $N = 12$ replicates in (**a**) and (**c**), $n = 18$ in d, $n = 9$ in (**b**), (**c**) and (**e–h**), $n = 2$ in (**i–k**).

vector, which also expresses firefly luciferase as internal control. Plasmids were then co-transfected into HEK293 cells with different combinations of miRNA mimics and luciferase activity was evaluated in cell lysates 48 h later. The fold change of *Renilla*/firefly luciferase signal was normalized to a control group containing either a non-targeting siRNA or a miRNA mimic without a predicted binding site in the 3'UTR fragment of the target gene.

The first gene we investigated, *Neurod1*, is an important transcription factor regulating neuronal differentiation and migration in the developing cerebral cortex[42]. *Neurod1* contains binding sites for miR-137-3p and miR-

https://doi.org/10.1038/s42003-024-07092-7 Article

153-3p that were previously demonstrated to co-operatively repress the gene's expression[20]. Therefore, we used this experiment as a positive control. We independently cloned two *Neurod1* 3' UTR fragments with different lengths (274 bp and 1188 bp, respectively). The luciferase activity was significantly reduced in cells transfected with the combination of miR-137-3p and miR-153-3p compared to individual miRNAs as well as two different negative controls (siRNA and miR-128-3p), thereby confirming the co-targeting effect previously observed (Fig. 7a, b).

*Src*, a proto-oncogene that codes for a non-receptor protein tyrosine kinase is another important neurodevelopmental regulator that contains binding sites for both miR-137-3p and miR-153-3p in its 3'UTR. *Src* is expressed at steadily high levels in the mouse neocortex from E12.5 to P1 and overexpression of this gene leads to impaired neuronal migration due to altered adhesion properties and cytoskeletal dynamics[43]. We observed that the combination of both miRNAs exerted a significantly stronger repressive effect on *Src* compared to each individual miRNA (Fig. 7c).

As an additional target gene for the reporter assays, we selected *Cxcl12* which is also an important regulator of early brain development. *Cxcl12* is involved in migration of NPCs, early localization of Cajal-Retzius cells in the developing cortex, and in axon guidance and pathfinding[44,45]. *Cxcl12* is a predicted target of miR-137-3p and miR-135b-5p. Luciferase reporter assays showed that co-transfection with both miRNAs significantly increased the repressive effect compared to the negative siRNA control and treatment with each miRNA separately (Fig. 7d).

In contrast, we did not observe a significant co-targeting effect for miR-153-3p with miR-129-5p and miR-137-3p with miR-128-3p in reporter assays with *Apc* and *Ndst1*, respectively (Supplementary Fig. 5a, c). Furthermore, we aimed to investigate if higher-order co-targeting interactions, including three miRNAs would exert stronger silencing effects on gene expression. To this end, we co-transfected cells with plasmids containing the 3' UTR fragment of the *Dcx* gene and mimics of miR-128-3p, miR-129-5p, and miR-135b-5p (Supplementary Fig. 5b). In an additional assay, we cloned the 3' UTR of *Zeb2* and co-transfected cells with its targeting miRNAs – miR-129-5p, miR-137-3p and miR-153-3p (Supplementary Fig. 5d). Treatment with different miRNA mimics significantly reduced luciferase activity compared to the siRNA control in the *Zeb2* assays. However, we did not observe a significant cooperative repressive effect for either *Dcx* or *Zeb2*.

To confirm that the cooperative silencing effect for *Neurod1, Src*, and *Cxcl12* was mediated via direct binding of the miRNAs, we employed in vitro site-directed mutagenesis to introduce mutations in the miRNA binding sites of the 3' UTRs. We generated plasmids carrying a mutation in one of the binding sites or in both binding sites of the respective co-targeting pair. For all three genes, we observed the highest luciferase activity in the cell lysates where both miRNA binding sites were mutated. Conversely, the strongest repressive effect was detected when both binding sites were intact, thereby confirming that miRNAs acted co-operatively to exert stronger gene silencing (Fig. 7e–h). Furthermore, we investigated the expression patterns of these three genes by employing the data from Weyn-Vanhentenryck et al.[37]. *Neurod1* was significantly downregulated at P0 compared to E14.5 and E16.5, correlating negatively with the expression pattern of the co-targeting pair miR-137-3p and miR-153-3p (Fig. 7i, Supplementary Fig. 6a). While *Src* was not differentially regulated, it still had its expression minimum at P0 (Fig. 7j, Supplementary Fig. 6b). Interestingly, *Cxcl12* had a significantly reduced expression only at E16.5 compared to E14.5, but this pattern negatively correlated with the expression peak of miR-135b-5p at E17 (Fig. 7k, Supplementary Fig. 6c). These matching in vivo expression patterns of the miRNAs and the genes they co-target lend further support to the biological relevance of the co-operative miRNA gene silencing we observed in the luciferase assays.

## Discussion

Our study provides a detailed map of the longitudinal changes in miRNA expression patterns that occur in the transition between NPCs and neurons as well as in vivo at key stages of embryonic cortical development in the mouse. While previous studies have already employed high-throughput sequencing to examine miRNA composition in the embryonic cortex, they have focused on a single time point only[29,46]. In contrast, in situ hybridization-based technologies have successfully profiled miRNA expression in different embryonic brain structures and at multiple time points[47], however, this analysis has been limited to a pre-selected set of miRNAs. To our knowledge, this is the first high-throughput longitudinal investigation, therefore providing a valuable resource for elucidating the regulatory role miRNAs play during murine embryonic corticogenesis.

Remarkably, the majority of the miRNAs significantly altered their expression level already at the transition from E14 to E17. This predominantly neurogenic phase is characterized by a complex interplay of multiple processes that shape late-stage embryonic corticogenesis[48]. At E14, radial glia cells in the ventricular zone have switched from symmetrical to asymmetrical divisions to give rise to the basal progenitors that later generate neurons. Subsequently, newly born neurons migrate out of the ventricular zone to the upper layers of the neocortex where they differentiate into mature neurons. Upon neurogenesis completion at around E17, neural stem cells give rise to the other brain cell types including astrocytes and oligodendrocytes[28,30]. Cell fate commitment and neuronal identity are determined by specialized transcriptional programs that occur in sequential waves and eventually result in the immense cell type diversity observed in the brain[49,50]. The dynamic changes of miRNA expression we detected indicate that miRNA networks can act as quick regulators of these transcriptional programs by controlling the expression of cell-type specific genes[51]. miRNA-mediated transcriptional inhibition could also contribute to reducing excess levels of target mRNA arising as noise from transcriptional bursts and thereby ensuring appropriate cell-type or developmental-stage specific expression.

By employing a co-expression network analysis, we detected sets of co-regulated miRNAs with individual miRNAs acting as hubs at early (e.g., miR-92a/b) and late (e.g., miR-124 and miR-137) stages of neurogenesis. miR-92 is a part of the miR-17-92 cluster that is involved in the maintenance of neural stem cells, and its genetic ablation results in a reduced pool of neural stem and radial glia cells and a premature transition to intermediate progenitors[52]. Furthermore, miR-137 has been reported previously to influence neuronal differentiation via a regulatory loop between TLX and miR-137' downstream target LSD1[53].

Interestingly, we observed an enrichment of downregulated genes at P0 compared to E14, which were validated targets of hub miRNAs in the green module (Fig. 4e). This module consisted of miRNAs that were upregulated at P0. A GO annotation analysis revealed that many of these genes are regulators of key processes that are responsible for keeping neural stem cells in a proliferative state and blocking neuronal differentiation. For instance, the canonical NPC marker *Sox2* is crucial for the maintenance and self-renewal of progenitors[54,55], and silencing its expression promotes neuronal differentiation[54]. Another member of the SOX transcription factor family—*Sox9*, also plays an important role in maintaining neural stem cells in the early embryonic neocortex and its expression levels determine self-renewal and neurogenic division behavior of radial glial cells[56]. In fact, a recent review highlighted a complex regulatory interplay between SOX transcription factors and miRNAs that guide distinct cellular activities in the developing and adult brain under physiological and pathological conditions[57].

Green module hub miRNA targets that were downregulated at P0 also included positive regulators of Notch signaling and negative regulators of the Wnt pathway. Activation of the Notch pathway indeed leads to maintaining the neural progenitor pool[58]. Furthermore, inhibiting Wnt signaling during mid and late stages of neurogenesis in the neocortex was previously reported to result in reduced neuronal production[59].

Another crucial mechanism through which miRNAs can influence the development of the cerebral cortex is via the regulation of RNA-binding proteins. In line with this, we observed that several effectors of alternative splicing whose expression significantly changed during embryonic corticogenesis were validated targets of hub miRNAs (Fig. 4f). Alternative splicing plays a pivotal role in neuronal differentiation[60], axonogenesis[61] and

https://doi.org/10.1038/s42003-024-07092-7 **Article**

synapse formation[62]. In this context, miR-124 represents one of the most well-studied examples in neuronal differentiation. miR-124 targets PTBP1, a protein that represses neuronal splice patterns. The upregulation of miR-124 in neurons is sufficient to suppress the expression of *Ptbp1* and thereby induce the necessary splicing changes for the transition from NPCs to neurons[39]. Thus, miRNAs could act as a post-transcriptional mechanism ensuring the precise spatio-temporal expression of RNA-binding proteins which is critical for proper development of the central nervous system[63].

Surprisingly, the gene silencing effect of most miRNAs is modest despite their crucial regulatory potential[64], indicating that—with the exception of hub miRNAs—they might be fine tuners rather than master regulators of embryonic brain development. However, the redundancy of multiple co-expressed miRNAs sharing the same target genes supports the mechanism of co-operative binding to enhance the gene-silencing effect of individual miRNAs[20]. Accordingly, we confirmed the co-targeting for several neurodevelopmentally relevant genes in luciferase assays (Fig. 7). Furthermore, the negative correlation between the in vivo miRNA and target expression peaks strongly suggests that co-targeting is a biological phenomenon that can occur during embryonic cortical development. As 3' UTRs of mRNAs expressed in the brain are longer compared to other tissues[65] and this length even increases in neuronal transcripts[66], the brain indeed offers extremely favorable conditions for the emergence of miRNA multi-targeting networks[20].

Notably, significant co-targeting relationships between co-expressed miRNAs were as likely as co-targeting associations between miRNAs regulated in opposite directions. Apart from simultaneous cooperative biding to enhance gene silencing, this observation points to an alternative evolutionary need for the presence of multiple binding sites for distinct miRNAs in the same gene, namely regulating the expression at different time points or in diverse cell types. Accordingly, Nowakowski and colleagues recently reported cell-type specific miRNA-mRNA interactions in the developing human cortex using a single-cell qPCR profiling strategy[51]. Thus, distinct miRNAs might be responsible for silencing temporally or spatially abnormal expression of an overlapping set of genes. This explains our observation of miRNAs with opposite expression patterns that share more targets than expected by chance.

In summary, we detected dynamic changes in miRNA expression during embryonic brain development with distinct miRNAs acting as hubs in co-expression and co-targeting networks. Furthermore, we showed that miRNAs might be particularly important for controlling cell fate commitment and neuronal differentiation by silencing the expression of genes that promote neural stem cell proliferation and maintenance as well as NPC-like splicing patterns. Our study also provides additional evidence that simultaneous binding to common targets increases the transcriptional repression effect of miRNAs. To further resolve the complexity of mRNA-miRNA as well as miRNA co-targeting networks in distinct cell types in vivo, future studies should focus on single-cell high-throughput profiling techniques.

## Methods

### miRNA sequencing of the developing mouse cerebral cortex and in NPCs/neurons

For bulk RNA sequencing of cerebral cortex samples as E14, E17 and P0, the two cortical hemispheres of each embryo were dissected from the brains, the meninges were removed, and the cortices were stored in RNAlater solution (Sigma). To isolate total RNA (including miRNAs) from the embryonic cortices, the Trizol/Chloroform method was used. For NPC/neuron culture, the cortices of E14.5 NMRI embryos (Janvier Labs; Le Genest-Saint-Isle, France) were dissected and collected in cooled DMEM high glucose media (Gibco Life Technologies) and processed into single cells by trypsin digestion. For NPC and neuron culture, $0.2 \times 10^6$ cells per well and $1.4 \times 10^6$ cells per well, respectively, were seeded on Poly-L-ornithin and Laminin coated 6 well plates. The NPCs were cultured in neurobasal medium containing 2% B27 -VitA supplement (Gibco Life Technologies), 500 µM Glutamax (Gibco Life Technologies) and EGF (10 ng/ml) and FGF (10 ng/ml). For neural differentiation, the cells were cultured in neurobasal medium containing 2% B27 supplement (Gibco Life Technologies) and 500 µM Glutamax (Gibco Life Technologies). Total RNA, including miRNA, was isolated from the NPCs and neurons as well as from cortices of female and male NMRI embryos (Janvier Labs; Le Genest-Saint-Isle, France) at the time points E14, E17 and P0 ($n = 6$ embryos per sex and time point) using the Qiagen miRNeasy mini kit (CatNo. 217004; Qiagen; Hilden, Germany). To determine the concentration of the isolated RNA a NanodropOne Spectrometer was used (ThermoScientific). 500 ng of total RNA, including miRNA, were used as an input for library preparation with the Bioo Scientific NextFlex small RNA v3 Seq Kit (CatNo. NOVA-5132-05; Bioo Scientific; Austin, USA). Library preparation was conducted according to the kit manual. Size distribution and concentrations of the prepared libraries were checked by Qubit dsDNA High Sensitivity Assay (CatNo. Q32851; Thermo Scientific; Waltham, USA). 0.5 nanomoles (NPCs/neurons) or 4 nanomoles (cerebral cortex samples) of the prepared miRNA libraries were loaded on a High Output v2 kit (75 cycles) Illumina cartridge which was run on a NextSeq 500 device.

### miRNA sequencing data pre-processing

After the sequencing, bcl2fastq v2.17.1.14 conversion software (Illumina, Inc.) was used to demultiplex sequencing data and convert base call (BCL) files into fastq files. The trimming of the fastq files was conducted in two steps as suggested by the NEXTflex™ Small RNA Trimming Instructions. Briefly, sequencing adapters (TGGAATTCTCGGGTGCCAAGG) were trimmed and reads shorter than 15 nucleotides were removed from further analysis. Afterwards, 4 bases from either side of each read were trimmed using Cutadapt v1.18. Quality control checks were performed on the trimmed data with FastQC v0.11.7.

### miNRA differential expression analysis

miRNA samples with at least 20 million reads were further analyzed, thus 2 female samples at E14 not meeting this criteria were excluded. Using miRDeep's v2.0.1.2 *mapper.pl* script, miRNA reads were mapped to the *Mus musculus* GRCm38 genome. Afterwards, known and novel miRNA were identified using the *miRDeep2.pl* script. Prior to differential expression analysis, miRNAs with CPM expression values less than 10 were filtered out using edgeR v3.30.3. Differential expression analysis was then performed with DESeq2 v1.28.1. miRNAs with an adjusted $p$-value < 0.05 and an absolute log fold change exceeding 0.5 were considered differentially expressed. $P$-values were corrected for multiple comparisons with the Benjamini–Hochberg method.

### Weighted gene co-expression network analysis

We performed a Weighted Correlation Network Analysis (WGCNA)[36] to find clusters or "modules" of co-expressed miRNAs. For the analysis, a *bicor* correlation type and a *signed* network type with soft-thresholding power of 24, minimal module size of 5 and dynamic tree cut height of 0.2 were applied. Target prediction of the miRNAs in each module was performed using the TargetScanMouse database v7.2[67]. Functional enrichment analysis of the different modules in the co-expression network was conducted using the clusterProfiler v4.6.2 R package and the target genes of the miRNAs in the respective module as input.

### Key driver analysis

To identify hub (or key driver) miRNAs in the modules of the co-expression network, we performed a key driver analysis as previously described[34,35]. First, we used the algorithm for the reconstruction of cellular networks (ARACNE)[68] as implemented in the bnlearn R package v4.8.3 to obtain an undirected gene regulatory network from the expression levels of the miRNAs in the respective WGCNA module. Next, we performed key driver analysis on the ARACNE reconstructed network using the KDA R package v0.2.2 (https://github.com/mw201608/mnml-public/tree/master/pkgs) to identify important regulatory miRNAs.

https://doi.org/10.1038/s42003-024-07092-7 Article

### Analysis of publicly available bulk RNA-seq data of the developing mouse cortex

To explore the expression of target genes during cortical development, we re-analyzed publicly available data from the study by Weyn-Vanhentenryck et al.[37] containing RNA-seq of the mouse cortex. We focused on E14.5, E16.5, P0 as these were comparable with the time points in our study. Fastq files were downloaded from the NCBI Short Read Archive, accession number SRP055008. After trimming with BBDuk v39.01, reads were mapped to the Gencode mm39 reference genome (released 19.10.2022) using STAR v2.7.10b. A count matrix was obtained using FeatureCounts provided by SubRead v2.0.6. Differential expression analysis was performed with DESeq2 v1.40.1 with default settings. Genes with an adjusted *p*-value (Benjamini–Hochberg method) <0.05 were considered to be differentially expressed.

### miRNA expression profiling using RT-qPCR

miRNA expression patterns identified by small RNA sequencing were validated with the TaqMan MicroRNA Assay (Applied Biosystems). Reverse transcription was performed using the TaqMan MicroRNA Reverse Transcription Kit (Applied Biosystems; CatNo. 4366596). RT-qPCRs were conducted with the TaqMan Universal Master Mix II, no UNG (Applied Biosystems; CatNo. 4440040) on a StepOnePlus Real-Time PCR System (Applied Biosystems). The U6 snRNA was used as a control for normalization of experimental samples. Relative quantification (RQ) values of miRNA expression were calculated with the ΔΔCT method. Expression levels in NPCs and E14 samples, respectively, were used as reference groups. Primers used for the RT-qPCR analysis are shown in Supplementary Table 1.

### miRNA co-targeting prediction

miRNA co-targeting analysis was performed using a custom R script. We employed the TargetScanMouse database v7.2 to identify the broadly conserved mRNA targets for each miRNA. miRNAs which belong to the same broadly conserved family and therefore have identical gene target sets were grouped together for further analysis. Additionally, we only kept miRNAs with at least 300 targets[20].

Subsequently, we created a custom control set for each miRNA, containing genes with similar 3' UTR length, GC content, and sequence conservation as the actual genes included in the respective target set based on a case-control strategy. To select the best matching control for a gene *X* from the respective target set (case), first we filtered the potential pool of candidates for genes with a 3' UTR length within the range of 0.85–1.15 of the 3'UTR length of target gene *X*. Then, we filtered out genes with a GC content outside the range of 0.95–1.05 of the GC content of gene *X*. Finally, we eliminated candidates with a phyloP score outside the range of 0.8–1.2 for gene *X*. If more than one candidate remained after the filtering steps, a control gene *Y* for the target gene *X* was picked randomly. If the filtering steps returned an empty set, no control gene was selected for the respective target. This procedure was repeated for all genes included in the target set for the miRNA. The filtering cut-off values were selected empirically to maximize the number of controls while simultaneously minimizing the difference in the 3' UTR length, GC content, and phyloP score distributions of genes in the target and control sets. The similarity of the distributions of the three parameters between the control and target sets was ensured by non-significant pairwise Wilcoxon tests.

We considered miRNA *A* and miRNA *B* to be a co-targeting pair if the intersection of their target sets contained more genes than what would be expected by chance. To this end, we compared the observed number of common targets with the expected number obtained by intersecting the target set of miRNA *A* with the control set of miRNA *B* and vice versa. This yields two comparisons for each pair of miRNAs whose significance was evaluated with a Fisher's exact test. If both tests were statistically significant after a false discovery rate *p*-value adjustment (Benjamini–Hochberg method), then we considered miRNA *A* and miRNA *B* to be a bidirectional co-targeting pair. To quantify the magnitude of the co-targeting relationship, we calculated the odds ratios with values significantly higher than 1 corresponding to a pair of miRNAs sharing a significantly higher number of targets than what would be expected by chance. Higher odds ratios indicate a higher number of shared targets. To ensure that co-targeting pairs do not originate from identical seed sequences, miRNAs having identical seeds up to one mismatch were excluded a priori from the statistical analysis.

**Table 1 | Contingency table used to calculate the association between intra- and inter-modular miRNA co-targeting relationships for the black and green WGCNA modules**

| | Significant co-targeting relationship | Non-significant co-targeting relationship |
|---|---|---|
| Intra-modular | *m* | *M–m* |
| Inter-modular | *n* | *N–n* |

*m* represents the number of significant intra-modular co-targeting relationships, *M* corresponds to the total number of possible intra-modular relationships, *n* corresponds to the number of significant inter-modular relationships and *N* refers to the total number of possible inter-modular relationships. We used the following formula to calculate *M*:

$M = x(x-1)/2$

where *x* corresponds to the number of miRNAs in the respective module. The total number of possible inter-modular relationships was estimated with the formula:

$N = xy$

with *x* being the number of miRNAs in the module of interest and *y* corresponding to the number of miRNAs in the remaining modules.

### Comparing the number of intra- and inter-modular co-targeting relationships

To investigate if the black or green WGCNA modules contain more intra-modular (miRNAs of the same module) than inter-modular (miRNAs from different modules) co-targeting relationships, we performed a Fisher's exact test on the contingency table shown in Table 1.

### Luciferase reporter assays

3' UTR fragments of miRNA target genes (for primer sequences see Supplementary Table 2) were cloned into the XhoI/NotI sites downstream of the synthetic *Renilla* luciferase gene of the psiCHECK-2 vector (Promega; CatNo. C8021). Mutations in the miRNA binding sites were introduced using the QuikChange II XL system (Agilent Technologies; CatNo. 200521-5). Primers used are shown in Supplementary Table 2. $5 \times 10^4$ HEK293 cells were seeded into each well of a 12-well plate. 24 h later, 200 ng psiCHECK-2 reporter plasmid were co-transfected with 5 µl miScript miRNA mimics (Qiagen; CatNo. 219600) using 4 µl Lipofectamine 2000 Transfection Reagent (Thermo Fisher Scientific; CatNo. 11668019). Luciferase reporter assays were conducted 48 h later using the Dual-Luciferase Reporter Assay System (Promega; CatNo. E1980). Luciferase activity was measured on a CentroXS LB 960 (Berthold Technologies).

### Statistics and Reproducibility

In the analysis of qPCR and luciferase reporter assay data, two groups were compared statistically using an unpaired *t*-test or Welch's *t*-test in case of unequal variance between groups. For comparisons of three groups, a one- or two-way analysis of variance (ANOVA) followed by Tukey's post hoc test was performed. The assumptions of the linear model were evaluated by inspecting Q-Q plots and fitted values vs. residuals plots. Relative quantification values from the RT-qPCR assays were $\log_e$-transformed prior to statistical testing. All *p*-values are two-tailed and a *p*-value ≤0.05 was considered statistically significant. Statistical analysis was performed using R v. 4.2.2.

### Reporting summary

Further information on research design is available in the Nature Portfolio Reporting Summary linked to this article.

## Data availability

The raw RNA-seq data were uploaded to the Sequence Read Archive (SRA) data base under the accession number PRJNA1018560. Individual values underlying figures are provided in Supplementary data 5.

https://doi.org/10.1038/s42003-024-07092-7 **Article**

## Code availability

All analysis scripts can be obtained from the corresponding authors upon reasonable request.

Received: 14 May 2024; Accepted: 16 October 2024;
Published online: 22 October 2024

## References

1. Lee, Y. et al. MicroRNA genes are transcribed by RNA polymerase II. *EMBO J* **23**, 4051–4060 (2004).
2. Borchert, G. M., Lanier, W. & Davidson, B. L. RNA polymerase III transcribes human microRNAs. *Nat Struct Mol Biol* **13**, 1097–1101 (2006).
3. Denli, A. M., Tops, B. B., Plasterk, R. H., Ketting, R. F. & Hannon, G. J. Processing of primary microRNAs by the Microprocessor complex. *Nature* **432**, 231–235 (2004).
4. Gregory, R. I. et al. The Microprocessor complex mediates the genesis of microRNAs. *Nature* **432**, 235–240 (2004).
5. Han, J. et al. The Drosha-DGCR8 complex in primary microRNA processing. *Genes Dev* **18**, 3016–3027 (2004).
6. Yi, R., Qin, Y., Macara, I. G. & Cullen, B. R. Exportin-5 mediates the nuclear export of pre-microRNAs and short hairpin RNAs. *Genes Dev* **17**, 3011–3016 (2003).
7. Ketting, R. F. et al. Dicer functions in RNA interference and in synthesis of small RNA involved in developmental timing in C. elegans. *Genes Dev* **15**, 2654–2659 (2001).
8. O'Brien, J., Hayder, H., Zayed, Y. & Peng, C. Overview of MicroRNA Biogenesis, Mechanisms of Actions, and Circulation. *Front Endocrinol (Lausanne)* **9**, 402 (2018).
9. Davis, T. H. et al. Conditional loss of Dicer disrupts cellular and tissue morphogenesis in the cortex and hippocampus. *J Neurosci* **28**, 4322–4330 (2008).
10. McLoughlin, H. S., Fineberg, S. K., Ghosh, L. L., Tecedor, L. & Davidson, B. L. Dicer is required for proliferation, viability, migration and differentiation in corticoneurogenesis. *Neuroscience* **223**, 285–295 (2012).
11. Kawase-Koga, Y., Otaegi, G. & Sun, T. Different timings of Dicer deletion affect neurogenesis and gliogenesis in the developing mouse central nervous system. *Dev Dyn* **238**, 2800–2812 (2009).
12. Nowakowski, T. J., Mysiak, K. S., Pratt, T. & Price, D. J. Functional dicer is necessary for appropriate specification of radial glia during early development of mouse telencephalon. *PLoS One* **6**, e23013 (2011).
13. Saurat, N., Andersson, T., Vasistha, N. A., Molnar, Z. & Livesey, F. J. Dicer is required for neural stem cell multipotency and lineage progression during cerebral cortex development. *Neural Dev* **8**, 14 (2013).
14. De Pietri Tonelli, D. et al. miRNAs are essential for survival and differentiation of newborn neurons but not for expansion of neural progenitors during early neurogenesis in the mouse embryonic neocortex. *Development* **135**, 3911–3921 (2008).
15. De Pietri Tonelli, D., Clovis, Y. M. & Huttner, W. B. Detection and monitoring of microRNA expression in developing mouse brain and fixed brain cryosections. *Methods Mol Biol* **1092**, 31–42 (2014).
16. Alles, J. et al. An estimate of the total number of true human miRNAs. *Nucleic Acids Res* **47**, 3353–3364 (2019).
17. Prieto-Colomina, A., Fernández, V., Chinnappa, K. & Borrell, V. MiRNAs in early brain development and pediatric cancer: At the intersection between healthy and diseased embryonic development. *Bioessays* **43**, e2100073 (2021).
18. Winter, J. MicroRNAs of the miR379-410 cluster: New players in embryonic neurogenesis and regulators of neuronal function. *Neurogenesis (Austin)* **2**, e1004970 (2015).
19. Rago, L., Beattie, R., Taylor, V. & Winter, J. miR379-410 cluster miRNAs regulate neurogenesis and neuronal migration by fine-tuning N-cadherin. *EMBO J* **33**, 906–920 (2014).
20. Cherone, J. M., Jorgji, V. & Burge, C. B. Cotargeting among microRNAs in the brain. *Genome Res* **29**, 1791–1804 (2019).
21. Krek, A. et al. Combinatorial microRNA target predictions. *Nat Genet* **37**, 495–500 (2005).
22. Nielsen, C. B. et al. Determinants of targeting by endogenous and exogenous microRNAs and siRNAs. *RNA* **13**, 1894–1910 (2007).
23. Grimson, A. et al. MicroRNA targeting specificity in mammals: determinants beyond seed pairing. *Mol Cell* **27**, 91–105 (2007).
24. Saetrom, P. et al. Distance constraints between microRNA target sites dictate efficacy and cooperativity. *Nucleic Acids Res* **35**, 2333–2342 (2007).
25. Doench, J. G. & Sharp, P. A. Specificity of microRNA target selection in translational repression. *Genes Dev* **18**, 504–511 (2004).
26. Wu, S. et al. Multiple microRNAs modulate p21Cip1/Waf1 expression by directly targeting its 3' untranslated region. *Oncogene* **29**, 2302–2308 (2010).
27. Loo, L. et al. Single-cell transcriptomic analysis of mouse neocortical development. *Nature Communications* **10**, 134 (2019).
28. Mukhtar, T. & Taylor, V. Untangling Cortical Complexity During Development. *Journal of Experimental Neuroscience* **12**, 1179069518759332 (2018).
29. Ling, K.-H. et al. Deep sequencing analysis of the developing mouse brain reveals a novel microRNA. *BMC Genomics* **12**, 176 (2011).
30. Cadwell, C. R., Bhaduri, A., Mostajo-Radji, M. A., Keefe, M. G. & Nowakowski, T. J. Development and Arealization of the Cerebral Cortex. *Neuron* **103**, 980–1004 (2019).
31. Naka-Kaneda, H. et al. The miR-17/106–p38 axis is a key regulator of the neurogenic-to-gliogenic transition in developing neural stem/progenitor cells. *Proceedings of the National Academy of Sciences* **111**, 1604–1609 (2014).
32. Rajman, M. & Schratt, G. MicroRNAs in neural development: from master regulators to fine-tuners. *Development* **144**, 2310–2322 (2017).
33. Tsuyama, J. et al. MicroRNA-153 Regulates the Acquisition of Gliogenic Competence by Neural Stem Cells. *Stem Cell Reports* **5**, 365–377 (2015).
34. Bagot, R. C. et al. Circuit-wide Transcriptional Profiling Reveals Brain Region-Specific Gene Networks Regulating Depression Susceptibility. *Neuron* **90**, 969–983 (2016).
35. Lorsch, Z. S. et al. Stress resilience is promoted by a Zfp189-driven transcriptional network in prefrontal cortex. *Nature Neuroscience* **22**, 1413–1423 (2019).
36. Langfelder, P. & Horvath, S. WGCNA: an R package for weighted correlation network analysis. *BMC Bioinformatics* **9**, 559 (2008).
37. Weyn-Vanhentenryck, S. M. et al. Precise temporal regulation of alternative splicing during neural development. *Nature Communications* **9**, 2189 (2018).
38. Huang, H. Y. et al. miRTarBase update 2022: an informative resource for experimentally validated miRNA-target interactions. *Nucleic Acids Res* **50**, D222–d230 (2022).
39. Makeyev, E. V., Zhang, J., Carrasco, M. A. & Maniatis, T. The MicroRNA miR-124 promotes neuronal differentiation by triggering brain-specific alternative pre-mRNA splicing. *Mol Cell* **27**, 435–448 (2007).
40. Jensen, K. B. et al. Nova-1 regulates neuron-specific alternative splicing and is essential for neuronal viability. *Neuron* **25**, 359–371 (2000).
41. Ule, J. et al. Nova regulates brain-specific splicing to shape the synapse. *Nat Genet* **37**, 844–852 (2005).
42. Tutukova, S., Tarabykin, V. & Hernandez-Miranda, L. R. The Role of Neurod Genes in Brain Development, Function, and Disease. *Frontiers in Molecular Neuroscience* **14**, https://doi.org/10.3389/fnmol.2021.662774 (2021).
43. Wang, J. T. et al. Src controls neuronal migration by regulating the activity of FAK and cofilin. *Neuroscience* **292**, 90–100 (2015).
44. Li, M. & Ransohoff, R. M. Multiple roles of chemokine CXCL12 in the central nervous system: a migration from immunology to neurobiology. *Prog Neurobiol* **84**, 116–131 (2008).

https://doi.org/10.1038/s42003-024-07092-7 **Article**


45. Mithal, D. S., Banisadr, G. & Miller, R. J. CXCL12 signaling in the development of the nervous system. *J Neuroimmune Pharmacol* **7**, 820–834 (2012).
46. Dori, M. *et al*. MicroRNA profiling of mouse cortical progenitors and neurons reveals miR-486-5p as a regulator of neurogenesis. *Development* **147**, https://doi.org/10.1242/dev.190520 (2020).
47. Shu, P. et al. The spatiotemporal expression pattern of microRNAs in the developing mouse nervous system. *Journal of Biological Chemistry* **294**, 3444–3453 (2019).
48. Pilaz, L.-J. & Silver, D. L. Post-transcriptional regulation in corticogenesis: how RNA-binding proteins help build the brain. *WIREs RNA* **6**, 501–515 (2015).
49. Mukhtar, T. et al. Temporal and sequential transcriptional dynamics define lineage shifts in corticogenesis. *Embo j* **41**, e111132 (2022).
50. Telley, L. et al. Sequential transcriptional waves direct the differentiation of newborn neurons in the mouse neocortex. *Science* **351**, 1443–1446 (2016).
51. Nowakowski, T. J. et al. Regulation of cell-type-specific transcriptomes by microRNA networks during human brain development. *Nature Neuroscience* **21**, 1784–1792 (2018).
52. Bian, S. et al. MicroRNA cluster miR-17-92 regulates neural stem cell expansion and transition to intermediate progenitors in the developing mouse neocortex. *Cell Rep* **3**, 1398–1406 (2013).
53. Sun, G. et al. miR-137 forms a regulatory loop with nuclear receptor TLX and LSD1 in neural stem cells. *Nat Commun* **2**, 529 (2011).
54. Graham, V., Khudyakov, J., Ellis, P. & Pevny, L. SOX2 Functions to Maintain Neural Progenitor Identity. *Neuron* **39**, 749–765 (2003).
55. Hagey, D. W. & Muhr, J. Sox2 Acts in a Dose-Dependent Fashion to Regulate Proliferation of Cortical Progenitors. *Cell Reports* **9**, 1908–1920 (2014).
56. Fabra-Beser, J. et al. Differential Expression Levels of Sox9 in Early Neocortical Radial Glial Cells Regulate the Decision between Stem Cell Maintenance and Differentiation. *J Neurosci* **41**, 6969–6986 (2021).
57. Stevanovic, M., Stanisavljevic Ninkovic, D., Mojsin, M., Drakulic, D. & Schwirtlich, M. Interplay of SOX transcription factors and microRNAs in the brain under physiological and pathological conditions. *Neural Regen Res* **17**, 2325–2334, (2022).
58. Imayoshi, I., Sakamoto, M., Masahiro, Y., Mori, K. & Kageyama, R. Essential Roles of Notch Signaling in Maintenance of Neural Stem Cells in Developing and Adult Brains. *The Journal of Neuroscience* **30**, 3489 (2010).
59. Munji, R. N., Choe, Y., Li, G., Siegenthaler, J. A. & Pleasure, S. J. Wnt signaling regulates neuronal differentiation of cortical intermediate progenitors. *J Neurosci* **31**, 1676–1687 (2011).
60. Zhang, X. et al. Cell-Type-Specific Alternative Splicing Governs Cell Fate in the Developing Cerebral Cortex. *Cell* **166**, 1147–1162.e1115 (2016).
61. Zhang, M. et al. Axonogenesis Is Coordinated by Neuron-Specific Alternative Splicing Programming and Splicing Regulator PTBP2. *Neuron* **101**, 690–706.e610 (2019).
62. Lin, Y. S. et al. Neuronal Splicing Regulator RBFOX3 (NeuN) Regulates Adult Hippocampal Neurogenesis and Synaptogenesis. *PLoS One* **11**, e0164164 (2016).
63. Vuong, C. K., Black, D. L. & Zheng, S. The neurogenetics of alternative splicing. *Nature Reviews Neuroscience* **17**, 265–281 (2016).
64. Linsen, S. E. V., Tops, B. B. J. & Cuppen, E. miRNAs: small changes, widespread effects. *Cell Research* **18**, 1157–1159 (2008).
65. Ramsköld, D., Wang, E. T., Burge, C. B. & Sandberg, R. An abundance of ubiquitously expressed genes revealed by tissue transcriptome sequence data. *PLoS Comput Biol* **5**, e1000598 (2009).
66. Miura, P., Shenker, S., Andreu-Agullo, C., Westholm, J. O. & Lai, E. C. Widespread and extensive lengthening of 3' UTRs in the mammalian brain. *Genome Res* **23**, 812–825 (2013).
67. Agarwal, V., Bell, G. W., Nam, J.-W. & Bartel, D. P. Predicting effective microRNA target sites in mammalian mRNAs. *eLife* **4**, e05005 (2015).
68. Margolin, A. A. et al. ARACNE: An Algorithm for the Reconstruction of Gene Regulatory Networks in a Mammalian Cellular Context. *BMC Bioinformatics* **7**, S7 (2006).



## Acknowledgements
H.T. and S.G. acknowledge funding by the Landesinitiative Rheinland-Pfalz and the Resilience, Adaptation, and Longevity (ReALity) initiative of the Johannes Gutenberg University of Mainz. S.W. was funded by the Emergent Algorithmic Intelligence initiative of the Johannes Gutenberg University Mainz supported by the Carl-Zeiss foundation. J.W. acknowledges funding from the Deutsche Forschungsgemeinschaft (WI-3837 / 8-1).


## Author contributions
H.T., D.H., and S.W. performed the bioinformatics analysis. L.S. and H.M. performed miRNA sequencing, RT-qPCR and luciferase experiments. H.T. and J.W. wrote the manuscript. S.G. and J.W. supervised the study. All authors read and approved the final version of the manuscript.


## Funding
Open Access funding enabled and organized by Projekt DEAL.


## Competing interests
The authors declare no competing interests.

## Ethics
We have complied with all relevant ethical regulations for animal use. Ethical review and approval were not required for the animal study because the study did not include any animal experiments requiring approval. To carry out this study, mice were killed for organ removal. In Germany, this procedure is notifiable but does not require approval by an ethics committee.

## Additional information
**Supplementary information** The online version contains supplementary material available at https://doi.org/10.1038/s42003-024-07092-7.

**Correspondence** and requests for materials should be addressed to Susanne Gerber or Jennifer Winter.

**Peer review information** *Communications Biology* thanks the anonymous reviewers for their contribution to the peer review of this work. Primary Handling Editors: Kaliya Georgieva. A peer review file is available.

**Stage-specific expression patterns and co-targeting relationships among miRNAs in the developing mouse cerebral cortex**

Hristo Todorov, Stephan Weißbach, Laura Schlichtholz, Hanna Mueller, Dewi Hartwich, Susanne Gerber, Jennifer Winter

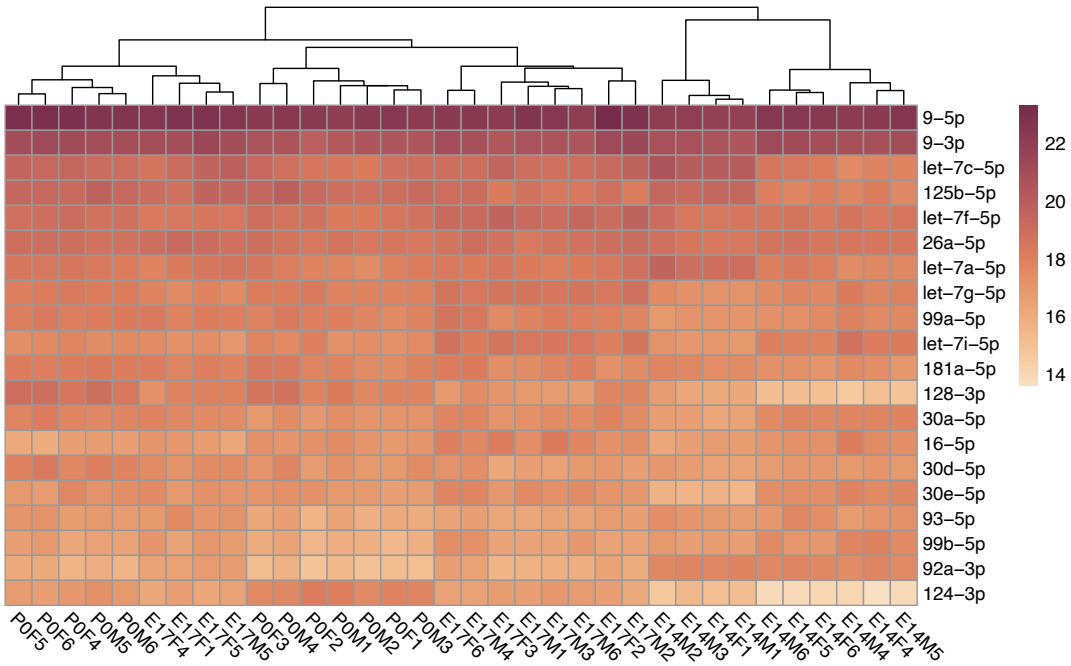


**Supplementary Figure 1. Top 20 most highly expressed miRNAs in E14, E17 and P0 mouse cortical samples.** Values in the heatmap correspond to log2-transformed normalized counts. M – males, F – females.

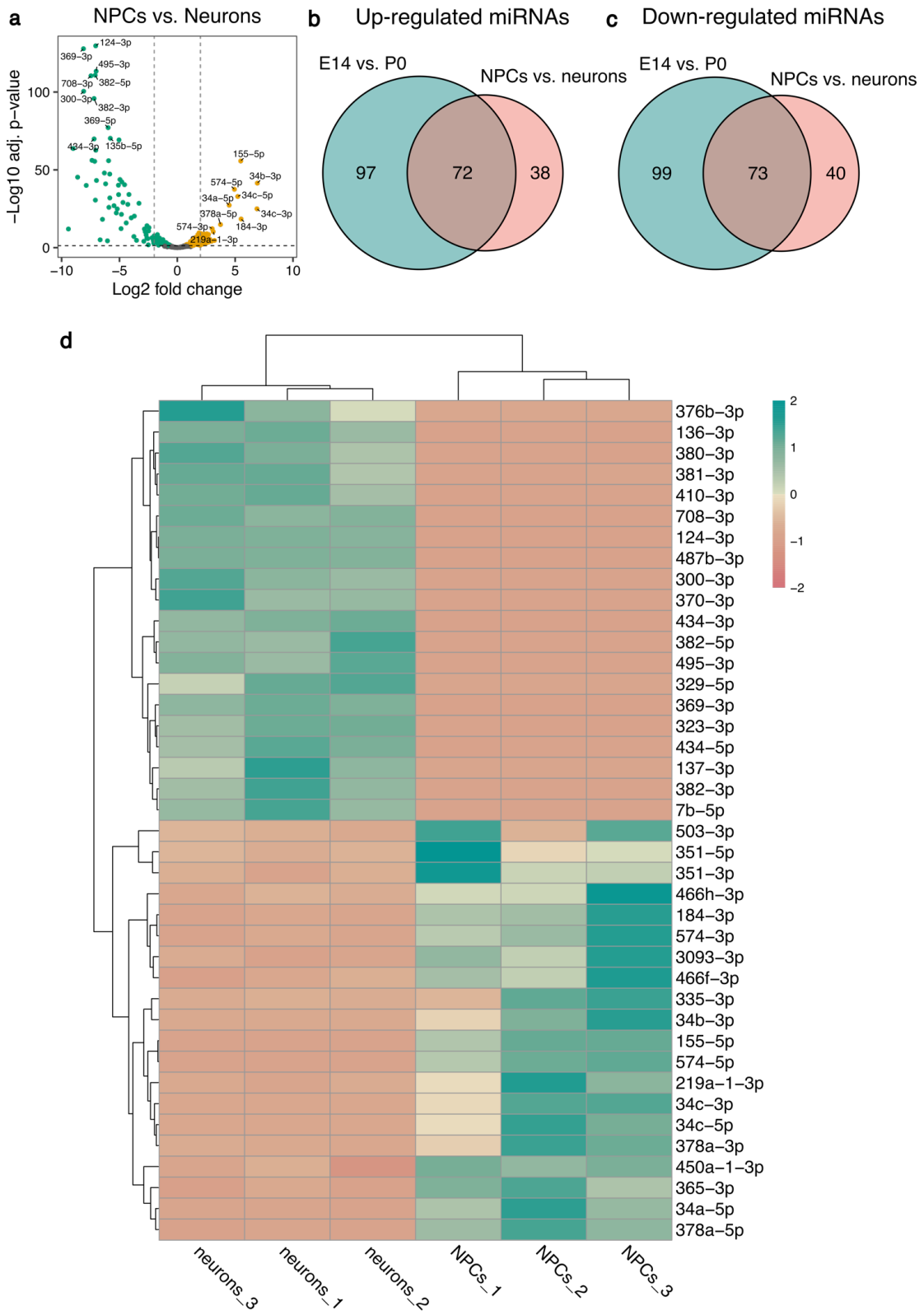
a
NPCs vs. Neurons
−Log10 adj. p−value
Log2 fold change
124−3p
369−3p
495−3p
708−3p
382−5p
300−3p
382−3p
369−5p
484−3p
135b−5p
155−5p
34b−3p
574−5p
34a−5p
34c−5p
378a−5p
34c−3p
574−3p
184−3p
219a−1−3p
b
Up-regulated miRNAs
E14 vs. P0
NPCs vs. neurons
97
72
38
c
Down-regulated miRNAs
E14 vs. P0
NPCs vs. neurons
99
73
40
d
376b−3p
136−3p
380−3p
381−3p
410−3p
708−3p
124−3p
487b−3p
300−3p
370−3p
434−3p
382−5p
495−3p
329−5p
369−3p
323−3p
434−5p
137−3p
382−3p
7b−5p
503−3p
351−5p
351−3p
466h−3p
184−3p
574−3p
3093−3p
466f−3p
335−3p
34b−3p
155−5p
574−5p
219a−1−3p
34c−3p
34c−5p
378a−3p
450a−1−3p
365−3p
34a−5p
378a−5p
neurons_3
neurons_1
neurons_2
NPCs_1
NPCs_2
NPCs_3

**Supplementary Figure 2. Differential expression analysis of miRNAs in neuronal progenitor cells (NPCs) vs. neurons. a** Volcano plot of differentially expressed miRNAs. Orange dots correspond to miRNAs up-regulated in NPCs, blue dots signify miRNAs that are up-regulated in neurons. Non-significant results are shown in gray, n = 3 biological replicates per group. **a-c** Venn diagrams showing the overlap of miRNAs that were up- or down-regulated in bulk cortical samples from E14 vs. P0 and NPCs vs. neurons. **d** Heatmap showing the expression levels of the top 20 down- and top 20 up-regulated miRNAs in NPCs vs. neurons. Values correspond to z-scores of normalized miRNA expression.

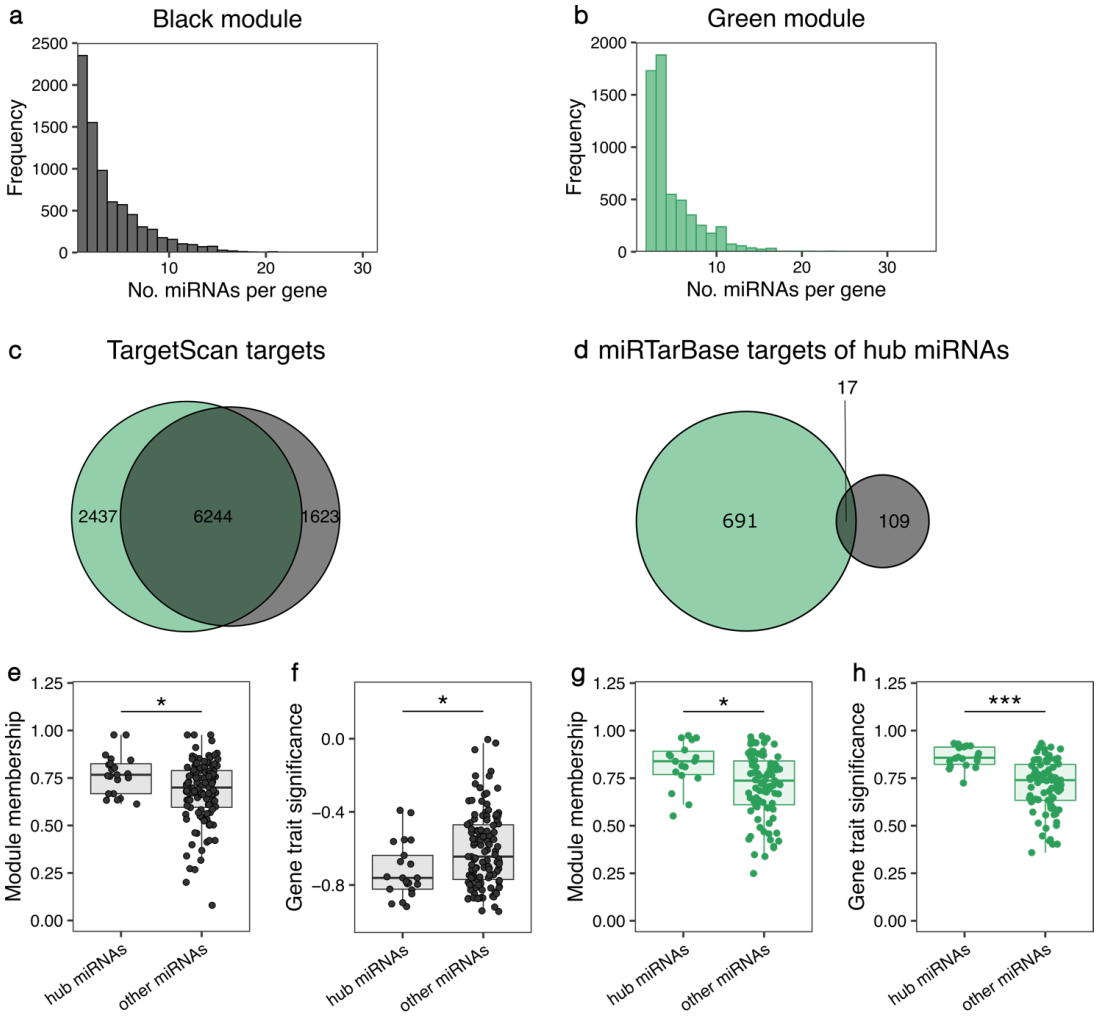


**Supplementary Figure 3. Weighted gene co-expression network analysis.** Histograms show the frequency distribution for the number of miRNAs targeting a gene for the black (**a)** and green (**b**) modules. **c** Venn diagram with the overlap of common genes targeted by miRNAs in the black and green modules. Target predictions were obtained from TargetScan using conserved miRNA families and binding sites. **d** Venn diagram with validated targets for conserved hub miRNAs from the black and green module obtained from miRTarBase. **e-h** Box

plots with the module membership and gene-trait significance values for the hub miRNAs and the remaining miRNAs in the black and green modules. ***p<0.001, * p<0.05, unpaired t-test.

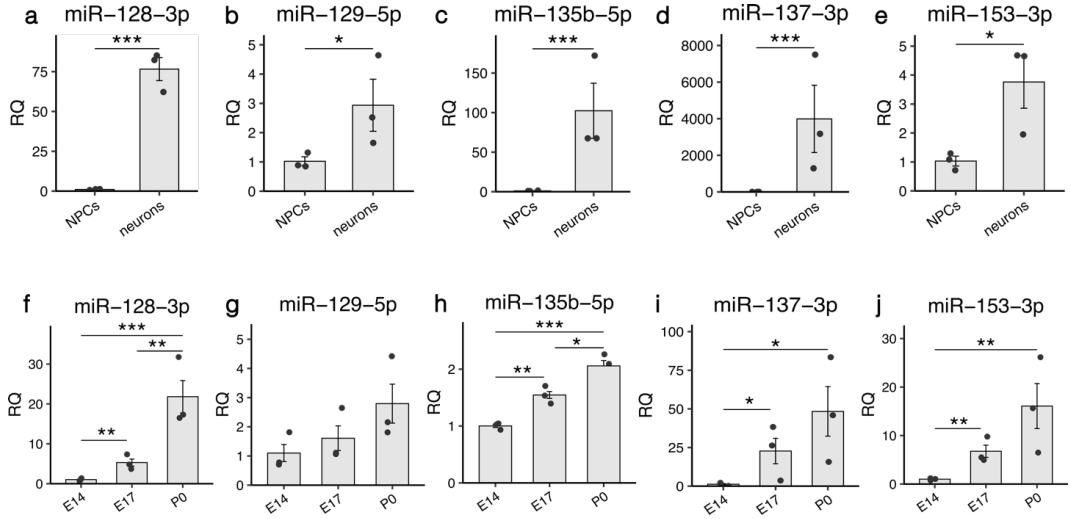


**Supplementary Figure 4. Relative quantification of miRNA expression using RT-qPCR.** **a-e** Expression levels of miRNAs selected for luciferase experiments in neuronal progenitor cells (NPCs) versus neurons. Relative quantification (RQ) values were normalized to the mean expression in NPCs.**f-j** Expression levels in cortical samples at E14, E17 and P0. RQ values were normalized to the mean expression in the E14 group.
Data are shown as mean ± standard error of the mean and individual values, n=3 biological replicates per group. *p<0.05, ** p<0.01, *** p<0.001, unpaired t-test of log-transformed RQ values.

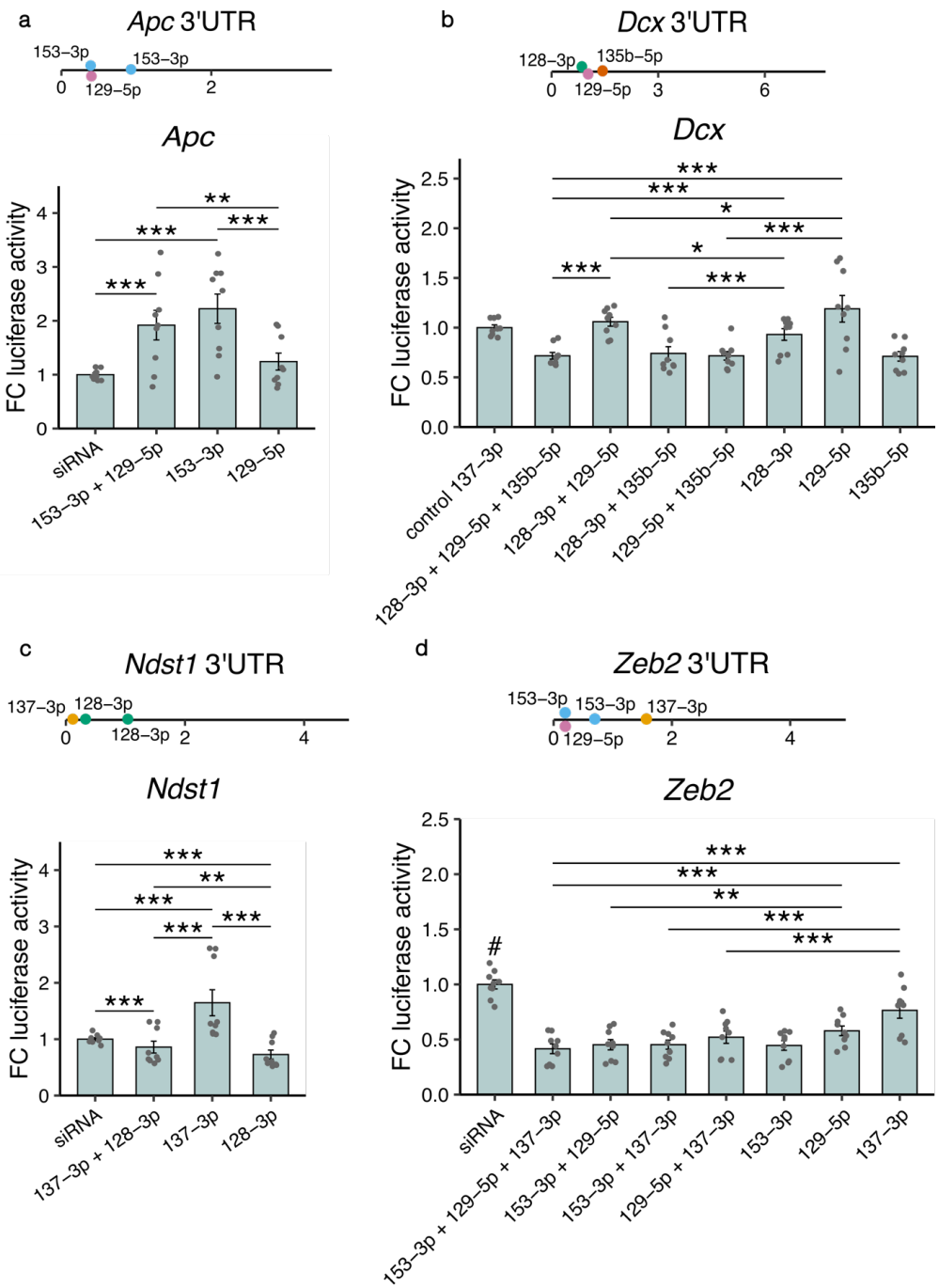


**Supplementary Figure 5. Luciferase activity in lysates of HEK293 cells transfected with plasmids containing 3' UTR fragments of target genes.** Lysates were co-transfected with different combinations of miRNA mimics. Fold change (FC) of luciferase activity was obtained by calculating the ratio of *Renilla* luciferace and firefly luciferase activity and then normalizing to the mean of the control siRNA or miRNA group. Locations of the binding sites in the 3' UTR of the respective gene are represented by colored dots. The length of the 3' UTRs is indicated in kbp. Data are shown as mean ± standard error of the mean and individual values, n=9

replicates per group. *p<0.05, ** p<0.01, *** p<0.001, only statistical comparisons containing groups with at least two miRNA mimics are shown, #p<0.05 siRNA control vs. all other groups, two-way analysis of variance followed by Tukey's post-hoc test.

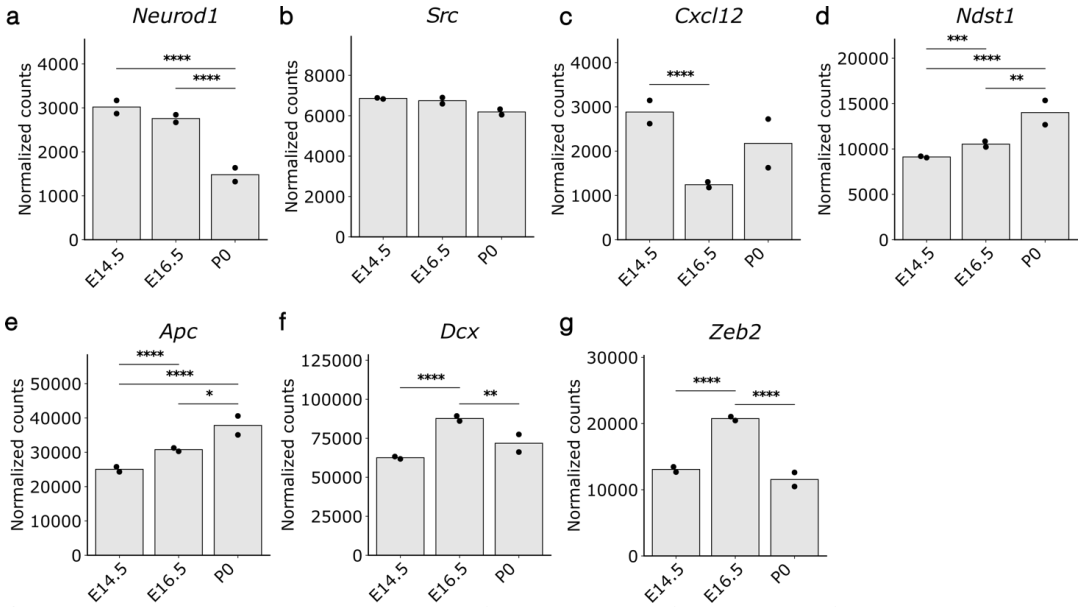


**Supplementary Figure 6. Expression of target genes from the luciferase assay at different developmental time points.** Bar plots show DESeq2-normalized counts for target genes that were used in the luciferase experiments at E14.5, E16.5 and P0 of cortical development. Data are depicted as mean and individual values. ** p<0.01, ***p<0.001, ***p<0.0001, Wald test from DESeq2, n=2 biological replicates per group. The expression values of genes were obtained by reprocessing data from the bulk RNA-seq study of the developing cerebral cortex by Weyn-Vanhentenryck et al. [1]

**Supplementary Table 1. Primers used for PCR and nested PCR of target genes used in luciferase assays.**

| Primer name | Sequence 5' to 3' | PCR product size |
|---|---|---|
| **Neurod1_XhoI_forw** | ACGTCTCGAGGCCTTTGGAAGAAACAGGGG | 274 bp |
| **Neurod1_NotI_rev** | ACGTGCGGCCGCGGTCACAGGTAGTAAAATGCTGG | |
| **Neurod1_lo_XhoI_for** | ACGTCTCGAGCGTCAGTTTCACTATTCCCGG | 1188 bp |
| **Neurod1_lo_NotI_rev** | ACGTGCGGCCGCCAGCACTTATTCTGGACTGCA | |
| **Zeb2_XhoI_forw** | ACGTCTCGAGCCAGGAAGCTGTAGAGAGGG | 1555 bp |
| **Zeb2_NotI_rev** | ACGTGCGGCCGCCAGGATCAGTTGAGAAAAGCTGT | |
| **Dcx_XhoI_forw** | ACGTCTCGAGGTTTGGGGTACATGATGTCACA | 1022 bp |
| **Dcx_NotI_rev** | ACGTGCGGCCGCCATCAGCAATGCCACCAAGT | |
| **Ndst1_XhoI_forw** | ACGTCTCGAGCTTGTGTTCGCAGGGATGTC | 1221 bp |
| **Ndst1_NotI_rev** | ACGTGCGGCCGCAGGACCCTTCAAGACTTCGC | |
| **Src_XhoI_forw** | ACGTCTCGAGCCCTGTGTGTGTGTGTTTGT | 484 bp |
| **Src_NotI_rev** | ACGTGCGGCCGCTACAACAAGTCTGGGTCCCC | |
| **Cxcl12_XhoI_forw** | ACGTCTCGAGACAGTGGGGATTCTGGGTTC | 407 bp |
| **Cxcl12_NotI_rev** | ACGTGCGGCCGCACGGTAGGAGGTTTACAGCA | |
| **Nipbl_XhoI_forw** | ACGTCTCGAGACATGCAGCCAAATTTACAGG | 748 bp |
| **Nipbl_NotI_rev** | ACGTGCGGCCGCAAGTCAGCCTGTACAAACTGT | |
| **Cited2_XhoI_forw** | ACGTCTCGAGCACAAACTGCCATCTCGCTT | 311 bp |
| **Cited2_NotI_rev** | ACGTGCGGCCGCCCTAAAAAGCTTTCAACACAGTAG | |
| **Nfib_1_XhoI_forw** | ACGTCTCGAGACATTACGTGCCTTGCCTTG | 2529 bp |
| **Nfib_1_NotI_rev** | ACGTGCGGCCGCCTTCTCTCTCCTCGCAGCTT | |
| **Nfib_2_XhoI_forw** | ACGTCTCGAGATGCATTCTTCATCGAGGGC | 957 bp |
| **Nfib_2_NotI_rev** | ACGTGCGGCCGCGTCTGTAGCATAGCTCATTT | |
| **Apc_nested_forw** | GAGCCCAAAGTCCTAAACGC | 1304 bp |

| | | |
|---|---|---|
| **Apc_nested_rev** | CGGAGAAGATGACGGGGTAA | |
| **Apc_XhoI_forw** | ACGTCTCGAGCTGGTCATTTTGGGAGGCAC | 962 bp |
| **Apc_XhoI_forw** | ACGTGCGGCCGCGCCCTTATGTCCAGTGCCTA | |

**Supplementary Table 2. Primers used for targeted in vitro mutagenesis of miRNA binding sites.**

| Primer name | Sequence 5' to 3' |
|---|---|
| **Neurod1_Mut137_forw** | CTGATCGGGATAAAAAAAATCACAAACGATAATTAGGATC |
| **Neurod1_Mut137_rev** | GATCCTAATTATCGTTTGTGATTTTTTTTATCCCGATCAG |
| **Neurod1_Mut153_forw** | TAATTAGGATCTGTACAATTTTTAAACTAGTAATGGGCC |
| **Neurod1_Mut153_rev** | GGCCCATTACTAGTTTAAAAATTGTACAGATCCTAATTA |
| **Cxcl12_Mut135b_forw** | ATATATTTGAAGTGGAGCTACAGTAATGCCAGTAGAT |
| **Cxcl12_Mut135b_rev** | ATCTACTGGCATTACTGTAGCTCCACTTCAAATATAT |
| **Cxcl12_Mut137_forw** | CTGTGACATTATATGCACTAACGATAAAATGCTAATTGTTTC |
| **Cxcl12_Mut137_rev** | GAAACAATTAGCATTTTATCGTTAGTGCATATAATGTCACAG |
| **Src_Mut137_forw** | CCATTGCCCCATCACAACGATAATGTCCCCGCTACTGG |
| **Src_Mut137_rev** | CCAGTAGCGGGGACATTATCGTTGTGATGGGGCAATGG |
| **Src_Mut153_forw** | GTAGATTTCAGATGACTGATCAGAGGCCTTGGGGACC |
| **Src_Mut153_rev** | GGTCCCCAAGGCCTCTGATCAGTCATCTGAAATCTAC |

## References

1 Weyn-Vanhentenryck, S. M. *et al.* Precise temporal regulation of alternative splicing during neural development. *Nature Communications* **9**, 2189, doi:10.1038/s41467-018-04559-0 (2018).

## 2.3 Cortexa: a comprehensive resource for studying gene expression and alternative splicing in the murine brain.

Authors: **Stephan Weißbach**, Jonas Milkovits, Stefan Pastore, Martin Heine, Susanne Gerber, Hristo Todorov

This article is published in *BMC Bioinformatics* (doi: https://doi.org/10.1186/s12859-024-05919-y).

My contributions to this article are listed in 6.1 Contribution to individual publications.

Weißbach *et al. BMC Bioinformatics* (2024) 25:293
https://doi.org/10.1186/s12859-024-05919-y

BMC Bioinformatics

DATABASE Open Access

# Cortexa: a comprehensive resource for studying gene expression and alternative splicing in the murine brain

Stephan Weißbach[1,2], Jonas Milkovits[1], Stefan Pastore[2,3], Martin Heine[1], Susanne Gerber[2*] and Hristo Todorov[2*]

*Correspondence:
sugerber@uni-mainz.de; hristo.todorov@uni-mainz.de

[1] Institute of Developmental Biology and Neurobiology (iDN), Johannes Gutenberg University Mainz, 55128 Mainz, Germany
[2] Institute of Human Genetics, University Medical Center, Johannes Gutenberg University Mainz, 55131 Mainz, Germany
[3] Institute of Pharmaceutical and Biomedical Sciences, Johannes Gutenberg University Mainz, 55128 Mainz, Germany

## Abstract

**Background:** Gene expression and alternative splicing are strictly regulated processes that shape brain development and determine the cellular identity of differentiated neural cell populations. Despite the availability of multiple valuable datasets, many functional implications, especially those related to alternative splicing, remain poorly understood. Moreover, neuroscientists working primarily experimentally often lack the bioinformatics expertise required to process alternative splicing data and produce meaningful and interpretable results. Notably, re-analyzing publicly available datasets and integrating them with in-house data can provide substantial novel insights. However, such analyses necessitate developing harmonized data handling and processing pipelines which in turn require considerable computational resources and in-depth bioinformatics expertise.

**Results:** Here, we present Cortexa—a comprehensive web portal that incorporates RNA-sequencing datasets from the mouse cerebral cortex (longitudinal or cell-specific) and the hippocampus. Cortexa facilitates understandable visualization of the expression and alternative splicing patterns of individual genes. Our platform provides SplicePCA—a tool that allows users to integrate their alternative splicing dataset and compare it to cell-specific or developmental neocortical splicing patterns. All standardized gene expression and alternative splicing datasets can be downloaded for further in-depth downstream analysis without the need for extensive preprocessing.

**Conclusions:** Cortexa provides a robust and readily available resource for unraveling the complexity of gene expression and alternative splicing regulatory processes in the mouse brain. The data portal is available at https://cortexa-rna.com/

**Keywords:** Alternative splicing, Gene expression, Cerebral cortex, Hippocampus, Embryonic brain development

## Background

Transcriptional regulation plays a crucial role in the developing and adult mammalian brain [1–3]. Major changes during development can be observed particularly in gene expression [4, 5] and alternative splicing [6–9] patterns.

Gene expression is the best-understood, and most extensively studied among these processes. It has been a major focus in the study of brain development [10], cell identity [11, 12], and disease-related alterations [13–15]. However, a common issue with gene expression analysis when comparing results from heterogenous sources is the occurrence of batch effects that are unrelated to biological factors, due to differences in sequencing technology, experimental handling, and bioinformatic processing [16–20].

Alternative splicing (AS) of precursor mRNA is a fundamental process that enables the generation of various transcripts and subsequent proteins from the same gene. Therefore, it significantly increases the available transcriptomic variability [21]. AS is particularly important in the central nervous system, playing a vital role during cortical development [6, 21] and in the determination and maintenance of neuronal cell identity [22]. Moreover, AS is an important regulator of gene expression since it can initiate the degradation of mRNA by introducing premature stop codons which leads to nonsense-mediated decay [23].

Although several high-quality datasets focusing on AS in the murine brain are freely available, interpreting the different types of splicing events for individual genes remains challenging. Moreover, harnessing the potential of multiple datasets requires a harmonized processing strategy to ensure the comparability of results. A limitation of existing data portals, namely, the single cell atlas of the Allen Brain Institute [24], Neuron Subtype Transcriptome [25], or Brain RNA-Seq [26], is that they are focused on gene expression and do not offer the analysis of custom data in the context of cell-specific or developmental changes in alternative splicing.

Here, we introduce Cortexa—a novel data portal for accessing a variety of high-quality neocortical and hippocampal transcriptomic datasets, analyzed for gene expression and alternative splicing. Batch effects between different studies have been minimized using a standardized analysis pipeline ( Figure1a). We offer easily interpretable summaries and visualization of results that allow a broad range of scientists to explore the expression and AS patterns of individual genes. Additionally, we developed SplicePCA—a tool that performs a principal component analysis of splicing events for a selected gene set and enables the investigation of splicing patterns related to developmental changes or variations across cell types [6, 27–29]. All standardized datasets included in Cortexa are publicly available for download, allowing users to integrate them into their research easily.

## Construction and content

### Datasets

We analyzed publicly available in vivo paired-end RNA sequencing data of the mouse cerebral cortex and hippocampus as well as in vivo data from neural progenitor cells (NPCs) and neurons (Fig. 1c) with a minimum read length of 100 bp. We downloaded the sequencing data from NCBI SRA or GEO respectively. Specifically, we used SRP055008 [6], GSE133291 [22], and GSE96950 [9]. Further datasets can easily be integrated, refer to https://cortexa-rna.com/datasets.

### RNA-seq analysis

We used a standardized RNA-seq pipeline (Fig. 1a) to analyze the transcriptomic data for gene expression and alternative splicing. In brief, we trimmed the reads for

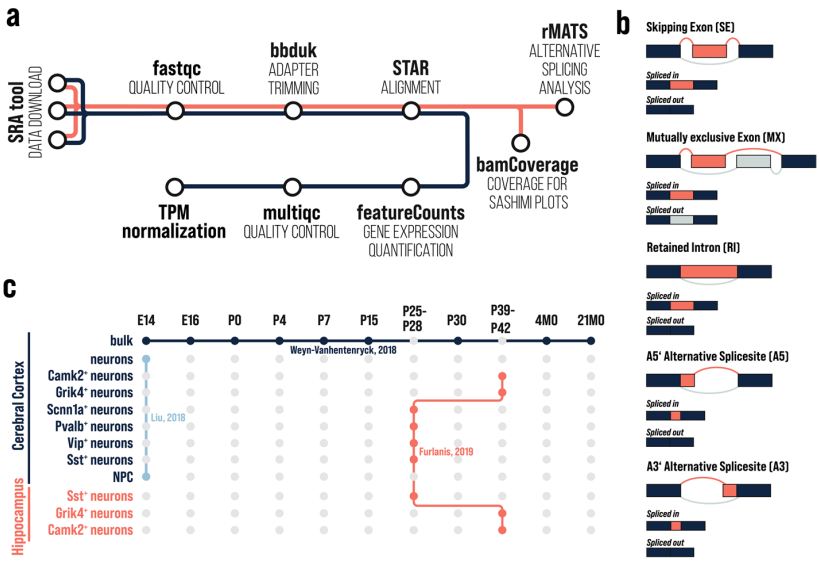


**Fig. 1** **a** Standardized RNA-seq pipeline used for gene expression (blue) and alternative splicing (orange). **b** Visualization of possible alternative splicing events and the splicing outcome referred to as spliced-in and spliced-out. **c** Publicly available datasets integrated into Cortexa: SRP055008 [6], GSE133291 [22], and GSE96950 [9]

adapter sequences with BBDuk (version 39.01) [30]. The trimmed reads were aligned to the reference genome mm39 (released 19.10.2022) downloaded from Gencode using STAR (version 2.7.10b) [31] and indexed using samtools (version 1.18) [32]. FeatureCounts, provided by SubRead (version 2.0.6) [33], was used to quantify the expression of each respective gene. All gene expression counts were normalized to transcripts per million (TPM).

We utilized rMATS turbo (version 4.1.2) [34] with default settings to detect AS events. We analyzed the data for five alternative splicing events: cassette exon (skipping exon), mutually exclusive exons, intron retention, alternative A5′ splice site, and alternative A3′ splice site (Fig. 1b), as defined in rMATS [34]. The coverage for sashimi plots was analyzed in 10 bp steps with bamCoverage (version 3.5.2) from deepTools2 [35] converted to wig with Encode bigWigToWig.

### Webapp

The web application was built with Next.js frontend framework, utilizing SQLite database for backend data storage. TypeScript enhances code maintainability and type safety, while Tailwind CSS streamlined styling. Prisma serves as the ORM tool for efficient database management. The application follows the REST principles for communication between frontend and backend components, optimizing interoperability and scalability. The website is hosted on servers of the Johannes Gutenberg University, Mainz, Germany. A detailed tutorial on how to interpret alternative splicing events presented in Cortexa is provided at https://cortexa-rna.com/tutorial.

#### Visualization of genes

Gene expression was normalized to transcripts per million (TPM) and represented as a barplot for each dataset. Alternative splicing events (Fig. 1b) are visualized as sashimi plots.

#### SplicePCA

SplicePCA performs principal component analysis (PCA) on averaged percentage spliced-in (PSI) values (Fig. 2a). Initially, the user can either select a subset of genes or perform SplicePCA on all genes. All events that have missing values are removed from the subsequent analysis. Next, PSI values are averaged within their respective group (e.g. E14.5 from the developmental data set [6]). These averaged PSI values are the input for the PCA, and the resulting values are plotted and available for download. Moreover, SplicePCA allows users to integrate their in-house analyzed output files (rMATS). We recommend processing the files as described in Sect. 3.2 and in the tutorial available at https://github.com/s-weissbach/cortexa_SplicePCA_example/.

#### Example usage of SplicePCA

To demonstrate the use of SplicePCA, we obtained *Nova2-* knock-out (KO) and wild-type (WT) data from NCBI GEO with the accession number GSE103314 [36]. We performed quality control, trimming, alignment, and alternative splicing analysis as described in Sect. 3.2 RNA-seq analysis.

Subsequently, the cassette exons from the rMATS output file were uploaded to https://cortexa-rna.com/pca and analyzed in the context of developmental [6] and NPC/neuron-specific [9] alternative splicing events. Next, the results from SplicePCA were downloaded and plotted using matplotlib (version 3.9.0) [37].

#### Utility and discussion

Alternative splicing is a prevalent regulatory mechanism in the brain that plays an important role during development and in specifying and maintaining neural cell types [6, 7, 9, 22, 28, 36, 38]. However, *Mus musculus* has ~ 22,000 protein-coding genes [39] of which almost all multi-exon genes undergo alternative splicing [40]. Functional implications of these alternative splicing events remain in many cases elusive. Cortexa is an easy-to-use web tool to access alternative splicing events for genes of interest in a developmental and neuronal cell-type-specific context to formulate and investigate research hypotheses.

Additionally, principal component analysis has proven to be a powerful tool to summarize alterations in the alternative splicing landscape [6, 27–29]. Representation of samples in two-dimensional space allows investigating the similarity or divergence of global splicing patterns between different experimental conditions. In our analysis of developmental alternative splicing, we observed a characteristic bell-shaped trajectory across diverse iterations, which aligns with findings reported in the literature [6]. However, the interpretation of principal components can be challenging in terms of associating them with biologically meaningful factors. By design, principal components capture the direction of maximal variance tin the original data [41] which

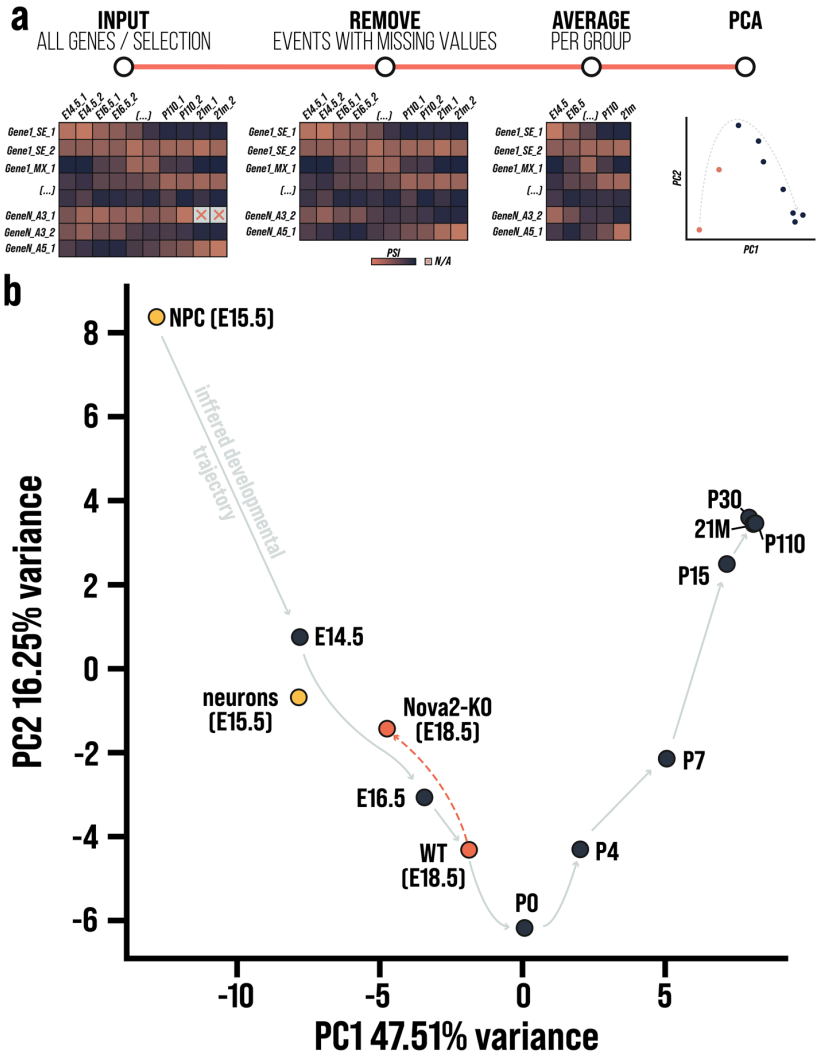


**Fig. 2** **a** Schematic representation of SplicePCA. SplicePCA takes percentage spliced-in (PSI) values for all genes or a selected subset of genes as input. Alternative spicing events with missing values are removed from the dataset. The remaining PSI values are averaged over individual replicates per experimental group. Finally, PCA is performed on the averaged data, resulting in a representation of splicing patterns across groups in two-dimensional space. **b** *Cassette exon data of cortical samples of WT (E18.5) and Nova2-KO (E18.5), analyzed with SplicePCA and compared to splicing changes across normal development of the mouse cortex. PCA of alternative splicing data across cortical development forms a characteristic bell-shaped trajectory (indicated by gray arrows) with P0 as its inflection point. The conditional knock-out of Nova2 resulted in a substantial deviation from the inferred normal splicing trajectory. Nova2-KO samples (E18.5) were associated with a less mature splicing pattern than E16.5 wild-type samples*

does not necessarily reflect experimental or biological factors. Despite these limitations, PCA remains a valuable exploratory tool, and SplicePCA offers a user-friendly method for investigating alternative splicing in the context of development or different cell types.

Using SplicePCA, researchers can select splice events for specific genes, integrate their data, and interpret results in the context of cortical development and specific neuronal cell types. To showcase the usefulness of this approach, we re-analyzed cortical *Nova2*-KO and WT samples at embryonic day E18.5 [36] and used the SplicePCA tool. NOVA2 belongs to the class of RNA-binding proteins, governing alternative splicing during cortical development and in mature neurons [42]. Specifically, NOVA2 is required to regulate neuronal migration through splicing *Dab1* which is part of the Reelin pathway [2]. By using SplicePCA, we revealed a striking effect of *Nova2*-KO during cortical development. E18.5 knockout samples were located between E14.5 and E16.5 wild-type samples on the inferred developmental splicing trajectory, indicating a less mature splicing pattern (Fig. 2b). Thus, NOVA2 splicing activity contributes significantly to the splicing changes between E14.5 to E18.5, as reported previously [2, 36, 43]. These results support the relevance of SplicePCA which combines available datasets with new datasets. Cortexa thus allows the use of publicly available data without extensive re-analysis, which would otherwise require significant computational resources.

## Conclusions

In summary, Cortexa gives access to high-quality, publicly available transcriptomic data to a broad range of scientists without the need to gain expertise in the computational aspects of gene expression and alternative splicing analysis. For experienced users, SplicePCA offers a powerful tool to summarize alterations in the alternative splicing landscapes upon experimental manipulation and compare results to the normal splicing trajectory during cerebral cortical development or in distinct neuronal cell types. Ultimately, Cortexa offers an easy-to-use extensive platform for gaining novel insights into gene expression and alternative splicing regulatory processes of the mouse brain.

**Acknowledgements**
Not applicable.

**Author contributions**
S.W. and H.T. conceived the idea and conceptualized the work. H.T., S.G., and M.H. supervised the project. S.W. and S.P. performed the bioinformatic analysis. J.M. and S.W. implemented and tested the website. S.W. created visualizations. S.W. and H.T. wrote the manuscript. M.H. and S.G. acquired funding and edited the manuscript.

**Funding**
Open Access funding enabled and organized by Projekt DEAL. This work has been supported by the Emergent Algorithmic Intelligence Centre of the Johannes Gutenberg University Mainz, funded by the Carl-Zeiss Foundation.

**Availability of data and materials**
Publicly available sequencing data were downloaded from NCBI SRA or GEO respectively. Specifically, we used SRP0550086, GSE13329122, and GSE969509. The Nova2-KO data that were used to test SplicePCA and a tutorial are available on GitHub at https://github.com/s-weissbach/cortexa_SplicePCA_example/. All processed datasets used in this study are available on Zenodo at https://zenodo.org/records/13170518.

## Declarations

**Ethics approval and consent to participate**
Not applicable.

**Consent for publication**
Not applicable.

**Competing interests**
The authors declare no competing interests.

Received: 6 June 2024 Accepted: 28 August 2024
Published online: 05 September 2024

**References**

1. Lennox AL, Mao H, Silver DL. RNA on the brain: emerging layers of post-transcriptional regulation in cerebral cortex development. WIREs Dev Biol. 2018;7: e290.
2. Vuong CK, Black DL, Zheng S. The neurogenetics of alternative splicing. Nat Rev Neurosci. 2016;17:265–81.
3. He X, Rosenfeld MG. Mechanisms of complex transcriptional regulation: implications for brain development. Neuron. 1991;7:183–96.
4. Loo L, et al. Single-cell transcriptomic analysis of mouse neocortical development. Nat Commun. 2019;10:134.
5. Telley L, et al. Sequential transcriptional waves direct the differentiation of newborn neurons in the mouse neocortex. Science. 2016;351:1443–6.
6. Weyn-Vanhentenryck SM, et al. Precise temporal regulation of alternative splicing during neural development. Nat Commun. 2018;9:2189.
7. Zhang X, et al. Cell-type-specific alternative splicing governs cell fate in the developing cerebral cortex. Cell. 2016;166:1147-1162.e15.
8. Baralle FE, Giudice J. Alternative splicing as a regulator of development and tissue identity. Nat Rev Mol Cell Biol. 2017;18:437–51.
9. Liu J, Geng A, Wu X, Lin R-J, Lu Q. Alternative RNA splicing associated with mammalian neuronal differentiation. Cereb Cortex. 2018;28:2810–6.
10. Kang HJ, et al. Spatio-temporal transcriptome of the human brain. Nature. 2011;478:483–9.
11. Scholpp S, et al. Her6 regulates the neurogenetic gradient and neuronal identity in the thalamus. Proc Natl Acad Sci. 2009;106:19895–900.
12. Bedogni F, et al. Tbr1 regulates regional and laminar identity of postmitotic neurons in developing neocortex. Proc Natl Acad Sci. 2010;107:13129–34.
13. Fromer M, et al. Gene expression elucidates functional impact of polygenic risk for schizophrenia. Nat Neurosci. 2016;19:1442–53.
14. Zhang B, et al. Integrated systems approach identifies genetic nodes and networks in late-onset Alzheimer's disease. Cell. 2013;153:707–20.
15. Voineagu I, et al. Transcriptomic analysis of autistic brain reveals convergent molecular pathology. Nature. 2011;474:380–4.
16. Goh WWB, Wang W, Wong L. Why batch effects matter in omics data, and how to avoid them. Trends Biotechnol. 2017;35:498–507.
17. Zheng W, Chung LM, Zhao H. Bias detection and correction in RNA-Sequencing data. BMC Bioinform. 2011;12:290.
18. Weißbach S, et al. Reliability of genomic variants across different next-generation sequencing platforms and bioinformatic processing pipelines. BMC Genom. 2021;22:1–15.
19. Zhang Y, Parmigiani G, Johnson WE. ComBat-seq: batch effect adjustment for RNA-seq count data. NAR Genom Bioinform. 2020;2:lqaa078.
20. O'Rawe J, et al. Low concordance of multiple variant-calling pipelines: practical implications for exome and genome sequencing. Genome Med. 2013;5:28.
21. Raj B, Blencowe BJ. Alternative splicing in the mammalian nervous system: Recent insights into mechanisms and functional roles. Neuron. 2015;87:14–27.
22. Furlanis E, Traunmüller L, Fucile G, Scheiffele P. Landscape of ribosome-engaged transcript isoforms reveals extensive neuronal-cell-class-specific alternative splicing programs. Nat Neurosci. 2019;22:1709–17.
23. Lewis BP, Green RE, Brenner SE. Evidence for the widespread coupling of alternative splicing and nonsense-mediated mRNA decay in humans. Proc Natl Acad Sci. 2003;100:189–92.
24. Yao Z, et al. A high-resolution transcriptomic and spatial atlas of cell types in the whole mouse brain. Nature. 2023;624:317–32.
25. Huntley MA, et al. Genome-wide analysis of differential gene expression and splicing in excitatory neurons and interneuron subtypes. J Neurosci. 2020;40:958–73.
26. Zhang Y, et al. An RNA-sequencing transcriptome and splicing database of glia, neurons, and vascular cells of the cerebral cortex. J Neurosci. 2014;34:11929–47.
27. Feng H, et al. Complexity and graded regulation of neuronal cell-type–specific alternative splicing revealed by single-cell RNA sequencing. Proc Natl Acad Sci. 2021;118: e2013056118.
28. Jacko M, et al. Rbfox splicing factors promote neuronal maturation and axon initial segment assembly. Neuron. 2018;97:853-868.e6.
29. Martí-Gómez C, et al. Functional impact and regulation of alternative splicing in mouse heart development and disease. J Cardiovasc Transl Res. 2022;15:1239–55.
30. BBMap. SourceForge https://sourceforge.net/projects/bbmap/ (2022).
31. Dobin A, et al. STAR: ultrafast universal RNA-seq aligner. Bioinformatics. 2013;29:15–21.
32. Danecek P, et al. Twelve years of SAMtools and BCFtools. GigaScience. 2021;10:giab008.
33. Liao Y, Smyth GK, Shi W. featureCounts: an efficient general purpose program for assigning sequence reads to genomic features. Bioinformatics. 2014;30:923–30.
34. Shen S. rMATS: robust and flexible detection of differential alternative splicing from replicate RNA-Seq data | PNAS. Proc Natl Acad Sci. 2014. https://doi.org/10.1073/pnas.1419161111.
35. Ramírez F, et al. deepTools2: a next generation web server for deep-sequencing data analysis. Nucleic Acids Res. 2016;44:W160–5.

36. Saito Y, et al. Differential NOVA2-mediated splicing in excitatory and inhibitory neurons regulates cortical development and cerebellar function: neuron. Neuron. 2019;101:707-720.E5.
37. Ari N, Ustazhanov M. Matplotlib: a 2D graphics environment. IEEE J Mag. 2014.
38. Heck J, et al. More than a pore: how voltage-gated calcium channels act on different levels of neuronal communication regulation. Channels. 2021;15:322–38.
39. Breschi A, Gingeras TR, Guigó R. Comparative transcriptomics in human and mouse. Nat Rev Genet. 2017;18:425–40.
40. Jiang W, Chen L. Alternative splicing: Human disease and quantitative analysis from high-throughput sequencing. Comput Struct Biotechnol J. 2021;19:183–95.
41. Todorov H, Fournier D, Gerber S. Principal components analysis: theory and application to gene expression data analysis. Genom Comput Biol. 2018;4: 100041.
42. Meldolesi J. Alternative splicing by NOVA factors: from gene expression to cell physiology and pathology. Int J Mol Sci. 2020;21:3941.
43. Yano M, Hayakawa-Yano Y, Mele A, Darnell RB. Nova2 regulates neuronal migration through an RNA switch in disabled-1 signaling. Neuron. 2010;66:848–58.

## Publisher's Note

## 2.4 More than a pore: How voltage-gated calcium channels act on different levels of neuronal communication regulation

Authors: Jennifer Heck, Carolina Palmeira, **Stephan Weißbach**, Abderazzaq El Khallouqi, Arthur Bikbaev, Martin Heine

This article is published in *Channels* (doi: https://doi.org/10.1080/19336950.2021.1900024)

My contributions to this article are listed in 6.1 Contribution to individual publications.

CHANNELS
2021, VOL. 15, NO. 1, 322–338
https://doi.org/10.1080/19336950.2021.1900024

Taylor & Francis
Taylor & Francis Group

REVIEW



# More than a pore: How voltage-gated calcium channels act on different levels of neuronal communication regulation

Jennifer Heck [a], Ana Carolina Palmeira Do Amaral[a], Stephan Weißbach[a,b], Abderazzaq El Khallouqi[a], Arthur Bikbaev[a], and Martin Heine[a]

[a]Functional Neurobiology, Johannes Gutenberg-University Mainz, Institute for Developmental Biology and Neurobiology, Mainz, Germany; [b]Computational Genomics and Bioinformatics, Johannes Gutenberg-University Mainz, University Medical Center Mainz, Institute for Human Genetics, Mainz, Germany

**ABSTRACT**

Voltage-gated calcium channels (VGCCs) represent key regulators of the calcium influx through the plasma membrane of excitable cells, like neurons. Activated by the depolarization of the membrane, the opening of VGCCs induces very transient and local changes in the intracellular calcium concentration, known as calcium nanodomains, that in turn trigger calcium-dependent signaling cascades and the release of chemical neurotransmitters. Based on their central importance as concierges of excitation-secretion coupling and therefore neuronal communication, VGCCs have been studied in multiple aspects of neuronal function and malfunction. However, studies on molecular interaction partners and recent progress in omics technologies have extended the actual concept of these molecules. With this review, we want to illustrate some new perspectives of VGCCs reaching beyond their function as calcium-permeable pores in the plasma membrane. Therefore, we will discuss the relevance of VGCCs as voltage sensors in functional complexes with ryanodine receptors, channel-independent actions of auxiliary VGCC subunits, and provide an insight into how VGCCs even directly participate in gene regulation. Furthermore, we will illustrate how structural changes in the intracellular C-terminus of VGCCs generated by alternative splicing events might not only affect the biophysical channel characteristics but rather determine their molecular environment and downstream signaling pathways.

**ARTICLE HISTORY**
Received 19 January 2021
Revised 4 March 2021
Accepted 4 March 2021

**KEYWORDS**
Ion channels; voltage-gated calcium channels; VGCC auxiliary subunits; $\alpha_2\delta$ subunits; $Ca_v\beta$ subunits; synaptogenesis; gene regulation; synaptic transmission; voltage-induced calcium release; alternative splicing

## Introduction

Transient changes of the intracellular calcium concentration are a major trigger for many signaling cascades and cellular processes. Besides being a key parameter for neuronal communication, intracellular calcium levels control the entire cell life from fertilization to programmed cell death and regulate, inter alia, gene expression, heart and muscle contraction, as well as enzyme activity within subcellular compartments [1–3]. In excitable cells like neurons, voltage-gated calcium channels (VGCCs) are important regulators of the calcium concentration by controlling the influx of calcium ions ($Ca^{2+}$) across the plasma membrane [4–6]. The huge signaling power of $Ca^{2+}$ , which is the most widely used and at the same time most strictly controlled second messenger molecule [1,7], might account for the fact that mutations in VGCCs have been reported in the context of severe disorders reaching from cardiovascular channelopathies to neurological and psychiatric conditions such as ataxic and epileptic phenotypes, chronic pain, autism, schizophrenia, and depression [8–10]. However, there is a growing body of evidence suggesting that the functional relevance of VGCCs goes beyond their central role as $Ca^{2+}$ -conducting elements. One structural feature that might facilitate such a many-sided picture of VGCCs is their design as multi-subunit complexes. The basic $Ca^{2+}$ -conducting pore is formed by the $\alpha_1$ subunit, a 190–270 kDa membrane-spanning protein. Today, ten variants of the pore forming $\alpha_1$ calcium channel subunits have been described and grouped into three families, termed $Ca_V1$, $Ca_V2$ and $Ca_V3$, based on their biophysical kinetics and pharmacological properties [4,11]. This diversity of calcium channel phenotypes is strongly increased by the association of

**CONTACT** Jennifer Heck PhD jeheck@uni-mainz.de Johannes Gutenberg-University Mainz, Institute for Developmental Biology and Neurobiology, Functional Neurobiology, Hanns-Dieter Hüsch Weg 15, 55128 Mainz, Germany

the auxiliary subunits β, $\alpha_2\delta$, and γ as well as many other regulatory proteins that interact with specific binding domains located in the intracellular loops of $\alpha_1$[9,12]. Historically, the functional importance of auxiliary VGCC subunits was considered primarily in association with the $\alpha_1$ pore of $Ca_V1$ and $Ca_V2$ high-voltage-activated (HVA) VGCCs. From this point of view, β and $\alpha_2\delta$ isoforms were extensively shown to promote the trafficking of the channel to the membrane, as well as to significantly modulate the biophysical properties of the multi-subunit channel complex [13,14]. However, several reports published over the last two decades demonstrate that VGCC auxiliary subunits can serve additional functions, which do not necessarily involve or require a direct interaction with the channel pore. Furthermore, there are studies suggesting that the pore-forming subunit of VGCCs, besides being the traditional source of $Ca^{2+}$ from the extracellular space, has some side-functions, e.g. as voltage sensor and interaction partner for signaling complexes as well as in gene expression. These extended roles of VGCCs will be discussed in the following to illustrate some possibilities of how VGCCs might participate in neuronal network development, maintenance, and plasticity.

## VGCCs: Not only voltage-gating but voltage-sensing

As already mentioned above, VGCCs are key regulators of the $Ca^{2+}$ influx across the plasma membrane of excitable cells. In neurons, they have been widely described to shape neuronal communication by initializing the release of neurotransmitter molecules. This process mainly involves the transient influx of $Ca^{2+}$ in response to the depolarization of the plasma membrane triggered by an arriving action potential and is therefore known as excitation-secretion coupling [4–6]. However, besides the $Ca^{2+}$-conducting aspect, a second key feature of VGCCs is their ability to sense membrane depolarization to initialize channel gating. The role VGCCs as voltage sensors was firstly described in skeletal muscle. Here, the excitation-contraction coupling does not require the influx of extracellular $Ca^{2+}$ via VGCCs but rather depends on their voltage-sensing properties to trigger the release of $Ca^{2+}$ from intracellular stores of the sarcoplasmic reticulum [15–17]. This functional coupling involves the physical interaction of $Ca_V1.1$, a member of the $Ca_V1$ family, and calcium release channels in the sarcoplasmic reticulum called ryanodine receptors (RyR), especially the isoform 1, called RyR1. When binding to the skeletal RyR1, $Ca_V1.1$ transduces the sarcolemma depolarization to directly induce a mechanical gating of RyR1 by conformational interaction resulting in calcium release from intracellular stores [18,19]. Interestingly, the molecular basics and, more importantly, a similar process of voltage-induced calcium release (also called depolarization-induced calcium release) has been documented in the brain and spinal cord [20–23]. Mouton and colleagues have found RyR1 channels, although poorly expressed in the brain when compared to the other RyR isoforms 2 and 3 [23–27], in a complex with the pore-forming subunits of the $Ca_V1$ family members $Ca_V1.2$ and $Ca_V1.3$ in the rat brain [22]. The mechanical coupling between RyR1 and $Ca_V1$ channels was later shown to be specific for $Ca_V1.2$, while RyR2 was associated with $Ca_V1.3$ in spinal cord dorsal columns and whole brain [20]. A study by Kim et al. has further characterized the specific interaction of $Ca_V1.3$ and RyR2 in the rat hippocampus and demonstrated the importance of both N termini of $Ca_V1.3$ and RyR2 for their functional coupling [23]. Notably, also the activation of RyR2 in hippocampal neurons seems to be independent of the $Ca^{2+}$ influx through $Ca_V1.3$ since RyR2 opening was also triggered in $Ca^{2+}$ -free extracellular solution [23]. This highlights the function of $Ca_V1.3$ as a voltage sensor in neurons, which seems to differ from its classical role in the cardiac muscle where $Ca_V1.3$ opening has been widely reported to trigger calcium-induced calcium release [28]. Although the co-localization of Cav1 isoforms and RyRs in neurons was confirmed using immunocytochemistry and super-resolution microscopy [23,29], it has been noted that only a few of the $Ca_V1$-RyR complexes appear co-localized and are sparsely distributed along axon cylinders [20]. More recently, studies have revealed additional interaction partners, including potassium channels and junctophilin proteins, participating in a multi-protein complex on the junction between the outer plasma membrane and the ER in mammalian

neurons (Fig.1) [29,30]. However, further investigation is necessary to evaluate the stability of these complexes and their functional implication for, e.g. synaptic plasticity. Suggestions have been made on a role in activity-dependent transport of signaling molecules [20], neuronal excitability [29], and a possible link to transmit membrane activity to gene expression in the nucleus [22]. From a pathophysiological perspective, it has been shown that RyR1 mediates the release of damaging quantities of $Ca^{2+}$ from the ER when triggered by ischemic depolarizations sensed by $Ca_V1.2$ in rat dorsal columns [20]. Therefore, the voltage-sensing contribution of VGCCs in the release of $Ca^{2+}$ from intracellular stores should be considered when studying pathophysiological elevations of calcium levels involved in, e.g. axonal damage [31]. Although a participation of the $Ca^{2+}$ influx through VGCCs cannot be ruled out completely, especially for $Ca_V1.3$-RyR2-complexes, this functional coupling is a first example of how VGCCs, as calcium sensors and interaction partners, can contribute to more complex signaling mechanisms.

## C-terminal fragments of the VGCC pore and $Ca_V\beta$ subunits participate in gene regulation

Since intracellular $Ca^{2+}$ acts as a second messenger molecule in a plethora of signaling pathways [1], it is evident that VGCCs, beeing main plasma membrane $Ca^{2+}$ sources in excitable cells, contribute to transcriptional regulation processes [32]. This excitation-transcription coupling allows the conversion of activity-induced, very local calcium transients into long-term effects on gene regulation pathways with distinct transcription factors. Early studies have already demonstrated that the genes regulated via VGCC-induced $Ca^{2+}$ influx differ from those targeted by other $Ca^{2+}$ origins, for example, receptor-activated $Ca^{2+}$ channels like NMDA receptors, store-operated $Ca^{2+}$ channels like ORAI and TRP members, or by $Ca^{2+}$ release from intracellular stores [33,34]. To date, many pathways orchestrating neuronal development, survival, and communication have been identified that specifically involve VGCCs' $Ca^{2+}$ signaling to activate CREB [35,36], NFAT [37] or downstream regulator element antagonist modulator (DREAM) transcription factors [38], to name only a few [32].

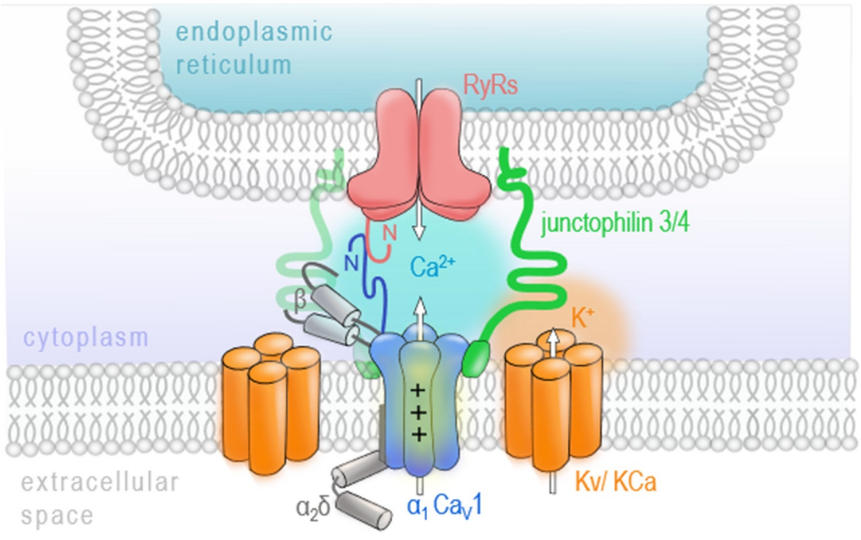


**Figure 1.** VGCCs as voltage sensors.
As known from the skeletal muscle, also in neurons VGCCs have been shown to colocalize with ryanodine receptors (RyR) in the endoplasmic reticulum and trigger RyR-mediated $Ca^{2+}$release from intracellular stores. Importantly, the RyR opening, especially of RyR isoform 1, was shown to be independent of the ionic activity of the VGCCs but rather require the conformational change of the voltage-sensing transmembrane helices of the VGCC pore induced by membrane depolarization, a process called voltage-induced calcium release. Additional interaction partners like voltage-gated (Kv) or $Ca^{2+}$-activated (KCa) potassium channel and membrane-binding proteins, junctophilins, might complement and stabilize this functional complex.

Even if the specific contribution of VGCCs has been reported to initialize these pathways, it is the transcriptional signaling power of $Ca^{2+}$ in combination with accessory $Ca^{2+}$-binding proteins that allows for the nuclear forwarding and transcriptional action described above. However, several observations have been made, underpinning the idea that VGCC subunits and intracellular domains might also directly act as gene regulators (Fig.2).

In 2006, two independent studies have reported C-terminal fragments of $Ca_V1.2$ and $Ca_V2.1$ that translocate to the nucleus of neurons in vitro and in vivo [39,40]. Gomez-Ospina et al. describe a so-called calcium channel associated transcriptional regulator (CCAT), a C-terminal fragment of the $Ca_V1.2$ channel subunit. Initially, it was assumed that CCAT is proteolytically processed from the full-length $Ca_V1.2$. However, later studies have shown that an internal promoter located in exon 46 of the *CACNA1C* gene might drive CCAT's expression independently of the $Ca_V1.2$ channel protein [41]. CCAT was verified in many different neuronal cell types throughout the brain, with a strong nuclear expression in GAD65-positive inhibitory neurons [39,41]. Notably, its nuclear localization is developmentally regulated and controlled by changes in intracellular calcium levels [39]. In the nucleus, CCAT associates with the transcriptional regulator p54(nrb)/NonO [39] and can activate transcription reporters and endogenous genes affecting, for example, cell excitability, neurite extension, and neural differentiation [42]. A similar observation has been made by Kordasiewicz and colleagues, who have found a C-terminal fragment of the neuronal $Ca_V2.1$ VGCC, which they have termed $\alpha_1$ACT, enriched in nuclei of cerebellar neurons [40]. The expression of $\alpha_1$ACT was proven to involve the cap-independent translation as a second gene product via an internal ribosomal entry site (IRES) located in the C-terminus of the *CACNA1A* gene [43]. Using chromatin immunoprecipitation-based sequencing and high-throughput RNA sequencing (RNA-seq), $\alpha_1$ACT was shown to orchestrate a complex network of neuronal genes associated with neurogenesis (*Dusp4, Efnb2, Fgfr3, Gfra2, Ntn1, Ptger3, Penk*, and *Odc1*), synaptic transmission (*Hcn4, Slc18A3*, and *Syn2*), and cell adhesion (*L1cam*) essential for early cerebellar development and neonatal survival [43,44]. Tet-off transgenic reintroduction of $\alpha_1$ACT in Purkinje cells of knockin-knockout compound heterozygote mice (KIKO), which exhibit a marked reduction of the full-length $Ca_V2.1$ mRNA isoform (+exon47), improved mouse survival and early motor development demonstrating a highly age-dependent operation window of $\alpha_1$ACT in early life [44]. Importantly, $\alpha_1$ACT was further shown to partially rescue the *CACNA1A* knockout phenotype associated with seizures, dystonia, ataxia, and death by postnatal days P18–P21 [45], at behavioral, histological, and electrophysiological levels [44]. These results demonstrate that both gene products, the ion channel and a nuclear protein $\alpha_1$ACT, play an important role in neuronal development and that in the case of perinatally decreased *CACNA1A* gene expression, the reintroduction of $\alpha_1$ACT might be a potential early intervention therapy [44]. Taken together with the results from $Ca_V1.2$ and recent reports on C-terminal proteins identified across all functional VGCC classes (also $Ca_V1.3$ [46] and $Ca_V3.2$ [44]), it seems likely that the bicistronic expression of calcium channel proteins might be conserved across the gene family, even if a nuclear protein has not been documented for all channel isoforms, yet, and the nature of its expression mechanism is currently not fully elucidated.

Notably, not only intracellular domains of the VGCC pore have been identified to participate in transcriptional regulation, but also some isoforms of the auxiliary $Ca_V\beta$ subunit of the VGCC complex have been found in the nucleus. This intracellular family of VGCC subunits is widely known to support the trafficking and expression of functional VGCCs. Four isoforms of the $Ca_V\beta$ subunit are described ($\beta_1$-$\beta_4$), each having different splice variants that might interact with any $\alpha_1$ channel isoform in a tissue-dependent manner [11,47]. In addition to their essential effect on the forward trafficking of VGCCs [48,49], β subunits can also modulate the channel's kinetics, reported as a shift of the activation potential and raise of the opening probability of HVA channels resulting in larger current densities [14,50,51]. More surprisingly, several studies uncovered a calcium channel-independent function of $\beta_4$ which has been shown to translocate to the nucleus and might be directly

involved in activity-dependent gene regulation. At first, Hibino and colleagues have described an atypical short splice variant of the $\beta_4$ subunit, namely $\beta_{4C}$, to directly interact with the chromo shadow domain of chromobox protein 2/heterochromatin protein 1γ (CHCB2/HP1γ), a nuclear protein involved in the epigenetic control of gene regulation and gene silencing. While having only slight effects on channel activation and inactivation kinetics, the co-expression of $\beta_{4C}$ with CHCB2/HP1γ fosters the recruitment of $\beta_{4C}$ to the nuclei of mammalian cells and significantly reduces its transcriptional repression activity [52]. Despite some controversial results about the molecular underpinnings, a number of studies have now confirmed the nuclear targeting of various $\beta_4$ variants [52–55] and their direct involvement in gene regulation via interactions with proteins of the epigenetic machinery such as HP1s [52,56] or the regulatory subunit of protein phosphatases-2A [57,58]. Notably, the subcellular localization and thus the function of $\beta_4$, either as a VGCC channel subunit or transcription regulator, was shown to be under the control of electrical activity and $Ca^{2+}$ influx [54,57]. Subramanyam et al. further interpret this activity-dependent shuttling of $\beta_{4b}$ into and out of the nucleus, and probably its switch between two independent physiological functions, as a possible mechanism of VGCCs to communicate their state of activity to the nucleus. Reconstitution experiments performed on cultured hippocampal neurons and cerebellar granule cells prepared from E17 lethargic ($\beta_4$-null) mice have shown that the extent of $\beta_4$ nuclear targeting significantly varied for the tested $\beta_4$ splice variants which localized in neuronal nuclei with a rank order of $\beta_{4b} > \beta_{4a} > \beta_{4e}$ [55]. The differential subcellular distribution of $\beta_4$ splice variants suggests that they might regulate distinct genetic programs. Indeed, Etemad and colleagues report that the gene regulatory power of $\beta_4$ splice variants correlates with their nuclear-targeting properties. However, they further point out that the nature of regulated genes, which are mainly implicated in cellular signaling, membrane/vesicle transport, and neuronal development, is quite similar for the tested $\beta_4$ splice variants [55]. This could indeed indicate an identical gene regulatory mechanism but remains to be explored in more detail.

## α2δ subunits are many-sided extracellular interaction partners involved in synaptogenesis

In the extracellular space, VGCCs are represented by the auxiliary $\alpha_2\delta$ subunits that are attached to the outer loops of the $\alpha_1$ subunits. To date, four $\alpha_2\delta$ isoforms ($\alpha_2\delta_1$-$\alpha_2\delta_4$), encoded by the *CACNA2D1-CACNA2D4* genes, have been identified [13,14]. Being transcribed from a single gene [59], the $\alpha_2\delta$ protein undergoes post-translational proteolytic cleavage into $\alpha_2$ and δ polypeptides [60] that remain linked via disulfide bonds [61]. Although it is generally assumed that every $\alpha_2\delta$ isoform can associate with any HVA $\alpha_1$ pore-forming subunit, recent findings suggest distinct $\alpha_1$-preferences for some $\alpha_2\delta$ isoforms [62–65]. Hence, the observed differences in the distribution and expression levels of the individual $\alpha_2\delta$ isoforms across tissues and brain regions [66–71] might reflect such preferential interaction between $\alpha_2\delta$ and $\alpha_1$ subunits. Experimental and clinical data on $\alpha_2\delta$ knockouts or mutations in $\alpha_2\delta$ genes revealed their important role for the development of neuronal networks and establishment of excitation-to-inhibition balance. In particular, genetic aberrations in *CACNA2D1* and *CACNA2D2* in humans are associated with a developmental delay, mental disability and symptomatic epilepsy [72,73]. In several studies of normotypic and autistic individuals, mutations in *CACNA2D3* were consistently identified as a risk factor for autism spectrum disorders [74]. In the last few years, several new interaction partners of $\alpha_2\delta$ subunits were identified, including thrombospondin [75], prion protein [76], LRP1 [77], BK channels [78], NMDA receptors [79], and α-neurexin [62,63]. Given the wide range of possible interactions, the idea that $\alpha_2\delta$ subunits can exert calcium channel-independent functions is increasingly gaining favor (Fig.3).

One of the most intriguing aspects related to such autonomous functions of $\alpha_2\delta$ subunits is their ability to trigger synaptogenesis in developing neurons. The $\alpha_2\delta_1$ subunit was shown to induce glutamatergic synapse formation in murine neurons through a process requiring interaction with

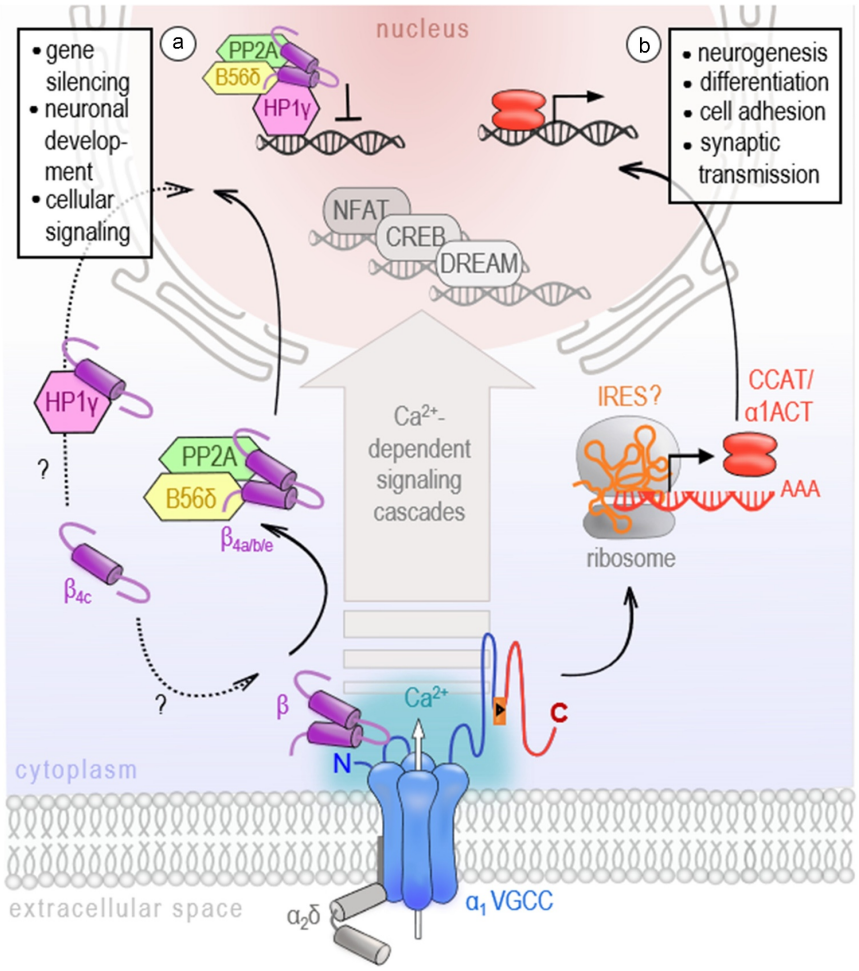


**Figure 2.** VGCCs participate in gene regulation.

Besides $Ca^{2+}$-dependent signaling cascades activating NFAT, CREB, or DREAM, VGCC $\beta_4$ subunits (A, left) and $\alpha_1$ C-terminal domains (B, right) also act as transcription factors. A) $\beta_4$ splice variants interact with proteins of the epigenetic machinery such as HP1s or the B56δ regulatory subunit of protein phosphatases-2A (PP2A) and translocate to the nucleus with a rank order of $^{\beta}{}_{4b} > {}^{\beta}{}_{4a} > {}^{\beta}{}_{4e}$. B) CCAT and $\alpha_1$ACT are fragments directly derived from the carboxyl-terminus of the pore-forming $\alpha_1$ subunit of $Ca_V1.2$ and $Ca_V2.1$ channels, respectively. Their expression via an internal ribosomal entry site (IRES) or an unknown exonic promoter is controversially discussed. They have been shown to translocate to the nucleus and regulate gene activity associated with neurodevelopment and synaptic transmission. Modelled after Barbado et al. 2009[32] and Tadmouri et al. 2012[57].

thrombospondins, extracellular matrix proteins released by young astrocytes [75]. Similarly, *straightjacket* (the ortholog of $\alpha_2\delta_3$) was reported to be essential for the development of excitatory synaptic boutons in *Drosophila*, with the extracellular $\alpha_2$ peptide chain being necessary and sufficient for bouton formation [80]. The finding of Kurshan and colleagues that the synapse establishment was significantly impaired upon deletion of *straightjacket*, but was not affected by the knockout of the pore-forming subunit *cacophony* [80], provided one of the first pieces of evidence that synaptogenic function of $\alpha_2\delta$ subunits is independent of the $\alpha_1$ subunit. A more recent report provided further compelling evidence for the channel-independent action of $\alpha_2\delta$ subunits on the formation of presynaptic release machinery and transsynaptic organization. In cultured

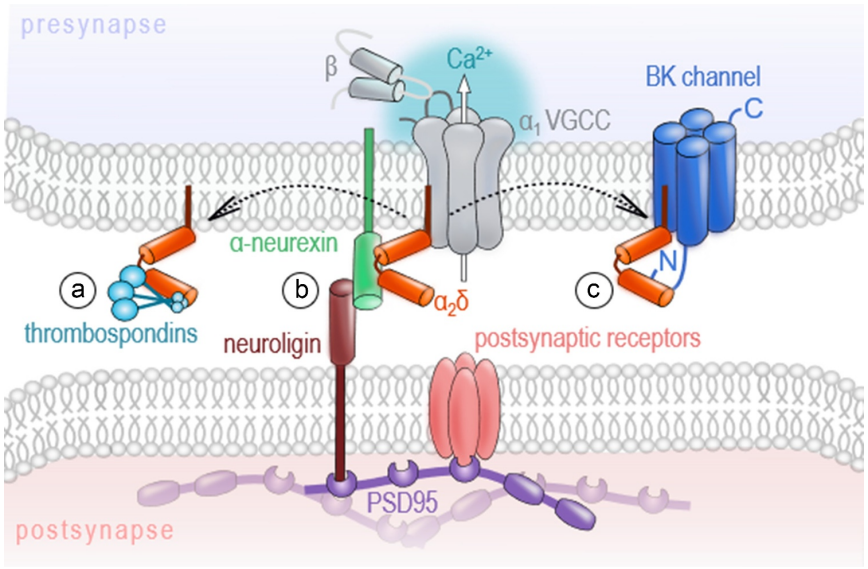


**Figure 3.** Channel-independent functions of the auxiliary $\alpha_2$ δ subunit.

A) Excitatory and inhibitory synaptogenesis: As interaction partners of thrombospondins, $\alpha_2\delta$s were shown to foster glutamatergic synapse formation. Further, $\alpha_2\delta$ subunits participate in GABAergic synaptogenesis. B) Transsynaptic signaling: $\alpha_2\delta$ subunits interact with α-neurexin, which is involved in the formation of transsynaptic complexes supporting synapse specification, establishment, maturation, and plasticity. C) Competition of other interaction partners, like the large conductance (big) potassium (BK) α subunit, for $\alpha_2\delta$.

hippocampal neurons and at the calyx of Held, triple knockout of $Ca_V2.1$, $Ca_V2.2$, and $Ca_V2.3$ strongly impaired evoked vesicle release but did not alter the structure of presynaptic terminals or transsynaptic organization [81]. Importantly, the localization of the $\alpha_2\delta_1$ in nerve terminals was not affected by the knockout of $Ca_V2$ channels as compared to control neurons, hence demonstrating that the synaptic localization of the $\alpha_2\delta_1$ is independent of the channel pore [81]. Furthermore, the total deletion of $\alpha_2\delta$ subunits in hippocampal neurons supported their relevance as a nucleation point for the formation of glutamatergic synapses [82]. Consistent with the role of $\alpha_2\delta_1$ subunits in glutamatergic synaptogenesis, the overexpression of $\alpha_2\delta_1$ in adult mice leads to cortical hyperexcitability, epileptiform activity, and an increased glutamatergic synaptic density [83], while a significant decrease in the number of excitatory synapses was shown for cortical neurons of $\alpha_2\delta_1$ knockout mice [84]. We have recently demonstrated that $\alpha_2\delta$ subunits can trigger the formation of not only excitatory, but also inhibitory synapses in an isoform-specific manner [64]. While $\alpha_2\delta_1$ subunits selectively improved neurotransmitter release in glutamatergic synapses, the upregulation of the $\alpha_2\delta_3$, but not $\alpha_2\delta_1$, resulted in a significantly higher density of GABAergic synapses and facilitated both the axonal growth in GAD67-positive interneurons and spontaneous GABA release during early development [64]. Although modulatory effects on the channel pore cannot be completely ruled out, the expression, surface delivery, and major current properties of $Ca_V2.1$ and $Ca_V2.2$ channels were not affected by association with either $\alpha_2\delta_1$ or $\alpha_2\delta_3$ in heterologous expression systems [64].

A strong argument for the autonomous function of $\alpha_2\delta$ subunits is the plurality of their additional interaction partners. At the nanoscale organization of a synapse, their interaction of $\alpha_2\delta$ subunits with the synaptic cell adhesion molecule α-neurexin might be particularly interesting in the context of transcellular units, so-called nanocolumns [85,86]. These structures have been recently reported to align the presynaptic nerve terminal,

synaptic cleft, and postsynaptic compartment fostering efficient neurotransmission [85,86]. Similarly to $\alpha_2\delta$ subunits, α-neurexins exhibit a wide array of potential binding partners, including the postsynaptic neuroligin [87,88], neurexophilin [89], dystroglycan [90], LRRTM proteins [91,92], and cerebellin [93]. The complex formed by neurexin isoforms and neuroligins, for example, has been described as a transsynaptic assembly found at excitatory and inhibitory synapses that is involved in synapse specification, establishment, maturation, and plasticity [94]. Notably, Tong and colleagues have reported a selective interaction of the $\alpha_2\delta_3$ protein with neurexin1α[62]. Since the confirmation of a specific association between $\alpha_2\delta$ isoforms and α-neurexin failed in overexpression experiments [63], the physiological interaction could be regulated rather via a cell type- or synapse-specific expression of these molecules than selective binding mechanisms. It is also conceivable that slight differences in the binding affinities can dynamically influence these molecular interactions. This could transiently modulate the calcium channel properties and, in turn, synaptic transmission and plasticity in an activity- or synapse-specific manner. Indeed, other partners, besides α-neurexin, e.g. BK potassium channels [80], have been also described to compete with the channel pore for the $\alpha_2\delta$ subunits [78]. Moreover, the channel-to-$\alpha_2\delta$ coupling is expected to be rather loose [95–97] and the analysis of surface dynamics of the $\alpha_2\delta_1$ subunits and various $\alpha_1$ proteins further revealed, apart from a pool of $\alpha_2\delta_1$ bound to the channel, two subpopulations of the $\alpha_2\delta_1$ and $\alpha_1$ subunits that are not interacting with each other [98]. Whether the dissociation of the $\alpha_2\delta$ subunit from the channel pore located in the plasma membrane has direct consequences on the channel gating, stability or turn-over rates has been discussed in some studies but requires more attention to resolve the molecular mechanism [78,99,100]. Besides gating or stability effects on the channel, changes in channel positioning or in the multi-subunit complex organization could also be possible.

To summarize, the VGCC pore-forming subunit as well as the auxiliary β and $\alpha_2\delta$ subunits play an essential role in voltage-induced calcium release, gene regulation, neuronal synaptogenesis, and transsynaptic signaling, which do not necessarily involve the $Ca^{2+}$ transients of the channel complexes. The modular expression as multi-subunit complexes provides a first basis for the diversity and functional range of these molecules. We aim to further develop the idea that the functional diversity of VGCCs could not only arise from different basic channel kinetic and ion-conducting properties but rather from variations in their interaction partners or molecular environment. Some interesting findings pointing in this direction come from studies of alternative splice variants of VGCCs, which will be in the focus of the last section of this review.

## Alternative splicing: How VGCC transcript variants shape neuronal phenotypes or vice versa?

Alternative splicing is crucial for increasing the proteomic diversity of the finite number of genes, which allows for a massive expansion of the coding power of the metazoan genome [101,102]. To explain the high functional diversity of neuronal phenotypes observed in distinct brain areas and over development, many studies have focused on the regulatory role of alternative splicing for molecules involved in neurotransmission, including large multi exon ion channels and postsynaptic receptors [103–108]. Nowadays, genome-wide analysis of splicing events strongly supports the idea of specialized splicing patterns in distinct neuronal phenotypes [109–111]. In the case of VGCCs, nine of the ten genes that encode the pore-forming $\alpha_1$ calcium channel subunit are expressed in the mammalian brain, and each $\alpha_1$ subunit contains multiple sites that are hotspots for splicing events [103,112]. However, whether VGCCs are indeed spliced in a cell type-specific manner has not been comprehensively assessed, yet. For a first estimation, we have analyzed raw sequencing data generated by Furlanis and colleagues (accession code: GSE133291 [110]; Fig. 4) from ribosome-associated transcript isoforms in genetically defined neuron types of the mouse forebrain. The data indicate that some classes of neurons indeed stand out for the splicing events of VGCCs,

annotated to date. Especially the class of parvalbumin (PV)-positive cells, which have been described as fast-spiking GABAergic interneurons [113], show a distinct VGCC splicing pattern (Fig. 4C). Hence, there might be a link between neuronal cell identity and VGCC splicing. The structural changes induced by alternative splicing might affect channel gating and conductance, which then leads to different functional properties of neuronal phenotypes. There is an extensive literature accumulated over the last decades that clearly demonstrates major effects of VGCCs' splicing on the channel's pharmacology, gating, surface expression, but also on its molecular interactions [103,114,115]. Here, we want to present some examples, showing that alternative splicing has no direct consequence on the channel gating but rather affects their coupling to downstream interaction partners triggering different signaling pathways.

One interesting VGCC splice event is the usage of two mutually exclusive exons 37a and 37b found in the C-terminus of the neuronal $Ca_V2$ calcium channels ($Ca_V2.1$ [123], $Ca_V2.2$ [124] and $Ca_V2.3$ [116]). Independent studies have shown that the splicing of exons 37a and 37b generates two variants, EFa (or 37a) or EFb (or 37b), of the EF-hand-like $Ca^{2+}$-binding motif that acts as a molecular switch for calcium-dependent facilitation and might modulate different neuronal phenotypes in a spatiotemporal manner [105,123–127]. The recent analysis of RNA-seq data obtained from specialized neuronal cell types mapped the differential usage of exon37 for $Ca_V2.1$ channels across excitatory and inhibitory neurons [111]. Huntley et al. confirmed that the mutually exclusive usage of exon37 correlates with opposite short-term plasticity behavior observed for principal excitatory neurons versus inhibitory cells (like PV interneurons). These results are in line with the electrophysiological characterization of rat hippocampal neurons where the expression of $Ca_V2.1$[EFa] was shown to promote synaptic depression, while $Ca_V2.1$[EFb] favored synaptic facilitation [105]. Thalhammer and colleagues have further demonstrated that $Ca_V2.1$[EFa] is more tightly coupled to presynaptic scaffold proteins and the neurotransmitter release machinery when compared to $Ca_V2.1$[EFb], which is characterized by a rather loose coupling [105]. Although a contribution of differing biophysical properties for $Ca_V2.1$[EFa] and $Ca_V2.1$[EFb] cannot be excluded, the authors pointed out that the variation of the synaptic efficacy between these splice variants is likely due to a differential organization and molecular coupling at the presynaptic site [105]. This suggests that the tighter coupling of $Ca_V2.1$[EFa], preferentially expressed in PV neurons, might be necessary to define the PV phenotype, whereas excitatory neurons use the $Ca_V2.1$[EFb] variant. As previously mentioned, the mutually exclusive usage of exon37 is conserved across neuronal $Ca_V2$ channels [116,123,124]. For $Ca_V2.2$ channels, it has been shown that alternative splicing of the exon37 plays an important role in voltage-independent inhibition via G proteins. The inclusion of exon37a results in the expression of a tyrosine residue (Y1747), which is absent in exon37b, that triggers a voltage-independent inhibitory pathway that increases the sensitivity of $Ca_V2.2$ channels to opiates and the inhibitory neurotransmitter GABA [128]. In a following study, the Lipscombe laboratory has further demonstrated the importance of activity-independent inhibition of $Ca_V2.2$ channels expressing exon37a for its function in nociceptors and morphine analgesia sensitivity *in vivo*, and thus the relevance for the pain pathway [129].

As already indicated above, the C-terminus of neuronal VGCCs has been described for its central role for the channel's synaptic targeting and organization [108,130], interaction with scaffolding proteins [105,131–135], G protein signaling [128,129], gating [112,125,136–139], and consequently, for synaptic transmission and short-term plasticity[105,108]. Therefore, we now want to pay attention to another splice event in the distal part of the VGCC's C-terminus that critically affects the length and binding sites expressed by this important structure. The expression of truncated VGCCs arising from alternative splicing events has been reported across neuronal calcium channel isoforms [114,140]. In the case of $Ca_V2.1$ channels, a premature stop codon results in the expression of a channel variant lacking exon47, termed Δ47, that exhibits a 150–250 amino acids (depending on the species) shorter C-terminus compared to the fully expressed exon 47 (+47) [112,141]. This

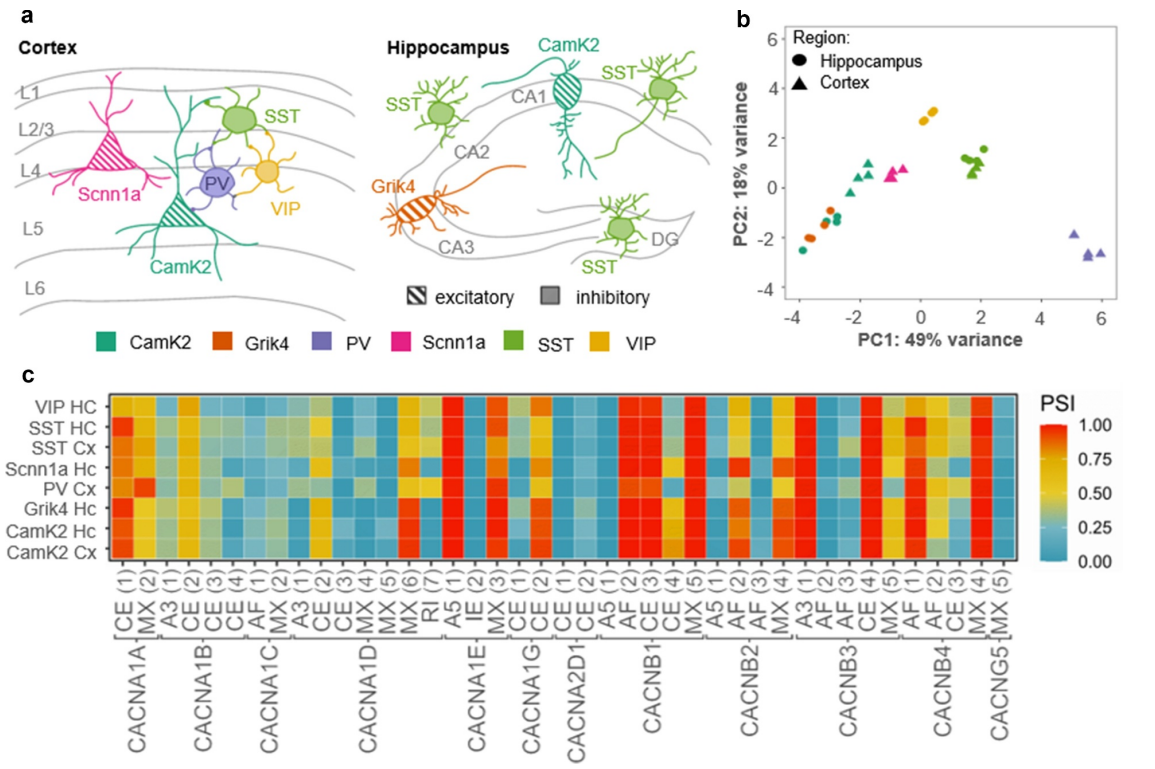


**Figure 4.** VGCC genes are spliced differently across neuronal cell types.

A) Schematic overview representing different neuronal cell populations included in the RNA sequencing data (data is publicly available; accession code: GSE133291[110]). The scheme was adapted from Furlanis and colleagues. The color-code for the cell types is used in B. CamK2= $Ca^{2+}$/calmodulin-dependent protein kinase II; Grik4= glutamate receptor, ionotropic, kainite 4; PV= parvalbumin; Scnn1a=α subunit of the epithelial sodium channel ENaC; SSTsomatostatin; VIP- vasoactive intestinal peptide. B) The principal component analysis (PCA) of the gene expression demonstrates a differential regulation of VGCC genes across excitatory and inhibitory neuronal cell types. Especially, the cluster of PV interneurons localizes with asignificant gap to other neuron types on principal component 1, which explains roughly fifty percent of the observed variance. Data analysis: The fastq-files were mapped to the mm10 reference genome using STAR[117]. The PCA was performed with DESeq2 in R[118,119] and plotted with ggplot2[120]. C) Heatmap of alternatively spliced transcripts of VGCC genes. We have analyzed the occurrence of the following splice events: cassette exon (CE), mutually exclusive exon (MX), retained intron (RI), alternative 5′ splice-site (A5), alternative 3′ splice-site (A3) and alternative first exon (AF), schematically shown in the lower part of C. Only those events that show a significant variance between the samples (ANOVA p-value < 0.01) were included. Overall, a difference between the PV neurons and the remaining samples in the splice patterns for the VGCC genes can be observed (e.g. *CACNA1A* MX(2), *CACNB1* CE(4) or *CANB3* MX (5)). Since the exon numbering depends on the transcript variant of a respective gene, the exact position for the splice variants (for instance, the start and end coordinates of the included exon) of the heatmap are listed here: *CACNA1A*: CE (1) chr8:84601756–84601821, MX (2) chr8:84614695–84614791, *CACNA1B*: A3 (1) chr2:4718122, CE (2) chr2:24642853–24642858, CE (3) chr2:24656711–24656722, CE (4) chr2:24682976–24683038, *CACNA1C*: AF (1) chr6:119196231–119196093, MX (2) chr6:118637730 –118637813, *CACNA1D*: A3 (1) chr14:30129848, CE (2) chr14:30129789–30129848, CE (3) chr14:30137041–30137124, MX (4) chr14:30089296–30089379, MX (5) chr14:30107653–30107712, MX (6) chr14:30171296–30171399, RI (7) chr14:30128798–30129789, *CACNA1E*: A5 (1)chr1:154471338, CE (2) chr1:154404885–154405013, MX (3) chr1:154416061–154416157, *CACNA1G*: CE (1) chr11:94423671–94423724, CE (2) chr11:94439709–94439777,*CACNA2D1*: CE (1) chr5:16322539–16322595, CE (2) chr5:16341990 –16342010, *CACNB1*:A5 (1) chr11:98010004, AF (2) chr11:98023034–98022887, CE (3) chr11:98010627–98010646, CE (4) chr11:98011343–98011497, MX (5) chr11:98010627–98010646, *CACNB2*: A5 (1) chr2:4971646, AF (2) chr2:4739216–14739763,AF (3) chr2:4763129–14763992, MX (4) chr2:14967942–14968075, *CACNB3*: A3 (1)chr15:98640686, AF (2) chr15:98631805–98631931, AF (3) chr15:98632376–98632520, CE (4) chr15:98640959–98640978, MX (5) chr15:98640959–98640978, *CACNB4*: AF (1)chr2:52676582 –52676271, AF (2) chr2:52676831–52676271, CE (3) chr2:52556202–52556361, MX (4) chr2:52465894–52465913, *CACNG5*: AF (1) chr11:107915055–107914900. For this analysis, the fastq-files were mapped to the referencegenome (mm10) with Salmon[121] and the percentage-spliced in (PSI) values were computedusing SUPPA2[122].

truncation was shown to affect the channel's trafficking, its molecular arrangement, as well as synaptic transmission properties including short-term plasticity [108,142]. However, only mild effects on the channel kinetics have been reported so far [108,142]. Moreover, a study by Aikawa et al. using a knockin mouse line, which exclusively expresses $Ca_V2.1_{\Delta 47}$ (*CACNA1A*$^{CtmKO/CtmKO}$), has shown that in cerebellar Purkinje cells, exon47 was not required to maintain such basic channel electrophysiological properties as current density-voltage relationships and channel inactivation. Instead, in the cerebellum, exon47 has a more important role in establishing channel interactions with scaffold proteins such as RIM-binding protein 2 and the auxiliary subunit $\beta_4$. Surprisingly, the absence of exon47 did not only reduce interactions to scaffold proteins but also promoted the binding to $GABA_{B2}$, a principal subunit of the G protein-coupled receptor for GABA, in the cerebellum of *CACNA1A*$^{CtmKO/CtmKO}$ mice. This enhancement of $Ca_V2.1$–$GABA_{B2}$ interaction might contribute to the pathogenesis of absence seizures and motor incoordination observed in these animals [143–147].

These examples demonstrate that changes in the structure of VGCCs induced by splicing events also affect their interaction to partner molecules and suggest that significant functional implications cannot be reduced to their ionic activity.

## Outlook and perspectives

Although this review cannot fully capture the functional range of VGCCs, we aimed to draw attention to some side functions of VGCCs that go beyond their classical role as ion channels to induce local $Ca^{2+}$ nanodomains necessary for neurotransmission or downstream $Ca^{2+}$ signaling pathways. When associated with ryanodine receptors, VGCCs contribute to a functional complex to trigger voltage-induced $Ca^{2+}$ release from intracellular stores, a process that is independent of their ionic activity. Further, VGCC auxiliary subunits as well as C-terminal domains of the $\alpha_1$ channel pore participate in gene regulation. Their activity- and $Ca^{2+}$-dependent subcellular shuttling implicate a pathway how VGCCs communicate their own activity status to the nucleus and integrate transient $Ca^{2+}$ signaling into longer-lasting transcriptional processes. These transcriptomic alterations should be considered especially when evaluating the phenotype of channelopathies, where most of the studies have primarily focused on explaining the pathological consequences based on the loss or gain of calcium channel function so far. Moreover, we have shown that $\alpha_2\delta$ auxiliary subunits are directly involved into neuronal network development and maintenance by fostering excitatory and inhibitory synaptogenesis and transsynaptic signaling. We have introduced some examples where structural changes in critical VGCC domains result in distinct synaptic plasticity behaviors and contribute, at least to some extent, to the specification of neuronal phenotypes. Notably, these changes in the channel structure do not necessarily involve differences in basic channel gating but might rather involve different protein environments or downstream pathways. Considering the many interaction partners of VGCCs, and from a molecular dynamics point of view, we want to point out the possibility that these large molecules could also serve as seeding points for molecular interactions. The question remains open at this point to what extent VGCCs can shape their environment by acting as a basic element bringing together important signaling molecules or how specific interaction partners that are present, e.g. in distinct neuronal phenotypes, regulate VGCCs' functional diversity.

## Acknowledgements

We thank the Scheiffele Lab from the University of Basel for sharing the extensive dataset of ribosome-associated mRNAs from major neuron classes published in Furlanis et al. 2019 and for interesting discussions about neuronal cell class-specific alternative splicing.

## Disclosure statement

No potential conflict of interest was reported by the authors.

## Disclosure of interest

The authors declare that there are no competing interests associated with this manuscript.

## Abbreviations

| | |
|---|---|
| $\alpha_1$ACT | C-terminal fragment of the neuronal $Ca_V2.1$ VGCC |
| A3 | alternative 3′ splice site |
| A5 | alternative 5′ splice site |
| AF | alternative 3′ splice site |
| BK | big potassium |
| $Ca^{2+}$ | calcium ions |
| CamK2 | $Ca^{2+}$/calmodulin-dependent protein kinase II |
| CCAT | calcium channel associated transcriptional regulator |
| CE | cassette exon |
| CHCB2/HP1γ | chromobox protein 2/heterochromatin protein 1γ |
| CREB | cAMP response element-binding protein |
| DREAM | downstream regulator element antagonist modulator |
| ER | endoplasmic reticulum |
| GABA | gamma-aminobutyric acid |
| GAD65/GAD67 | glutamic acid decarboxylase 65/67 |
| Grik4 | glutamate receptor, ionotropic, kainate 4 |
| HVA | high voltage-activated |
| IRES | internal ribosomal entry site |
| Kv | voltage-gated potassium channels |
| KCa | callcium-activated potassium channels |
| KIKO | knockin-knockout compound heterozygote mice |
| LRRM | leucine -rich repeat transmembrane proteins |
| mEPSCs | miniature excitatory postsynaptic currents |
| mIPSCs | miniature inhibitory postsynaptic currents |
| MX | mutually exclusive exon |
| NFAT | nuclear factor of activated T-cells |
| NMDA | N-methyl-D-aspartate |
| ORAI | calcium release-activated calcium channel protein |
| PCA | principal component analysis |
| PP2A | protein phosphatases 2A |
| PSI | percentage spliced in |
| PV | parvalbumin |
| RI | retained intron |
| RNA-seq | high-throughput RNA sequencing |
| RyR | ryanodine receptor |
| SCA6 | spinocerebellar ataxia type 6 |
| Scnn1a | α subunit of the epithelial sodium channel ENaC |
| SST | somatostatin |
| Tet | tetracycline |
| TRP | transient receptor potential channels |
| VGCC | voltage-gated calcium channel |
| VIP | vasoactive intestinal peptide |

## Funding

This work was supported by the Schram Foundation (Arthur Bikbaev), the Carl-Zeiss Foundation (Stephan Weißbach), and internal university research funding of the Johannes Gutenberg-University (Jennifer Heck).

## ORCID

Jennifer Heck http://orcid.org/0000-0003-3694-2393

## References

[1] Clapham D. Calcium signaling. Cell. 1995;80(2):259–268.
[2] Brini M, Calì T, Ottolini D, et al. Intracellular calcium homeostasis and signaling. 2013.
[3] Campbell A Intracellular calcium. 2015.Intracellular Ca2+ – Principles and Terminology. Intracellular Calcium, 2014:39-80.
[4] Catterall WA. Voltage-Gated Calcium Channels. Cold Spring Harbor Perspectives in Biology. 2011; 3:a003947
[5] Tsien RW, Lipscombe D, Madison DV, et al. Multiple types of neuronal calcium channels and their selective modulation. Trends Neurosci. 1988;11 (10):431–438.
[6] Dunlap K, Luebke JI, Turner TJ. Exocytotic Ca2+ channels in mammalian central neurons. Trends Neurosci. 1995;18(2):89–98.
[7] Carafoli E, Krebs J. Why calcium? How calcium became the best communicator. J Biol Chem. 2016;291(40):20849–20857.Carafoli E, Krebs J. Why Calcium? How Calcium Became the Best Communicator. J Biol Chem 2016; 291:20849-57.
[8] Zamponi GW, Striessnig J, Koschak A, et al. The physiology, pathology, and pharmacology of voltage-gated calcium channels and their future therapeutic potential. Pharmacol Rev. 2015;67:821–870.
[9] Dolphin AC. Voltage-gated calcium channels and their auxiliary subunits: physiology and pathophysiology and pharmacology. J Physiol. 2016;594 (19):5369–5390.Dolphin AC. Voltage-gated calcium channels and their auxiliary subunits: physiology and pathophysiology and pharmacology. J Physiol 2016; 594:5369-90.
[10] Striessnig J. Voltage-gated calcium channels - from basic mechanisms to disease. J Physiol. 2016;594 (20):5817–5821.
[11] Lacinova L. Voltage-dependent calcium channels. Gen Physiol Biophys. 2005;24 Suppl 1:24.
[12] Campiglio M, Flucher BE. The role of auxiliary subunits for the functional diversity of voltage-gated calcium channels. J Cell Physiol. 2015;230(9):2019–2031.
[13] Arikkath J, Campbell KP. Auxiliary subunits: essential components of the voltage-gated calcium channel complex. Curr Opin Neurobiol. 2003;13(3):298–307. Arikkath J, Campbell KP. Auxiliary subunits: essential components of the voltage-gated calcium channel complex. Curr Opin Neurobiol 2003; 13:298-307.
[14] Dolphin AC. Calcium channel auxiliary α2δ and β subunits: trafficking and one step beyond. Nat Rev Neurosci. 2012;13(8):542.

[15] Melzer W, Herrmann-Frank A, Lüttgau H. The role of Ca2+ ions in excitation-contraction coupling of skeletal muscle fibres. 1995;1241:59–116. Biochimica et Biophysica Acta (BBA) - Reviews on Biomembranes.
[16] Leong P, MacLennan DH. Complex interactions between skeletal muscle ryanodine receptor and dihydropyridine receptor proteins. Biochem Cell Biol. 1998;76(5):681–694.
[17] Franzini-Armstrong C, Protasi F. Ryanodine receptors of striated muscles: a complex channel capable of multiple interactions. Physiol Rev. 1997;77:699–729. Franzini-Armstrong C, Protasi F. Ryanodine receptors of striated muscles: a complex channel capable of multiple interactions. Physiol Rev 1997; 77:699-729.
[18] Lu X, Xu L, Meer G. Activation of the skeletal muscle calcium release channel by a cytoplasmic loop of the dihydropyridine receptor. J Biol Chem. 1994;269 (9):6511–6516.
[19] Marty I, Robert M, Villaz M, et al. Biochemical evidence for a complex involving dihydropyridine receptor and ryanodine receptor in triad junctions of skeletal muscle. Proc Natl Acad Sci U S A. 1994;91(6):2270–2274.
[20] Ouardouz M, Nikolaeva MA, Coderre E, et al. Depolarization-induced Ca2+ release in ischemic spinal cord white matter involves L-type Ca2+ channel activation of ryanodine receptors. Neuron. 2003;40(1):53–63.
[21] Chavis P, Fagni L, Lansman JB, et al. Functional coupling between ryanodine receptors and L-type calcium channels in neurons. Nature. 1996;382 (6593):719–722.
[22] Mouton J, Marty I, Villaz M, et al. Molecular interaction of dihydropyridine receptors with type-1 ryanodine receptors in rat brain. Biochem J. 2001;354 (3):597–603.
[23] Kim S, Yun H-M, Baik J-H, et al. Functional interaction of neuronal Cav1.3 L-type calcium channel with ryanodine receptor Type 2 in the rat hippocampus *. J Biol Chem. 2007;282(45):32877–32889.
[24] Furuichi T, Furutama D, Hakamata Y, et al. Multiple types of ryanodine receptor/Ca2+ release channels are differentially expressed in rabbit brain. J Neurosci. 1994;14(8):4794.
[25] Kuwajima G, Futatsugi A, Niinobe M, et al. Two types of ryanodine receptors in mouse brain: skeletal muscle type exclusively in Purkinje cells and cardiac muscle type in various neurons. Neuron. 1992;9 (6):1133–1142.
[26] Walton PD, Airey JA, Sutko JL, et al. Ryanodine and inositol trisphosphate receptors coexist in avian cerebellar purkinje neurons. J Cell Biol. 1991;113 (5):1145–1157.
[27] Giannini G, Conti A, Mammarella S, et al. The ryanodine receptor/calcium channel genes are widely and differentially expressed in murine brain and peripheral tissues. J Cell Biol. 1995;128 (5):893–904.
[28] Striessnig J, Pinggera A, Kaur G, et al. L-type Ca2+ channels in heart and brain. Wiley Interdisciplinary Reviews: Membrane Transport and Signaling. 2014;3 (2):15–38. DOI:10.1002/wmts.102
[29] Sahu G, Wazen R-M, Colarusso P, et al. Junctophilin proteins tether a Cav1-RyR2-KCa3.1 tripartite complex to regulate neuronal excitability. Cell Rep. 2019;28(9):2427–2442.e6.
[30] Vierra NC, Kirmiz M, Van Der List D, et al. Kv2.1 mediates spatial and functional coupling of L-type calcium channels and ryanodine receptors in mammalian neurons. eLife. 2019;8:8:e49953.
[31] Stys PK. White matter injury mechanisms. Curr Mol Med. 2004;4(2):113–130.
[32] Barbado M, Fablet K, Ronjat M, et al. Gene regulation by voltage-dependent calcium channels. 2009;1793:1096–1104. Biochim Biophys Acta, Mol Cell Res.
[33] Greenberg M, Ziff E, Greene L. Stimulation of neuronal acetylcholine receptors induces rapid gene transcription. Science. 1986;234(4772):80.
[34] Morgan JI, Curran T. Role of ion flux in the control of c-fos expression. Nature. 1986;322(6079):552–555.
[35] Dolmetsch RE, Pajvani U, Fife K, et al. Signaling to the nucleus by an L-type calcium channel-calmodulin complex through the MAP kinase pathway. Science. 2001;294(5541):333–339.
[36] Zhao R, Liu L, Rittenhouse AR. Ca2+ influx through both L- and N-type Ca2+ channels increases c-fos expression by electrical stimulation of sympathetic neurons. Eur J Neurosci. 2007;25(4):1127–1135.
[37] Hernández-Ochoa EO, Contreras M, Cseresnyés Z, et al. Ca2+ signal summation and NFATc1 nuclear translocation in sympathetic ganglion neurons during repetitive action potentials. Cell Calcium. 2007;41 (6):559–571.
[38] Leclerc GM, Boockfor FR. Calcium influx and DREAM protein are required for GnRH gene expression pulse activity. Mol Cell Endocrinol. 2007;267(1–2):70–79.
[39] Gomez-Ospina N, Tsuruta F, Barreto-Chang O, et al. The C terminus of the L-type voltage-gated calcium channel Ca(V)1.2 encodes a transcription factor. Cell. 2006;127(3):591–606.
[40] Kordasiewicz HB, Thompson RM, Clark HB, et al. C-termini of P/Q-type Ca 2+ channel α1A subunits translocate to nuclei and promote polyglutamine-mediated toxicity. Hum Mol Genet. 2006;15 (10):1587–1599.
[41] Gomez-Ospina N, Panagiotakos G, Portmann T, et al. A promoter in the coding region of the calcium channel gene CACNA1C generates the transcription factor CCAT. PLoS One. 2013;8(4):e60526–e60526.
[42] Ge J, Ju Y, Xue Z, et al. Distal C terminus of CaV1.2 channels plays a crucial role in the neural

differentiation of dental pulp stem cells. PLoS One. 2013;8(11):e81332–e81332.
[43] Du X, Wang J, Zhu H, et al. Second cistron in CACNA1A gene encodes a transcription factor mediating cerebellar development and SCA6. Cell. 2013;154(1):118–133.
[44] Du X, Wei C, Hejazi Pastor DP, et al. α1ACT is essential for survival and early cerebellar programming in a critical neonatal window. Neuron. 2019;102(770–785):e7. DOI:10.1016/j.neuron.2019.02.036
[45] Jun K, Piedras-Rentería ES, Smith SM, et al. Ablation of P/Q-type $Ca^{2+}$ channel currents, altered synaptic transmission, and progressive ataxia in mice lacking the $\alpha_{1A}$-subunit. Proc Natl Acad Sci USA. 1999;96(26):15245.
[46] Lu L, Sirish P, Zhang Z, et al. Regulation of gene transcription by voltage-gated L-type calcium channel, Cav1.3. J Biol Chem. 2015;290(8):4663–4676.
[47] Dolphin AC. β subunits of voltage-gated calcium channels. J Bioenerg Biomembr. 2003;35(6):599–620.
[48] Altier C, Garcia-Caballero A, Simms B, et al. The Cavβ subunit prevents RFP2-mediated ubiquitination and proteasomal degradation of L-type channels. Nat Neurosci. 2010;14(2):173.Altier C, Garcia-Caballero A, Simms B, You H, Chen L, Walcher J, et al. The Cavbeta subunit prevents RFP2-mediated ubiquitination and proteasomal degradation of L-type channels. Nat Neurosci 2011; 14:173-80.
[49] Waithe D, Ferron L, Page KM, et al. β-Subunits promote the expression of Ca(V)2.2 channels by reducing their proteasomal degradation. The. J Biol Chem. 2011(286):9598–9611.Waithe D, Ferron L, Page KM, Chaggar K, Dolphin AC. Beta-subunits promote the expression of Ca(V)2.2 channels by reducing their proteasomal degradation. J Biol Chem 2011; 286:9598-611.
[50] Meir A, Bell DC, Stephens GJ, et al. Calcium channel beta subunit promotes voltage-dependent modulation of alpha 1 B by G beta gamma. Biophys J. 2000;79(2):731–746.Meir A, Bell DC, Stephens GJ, Page KM, Dolphin AC. Calcium channel beta subunit promotes voltage-dependent modulation of alpha 1 B by G beta gamma. Biophys J 2000; 79:731-46.
[51] Neely A, Garcia-Olivares J, Voswinkel S, et al. Folding of active calcium channel β1b -subunit by size-exclusion chromatography and its role on channel function. J Biol Chem. 2004;279(21):21689–21694.Neely A, Garcia-Olivares J, Voswinkel S, Horstkott H, Hidalgo P. Folding of active calcium channel beta(1b) -subunit by size-exclusion chromatography and its role on channel function. J Biol Chem 2004; 279:21689-94.
[52] Hibino H, Pironkova R, Onwumere O, et al. Direct interaction with a nuclear protein and regulation of gene silencing by a variant of the Ca2+-channel beta 4 subunit. Proc Natl Acad Sci U S A. 2003;100(1):307–312.
[53] Colecraft HM, Alseikhan B, Takahashi SX, et al. Novel functional properties of Ca2+ channel β subunits revealed by their expression in adult rat heart cells. J Physiol. 2002;541(2):435–452.
[54] Subramanyam P, Obermair GJ, Baumgartner S, et al. Activity and calcium regulate nuclear targeting of the calcium channel beta4b subunit in nerve and muscle cells. Channels (Austin, Tex). 2009;3(5):343–355.
[55] Etemad S, Obermair GJ, Bindreither D, et al. Differential neuronal targeting of a new and two known calcium channel β4 subunit splice variants correlates with their regulation of gene expression. The Journal of neuroscience : the official journal of the Society for Neuroscience. 2014;34(4):1446–1461. DOI:10.1523/JNEUROSCI.3935-13.2014
[56] Xu X, Lee YJ, Holm JB, et al. The Ca2+ Channel β4c subunit interacts with heterochromatin protein 1 via a PXVXL binding motif. J Biol Chem. 2011;286(11):9677–9687.
[57] Tadmouri A, Kiyonaka S, Barbado M, et al. Cacnb4 directly couples electrical activity to gene expression, a process defective in juvenile epilepsy. Embo J. 2012;31(18):3730–3744.
[58] Ronjat M, Kiyonaka S, Barbado M, et al. Nuclear life of the voltage-gated Cacnb4 subunit and its role in gene transcription regulation. null. 2013;7:119–125.
[59] De Jongh KS, Warner C, Catterall WA. Subunits of purified calcium channels. Alpha 2 and delta are encoded by the same gene. J Biol Chem. 1990;265:14738–14741.
[60] Jay SD, Sharp AH, Kahl SD, et al. Structural characterization of the dihydropyridine-sensitive calcium channel alpha 2-subunit and the associated delta peptides. J Biol Chem. 1991;266(5):3287–3293.
[61] Wu J, Yan Z, Li Z, et al. Structure of the voltage-gated calcium channel Cav1.1 at 3.6 Å resolution. Nature. 2016;537(7619):191.
[62] Tong X-J, López-Soto EJ, Li L, et al. Retrograde synaptic inhibition is mediated by α-neurexin binding to the α2δ subunits of N-type calcium channels. Neuron. 2017;95(326–340):e5.
[63] Brockhaus J, Schreitmüller M, Repetto D, et al., α-neurexins together with α2δ-1 auxiliary subunits regulate Ca 2+ Influx through Ca v 2.1 channels. J Neurosci. Internet. 2018;38(38):8277–8294. Available from http://www.jneurosci.org/content/early/2018/08/13/JNEUROSCI.0511-18.2018.abstract
[64] Bikbaev A, Ciuraszkiewicz-Wojciech A, Heck J, et al. Auxiliary α2δ1 and α2δ3 subunits of calcium channels drive excitatory and inhibitory neuronal network development. J Neurosci. 2020;40(25):4824. DOI:10.1523/JNEUROSCI.1707-19.2020
[65] Heinrich L, Ryglewski S. Different functions of two putative drosophila α2δ subunits in the same identified motoneurons. Sci Rep. 2020;10(1):13670.

[66] Klugbauer N, Lacinová L, Marais E, et al. Molecular diversity of the calcium channel α 2 δ subunit. J Neurosci. 1999;19(2):684–691.
[67] Gong HC, Hang J, Kohler W, et al. Tissue-specific expression and gabapentin-binding properties of calcium channel α2δ subunit subtypes. J Membr Biol. 2001;184(1):35–43.
[68] Klugbauer N, Marais E, Hofmann F. Calcium channel α2δ subunits: differential expression, function, and drug binding. J Bioenerg Biomembr. 2003;35 (6):639–647.
[69] Cole RL, Lechner SM, Williams ME, et al. Differential distribution of voltage-gated calcium channel alpha-2 delta (alpha2delta) subunit mRNA-containing cells in the rat central nervous system and the dorsal root ganglia. J Comp Neurol. 2005;491 (3):246–269.
[70] Davies A, Hendrich J, Van Minh AT, et al. Functional biology of the alpha(2)delta subunits of voltage-gated calcium channels. Trends Pharmacol Sci. 2007;28(5):220–228.
[71] Schlick B, Flucher BE, Obermair GJ. Voltage-activated calcium channel expression profiles in mouse brain and cultured hippocampal neurons. Neuroscience. 2010;167(3):786–798.
[72] Edvardson S, Oz S, Abulhijaa FA, et al. Early infantile epileptic encephalopathy associated with a high voltage gated calcium channelopathy. J Med Genet. 2013;50(2):118.
[73] Vergult S, Dheedene A, Meurs A, et al. Genomic aberrations of the CACNA2D1 gene in three patients with epilepsy and intellectual disability. Eur J Hum Genet. 2015;23(5):628–632.
[74] Iossifov I, Ronemus M, Levy D, et al. De novo gene disruptions in children on the autistic spectrum. Neuron. 2012;74(2):285–299. DOI:10.1016/j.neuron.2012.04.009
[75] Eroglu Ç, Allen NJ, Susman MW, et al. The gabapentin receptor α2δ-1 is the neuronal thrombospondin receptor responsible for excitatory CNS synaptogenesis. Cell. 2009;139(2):380–392. DOI:10.1016/j.cell.2009.09.025
[76] Senatore A, Colleoni S, Verderio C, et al. Mutant PrP suppresses glutamatergic neurotransmission in cerebellar granule neurons by impairing membrane delivery of VGCC α(2)δ-1 subunit. Neuron. 2012;74 (2):300–313. DOI:10.1016/j.neuron.2012.02.027
[77] Kadurin I, Rothwell SW, Lana B, et al. LRP1 influences trafficking of N-type calcium channels via interaction with the auxiliary α(2)δ-1 subunit. Sci Rep. 2017;7(1):43802.
[78] Zhang F-X, Gadotti VM, Souza IA, et al. Suppress Cavα2δ subunit function to reduce inflammatory and neuropathic pain. Cell Rep. 2018;22(8):1956–1964.
[79] Chen J, Li L, Chen S-R, et al. The α2δ-1-NMDA receptor complex is critically involved in neuropathic pain development and gabapentin therapeutic actions. Cell Rep. 2018;22(9):2307–2321. DOI:10.1016/j.celrep.2018.02.021
[80] Kurshan PT, Oztan A, Schwarz TL. Presynaptic alpha2delta-3 is required for synaptic morphogenesis independent of its Ca2+-channel functions. Nat Neurosci. 2009;12(11):1415–1423.
[81] Held RG, Liu C, Ma K, et al. Synapse and active zone assembly in the absence of presynaptic Ca2+ channels and Ca2+ Entry. Neuron. 2020;107(667–683):e9. DOI:10.1016/j.neuron.2020.05.032
[82] Schöpf CL, Geisler S, Stanika RI, et al. Presynaptic $\alpha_2\delta$ subunits are key organizers of glutamatergic synapses. bioRxiv. 2019;826016.
[83] Faria LC, Gu F, Parada I, et al. Epileptiform activity and behavioral arrests in mice overexpressing the calcium channel subunit α2δ-1. Neurobiol Dis. 2017;102:70–80.
[84] Risher WC, Kim N, Koh S, et al. Thrombospondin receptor α2δ-1 promotes synaptogenesis and spinogenesis via postsynaptic Rac1. J Cell Biol. 2018;217 (10):3747–3765. DOI:10.1083/jcb.201802057
[85] Tang A-H, Chen H, Li TP, et al. A trans-synaptic nanocolumn aligns neurotransmitter release to receptors. Nature. 2016;536(7615):210.
[86] Biederer T, Kaeser PS, Blanpied TA. Transcellular nanoalignment of synaptic function. Neuron. 2017;96:680–696.
[87] Ichtchenko K, Hata Y, Nguyen T, et al. Neuroligin 1: a splice site-specific ligand for β-neurexins. Cell. 1995;81(3):435–443.
[88] Boucard AA, Chubykin AA, Comoletti D, et al. Code for trans-synaptic cell adhesion mediated by binding of neuroligin 1 to α- and β-neurexins. Neuron. 2005;48(2):229–236.
[89] Missler M, Hammer RE, Südhof TC. Neurexophilin binding to α-Neurexins: a single LNS domain functions as an independently folding ligand-binding unit. J Biol Chem. 1998;273(52):34716–34723.
[90] Sugita S, Saito F, Tang J, et al. A stoichiometric complex of neurexins and dystroglycan in brain. J Cell Biol. 2001;154(2):435–446.
[91] Ko J, Fuccillo MV, Malenka RC, et al. LRRTM2 functions as a neurexin ligand in promoting excitatory synapse formation. Neuron. 2009;64(6):791–798.
[92] De Wit J, Sylwestrak E, O'Sullivan ML, et al. LRRTM2 interacts with neurexin1 and regulates excitatory synapse formation. Neuron. 2009;64(6):799–806.
[93] Uemura T, Lee S-J, Yasumura M, et al. Trans-synaptic interaction of GluRδ2 and neurexin through Cbln1 mediates synapse formation in the cerebellum. Cell. 2010;141(6):1068–1079.
[94] Reissner C, Runkel F, Missler M. Neurexins. Genome Biol. 2013;14(9):213.
[95] Gee NS, Brown JP, Dissanayake VUK, et al. The novel anticonvulsant drug, gabapentin (neurontin),

binds to the subunit of a calcium channel. J Biol Chem. 1996;271(10):5768–5776.
[96] Gurnett CA, De Waard M, Campbell KP. Dual function of the voltage-dependent ca2+ channel α2δ subunit in current stimulation and subunit interaction. Neuron. 1996;16(2):431–440.
[97] Müller CS, Haupt A, Bildl W, et al. Quantitative proteomics of the Cav2 channel nano-environments in the mammalian brain. Proc Natl Acad Sci U S A. 2010;107(34):14950–14957. DOI:10.1073/pnas.1005940107
[98] Voigt A, Freund R, Heck J, et al. Dynamic association of calcium channel subunits at the cellular membrane. Neurophotonics. 2016;3(4):041809.
[99] Kadurin I, Alvarez-Laviada A, Ng SFJ, et al. Calcium currents are enhanced by α2δ-1 lacking its membrane anchor. J Biol Chem. 2012;287(40):33554–33566.
[100] Davies A, Kadurin I, Alvarez-Laviada A, et al. The α(2)δ subunits of voltage-gated calcium channels form GPI-anchored proteins, a posttranslational modification essential for function. Proc Natl Acad Sci U S A. 2010;107(4):1654–1659.
[101] Nilsen TW, Graveley BR. Expansion of the eukaryotic proteome by alternative splicing. Nature. 2010;463(7280):457–463.
[102] Kalsotra A, Cooper TA. Functional consequences of developmentally regulated alternative splicing. Nat Rev Genet. 2011;12(10):715–729.
[103] Lipscombe D, Andrade A, Allen SE. Alternative splicing: functional diversity among voltage-gated calcium channels and behavioral consequences. Biochim Biophys Acta. 2013;1828(7):1522–1529.
[104] Zandany N, Marciano S, Magidovich E, et al. Alternative splicing modulates Kv channel clustering through a molecular ball and chain mechanism. Nat Commun. 2015;6(1):6488.
[105] Thalhammer A, Contestabile A, Ermolyuk YS, et al. Alternative splicing of P/Q-type Ca2+ channels shapes presynaptic plasticity. Cell Rep. 2017;20(2):333–343.
[106] Regan MC, Grant T, McDaniel MJ, et al. Structural mechanism of functional modulation by gene splicing in NMDA receptors. Neuron. 2018;98(521–529):e3.
[107] Bunda A, LaCarubba B, Bertolino M, et al. Cacna1b alternative splicing impacts excitatory neurotransmission and is linked to behavioral responses to aversive stimuli. Mol Brain. 2019;12(1):81.
[108] Heck J, Parutto P, Ciuraszkiewicz A, et al. Transient confinement of CaV2.1 Ca2+-channel splice variants shapes synaptic short-term plasticity. Neuron. 2019;103(1):66–79.e12.
[109] Zhang X, Chen MH, Wu X, et al. Cell-type-specific alternative splicing governs cell fate in the developing cerebral cortex. Cell. 2016;166(1147–1162):e15. DOI:10.1016/j.cell.2016.07.025
[110] Furlanis E, Traunmüller L, Fucile G, et al. Landscape of ribosome-engaged transcript isoforms reveals extensive neuronal-cell-class-specific alternative splicing programs. Nat Neurosci. 2019;22(10):1709–1717.
[111] Huntley MA, Srinivasan K, Friedman BA, et al. Genome-wide analysis of differential gene expression and splicing in excitatory neurons and interneuron subtypes. J Neurosci. 2020;40(5):958.
[112] Soong TW, DeMaria CD, Alvania RS, et al. Systematic identification of splice variants in human P/Q-type channel $\alpha_1$2.1 subunits: implications for current density and $Ca^{2+}$-dependent inactivation. J Neurosci. 2002;22(23):10142.
[113] Kawaguchi Y, Kubota Y. Neurochemical features and synaptic connections of large physiologically-identified GABAergic cells in the rat frontal cortex. Neuroscience. 1998;85(3):677–701.
[114] Liao P, Zhang HY, Soong TW. Alternative splicing of voltage-gated calcium channels: from molecular biology to disease. Pflügers Archiv - European Journal of Physiology. 2009;458(3):481–487. DOI:10.1007/s00424-009-0635-5
[115] Lipscombe D, Andrade A. Calcium channel $Ca_{V\alpha1}$ splice isoforms - tissue specificity and drug action. Curr Mol Pharmacol. 2015;8(1):22–31.
[116] Gray AC, Raingo J, Lipscombe D. Neuronal calcium channels: splicing for optimal performance. Cell Calcium. 2007;42(4–5):409–417.
[117] Dobin A, Davis CA, Schlesinger F, et al. STAR: ultrafast universal RNA-seq aligner. Bioinformatics. 2013;29(1):15–21.
[118] Team RC. R: a language and environment for statistical computing. Austria: Vienna; 2013.
[119] Love MI, Huber W, Anders S. Moderated estimation of fold change and dispersion for RNA-seq data with DESeq2. Genome Biol. 2014;15(12):550.
[120] Wickham H. Programming with ggplot2. ggplot2. Springer: 2016. page 241–253.
[121] Patro R, Duggal G, Love MI, et al. Salmon provides fast and bias-aware quantification of transcript expression. Nat Methods. 2017;14(4):417–419.
[122] Trincado JL, Entizne JC, Hysenaj G, et al. SUPPA2: fast, accurate, and uncertainty-aware differential splicing analysis across multiple conditions. Genome Biol. 2018;19(1):40.
[123] Bourinet E, Soong TW, Sutton K, et al. Splicing of α1A subunit gene generates phenotypic variants of P- and Q-type calcium channels. Nat Neurosci. 1999;2(5):407.
[124] Bell TJ, Thaler C, Castiglioni AJ, et al. Cell-specific alternative splicing increases calcium channel current density in the pain pathway. Neuron. 2004;41(1):127–138.
[125] Chaudhuri D, Chang S-Y, DeMaria CD, et al. Alternative splicing as a molecular switch for $Ca^{2+}$/Calmodulin-dependent facilitation of P/Q-Type $Ca^{2+}$ Channels. J Neurosci. 2004;24(28):6334.

[126] Chaudhuri D, Alseikhan BA, Chang SY, et al. Developmental activation of calmodulin-dependent facilitation of cerebellar P-type $Ca^{2+}$ current. J Neurosci. 2005;25(36):8282.
[127] Chang SY, Yong TF, Yu CY, et al. Age and gender-dependent alternative splicing of P/Q-type calcium channel EF-hand. Neuroscience. 2007;145(3):1026–1036.
[128] Raingo J, Castiglioni AJ, Lipscombe D. Alternative splicing controls G protein-dependent inhibition of N-type calcium channels in nociceptors. Nat Neurosci. 2007;10(3):285–292.
[129] Andrade A, Denome S, Jiang Y-Q, et al. Opioid inhibition of N-type Ca2+ channels and spinal analgesia couple to alternative splicing. Nat Neurosci. 2010;13(10):1249–1256.
[130] Maximov A, Bezprozvanny I. Synaptic targeting of N-type calcium channels in hippocampal neurons. J Neurosci. 2002;22(16):6939.
[131] Maximov A, Südhof TC, Bezprozvanny I. Association of neuronal calcium channels with modular adaptor proteins. J Biol Chem. 1999;274(35):24453–24456.
[132] Hibino H, Pironkova R, Onwumere O, et al. RIM binding proteins (RBPs) couple Rab3-interacting molecules (RIMs) to voltage-gated Ca2+ channels. Neuron. 2002;34(3):411–423.
[133] Kaeser PS, Deng L, Wang Y, et al. RIM proteins tether Ca2+ channels to presynaptic active zones via a direct PDZ-domain interaction. Cell. 2011;144(2):282–295.
[134] Davydova D, Marini C, King C, et al. Bassoon specifically controls presynaptic P/Q-type Ca2+ Channels via RIM-binding protein. Neuron. 2014;82(1):181–194. DOI:10.1016/j.neuron.2014.02.012
[135] Hirano M, Takada Y, Wong CF, et al. C-terminal splice variants of P/Q-type Ca(2+) channel Ca(V)2.1 α(1) subunits are differentially regulated by Rab3-interacting molecule proteins. The. J Biol Chem. 2017(292):9365–9381.
[136] Lee A, Wong ST, Gallagher D, et al. Ca2+/calmodulin binds to and modulates P/Q-type calcium channels. Nature. 1999;399(6732):155.
[137] Lee A, Scheuer T, Catterall WA. $Ca^{2+}$/Calmodulin-dependent facilitation and inactivation of P/Q-Type $Ca^{2+}$. J Neurosci. 2000;20(18):6830.
[138] DeMaria CD, Soong TW, Alseikhan BA, et al. Calmodulin bifurcates the local Ca2+ signal that modulates P/Q-type Ca2+ channels. Nature. 2001;411(6836):484.
[139] Moreno CM, Dixon RE, Tajada S, et al. Ca2+ entry into neurons is facilitated by cooperative gating of clustered CaV1.3 channels. eLife. 2016;5:e15744.
[140] Lipscombe D, Castiglioni AJ. Alternative Splicing in Voltage Gated Calcium Channels. Internet]. In: McDonough SI, editor. Calcium Channel Pharmacology. Boston, MA: Springer US; 2004. page 369–409. Available from: https://doi.org/10.1007/978-1-4419-9254-3_11
[141] Krovetz HS, Helton TD, Crews AL, et al. C-terminal alternative splicing changes the gating properties of a human spinal cord calcium channel α1A Subunit. J Neurosci. 2000;20(20):7564.
[142] Adams PJ, Garcia E, David LS, et al. CaV2.1 P/Q-type calcium channel alternative splicing affects the functional impact of familial hemiplegic migraine mutations: implications for calcium channelopathies. Channels. 2009;3:(2):110–121.
[143] Aikawa T, Watanabe T, Miyazaki T, et al. Alternative splicing in the C-terminal tail of Cav2.1 is essential for preventing a neurological disease in mice. Hum Mol Genet. 2017;26(16):3094–3104. DOI:10.1093/hmg/ddx193
[144] Zhuchenko O, Bailey J, Bonnen P, et al. Autosomal dominant cerebellar ataxia (SCA6) associated with small polyglutamine expansions in the α1A-voltage-dependent calcium channel. Nat Genet. 1997;15(1):62.
[145] Ishiguro T, Ishikawa K, Takahashi M, et al. The carboxy-terminal fragment of α1A calcium channel preferentially aggregates in the cytoplasm of human spinocerebellar ataxia type 6 Purkinje cells. Acta Neuropathol. 2010;119(4):447–464. DOI:10.1007/s00401-009-0630-0
[146] Heyes S, Pratt WS, Rees E, et al. Genetic disruption of voltage-gated calcium channels in psychiatric and neurological disorders. Prog Neurobiol. 2015;134:36–54.
[147] Clark MB, Wrzesinski T, Garcia AB, et al. Long-read sequencing reveals the complex splicing profile of the psychiatric risk gene CACNA1C in human brain. Mol Psychiatry. 2020;25(1):37–47.

## 2.5 Neuroimage Denoiser for removing noise from transient fluorescent signals in functional imaging

Authors: **Stephan Weißbach**, Jonas Milkovits, Michela Borghi, Carolina Amaral, Abderazzaq El Khallouqi, Susanne Gerber, Martin Heine

This article is available as a preprint in *biorXiv* (doi: https://doi.org/10.1101/2024.06.08.598061) and is under review at *Heliyon*.

My contributions to this article are listed in 6.1 Contribution to individual publications.

# Neuroimage Denoiser for removing noise from transient fluorescent signals in functional imaging.

Stephan Weißbach[1,2], Jonas Milkovits[1,2], Michela Borghi[1], Carolina Amaral[1], Abderazzaq El Khallouqi[1], Susanne Gerber[2], Martin Heine[1]

[1] Institute of Developmental Biology and Neurobiology (iDN), Johannes Gutenberg-University, 55128 Mainz, Germany,
[2] Institute of Human Genetics, University Medical Center, Johannes Gutenberg-University, 55131 Mainz, Germany

**Keywords**: glutamate imaging, functional imaging, iGluSnFR, denoising, deep learning

## Highlights

- Neuroimage Denoiser is a deep learning framework to remove noise from functional microscopic recordings, particularly trained and tested for glutamate imaging
- Neuroimage Denoiser balances the removal of noise while preserving the amplitude of responses
- Neuroimage Denoiser operates without re-training for different sensors (when the localization is similar) and recording frequencies

## Motivation

Accurate measurements of neuronal activity through functional imaging are critical in understanding mechanisms of synaptic plasticity and learning concerning changes in the molecular composition of single synapses. Traditional denoising methods, such as Gaussian or Median filters, indiscriminately smooth entire recordings, reducing temporal and spatial resolutions considerably. Existing frameworks are not suited to remove noise from glutamate recordings due to the fast dynamics of the sensor. Therefore, a specialized tool for the challenges imposed by glutamate recordings, i.e. faster dynamics, and synaptic localization, is needed.

## Summary

We developed Neuroimage Denoiser, a novel U-Net-based model that effectively removes noise from microscopic recordings of transient local fluorescent signals. The model makes the denoising process independent of the recording frequency and the kinetics of the sensor used. The framework is easy to use for denoising and training

and has minimal hardware requirements, thus, making it accessible for an average laboratory to create a custom version specific to their experimental setup. Neuroimage Denoiser significantly enhances the quality of functional microscopy recordings by effectively removing noise, thereby facilitating a more accurate and reliable analysis of neural activity.

## Introduction

Noise is a pervasive phenomenon impacting all experimental systems used in neuroscience. Accurate measurement of neuronal activity is crucial for understanding neuronal function, yet noise in imaging systems can severely distort data[1]. With the development of genetically encoded calcium or neurotransmitter sensors, the possibility reading the activity of neuronal subcellular compartments like synapses became feasible, based on fast time-lapse fluorescent imaging. In camera-based setups, noise affects pixels individually without any spatiotemporal relations, often uneven distributed over the field of view. However, the signal from fluorescent reporters that indicates neuronal activity in synapses or somata exhibits a high spatiotemporal correlation.

Traditional methods, such as Gaussian or Median filters, can be used to remove noise from microscopic recordings. While effective to some extent, these filters indiscriminately smooth the entire image, leading to reduced temporal and spatial resolutions[2]. Additionally, the manual selection of filter parameters can be labor-intensive and subjective, often resulting in suboptimal noise reduction.

There has been a considerable effort to remove noise from calcium imaging data and several frameworks have been proposed[3–7]. Notably, Lecoq et al. (2018) developed the deep-learning approach DeepInterpolation[3], a U-Net architecture framework that effectively reduces noise in various biological recordings, including somatic calcium imaging, fMRI, and MEA recordings. DeepInterpolation leverages the data's inherent spatial and temporal relationships to distinguish between true signals and noise, offering a more sophisticated and automated approach to noise reduction[3].

However, commonly used sensors like somatic GCaMP6f, which measure calcium influx, exhibit slower dynamics compared to diffusion-dominated local release of neurotransmitters. Monitoring the synaptic glutamate release needs considerably higher spatial and temporal resolution[8], accessible with camera-based approaches. This can be challenging for a tool that was particularly trained on data acquired using sensors with vastly slower kinetics, i.e. TITL-GCaMP6f, and TIT2L-GCaMP6f-ICL-tTA2[3,9,10]. The glutamate sensor iGluSnFR3.v857.SGZ[11] fluoresces upon glutamate release in the synaptic cleft and subsequent binding to the sensor, providing a much faster signal directly related to neuronal communication[8]. These synaptic signals originate from the fusion of individual transmitter vesicles within the presynaptic membrane and are accompanied by higher background noise compared to the larger somatic calcium signals.

To address these specific challenges, we developed Neuroimage Denoiser, a novel model that effectively removes independent noise from microscopic recordings. Unlike traditional methods, the training and architecture of Neuroimage Denoiser makes the denoising process independent of the recording frequency and the kinetics of the sensor used. This flexibility sets Neuroimage Denoiser apart from previous methods and makes it a versatile tool for various experimental setups, including fast calcium imaging.

Neuroimage Denoiser has minimal hardware requirements, making it accessible for many laboratories to create a custom version tailored to their specific experimental setup. Neuroimage Denoiser enables researchers to obtain high-quality, noise-reduced data without the need for extensive computational resources or expertise.

# Material and Methods

## Primary hippocampal mouse cultures

Primary mouse hippocampal cultures were generated from newborn pups[12]. Animals were sacrificed according to the European and local government (Rheinland-Pfalz, Germany) regulations for animal welfare. After dissociation with trypsin (Thermo Fisher Scientific; Cat#: 15090-046), cells were plated on poly-L-lysine-coated 18 mm glass coverslips with a density of 70,000 cells per coverslip. After 1 h incubation in Dulbecco's Modified Eagle Medium (Thermo Fisher, Gibco; Cat#: 41966-029/D6429) supplemented with 10% fetal bovine serum and 0.5% glutamate at 37°C, coverslips were transferred to 12-well plates containing 1mL of growth medium composed of Neurobasal-A (Thermo Fisher, Gibco; Cat#: 12349-015) with 2% GlutaMax (Thermo Fisher, Gibco; Cat#: 35050-038), 2% B27 (Thermo Fisher, Gibco; Cat#: 17504-044), 0.1 M sodium pyruvate (MERK, Sigma; Cat#: S8636). Cultures were maintained in a humidified incubator with an atmosphere of 95 % air and 5 % $CO_2$ at 37°C.

At DIV3-5 neurons were transfected with glutamate sensor iGluSnFR3.v857.SGZ (Addgene; Cat#: 178330)[11] to perform functional imaging experiments, using the calcium phosphate method. To validate the generalizability of the model, one culture was infected with iGluSnFR.S72A (Addgene; Cat#: 106176)[13]. Briefly, the neuron's growth medium was exchanged with 1 mL of pre-warmed Neurobasal-A medium, and the original medium was stored and kept at 37°C. In the meantime, per 18 mm coverslip, 30 $\mu$L of transfection buffer containing in mM: 274 NaCl, 9.5 KCl, 1.4 $Na_2HPO_4$, 15 Glucose, 15 HEPES, pH 7.14 were added to a solution containing 3 µg of DNA and 2 M $CaCl_2$ and 24 $\mu$L of $H_2O$ (q.s. 30 $\mu$L). The resulting DNA/$CaPO_4$ mix was incubated for 20 min at RT and then added in a proportion of 60 of mix per well. Incubation on neurons was maintained at 37°C until precipitate formation (40 min). Following DNA/$CaPO_4$ incubation, neurons were washed two times for 5 min with 1X HBS buffer containing in mM: 137 NaCl, 4.75 KCl, 0.7 Na2HPO4, 7.5 Glucose, 7.5 HEPES, pH 6.9 and for one time for 5 min with Neurobasal-A medium. Following the

washing steps, the original growth medium was added, and neurons were stored in the incubator at 37°C until live imaging experiments were performed at DIV16 - 19.

## Functional Imaging

All live experiments were conducted on hippocampal cultures 16 - 19 DIV at 37°C within a whole microscope incubator. Neurons were perfused with extracellular solution containing (in mM): 145 NaCl, 2.5 KCl, 10 HEPES, and 10 D-glucose 2 $MgCl_2$, 2 $CaCl_2$ (pH 7.4). Network activity was suppressed by adding 10 µM CNQX (Tocris; Cat#: 1045) and 10 µM D-AP5 (Tocris; Cat#: 0106) to the extracellular solution as indicated for the respective experiment. Experiments were performed with an inverted total internal reflection fluorescence (TIRF) setup composed of the eclipse Ti microscope (Nikon) equipped with a 60 x Apo TIRF oil objective (1.49 NA; Nikon). Fluorescence was excited with a combined laser system (Coherent; MPB Communications Inc.). Images were captured by a scientific CMOS camera (ORCA-Fusion C14440-20UP, Hamamatsu) at frame rates between 100 to 1000 Hz controlled by NIS-Elements Advanced Research acquisition software (Nikon). Electrical field stimulation was carried out using two platinum electrodes placed on the coverslip at a 10 mm distance. Extracellular stimulus sequences (0.9 ms; 50 mA; 1 s interval) were triggered by an isolated pulse generator (A&M Systems, Model 2100) and delivered via a stimulus isolator unit A385 (WPI). Images were acquired by image streaming for 2000 frames at 100 Hz within a defined region of interest (ROI) 800 x 800 pixels (100 Hz acquisition rate) or 250 x 250 pixels (1000 Hz acquisition rate) with a pixel size of 72nm. Triggered electrical field stimulation was used to elicit 20 action-potential-like stimuli.

## Synaptic ROI and Threshold

Circular synaptic ROIs were selected manually using Fiji (version 1.54f)[14] and set to a diameter of 9 pixels. The average traces along the z-axis of the synapses were extracted by either Fiji (version 1.54f)[14] or Python (version 3.10.14)[15] with roifile (version v2024.3.29)[16].

On the average traces, the threshold was computed using numpy (version 1.26.4)[17] based on the baseline frames up to the first stimulation, using the formula:

$$Threshold(x) = mean(x) + threshold_{mult} * std(x)$$

Whenever the average trace crossed the computed threshold (set by $threshold_{mult}$), this was considered to be a response.

## Preparing Training Data

Training deep learning models is sensitive to imbalances between foreground and background[18,19]. The microscopic recording of synaptic glutamate responses is dominated by background due to the small synapses that sparsely respond when defining a responding synapse as foreground. Therefore, the available data is filtered for active regions and frames to remove the background (Figure 1a). We transformed our recording frames into activity maps to filter efficiently. First, the data is transformed

by a pixel-wise rolling window (along 50 frames) z-normalization (Figure 1b). The rolling window adapts for potential bleaching in the recording.

$$z\ score_{frame} = \frac{x_{frame} - \mu_{window_{start}:window_{end}}}{\sigma_{window_{start}:window_{end}}}$$

An activity map is calculated framewise and represents the maximum z-score within a local region for each spatial position in each frame. Each frame is divided into crops of a predefined size of 32 x 32 pixels to compute the activity map. A crop is assigned with the maximum value of the kernel-averaged region, obtained by sliding a quadratic kernel over the crop (step size 1) and computing the average intensity within that kernel at each position (Figure 1c, right). The kernel size corresponds to the expected minimal region of interest (ROI) size, reflecting the spatial extent of the structures under investigation (6 pixels for synapses in our setup). The activity map effectively captures and highlights regions exhibiting high-intensity fluctuations that are potential indicators of neuronal activity, by assigning the maximum averaged kernel value to each crop. Next, these activity maps are filtered for crops that exceed a minimum z-score of 3. Subsequently, the pixel-wise z-score (without using a rolling window) is computed, and the transformed crop is stored in an h5 file for training, using h5py (version 3.11.0).

Neuroimage Denoiser can be run on an entire directory storing multiple recordings and will automatically prepare the training data without manual intervention. Additionally, a memory-optimized version is implemented that necessitates less RAM at the cost of a longer run-time.

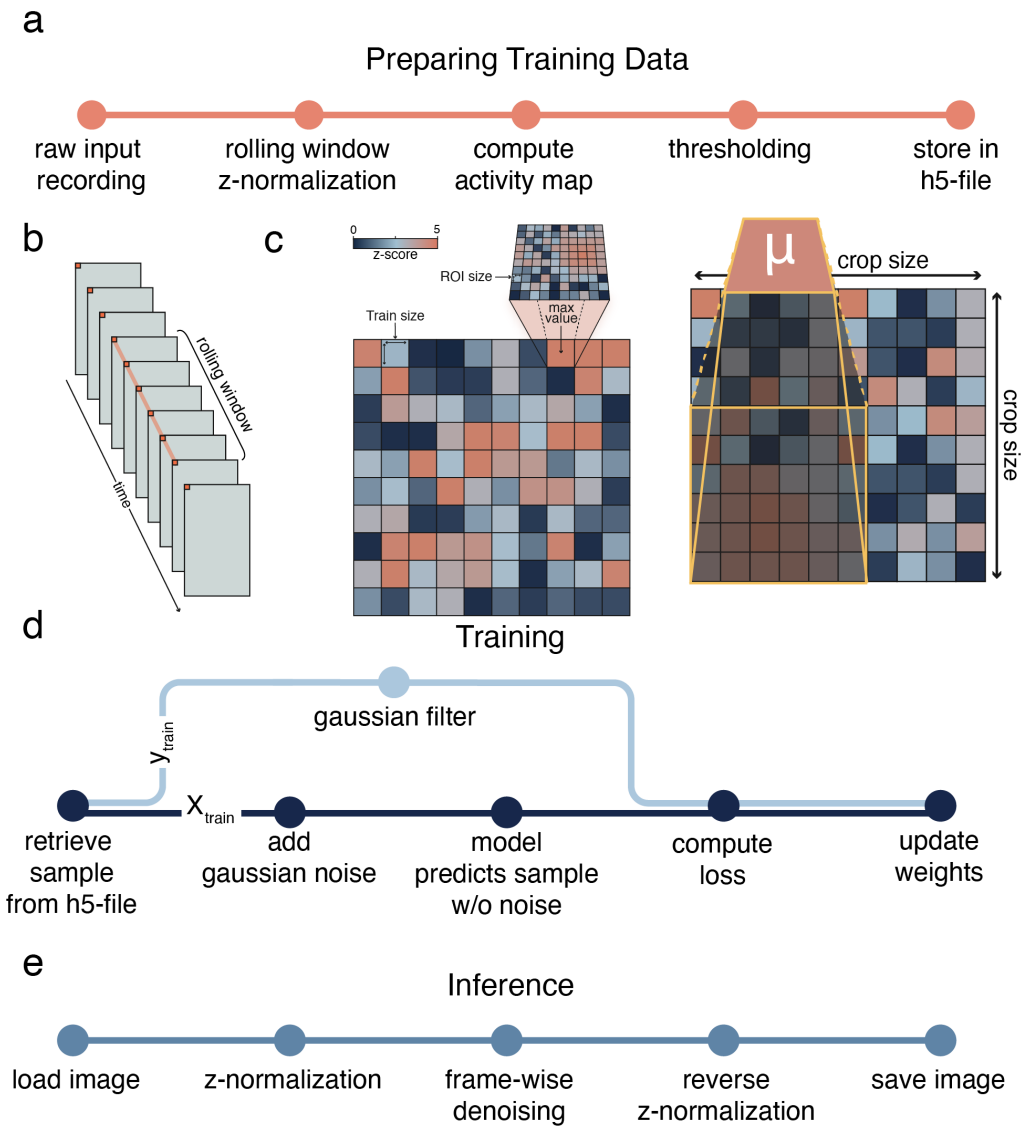


*Figure 1 a) Schematic representation of the preparation of the training data. The preparation aims to enrich the foreground (crops of the recording with responding synapses/somata) over the background (non-responding frames or crops) and store them in an h5 file for training. b) Z-normalization for training data preparation is computed per pixel using a rolling window to account for potential bleach occurring during the recording. c) Schematic representation of an activity map that is computed for each frame of a recording during the training data preparation step. The frame is divided into crops of equal size. Per crop, the average z-score per possible ROI of a given size is computed and whenever this averaged z-score exceeds a set threshold, the crop is added to the training data. Left: one frame divided into crops and applied average filter; right: average filter applied of ROI size 6 to a crop d) Schematic representation of the training routine. $X_{train}$ represents the input on which the model makes its prediction, and the result is compared to $y_{train}$. f) Schematic representation of the inference/denoising process. The inference is done on a z-normalized representation of the recording, which is reversed after denoising.*

## Model Architecture and Training

The U-Net model[20] is implemented in PyTorch (version 2.1.1.)[21] with a single input and output channel (Figure 1a). The U-Net architecture consists of an encoder and a

decoder. The encoder comprises blocks containing two 2D convolutional layers with 3x3 kernels, ReLU activation, and batch normalization, followed by a 2D max-pooling layer for downsampling. These blocks are referred to as down-blocks. Skip connections connect the corresponding down-blocks to the up-blocks in the decoder without any processing.

The decoder comprises up-blocks, each consisting of a 2D transpose convolutional layer for upsampling, followed by a concatenation with the respective feature map from the corresponding down-block (skip connection). This concatenated output is then processed by two 2D convolutional layers with 3x3 kernels, ReLU activation, and batch normalization. The final layer is a 1x1 2D convolutional layer that maps the feature vector to the denoised image. This architecture allows the network to capture both local and global features, enabling accurate denoising of the input image. Using a fully convolutional model without dense layers allows flexible input image sizes during inference, limited only by GPU memory, overcoming fixed training input constraints.

Training is performed on z-transformed patches containing active synapses for one epoch using a batch size of 64, the ADAM optimizer with a learning rate of 0.0001, on a consumer-grade NVIDIA GeForce 2060 super graphics card with 8GB of vRAM. A grid search for the parameters listed in Table 1 was performed to find a suitable combination of parameters for the training. The model's objective is to reduce noise in the recordings while maintaining the integrity of the peak response amplitudes.

To evaluate the model's performance in preserving the amplitude of neural responses, regions of interest (ROIs) exhibiting clear stimulus-evoked responses were manually identified in the raw recorded data. The peak response amplitudes within these ROIs were measured following the presentation of a stimulus. After training the model, the same ROIs were analyzed in the denoised output, and the corresponding peak response amplitudes were extracted. The model's accuracy in preserving the response amplitudes is quantified by calculating the Mean Absolute Percentage Error (MAPE) using scikit-learn (version 1.5.0)[22] between the raw and denoised peak amplitudes across all ROIs. The correlation between raw and denoised peak amplitudes was calculated using scipy[23].

$$MAPE = 100 * \frac{1}{n}\sum_{t=1}^{n}\left|\frac{peak_t^{raw} - peak_t^{denoised}}{peak_t^{raw}}\right|$$

Additionally, it is crucial that the model efficiently removes noise from the microscopic recordings. This is measured by the standard deviation of non-responding sections of the recordings.

Both metrics (MAPE and standard deviation) are ranked, and a combined score is calculated. The best-performing model is selected based on the minimal combined score achieved (supplementary table 1).

$$score = \frac{(Rank_{std} + 2 * Rank_{MAPE})}{3}$$

*Table 1 Model Optimization Parameters: This table presents the various parameters tested during the optimization of the Neuroimage Denoiser model. For each parameter, different variables were tested to determine*

*the most effective configuration. The "Best performing Model" column lists the values that yielded the best performance based on the evaluation metrics.*

| Parameter | Tested Variables | Best performing Model |
|---|---|---|
| Loss Function | L1, Smooth-L1, MSE, Huber | Smooth-L1 |
| Use Gaussian Filter on $y_{True}$ | True, False | True |
| Sigma Gaussian Filter | 0.5, 1.0 | 1.0 |
| Noise Center | 0, 0.5, 1.0 | 0 |
| Noise Scale | 0.5, 1.0, 1.5, 2.0, 3.0 | 2.0 |

## Inference/Denoising

The denoising (or inference) using Neuroimage Denoiser can be done on single images or entire directories containing multiple sub-directories while maintaining the original folder structure. The process is schematically visualized in Figure 1e. First, the input image is loaded in tiff or nd2 format using tifffile (version 2023.12.9)[24] or nd2 (version 0.8.1) respectively and a z-normalization (along the time axis; no rolling window) is applied. The mean and standard deviation per pixel is temporarily saved. Neuroimage Denoiser performs the denoising on the z-normalized frames and afterward, the resulting frames are transformed back into intensity values using the saved mean and standard deviation. The denoised image is saved as a tiff file using tifffile (version 2023.12.9)[24].

## Reimplementation of DeepInterpolation

To fairly compare the performance of DeepInterpolation[3] with the approach of Neuroimage Denoiser, we re-implemented the model in PyTorch (version 2.1.1)[21]. Therefore, the model can be trained on crops of active synapses (32 x 32 pixels) and comparability was ensured. The number of frames before and after the target frames was reduced to five frames to account for the faster dynamics of glutamate sensors (Supplementary Figure 1a). The model was trained using the ADAM optimizer with an L1 loss function, and a learning rate of 0.0001 on an NVIDIA GeForce GTX2060 super graphics card.

## Data Visualization

Data was visualized using Python (version 3.10.14)[15], matplotlib (version 3.9.0)[25], and seaborn (version 0.13.2)[26]. Schematic drawings were made using Adobe Illustrator.

# Results

Denoising glutamate imaging data presents unique challenges compared to calcium imaging, as glutamate sensors are orders of magnitude faster and the synaptic localization results in considerably less foreground signal relative to somatic calcium recordings. Here, we present Neuroimage Denoiser, a U-Net-based imaging denoising

tool (Figure 1a) specifically trained to remove noise from microscopic glutamate time-series recordings.

To curate a balanced training dataset adjusted to the challenges posed by glutamate imaging data, the recordings are automatically screened to identify frames and regions exhibiting active synaptic signals (Figure 1a) in the training preparation step without manual intervention. This screening can be adapted to different ROI sizes representing the size in pixels of the biological structure where the sensor is localized. We set the ROI size to 6 pixels to account for the size of synapses harboring the sensor in our microscopic set-up.

Initially, we explored training a model in the style of DeepInterpolation[3]. DeepInterpolation predicts a target frame based on a set number of frames preceding and succeeding the target frame ($n_{pre}$, $n_{post}$)[3]. To account for the fast dynamics of the iGluSnFR3 sensor compared to Gcamp6f, we set $n_{pre}$ = 5 and $n_{post}$ = 5 and the model predicts the target frame in the middle (Supplementary Figure 1a). However, this temporal interpolation approach, while effective for slower calcium dynamics, did not adequately preserve the fast glutamate response and led to artifacts in the amplitudes (Supplementary Figure 1b).

Given the limitations of the DeepInterpolation strategy for capturing these rapid synaptic signals, we turned to the Noise2Noise concept proposed by Lehtinen and colleagues[27]. Their work demonstrated image restoration without ground truth data by training networks to distinguish signals from noise patterns by adding artificial noise to noisy images. Leveraging this approach, Neuroimage Denoiser is trained according to the Noise2Noise[27] method on individual frames and subsequently circumvents the dependence on the recording frequency or the dynamics of the sensor. Therefore, a trained model can be applied to a broad range of sensors that have similar localization independently of the recording frequency.

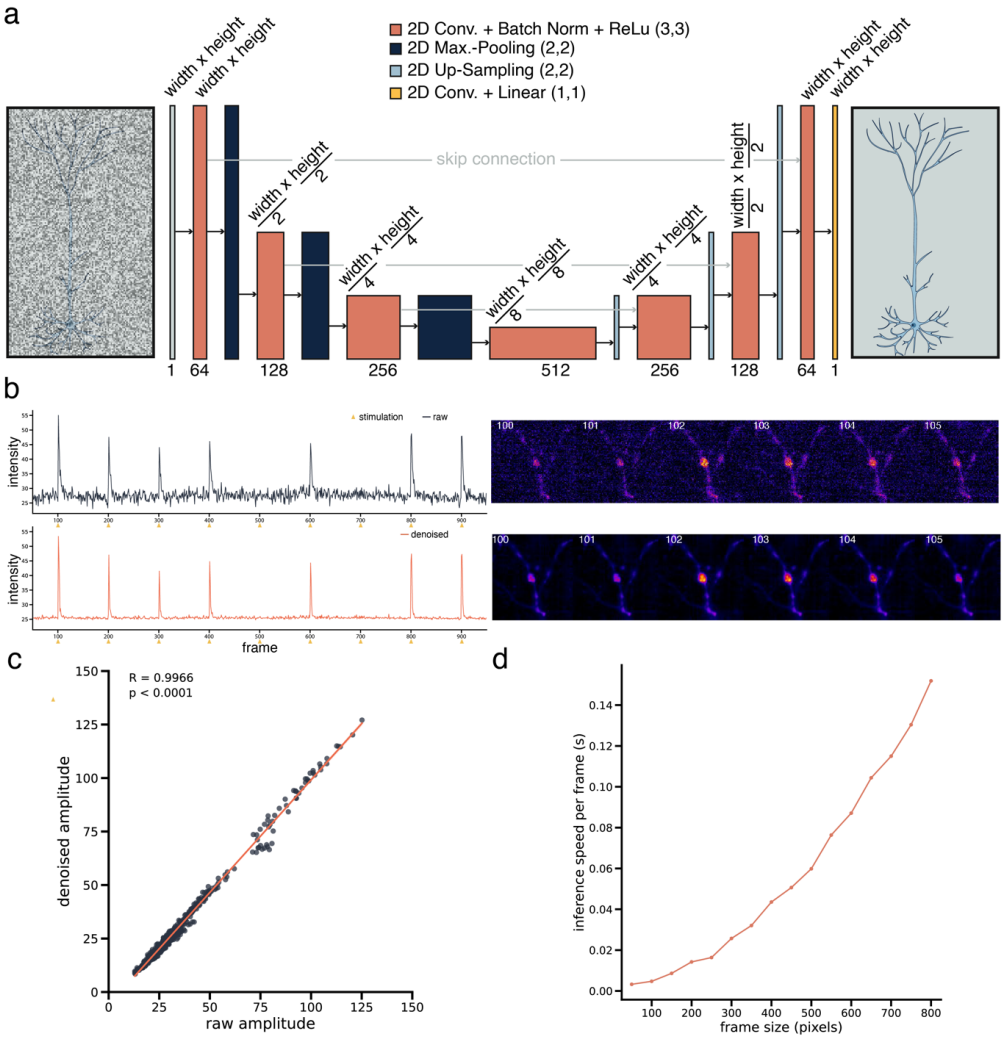


*Figure 2 a) Schematic representation of the architecture used for Neuroimage Denoiser is a U-Net[20] with one input and output channel. The data runs through the encoder and decoder part of the network while skip connections preserve untransformed data. Convolutional layers (orange) use a 3 by 3 filter with ReLu activation. The output layer is a linear layer that does not use an activation function. b) Representative area of a glutamate recording acquired at 100Hz. The stimulus is given in frame 100 and the peak response is in frame 102. After denoising, the amplitude height and time points are well preserved, and the noise level is minimal. c) Neuroimage Denoiser denoised amplitude heights of manually selected ROIs tested against the raw amplitude heights, showing a high correlation (R=0.9966, p<0.0001). d) Denoising inference speed (frames per second) tested for frame sizes 50 - 800 pixels (averaged values of three repetitions of recordings with 1,000 frames). The image was processed according to Figure 1e)*

We conducted a grid search to identify the optimal combination of training parameters (Table 1) and selected the model that best balanced noise removal and amplitude preservation (Supplementary Table 1). The best-performing model was trained using a smooth L1-loss. The training data included Gaussian noise added with a noise center of 0.0 and a noise scale of 2.0. Notably, higher noise scale and center values yielded models that removed noise more effectively but at the cost of less reliable amplitude

preservation (Supplementary Table 1). The selected model effectively removes noise from the raw recording, both visually as measured in the z-profile of the synaptic ROI (Figure 2b), while preserving the amplitudes well (Figure 2c), as evidenced by a significant correlation between raw and denoised amplitudes ($R=0.9966$, $p < 0.0001$). Neuroimage Denoiser demonstrates fast inference, as tested on three recordings of 1000 frames with varying spatial dimensions (50 to 800 pixels for x and y). The entire process, including normalization and reverse normalization, as shown in Figure 1e, requires between 0.0003 and 0.1519 seconds per frame (Figure 2d). Therefore, denoising 800 x 800 pixels recording of the length of 1,000 frames takes ~152 seconds.

## Neuroimage Denoiser enables precise Signal Localization across diverse Recording Conditions

Only infrequent spontaneous activity can be observed when recording a neuronal culture in the absence of electric stimulation. Specifically, it is challenging to differentiate the components at complex synapses, which comprise an accumulation of pre-synaptic inputs and post-synaptic receivers. These synapses often involve multiple release sites in close proximity, and the released glutamate can diffuse from its initial release site, leading to highly correlated signals at neighboring post-synaptic sites (Figure 3a, left). However, the maximum localization of a spontaneous release event indicates the release site. Due to the spatial proximity within these complex synapses, identifying and differentiating post-synaptic receiving sites is difficult when the signal is superimposed by noise (Figure 3a, top). After removing the noise using Neuroimage Denoiser, each of the three distinct sites within the complex synapse becomes visible and can be accurately localized (Figure 3a, bottom).

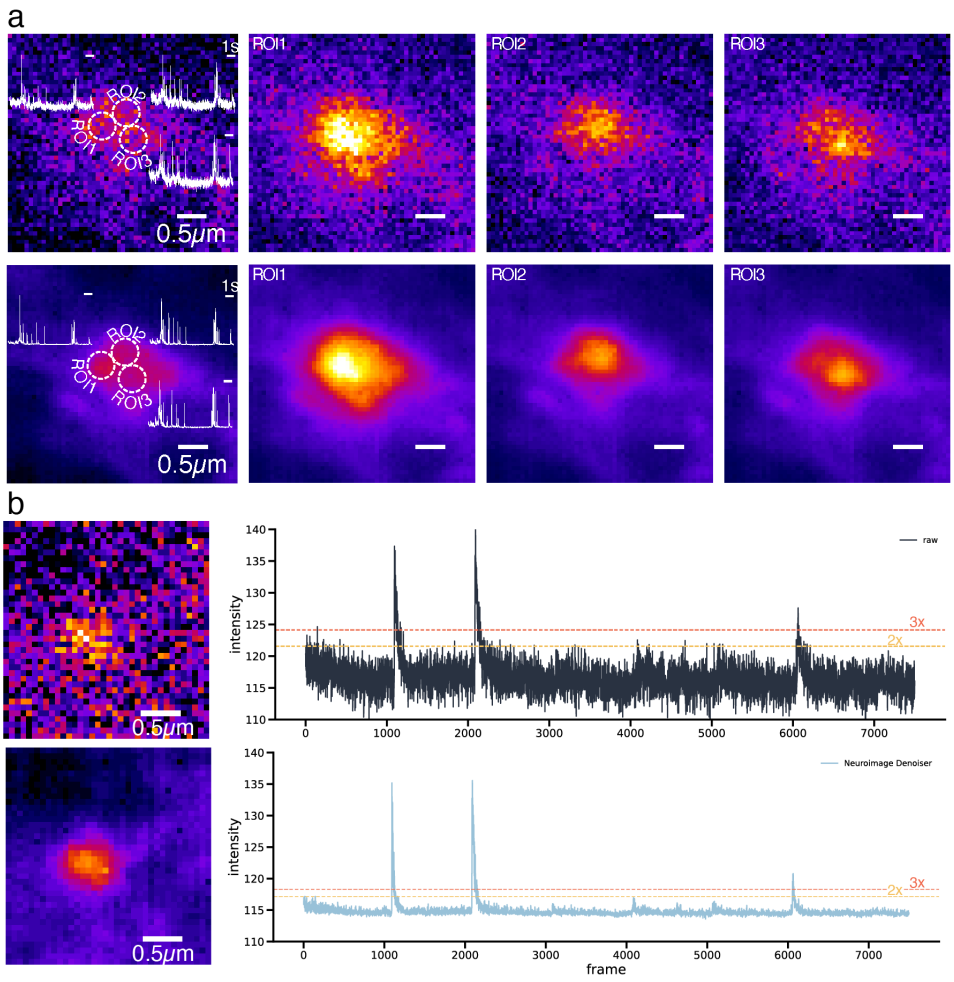


*Figure 3 a) Complex synapse with three sites that receive spontaneous input from different pre-synaptic sites. The top row shows the raw recording as it was acquired at the microscope and the bottom row shows the same frames denoised by Neuroimage Denoiser. The three different sites showing spontaneous activity are visible. The traces at these sites are highly correlated due to their proximity. b) Neuroimage Denoiser works on recordings acquired with very high recording frequencies (tested here with 1000Hz) although being trained on 100 Hz recordings exclusively.*

While Neuroimage Denoiser was trained exclusively on recordings done with 100 Hz, the model is capable of denoising recordings acquired at significantly higher acquisition rates, such as 1000 Hz (Figure 3b). The ability to acquire data at such high frequencies is valuable for capturing rapid synaptic events and amplitudes with high temporal precision. However, high noise levels often complicate these high-frequency recordings, making it challenging to identify true responses amidst false-positive threshold crossings (Figure 3b, top). The denoised recording, on the other hand, has a considerably improved signal-to-noise ratio (Figure 3b, bottom), like the improvement observed in previous recordings at 100 Hz. Therefore, Neuroimage Denoiser can facilitate the analysis of recordings acquired at very high frequencies without the need to re-train a new model. Acquiring at these high rates opens the door to various

applications, such as analyzing multi-vesicular or asynchronous releases from a single synapse, which would yield variable amplitudes and subsequent peaks, or resolving the precise time from stimulus to glutamate release with higher temporal resolution. Additionally, it enables the study of rapid synaptic plasticity mechanisms and the precise kinetics of neurotransmitter release and clearance. The camera-based imaging will allow the comparison of direct multiple synapses in the field of view, which will outcompete scanning microscopy-based approaches, where only single synapses can be imaged at necessary high acquisition rates (>100 Hz).

## Application of Neuroimage Denoiser on alternative Glutamate Sensor to study Synaptic Plasticity

Since Neuroimage Denoiser is not bound to a certain sensor and its associated kinetics but only to its localization, we applied the denoising to recordings of fast iGluSnFR.S72A[13]. This version of the sensor has faster kinetics, but a lower signal-to-noise ratio compared to iGluSnFR3.v857.SGZ[11] particularly due to the high noise level present in the baseline of the recording (until stimulation at frame 100). This noise in the baseline elevates the threshold above which a signal is considered a release event. iGluSnFR.S72A[13] is useful for plasticity studies since the kinetic properties allow the recording of synaptic release events up to 20 Hz pulse interval. Conventionally such recordings are done via patch-clamp[13], which will not allow reaching the single synapse resolution as easily as imaging approaches. Conversely, iGluSnFRs timing and localization of excitatory synaptic inputs[8] enable a more complete picture of the synaptic plasticity of a neuron under a given condition, which is of particular interest for investigating the molecular mechanisms underlying synaptic plasticity. Key plasticity metrics are the paired-pulse ratio, quantifying facilitation or depression of consecutive responses, and the failure rate, measuring the proportion of stimuli failing to evoke a response hence indicating release probability. Nevertheless, due to the low signal-to-noise level and the fast bleaching of the sensor, the recordings are superimposed by noise (Figure 4a, left) that considerably complicates the identification of responding synapses and to differentiate between response and failure within the average trace of a selected synapse (Figure 4b, top). The given example in Fig. 4 illustrates the impact of noise in fast pulse trains. Even though a very small threshold multiplier of two is applied to the raw average trace the responses to the stimulus given at frames 130 and 140 are not detected. Moreover, the noise in the raw data (Figure 4b, top) obscures these responses, while the denoised trace (Figure 4b, bottom) reveals clear and distinct responses upon each of the five stimuli. Thus, the failure rate can be determined to be 0% after applying denoising with Neuroimage Denoiser (threshold multiplier 2), contrary to 40% in the raw trace (threshold multiplier 2). Additionally, when computed with a multiplier of two (yellow dashed line, Figure 4b), the low threshold leads to the detection of false positive responses in the raw trace.

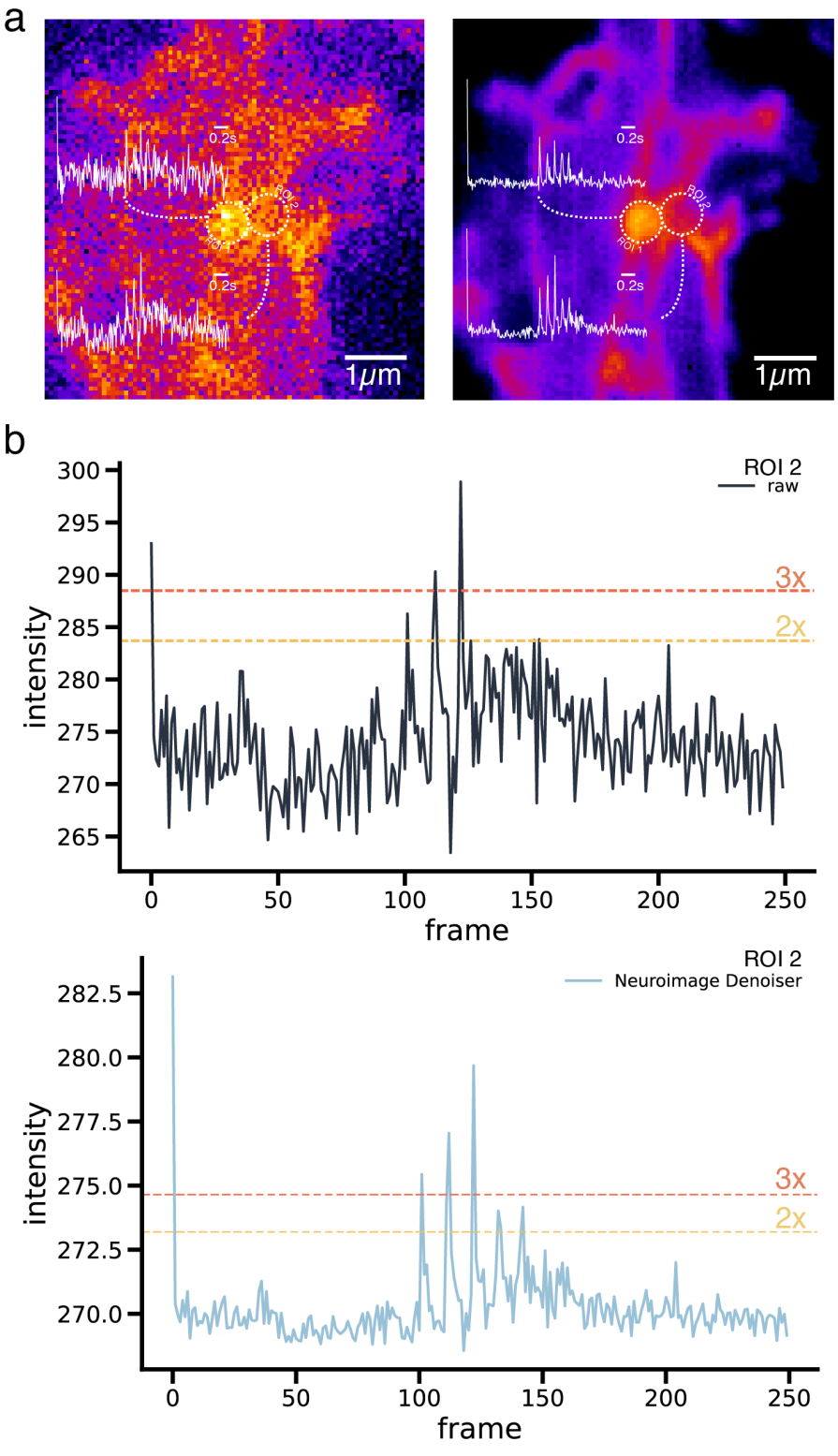

*Figure 4 a) A crop of the recording with iGluSnFR.S72A. The left panel represents the raw data with high noise levels, while the right panel shows the denoised data using Neuroimage Denoiser. b) Average intensity trace for ROI 2 over the recorded 250 frames. Stimulation is applied at frames 100, 110, 120, 130, and 140. The top graph is extracted from the raw recording and is characterized by significant noise and fluctuations. The bottom graph shows the denoised average intensity trace from ROI 2, where the noise level is substantially reduced, allowing clearer identification of responses to stimuli. Particularly, responses to the stimulation in frames 130 and 140, which are within the noise level in the raw trace, become visible in the denoised trace. The threshold for two low threshold multipliers is indicated as yellow and orange dashed lines, for multipliers two and three respectively.*

# Discussion

In this manuscript, we presented Neuroimage Denoiser – a U-Net-based[20] deep-learning framework to reduce noise levels in microscopic imaging recordings. By incorporating the concepts of Noise2Noise[27], the Neuroimage Denoiser framework is highly flexible for a wide array of experimental settings and does not require re-training for changed parameters. In the past, researchers developed several sensors to study functional neurobiology for the dynamics of calcium[28], GABA[29], dopamine[30], acetylcholine[31], and glutamate[11,29] on a single synapse level. These recordings are superimposed with noise regardless of the sensor and acquisition rate. Consequently, a unified model capable of denoising recordings when having the same localization would considerably ease the downstream processing. Therefore, we tested our model by applying the denoising routine to changed parameters, i.e. recording frequency (Figure 3) and sensor (Figure 4), and obtained convincing results. The proposed framework is capable of considerably reducing the noise in experiments with fast dynamics, as typical for glutamate imaging, which did lead to artifacts in responses when using previously described deep learning frameworks[3] (Supplementary Figure 1). One of the advantages of Neuroimage Denoiser is its ability to preserve the amplitude of synaptic responses, as evidenced by a high correlation ($R = 0.9966$, $p < 0.0001$) between denoised and raw responses (Figure 2c). Further, the improved signal-to-noise level helps to resolve complex synapses spatially (Figure 3) which can ease the analysis of spontaneous activity and be used as a functional readout for molecular manipulation to define release mechanisms in specific synapses.

We anticipate that Neuroimage Denoiser can be adopted in many laboratories as it has minimal hardware requirements, and the preparation of the training data is automatically balanced for optimal results. The framework is easy to use for data preparation, training, grid search, and inference (denoising) and does not require additional programming knowledge, making it accessible to a broad range of researchers in the field of neuroscience. Although glutamate imaging as a neural recording method can provide rich and diverse datasets, these data have a high complexity with many disruptive elements, such as noise, bright sensor depositions, or vesicular transport of sensor, that make the creation of ground truth data for training a model on responding regions of a recording challenging. Our training data preparation routine offers a way to balance the training data without time-consuming manual intervention and curation. We tested a several potential training parameters (Table 1)

to select the most performant parameter combination, however, users can freely choose a combination suited for their experimental set-up and analysis.
Neuroimage Denoiser is anticipated as a framework for fast responses and is specifically trained to denoise glutamate imaging recordings. However, its flexibility ensures that it is well-suited to work for a variety of typical functional experiments to improve the signal-to-noise ratio.

## Code availability

The code is available at https://github.com/s-weissbach/neuroimage_denoiser.

## Acknowledgment

The authors acknowledge financial support from the Emergent Algorithmic Intelligence Centre funded by the Carl-Zeiss Foundation. We thank Anita Heine, Nathalie Philipp, and Corinna Werkmann for technical support and excellent hippocampal culture preparation. The authors thank Stanislav Sys for critical feedback and discussion.

## Authors contribution

SW and MH conceived the idea and conceptualized the work. MB, CA, AK, and MH conducted experiments. SW conceptualized and implemented the Neuroimage Denoiser framework. SW and JM implemented the data preparation routine. SW created visualizations. SW, MB, and MH wrote the manuscript. SG revised the manuscript. MH and SG supervised the project and acquired funding.

## References

1. Wilt, B. A., Fitzgerald, J. E. & Schnitzer, M. J. Photon Shot Noise Limits on Optical Detection of Neuronal Spikes and Estimation of Spike Timing. *Biophys. J.* **104**, 51–62 (2013).
2. Buades, A., Coll, B. & Morel, J.-M. A non-local algorithm for image denoising. in *2005 IEEE Computer Society Conference on Computer Vision and Pattern Recognition (CVPR'05)* vol. 2 60–65 vol. 2 (2005).
3. Lecoq, J. *et al.* Removing independent noise in systems neuroscience data using DeepInterpolation. *Nat. Methods* **18**, 1401–1408 (2021).
4. Pnevmatikakis, E. A. *et al.* Simultaneous Denoising, Deconvolution, and Demixing of Calcium Imaging Data. *Neuron* **89**, 285–299 (2016).
5. Malik, W. Q., Schummers, J., Sur, M. & Brown, E. N. Denoising Two-Photon Calcium Imaging Data. *PLOS ONE* **6**, e20490 (2011).
6. Li, X. *et al.* Real-time denoising enables high-sensitivity fluorescence time-lapse imaging beyond the shot-noise limit. *Nat. Biotechnol.* **41**, 282–292 (2023).
7. Chaudhary, S., Moon, S. & Lu, H. Fast, efficient, and accurate neuro-imaging denoising via supervised deep learning. *Nat. Commun.* **13**, 5165 (2022).

469 8. Marvin, J. S. *et al.* An optimized fluorescent probe for visualizing glutamate
470 neurotransmission. *Nat. Methods* **10**, 162–170 (2013).
471 9. Madisen, L. *et al.* Transgenic Mice for Intersectional Targeting of Neural
472 Sensors and Effectors with High Specificity and Performance. *Neuron* **85**, 942–958
473 (2015).
474 10. Daigle, T. L. *et al.* A Suite of Transgenic Driver and Reporter Mouse Lines with
475 Enhanced Brain-Cell-Type Targeting and Functionality. *Cell* **174**, 465-480.e22
476 (2018).
477 11. Aggarwal, A. *et al.* Glutamate indicators with improved activation kinetics and
478 localization for imaging synaptic transmission. *Nat. Methods* **20**, 925–934 (2023).
479 12. Kaech, S. & Banker, G. Culturing hippocampal neurons. *Nat. Protoc.* **1**, 2406–
480 2415 (2006).
481 13. Marvin, J. S. *et al.* Stability, affinity, and chromatic variants of the glutamate
482 sensor iGluSnFR. *Nat. Methods* **15**, 936–939 (2018).
483 14. Schindelin, J. *et al.* Fiji: an open-source platform for biological-image analysis.
484 *Nat. Methods* **9**, 676–682 (2012).
485 15. The Python Language Reference — Python 3.10.12 documentation.
486 https://docs.python.org/3.10/reference/.
487 16. Gohlke, C. cgohlke/roifile: v2024.5.24. Zenodo
488 https://doi.org/10.5281/zenodo.11266632 (2024).
489 17. Harris, C. R. *et al.* Array programming with NumPy. *Nature* **585**, 357–362
490 (2020).
491 18. Saini, M. & Susan, S. Tackling class imbalance in computer vision: a
492 contemporary review. *Artif. Intell. Rev.* **56**, 1279–1335 (2023).
493 19. Chen, J., Wu, Q., Liu, D. & Xu, T. Foreground-Background Imbalance Problem
494 in Deep Object Detectors: A Review. in *2020 IEEE Conference on Multimedia*
495 *Information Processing and Retrieval (MIPR)* 285–290 (2020).
496 doi:10.1109/MIPR49039.2020.00066.
497 20. Ronneberger, O., Fischer, P. & Brox, T. U-Net: Convolutional Networks for
498 Biomedical Image Segmentation. Preprint at
499 https://doi.org/10.48550/arXiv.1505.04597 (2015).
500 21. Paszke, A. *et al.* PyTorch: An Imperative Style, High-Performance Deep
501 Learning Library. Preprint at https://doi.org/10.48550/arXiv.1912.01703 (2019).
502 22. Pedregosa, F. *et al.* Scikit-learn: Machine Learning in Python. *Mach. Learn.*
503 *PYTHON*.
504 23. Virtanen, P. *et al.* SciPy 1.0: fundamental algorithms for scientific computing in
505 Python. *Nat. Methods* **17**, 261–272 (2020).
506 24. Gohlke, C. cgohlke/tifffile: v2024.5.22. Zenodo
507 https://doi.org/10.5281/zenodo.11256883 (2024).
508 25. Ari, Niyazi & Ustazhanov, Makhamadsulton. Matplotlib: A 2D Graphics
509 Environment. *IEEE J. Mag.* (2014).
510 26. Waskom, M. L. seaborn: statistical data visualization. *J. Open Source Softw.* **6**,
511 3021 (2021).
512 27. Lehtinen, J. *et al.* Noise2Noise: Learning Image Restoration without Clean
513 Data. Preprint at http://arxiv.org/abs/1803.04189 (2018).
514 28. Chen, T.-W. *et al.* Ultrasensitive fluorescent proteins for imaging neuronal
515 activity. *Nature* **499**, 295–300 (2013).
516 29. Marvin, J. S. *et al.* A genetically encoded fluorescent sensor for in vivo
517 imaging of GABA. *Nat. Methods* **16**, 763–770 (2019).

518 30. Sun, F. *et al.* A Genetically Encoded Fluorescent Sensor Enables Rapid and
519 Specific Detection of Dopamine in Flies, Fish, and Mice. *Cell* **174**, 481-496.e19
520 (2018).
521 31. Borden, P. M. *et al.* A fast genetically encoded fluorescent sensor for faithful in
522 vivo acetylcholine detection in mice, fish, worms and flies. 2020.02.07.939504
523 Preprint at https://doi.org/10.1101/2020.02.07.939504 (2020).
524

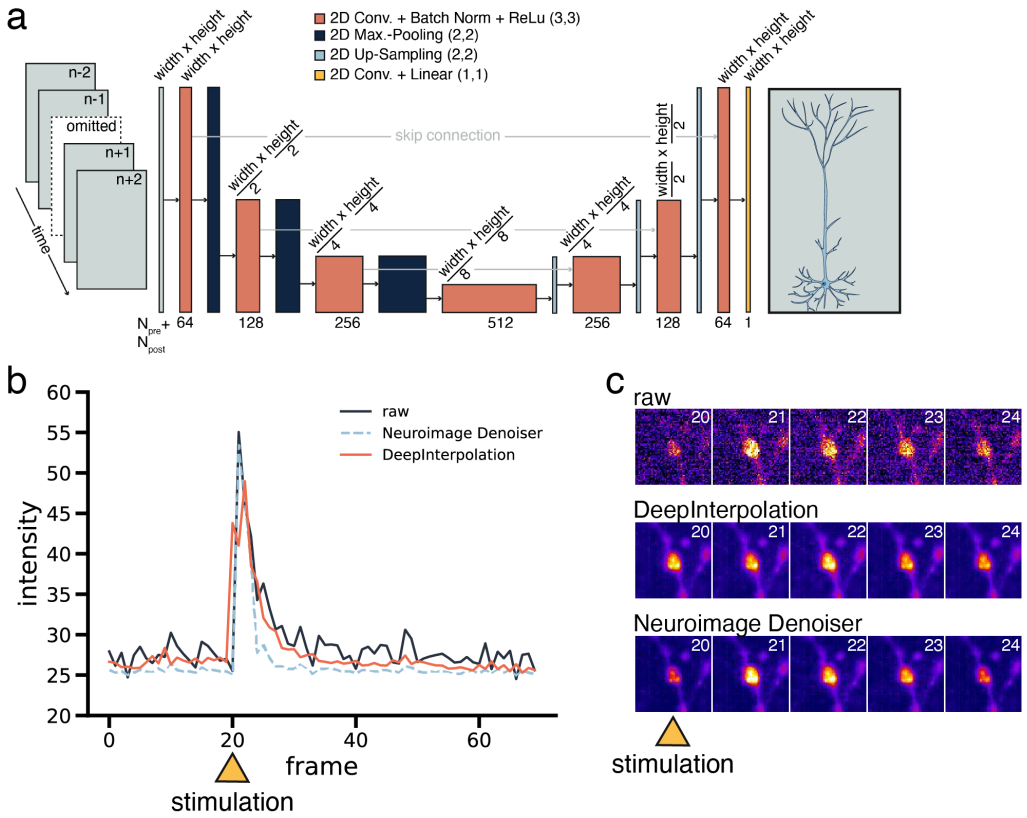


*Supplementary Figure 1 a) Schematic representation of a U-Net in the style of DeepInterpolation. Predictions are made based on five frames before and after the target frame (which is omitted). The model predicts tries to predict the omitted frame. b) Example of an artifact produced by a DeepInterpolation-styled approach (orange) to denoising for the fast kinetic of iGluSnFR. The peak is not preserved, instead, a double peak emerges with the original peak being of lower intensity than the preceding and succeeding frames. c) Raw, DeepInterpolation, and Neuroimage Denoiser denoised recordings of the synapse. Stimulation was applied at frame 20. It is visible that DeepInterpolation shifts the peak response from frame 21 to frame 22.*

# 3 Overall discussion and conclusion

The development of the neuronal networks within the cerebral cortex is a remarkably complex process requiring precise temporal, cell-type-specific, and spatial regulation of gene expression, posttranscriptional RNA processing, and protein diversity. Dysregulation of these mechanisms involving critical neurodevelopmental genes has been consistently linked with the pathogenesis of various neurodevelopmental disorders, such as autism spectrum disorder, epilepsy, and schizophrenia. For instance, misexpression, splicing, or mutations in the Reelin gene, essential for guiding neuronal migration, have been causally associated with these conditions[127–129]. While genetic mutations can disrupt gene expression, posttranscriptional RNA processing, and the resulting proteomic landscape, various regulatory mechanisms also play a crucial role in shaping gene expression and protein isoform composition during cortical development. This thesis explored these complex regulatory mechanisms through five interconnected studies, focusing on miRNA regulation and alternative splicing in cortical development. Key findings include the identification of crucial RNA-binding protein interactions, comprehensive miRNA expression profiling across key embryonic developmental stages, the implementation of a novel bioinformatics resource, and insights into cell type-specific alternative splicing of voltage-gated calcium channels.

The overarching aim of this thesis was to elucidate the critical roles of posttranscriptional regulatory mechanisms, specifically involving microRNAs and alternative splicing, in shaping the complex processes of cortical development. Across the five studies presented, several key findings emerged that collectively address this central research question. First, the regulation of RNA-binding proteins that guide the alternative splicing machinery was investigated. Here, this thesis focuses on RBFOX2 and elucidating its role during cortical development. Premature overexpression at an NPC-dominated stage of embryonic brain development disrupted the sensitive splicing balance and revealed an antagonistic relationship between RBFOX2 and PTBP2. Consequently, neuronal progenitor cells of the cerebral cortex failed to differentiate and migrate properly (**Figure 11**), highlighting the necessity for RNA-binding proteins to exhibit precisely timed and localized expression patterns. In this context, we demonstrated that the NPC-specific miR-92a-3p suppresses *Rbfox2* expression *in vivo*. Second, miRNA sequencing at distinct developmental stages of the cerebral

cortex (E14, E17, P0), as well as cell-specifically in NPCs/neurons, revealed changes in expression patterns throughout neuronal differentiation. The silencing effect was enhanced by the co-expression and cooperative binding of miRNAs to shared target mRNAs. Third, the web portal cortexa was developed to comprehensively analyze gene expression and alternative splicing dynamics across different developmental stages (E14 - 21 months) and cell types in the murine brain. Fourth, differences in alternative splicing patterns of voltage-gated calcium channels between neuronal cell types were studied. Alternative splicing events in the C-terminal region of VGCCs can regulate their coupling to scaffolding proteins, G-protein signaling, synaptic targeting, and, ultimately, synaptic transmission and plasticity across distinct neuronal populations. An impact on C-terminal splicing to channel gating and kinetics is shown in heterologous expression systems but must be confirmed in neurons. Finally, to bridge molecular mechanisms with functional outcomes, Neuroimage Denoiser, a deep-learning framework for removing noise from fluorescent signals in functional imaging and, therefore, considerably improving the quality of the recordings, was developed.

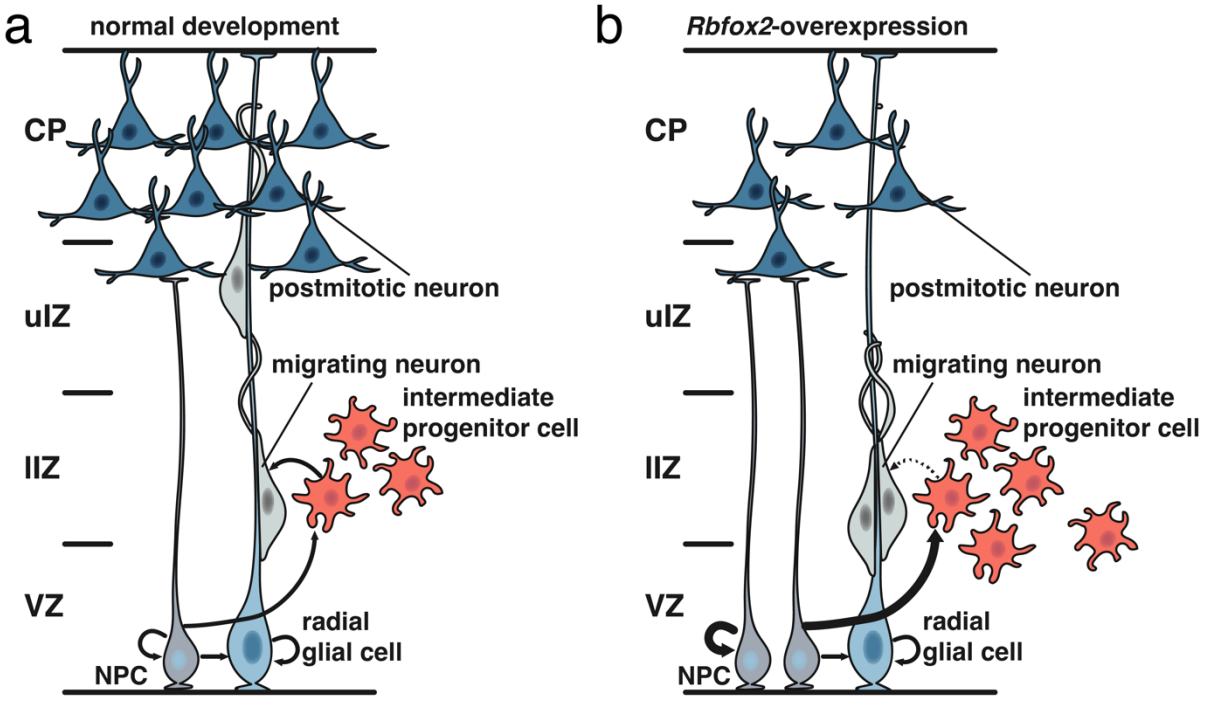


**Figure 11** Illustration depicting the effects of *Rbfox2* overexpression on cerebral cortex development. **a** normal development, showing the typical layered structure from the ventricular zone (VZ) at the bottom to the cortical plate (CP) at the top. Neural progenitor cells (NPCs) in the VZ give rise to radial glial cells that span the

developing cortex. Intermediate progenitor cells in the subventricular and intermediate zones (SVZ/IZ) produce neurons that migrate along radial glia to form the cortical layers. **b** Alterations caused by *Rbfox2* overexpression, leading to a reduction in neurons reaching the cortical plate (migration defect) and an increase in NPC and intermediate progenitor cells in the SVZ/IZ (differentiation defect).

Many regulatory mechanisms are often described as binary events, i.e., alternative splicing "switches"[8,21,130], miRNA "suppression" or "silencing." However, these processes usually involve more nuanced changes. For instance, miRNAs often fine-tune gene expression rather than completely silence their targets, thereby allowing for precise regulation of protein levels that can adapt to varying cellular conditions, and co-targeting offers yet another mechanism to modulate the magnitude of the silencing effect[47,85]. Similarly, alternative splicing can result in subtle shifts in isoform ratios rather than absolute switches, generating protein diversity crucial for specialized cellular functions. This thesis demonstrated that one of these fine-grained transitions in alternative splicing was moderated by a network of factors, including PTBP1, PTBP2, RBFOX2, miR-92a-3p, and miR-124-3p. PTBP1, a strong exon repressor, induces nonsense-mediated decay of PTBP2, ensuring a mutually exclusive expression of these two members of the PTBP family. Conversely, PTBP2 acts as a weaker exon repressor, allowing for more nuanced splicing regulation. RBFOX2 antagonistically regulates exons also targeted by PTBP, adding another layer of control. miR-124-3p, by repressing *Ptbp1* expression, promotes neuronal differentiation, while miR-92a-3p represses *Rbfox2* and is highly expressed in neural progenitor cells and at early development stages. This multifaceted regulatory network ensures a gradual change from exon skipping to inclusion in neurodevelopmentally-relevant target genes. Furthermore, the role of RBFOX2 in the maturation of miRNAs and the ability of miR-92a-3p to silence *Rbfox2* adds another layer of complexity to this regulatory system[38].

To further unravel the intricate miRNA-mediated and alternative splicing regulatory mechanisms underlying cortical development, our studies provided two valuable resources. On one hand, our comprehensive miRNA sequencing data span key developmental time points (E14, E17, P0), NPCs, and *in vitro* differentiated neurons in the murine cerebral cortex. This dataset offers insights into the expression patterns of miRNAs throughout neuronal differentiation and migration. On the other hand, the

cortexa web portal is a powerful bioinformatics resource for in-depth analysis of gene expression and alternative splicing dynamics across an extensive developmental timeline (E14 to 21 months) and diverse cell types in the murine brain. Taken together, these findings provide a valuable starting point for future research on posttranscriptional regulation in the developing and adult mammalian brain.

While transcriptomic analysis can provide crucial hypotheses for molecular mechanisms of cortical development, the changes induced by such mechanisms on the function of neurons must be experimentally validated. Here, functional imaging of neurotransmitters or secondary messengers is a valuable tool to observe the real-time consequences of these regulatory processes. However, the subtle changes in neuronal function resulting from posttranscriptional regulation can be challenging to detect and analyze because the small signal amplitudes are superimposed with noise. To facilitate functional imaging specifically in the case of minor changes due to posttranscriptional regulation, I developed Neuroimage Denoiser, a deep-learning framework designed to remove noise from transient fluorescent signals in functional imaging, particularly in glutamate imaging. This tool significantly improves the signal-to-noise ratio while preserving signal amplitudes, enabling more accurate detection and localization of synaptic responses. The preservation of the amplitude is important because subsequent measures such as the paired-pulse ratio or quantal content are dependent on unaltered amplitudes. By enhancing the ability to study complex synaptic structures, spontaneous activity, and synaptic plasticity at high temporal and spatial resolutions, Neuroimage Denoiser offers a way to bridge molecular-level regulation and functional outcomes in neuronal communication and development. The enhanced signal localization achieved through Neuroimage Denoiser, combined with precise particle localization using ThunderSTORM (ImageJ), enables a more detailed examination of how alternative splicing of calcium channels influences the spatial organization of active zones, providing novel insights into synaptic structure-function relationships (Amaral et al., in preparation).

While our research has focused on specific posttranscriptional regulatory mechanisms and their role in shaping cortical development, the broader context of neuronal classification and function is also an interesting aspect to consider. The complexity we have observed in miRNA regulation[47] and alternative splicing[37,38,131] suggests that

traditional methods of categorizing neuronal cell types may not fully capture the functional diversity present in the cerebral cortex. Traditionally, the classification of cell types is mostly performed on marker proteins, localization, and morphology for broad classification[132]. Using this approach, several proteins have been identified that can be used as markers for relatively specific cell types, e.g., VIP, CamKII, or PV[23,78]. Associated with these cell types, specific promoters have been described that allow researchers to specifically express constructs of interest in these cells[133,134]. Next-generation sequencing has been used to obtain the transcriptomes of these cell types by expressing a fluorescent marker under such a promoter and subsequently sorting these cells via fluorescence-activated cell sorting (FACS)[23,135,136]. With the rise of single-cell sequencing methods, the classification of cell types within the mammalian brain has attracted increasing interest. In one such approach, individual cells are encapsulated into droplets, and the adapter sequences contain a unique barcode for each cell. Thus, the expression of genes can be characterized at single-cell resolution, and a more complex analysis and classification of cells can be performed[137]. The Allen Brain Consortium conducted such an experiment on the neocortex and hippocampal formation and identified 388 transcriptomic types, including 364 neuronal types[12]. Remarkably, they identified inhibitory neurons that showed differing morphological and connectional patterns. However, since they share a transcriptomic profile, the correspondence between these cell clusters could be established[12]. Although the Allen Brain Consortium's transcriptomic atlas represents a significant advancement, it is important to recognize its limitations. The classification is primarily based on countable mRNA transcripts, which do not fully capture the true proteomic landscape of the cell. Several posttranscriptional mechanisms play crucial roles in shaping cellular function and identity, including alternative splicing, RNA modifications (such as m6A methylation), protein localization, protein-protein interactions, and posttranslational modifications. Moreover, translational efficiency, protein stability, and degradation rates all contribute to the final protein abundance and activity. These factors can lead to significant divergences between transcript levels and functional protein outcomes.

Furthermore, the Allen Brain Classification is based on a snapshot of gene expression in adult animals (P53 - P121)[12]. The mammalian brain undergoes dynamic changes throughout development and even in its mature state. This single timepoint approach fails to capture the temporal dynamics of gene expression and cell type identity, which

are known to evolve substantially over time. Cells that appear transcriptionally distinct at one stage might converge functionally at another or vice versa[138].

The complexity of cortical cell types likely extends beyond what is currently revealed by standard transcriptomics. The functional diversity of neurons and glia in the cortex is influenced by a multitude of factors, including their developmental history, local environment[139], and activity-dependent changes[140]. While these aspects are reflected in the transcriptome[141], current methods may not fully capture this information. A more complete transcriptomic picture reflecting the true functional differences among cells could be obtained by considering RNA modifications, splicing variants, and other posttranscriptional events. This evolving understanding of neuronal classification underscores the importance of posttranscriptional regulation in shaping cellular identity and function. The subtle changes in gene expression and protein isoforms that can be observed through miRNA regulation and alternative splicing likely contribute significantly to the functional diversity of neurons, even when their overall transcriptomic profiles are similar.

The nuanced understanding of transcriptomic complexity we have gained through our research is not merely an academic pursuit but also has significant clinical implications. While traditional clinical approaches often focus on genetic mutations identified by whole exome sequencing (WES) as the primary source of pathology, mounting evidence suggests that aberrations in posttranscriptional processes, particularly mis-splicing and miRNA dysregulation, play a crucial role in various neurological and psychiatric conditions and diseases[142].

For instance, splicing dysregulation has been linked to autism spectrum disorder[143,144], epilepsy[32,145–147], schizophrenia[148–151], cardiac hypertrophy[61,152], cancer[153–156], and other conditions and disorders[157]. Similarly, miRNA dysregulation has been implicated in cancer[158], cardiovascular diseases[159], and neurodevelopmental or neurodegenerative diseases[160,161]. Despite their significant impact on cellular processes and potential as biomarkers[162] and therapeutic targets[163], current diagnostic and treatment approaches typically neglect these posttranscriptional mechanisms[164]. Importantly, a considerable proportion (65-75 %) of rare diseases remain undiagnosed by traditional methods such as whole exome sequencing, microarrays, and gene

panels[164]. This gap in diagnosis highlights the potential importance of considering posttranscriptional regulatory processes in disease etiology and treatment.

In addition to miRNA regulation and alternative splicing, other posttranscriptional processes are attracting increasing interest in the fields of neurodevelopment and disease. RNA modifications are emerging as a crucial layer of gene regulation that may have significant implications for cortical development and neurological disorders. There are more than 100 known chemical RNA modifications that are significantly dysregulated in human cancers[165]. The most prevalent modification is N6-methyladenosine[166], which is applied to the 3'-UTR, 5'-UTR, untranslated intronic regions, and exonic regions[167]. Adenosine is methylated within the consensus motif of DRACH[3], and although this sequence is highly abundant, $m^6A$ modification is highly selective[167]. The m6A reader protein YTHDC1 interacts with two RBPs that antagonistically regulate alternative splicing events, SRSF3 and SRSF10. Interestingly, m6A modification and subsequent YTHDC1 binding promotes the binding of SRSF3 while decreasing the affinity of SRSF10[168], thereby enabling splicing regulation through RNA modifications. RNA modifications may also affect splicing outcomes directly by altering the binding affinity of RNA-binding proteins to RNA or changing the accessibility of the binding sites through altered RNA structure[169]. Pseudouridine, another RNA modification, is specifically enriched in the binding sites of many RBPs (e.g., U2AF2, KHSRP, and PTBP1). Furthermore, the knockout of pseudouridine synthases was linked to aberrant changes in the alternative splicing landscape[170]. Interestingly, pseudouridine was enriched (z score = 4.107) in the reported eCLIP peaks, while unmodified uridine was underrepresented for RBFOX2 (z score = -16.705). Thus, pseudouridine potentially modulates many RBP-RNA interactions, suggesting that this modification may also influence the binding preferences of RBFOX2 and subsequent splicing regulation. Although these first results imply a broad influence of RNA modifications on mRNA posttranscriptional processing and specifically on alternative splicing, many RNA modifications and their implications for alternative splicing have not yet been studied.

[3] R = purine, H = A, C, or U

In conclusion, this thesis revealed a complex landscape of posttranscriptional regulation, specifically focusing on miRNA regulation and alternative splicing during cortical development. This work, along with emerging research on RNA modifications and other regulatory mechanisms, underscores the need for a more comprehensive approach to understanding gene expression in the developing brain. Future research should aim to integrate these various layers of posttranscriptional regulation to build a more complete picture of how the remarkable complexity of the mammalian brain is achieved.

# 4 Outlook

The findings presented in this thesis contribute to our understanding of the complex landscape of posttranscriptional regulation in cortical development. As research is conducted to understand the intertwined regulation between miRNA regulation, alternative splicing, and emerging mechanisms such as RNA modifications, several key areas for future research appear. Moving forward, a primary focus should be integrating these various regulatory mechanisms to provide a more comprehensive view of posttranscriptional control. By combining data on miRNA regulation, alternative splicing, and RNA modifications, a more holistic understanding of how these processes collectively shape gene expression and protein diversity in the developing cortex can be reached.

The rise of single-cell methods has significantly advanced our understanding of gene expression within the central nervous system, with landmark studies conducted by the Allen Brain Institute leading to the classification of hundreds of transcriptomic cell types[12,171–173]. Recent studies have gradually shifted to focusing on epigenetic features at single-cell resolution in different compartments of the mammalian brain[174–177], with some resolving spatial resolution even for different nuclear compartments[178]. However, these assays often combine transcriptomics with a chromatin accessibility approach due to technical limitations of second-generation sequencing approaches (e.g., sequencing by synthesis as employed by the widely used Illumina systems) and do not allow for alternative splicing analysis, as they typically capture only the 3' end of transcripts. Thus, current approaches do not capture several posttranscriptional regulatory layers, i.e., miRNA regulation, alternative splicing, and RNA modifications. The rise of novel third-generation nanopore sequencing approaches paves the way for more comprehensive single-cell multi-omics analyses. These technologies offer the potential to sequence direct RNA with full-length transcripts, enabling the detection of alternative splicing events and RNA modifications at single-cell resolution. This advancement will lead to a deeper understanding of cellular heterogeneity and regulatory mechanisms, integrating multiple layers of gene regulation in individual cells of the brain.

Future research could explore how aberrations in posttranscriptional processes contribute to various neurological and psychiatric conditions. Given the limitations of

current diagnostic methods, investigating miRNA dysregulation, mis-splicing, and RNA modifications and their combinations could provide new insights into the etiology of rare and undiagnosed diseases. This line of research may also uncover novel biomarkers and therapeutic targets for conditions such as autism spectrum disorder, epilepsy, and schizophrenia, making recent developments in real-time sequencing highly relevant[179–181].

Building on our findings, future studies should aim to capture the temporal dynamics of posttranscriptional regulation throughout development and into adulthood at the single-cell level. This approach could reveal how regulatory networks evolve over time and contribute to different neuronal populations' functional maturation. Longitudinal studies combining transcriptomics, alternative splicing analysis, and miRNA profiling could provide a more nuanced understanding of brain development and cellular plasticity.

In conclusion, significant advancements have been made in the field of posttranscriptional regulation of gene expression. By integrating multiple regulatory layers and leveraging single-cell total RNA sequencing with nanopore technology, future research has the potential to broaden our understanding of brain development and function.

# 5 References

1. Schwartz, E. *et al.* Evolution of cortical geometry and its link to function, behaviour and ecology. *Nat. Commun.* **14**, 2252 (2023).
2. Florio, M. & Huttner, W. B. Neural progenitors, neurogenesis and the evolution of the neocortex. *Development* **141**, 2182–2194 (2014).
3. Barca-Mayo, O. & De Pietri Tonelli, D. Convergent microRNA actions coordinate neocortical development. *Cell. Mol. Life Sci.* **71**, 2975–2995 (2014).
4. Koo, B., Lee, K.-H., Ming, G., Yoon, K.-J. & Song, H. Setting the clock of neural progenitor cells during mammalian corticogenesis. *Semin. Cell Dev. Biol.* **142**, 43–53 (2023).
5. Miranda-Negrón, Y. & García-Arrarás, J. E. Radial glia and radial glia-like cells: Their role in neurogenesis and regeneration. *Front. Neurosci.* **16**, 1006037 (2022).
6. Borrell, V. & Götz, M. Role of radial glial cells in cerebral cortex folding. *Curr. Opin. Neurobiol.* **27**, 39–46 (2014).
7. Lennox, A. L., Mao, H. & Silver, D. L. RNA on the brain: emerging layers of post-transcriptional regulation in cerebral cortex development. *WIREs Dev. Biol.* **7**, e290 (2018).
8. Weyn-Vanhentenryck, S. M. *et al.* Precise temporal regulation of alternative splicing during neural development. *Nat. Commun.* **9**, 2189 (2018).
9. Krause, M. *et al.* tailfindr: alignment-free poly(A) length measurement for Oxford Nanopore RNA and DNA sequencing. *RNA* **25**, 1229–1241 (2019).
10. Frye, M., Harada, B. T., Behm, M. & He, C. RNA modifications modulate gene expression during development. *Science* **361**, 1346–1349 (2018).
11. Breschi, A., Gingeras, T. R. & Guigó, R. Comparative transcriptomics in human and mouse. *Nat. Rev. Genet.* **18**, 425–440 (2017).
12. Yao, Z. *et al.* A taxonomy of transcriptomic cell types across the isocortex and hippocampal formation. *Cell* **184**, 3222-3241.e26 (2021).
13. Baralle, F. E. & Giudice, J. Alternative splicing as a regulator of development and tissue identity. *Nat. Rev. Mol. Cell Biol.* **18**, 437–451 (2017).
14. Porter, R. S., Jaamour, F. & Iwase, S. Neuron-specific alternative splicing of transcriptional machineries: Implications for neurodevelopmental disorders. *Mol. Cell. Neurosci.* **87**, 35–45 (2018).
15. Wang, Y. *et al.* Mechanism of alternative splicing and its regulation (Review). *Biomed. Rep.* **3**, 152–158 (2015).
16. Wright, C. J., Smith, C. W. J. & Jiggins, C. D. Alternative splicing as a source of phenotypic diversity. *Nat. Rev. Genet.* **23**, 697–710 (2022).
17. Ren, P. *et al.* Alternative Splicing: A New Cause and Potential Therapeutic Target in Autoimmune Disease. *Front. Immunol.* **12**, (2021).
18. García-Moreno, J. F. & Romão, L. Perspective in Alternative Splicing Coupled to Nonsense-Mediated mRNA Decay. *Int. J. Mol. Sci.* **21**, 9424 (2020).
19. Shen Shihao *et al.* rMATS: Robust and flexible detection of differential alternative splicing from replicate RNA-Seq data | PNAS. *Proc. Natl. Acad. Sci.* **111**, (2014).
20. Corley, M., Burns, M. C. & Yeo, G. W. How RNA-Binding Proteins Interact with RNA: Molecules and Mechanisms. *Mol. Cell* **78**, 9–29 (2020).
21. Yano, M., Hayakawa-Yano, Y., Mele, A. & Darnell, R. B. Nova2 Regulates Neuronal

Migration through an RNA Switch in Disabled-1 Signaling. *Neuron* **66**, 848–858 (2010).
22. Weyn-Vanhentenryck, S. M. *et al.* HITS-CLIP and Integrative Modeling Define the Rbfox Splicing-Regulatory Network Linked to Brain Development and Autism. *Cell Rep.* **6**, 1139–1152 (2014).
23. Furlanis, E., Traunmüller, L., Fucile, G. & Scheiffele, P. Landscape of ribosome-engaged transcript isoforms reveals extensive neuronal-cell-class-specific alternative splicing programs. *Nat. Neurosci.* **22**, 1709–1717 (2019).
24. Huh, G. S. & Hynes, R. O. Regulation of alternative pre-mRNA splicing by a novel repeated hexanucleotide element. *Genes Dev.* **8**, 1561–1574 (1994).
25. Ule, J. *et al.* An RNA map predicting Nova-dependent splicing regulation. *Nature* **444**, 580–586 (2006).
26. Konieczny, P., Stepniak-Konieczna, E. & Sobczak, K. MBNL proteins and their target RNAs, interaction and splicing regulation. *Nucleic Acids Res.* **42**, 10873–10887 (2014).
27. Vuong, J. K. *et al.* PTBP1 and PTBP2 Serve Both Specific and Redundant Functions in Neuronal Pre-mRNA Splicing. *Cell Rep.* **17**, 2766–2775 (2016).
28. Makeyev, E. V., Zhang, J., Carrasco, M. A. & Maniatis, T. The MicroRNA miR-124 Promotes Neuronal Differentiation by Triggering Brain-Specific Alternative Pre-mRNA Splicing. *Mol. Cell* **27**, 435–448 (2007).
29. Gehman, L. T. *et al.* The splicing regulator Rbfox2 is required for both cerebellar development and mature motor function. *Genes Dev.* **26**, 445–460 (2012).
30. Vuong, C. K. *et al.* Rbfox1 Regulates Synaptic Transmission through the Inhibitory Neuron-Specific vSNARE Vamp1. *Neuron* **98**, 127-141.e7 (2018).
31. Liu, J., Geng, A., Wu, X., Lin, R.-J. & Lu, Q. Alternative RNA Splicing Associated With Mammalian Neuronal Differentiation. *Cereb. Cortex* **28**, 2810–2816 (2018).
32. Gehman, L. T. *et al.* The splicing regulator Rbfox1 (A2BP1) controls neuronal excitation in the mammalian brain. *Nat. Genet.* **43**, 706–711 (2011).
33. Paronetto, M. P., Passacantilli, I. & Sette, C. Alternative splicing and cell survival: from tissue homeostasis to disease. *Cell Death Differ.* **23**, 1919–1929 (2016).
34. Calarco, J. A., Zhen, M. & Blencowe, B. J. Networking in a global world: Establishing functional connections between neural splicing regulators and their target transcripts. *RNA* **17**, 775–791 (2011).
35. Zhang, X. *et al.* Cell-Type-Specific Alternative Splicing Governs Cell Fate in the Developing Cerebral Cortex. *Cell* **166**, 1147-1162.e15 (2016).
36. Weyn-Vanhentenryck, S. M. *et al.* Precise temporal regulation of alternative splicing during neural development. *Nat. Commun.* **9**, 2189 (2018).
37. Weißbach, S. *et al.* Cortexa: a comprehensive resource for studying gene expression and alternative splicing in the murine brain. *BMC Bioinformatics* **25**, 293 (2024).
38. Weißbach, S. *et al.* Premature upregulation of miR-92a's target RBFOX2 hijacks PTBP splicing and impairs cortical neuronal differentiation. 2024.09.20.614071 Preprint at https://doi.org/10.1101/2024.09.20.614071 (2024).
39. Leek, J. T. *et al.* Tackling the widespread and critical impact of batch effects in high-throughput data. *Nat. Rev. Genet.* **11**, 733–739 (2010).
40. Weißbach, S. *et al.* Reliability of genomic variants across different next-generation sequencing platforms and bioinformatic processing pipelines. *BMC Genomics* (2021).
41. Marín, O. & Müller, U. Lineage origins of GABAergic versus glutamatergic neurons in

the neocortex. *Curr. Opin. Neurobiol.* **26**, 132–141 (2014).
42. Mittal, N., Roy, N., Babu, M. M. & Janga, S. C. Dissecting the expression dynamics of RNA-binding proteins in posttranscriptional regulatory networks. *Proc. Natl. Acad. Sci.* **106**, 20300–20305 (2009).
43. Müller-McNicoll, M., Rossbach, O., Hui, J. & Medenbach, J. Auto-regulatory feedback by RNA-binding proteins. *J. Mol. Cell Biol.* **11**, 930–939 (2019).
44. Sun, Y. *et al.* Autoregulation of RBM10 and cross-regulation of RBM10/RBM5 via alternative splicing-coupled nonsense-mediated decay. *Nucleic Acids Res.* **45**, 8524–8540 (2017).
45. Makeyev, E. V., Zhang, J., Carrasco, M. A. & Maniatis, T. The MicroRNA miR-124 Promotes Neuronal Differentiation by Triggering Brain-Specific Alternative Pre-mRNA Splicing. *Mol. Cell* **27**, 435–448 (2007).
46. Sevignani, C., Calin, G. A., Siracusa, L. D. & Croce, C. M. Mammalian microRNAs: a small world for fine-tuning gene expression. *Mamm. Genome* **17**, 189–202 (2006).
47. Todorov, H. *et al.* Stage-specific expression patterns and co-targeting relationships among miRNAs in the developing mouse cerebral cortex. *Commun. Biol.* **7**, 1–14 (2024).
48. Keppetipola, N., Sharma, S., Li, Q. & Black, D. L. Neuronal regulation of pre-mRNA splicing by polypyrimidine tract binding proteins, PTBP1 and PTBP2. *Crit. Rev. Biochem. Mol. Biol.* **47**, 360–378 (2012).
49. Shibata, H., Duong, H. & Pulst, S.-M. novel protein with RNA-binding motifs interacts with ataxin-2 | Human Molecular Genetics | Oxford Academic. *Hum. Mol. Genet.* **9**, 1303–1313 (2000).
50. Mukherjee, A. & Nongthomba, U. To RNA-binding and beyond: Emerging facets of the role of Rbfox proteins in development and disease. *WIREs RNA* **15**, e1813 (2023).
51. Skipper, M., Milne, C. A. & Hodgkin, J. Genetic and Molecular Analysis of fox-1, a Numerator Element Involved in Caenorhabditis elegans Primary Sex Determination. *Genetics* **151**, 617–631 (1999).
52. Conboy, J. G. Developmental regulation of RNA processing by Rbfox proteins. *WIREs RNA* **8**, e1398 (2017).
53. Mullen, R. J., Buck, C. R. & Smith, A. M. NeuN, a neuronal specific nuclear protein in vertebratesxs. *Development* **116**, 201–211 (1992).
54. Feng, H. *et al.* Complexity and graded regulation of neuronal cell-type–specific alternative splicing revealed by single-cell RNA sequencing. *Proc. Natl. Acad. Sci.* **118**, e2013056118 (2021).
55. Damianov, A. & Black, D. L. Autoregulation of Fox protein expression to produce dominant negative splicing factors. *RNA* **16**, 405–416 (2010).
56. Dredge, B. K. & Jensen, K. B. NeuN/Rbfox3 Nuclear and Cytoplasmic Isoforms Differentially Regulate Alternative Splicing and Nonsense-Mediated Decay of Rbfox2. *PLOS ONE* **6**, e21585 (2011).
57. Rajman, M. *et al.* A microRNA-129-5p/Rbfox crosstalk coordinates homeostatic downscaling of excitatory synapses. *EMBO J.* **36**, 1770–1787 (2017).
58. Agarwal, V., Bell, G. W., Nam, J.-W. & Bartel, D. P. Predicting effective microRNA target sites in mammalian mRNAs. *eLife* **4**, e05005 (2015).
59. Corominas, R. *et al.* Protein interaction network of alternatively spliced isoforms from brain links genetic risk factors for autism. *Nat. Commun.* **5**, 3650 (2014).

60. Lal, D. *et al.* RBFOX1 and RBFOX3 Mutations in Rolandic Epilepsy. *PLOS ONE* **8**, e73323 (2013).
61. Nutter, C. A. *et al.* Dysregulation of RBFOX2 Is an Early Event in Cardiac Pathogenesis of Diabetes. *Cell Rep.* **15**, 2200–2213 (2016).
62. Homsy, J. *et al.* De novo mutations in congenital heart disease with neurodevelopmental and other congenital anomalies. *Science* **350**, 1262–1266 (2015).
63. Huang, D.-F. *et al.* Neuronal splicing regulator RBFOX3 mediates seizures via regulating Vamp1 expression preferentially in NPY-expressing GABAergic neurons. *Proc. Natl. Acad. Sci.* **119**, e2203632119 (2022).
64. Zhang, C. *et al.* Defining the regulatory network of the tissue-specific splicing factors Fox-1 and Fox-2. *Genes Dev.* **22**, 2550–2563 (2008).
65. Castle, J. C. *et al.* Expression of 24,426 human alternative splicing events and predicted cis regulation in 48 tissues and cell lines. *Nat. Genet.* **40**, 1416–1425 (2008).
66. Uhlén, M. *et al.* Tissue-based map of the human proteome. *Science* **347**, 1260419 (2015).
67. Tamura, K., Stecher, G. & Kumar, S. MEGA11: Molecular Evolutionary Genetics Analysis Version 11. *Mol. Biol. Evol.* **38**, 3022–3027 (2021).
68. Liu, J., Geng, A., Wu, X., Lin, R.-J. & Lu, Q. Alternative RNA Splicing Associated With Mammalian Neuronal Differentiation. *Cereb. Cortex* **28**, 2810–2816 (2018).
69. Damianov, A. *et al.* Rbfox Proteins Regulate Splicing as Part of a Large Multiprotein Complex LASR. *Cell* **165**, 606–619 (2016).
70. Chen, Y. *et al.* Rbfox proteins regulate microRNA biogenesis by sequence-specific binding to their precursors and target downstream Dicer | Nucleic Acids Research | Oxford Academic. *Nucleic Acids Res.* **44**, 4381–4395 (2016).
71. Kim, K. K., Yang, Y., Zhu, J., Adelstein, R. S. & Kawamoto, S. Rbfox3 Controls the Biogenesis of a Subset of MicroRNAs. *Nat. Struct. Mol. Biol.* **21**, 901–910 (2014).
72. Nakahata, S. & Kawamoto, S. Tissue-dependent isoforms of mammalian Fox-1 homologs are associated with tissue-specific splicing activities. *Nucleic Acids Res.* **33**, 2078–2089 (2005).
73. Lee, J.-A. *et al.* Cytoplasmic Rbfox1 Regulates the Expression of Synaptic and Autism-Related Genes. *Neuron* **89**, 113–128 (2016).
74. Carreira-Rosario, A. *et al.* Repression of Pumilio Protein Expression by Rbfox1 Promotes Germ Cell Differentiation. *Dev. Cell* **36**, 562–571 (2016).
75. Wei, C. *et al.* RBFox2 Binds Nascent RNA to Globally Regulate Polycomb Complex 2 Targeting in Mammalian Genomes. *Mol. Cell* **62**, 875–889 (2016).
76. Shang, R., Lee, S., Senavirathne, G. & Lai, E. C. microRNAs in action: biogenesis, function and regulation. *Nat. Rev. Genet.* **24**, 816–833 (2023).
77. Ambros, V. microRNAs: Tiny Regulators with Great Potential. *Cell* **107**, 823–826 (2001).
78. He, M. *et al.* Cell-Type-Based Analysis of MicroRNA Profiles in the Mouse Brain. *Neuron* **73**, 35–48 (2012).
79. Liu, J. Control of protein synthesis and mRNA degradation by microRNAs. *Curr. Opin. Cell Biol.* **20**, 214–221 (2008).
80. Kim, Y.-K., Kim, B. & Kim, V. N. Re-evaluation of the roles of DROSHA, Exportin 5, and DICER in microRNA biogenesis. *Proc. Natl. Acad. Sci.* **113**, E1881–E1889 (2016).

81. Kim, V. N. & Nam, J.-W. Genomics of microRNA. *Trends Genet.* **22**, 165–173 (2006).
82. Wu, K., He, J., Pu, W. & Peng, Y. The Role of Exportin-5 in MicroRNA Biogenesis and Cancer. *Genomics Proteomics Bioinformatics* **16**, 120–126 (2018).
83. Fridrich, A., Hazan, Y. & Moran, Y. Too Many False Targets for MicroRNAs: Challenges and Pitfalls in Prediction of miRNA Targets and Their Gene Ontology in Model and Non-model Organisms. *BioEssays* **41**, 1800169 (2019).
84. Lewis, B. P., Shih, I. -hung, Jones-Rhoades, M. W., Bartel, D. P. & Burge, C. B. Prediction of Mammalian MicroRNA Targets. *Cell* **115**, 787–798 (2003).
85. Cherone, J. M., Jorgji, V. & Burge, C. B. Cotargeting among microRNAs in the brain. *Genome Res.* **29**, 1791–1804 (2019).
86. Chong, M. M. W., Rasmussen, J. P., Rudensky, A. Y. & Littman, D. R. The RNAseIII enzyme Drosha is critical in T cells for preventing lethal inflammatory disease. *J. Exp. Med.* **205**, 2005–2017 (2008).
87. Hsu, R. *et al.* Loss of microRNAs in pyramidal neurons leads to specific changes in inhibitory synaptic transmission in the prefrontal cortex. *Mol. Cell. Neurosci.* **50**, 283–292 (2012).
88. Wang, Y., Medvid, R., Melton, C., Jaenisch, R. & Blelloch, R. DGCR8 is essential for microRNA biogenesis and silencing of embryonic stem cell self-renewal. *Nat. Genet.* **39**, 380–385 (2007).
89. Bennasser, Y. *et al.* Competition for XPO5 binding between Dicer mRNA, pre-miRNA and viral RNA regulates human Dicer levels. *Nat. Struct. Mol. Biol.* **18**, 323–327 (2011).
90. Bernstein, E. *et al.* Dicer is essential for mouse development. *Nat. Genet.* **35**, 215–217 (2003).
91. Davis, T. H. *et al.* Conditional Loss of Dicer Disrupts Cellular and Tissue Morphogenesis in the Cortex and Hippocampus. *J. Neurosci.* **28**, 4322–4330 (2008).
92. Kawase-Koga, Y., Otaegi, G. & Sun, T. Different timings of dicer deletion affect neurogenesis and gliogenesis in the developing mouse central nervous system. *Dev. Dyn.* **238**, 2800–2812 (2009).
93. Tonelli, D. D. P. *et al.* miRNAs are essential for survival and differentiation of newborn neurons but not for expansion of neural progenitors during early neurogenesis in the mouse embryonic neocortex. *Development* **135**, 3911–3921 (2008).
94. Wang, D. *et al.* Quantitative functions of Argonaute proteins in mammalian development. *Genes Dev.* **26**, 693–704 (2012).
95. Han, J. *et al.* Posttranscriptional Crossregulation between Drosha and DGCR8. *Cell* **136**, 75–84 (2009).
96. Triboulet, R., Chang, H.-M., LaPierre, R. J. & Gregory, R. I. Post-transcriptional control of DGCR8 expression by the Microprocessor. *RNA* **15**, 1005–1011 (2009).
97. Tang, X. *et al.* Acetylation of Drosha on the N-Terminus Inhibits Its Degradation by Ubiquitination. *PLOS ONE* **8**, e72503 (2013).
98. Di Carlo, V. *et al.* TDP-43 Regulates the Microprocessor Complex Activity During In Vitro Neuronal Differentiation. *Mol. Neurobiol.* **48**, 952–963 (2013).
99. Wang, I.-F., Wu, L.-S., Chang, H.-Y. & Shen, C.-K. J. TDP-43, the signature protein of FTLD-U, is a neuronal activity-responsive factor. *J. Neurochem.* **105**, 797–806 (2008).
100. Wada, T., Kikuchi, J. & Furukawa, Y. Histone deacetylase 1 enhances microRNA processing via deacetylation of DGCR8. *EMBO Rep.* **13**, 142–149 (2012).

101. Herbert, K. M., Pimienta, G., DeGregorio, S. J., Alexandrov, A. & Steitz, J. A. Phosphorylation of DGCR8 Increases Its Intracellular Stability and Induces a Progrowth miRNA Profile. *Cell Rep.* **5**, 1070–1081 (2013).
102. Cheng, T.-L. *et al.* MeCP2 Suppresses Nuclear MicroRNA Processing and Dendritic Growth by Regulating the DGCR8/Drosha Complex. *Dev. Cell* **28**, 547–560 (2014).
103. Tokumaru, S., Suzuki, M., Yamada, H., Nagino, M. & Takahashi, T. let-7 regulates Dicer expression and constitutes a negative feedback loop. *Carcinogenesis* **29**, 2073–2077 (2008).
104. Cohn, W. E. & Volkin, E. Nucleoside-5′-Phosphates from Ribonucleic Acid. *Nature* **167**, 483–484 (1951).
105. Mo, J., Weng, X. & Zhou, X. Detection, Clinical Application, and Manipulation of RNA Modifications. *Acc. Chem. Res.* **56**, 2788–2800 (2023).
106. Leger, A. *et al.* RNA modifications detection by comparative Nanopore direct RNA sequencing. *Nat. Commun.* **12**, 7198 (2021).
107. Stephenson, W. *et al.* Direct detection of RNA modifications and structure using single-molecule nanopore sequencing. *Cell Genomics* **2**, (2022).
108. Wu, Y. *et al.* Transfer learning enables identification of multiple types of RNA modifications using nanopore direct RNA sequencing. *Nat. Commun.* **15**, 4049 (2024).
109. Hendra, C. *et al.* Detection of m6A from direct RNA sequencing using a multiple instance learning framework. *Nat. Methods* **19**, 1590–1598 (2022).
110. Liu, H. *et al.* Accurate detection of m6A RNA modifications in native RNA sequences. *Nat. Commun.* **10**, 4079 (2019).
111. Hassan, D., Acevedo, D., Daulatabad, S. V., Mir, Q. & Janga, S. C. Penguin: A tool for predicting pseudouridine sites in direct RNA nanopore sequencing data. *Methods* **203**, 478–487 (2022).
112. Tavakoli, S. *et al.* Semi-quantitative detection of pseudouridine modifications and type I/II hypermodifications in human mRNAs using direct long-read sequencing. *Nat. Commun.* **14**, 334 (2023).
113. Widagdo, J. *et al.* Experience-Dependent Accumulation of N6-Methyladenosine in the Prefrontal Cortex Is Associated with Memory Processes in Mice. *J. Neurosci.* **36**, 6771–6777 (2016).
114. Chin, A. & Lécuyer, E. RNA localization: Making its way to the center stage. *Biochim. Biophys. Acta BBA - Gen. Subj.* **1861**, 2956–2970 (2017).
115. Cajigas, I. J. *et al.* The Local Transcriptome in the Synaptic Neuropil Revealed by Deep Sequencing and High-Resolution Imaging. *Neuron* **74**, 453–466 (2012).
116. Ainsley, J. A., Drane, L., Jacobs, J., Kittelberger, K. A. & Reijmers, L. G. Functionally diverse dendritic mRNAs rapidly associate with ribosomes following a novel experience. *Nat. Commun.* **5**, 4510 (2014).
117. Thelen, M. P. & Kye, M. J. The Role of RNA Binding Proteins for Local mRNA Translation: Implications in Neurological Disorders. *Front. Mol. Biosci.* **6**, (2020).
118. Wang, D. O., Martin, K. C. & Zukin, R. S. Spatially restricting gene expression by local translation at synapses. *Trends Neurosci.* **33**, 173–182 (2010).
119. Doyle, M. & Kiebler, M. A. Mechanisms of dendritic mRNA transport and its role in synaptic tagging. *EMBO J.* **30**, 3540–3552 (2011).
120. Krichevsky, A. M. & Kosik, K. S. Neuronal RNA Granules: A Link between RNA

Localization and Stimulation-Dependent Translation. *Neuron* **32**, 683–696 (2001).
121. Martin, K. C. & Zukin, R. S. RNA Trafficking and Local Protein Synthesis in Dendrites: An Overview. *J. Neurosci.* **26**, 7131–7134 (2006).
122. Kislauskis, E. H. & Singer, R. H. Determinants of mRNA localization. *Curr. Opin. Cell Biol.* **4**, 975–978 (1992).
123. Beilharz, T. H. & Preiss, T. Widespread use of poly(A) tail length control to accentuate expression of the yeast transcriptome. *RNA* **13**, 982–997 (2007).
124. Eckmann, C. R., Rammelt, C. & Wahle, E. Control of poly(A) tail length. *WIREs RNA* **2**, 348–361 (2011).
125. Bresson, S. M. & Conrad, N. K. The Human Nuclear Poly(A)-Binding Protein Promotes RNA Hyperadenylation and Decay. *PLOS Genet.* **9**, e1003893 (2013).
126. Di Giammartino, D. C., Nishida, K. & Manley, J. L. Mechanisms and Consequences of Alternative Polyadenylation. *Mol. Cell* **43**, 853–866 (2011).
127. Fatemi, S. H. *et al.* Reelin signaling is impaired in autism. *Biol. Psychiatry* **57**, 777–787 (2005).
128. Sánchez-Hidalgo, A. C., Martín-Cuevas, C., Crespo-Facorro, B. & Garrido-Torres, N. Reelin Alterations, Behavioral Phenotypes, and Brain Anomalies in Schizophrenia: A Systematic Review of Insights From Rodent Models. *Front. Neuroanat.* **16**, (2022).
129. Tissir, F. & Goffinet, A. M. Reelin and brain development. *Nat. Rev. Neurosci.* **4**, 496–505 (2003).
130. Fiszbein, A. & Kornblihtt, A. R. Alternative splicing switches: Important players in cell differentiation. *BioEssays* **39**, 1600157 (2017).
131. Heck, J. *et al.* More than a pore: How voltage-gated calcium channels act on different levels of neuronal communication regulation. *Channels* **15**, 322–338 (2021).
132. Zeng, H. & Sanes, J. R. Neuronal cell-type classification: challenges, opportunities and the path forward. *Nat. Rev. Neurosci.* **18**, 530–546 (2017).
133. Madisen, L. *et al.* A toolbox of Cre-dependent optogenetic transgenic mice for light-induced activation and silencing. *Nat. Neurosci.* **15**, 793–802 (2012).
134. McKenzie, A. T. *et al.* Brain Cell Type Specific Gene Expression and Co-expression Network Architectures. *Sci. Rep.* **8**, 8868 (2018).
135. Martin, D., Xu, J., Porretta, C. & Nichols, C. D. Neurocytometry: Flow cytometric sorting of specific neuronal populations from human and rodent brain. *ACS Chem. Neurosci.* **8**, 356 (2017).
136. Kim, H. J., Tam, P. P. L. & Yang, P. Defining cell identity beyond the premise of differential gene expression. *Cell Regen.* **10**, 20 (2021).
137. Salomon, R. *et al.* Droplet-based single cell RNAseq tools: a practical guide. *Lab. Chip* **19**, 1706–1727 (2019).
138. Kotliar, D. *et al.* Identifying gene expression programs of cell-type identity and cellular activity with single-cell RNA-Seq. *eLife* **8**, e43803 (2019).
139. Miterko, L. N., Lackey, E. P., Heck, D. H. & Sillitoe, R. V. Shaping Diversity Into the Brain's Form and Function. *Front. Neural Circuits* **12**, (2018).
140. Ganguly, K. & Poo, M. Activity-Dependent Neural Plasticity from Bench to Bedside. *Neuron* **80**, 729–741 (2013).
141. Tropea, D. *et al.* Gene expression changes and molecular pathways mediating activity-dependent plasticity in visual cortex. *Nat. Neurosci.* **9**, 660–668 (2006).

142. Peymani, F., Farzeen, A. & Prokisch, H. RNA sequencing role and application in clinical diagnostic. *Pediatr. Investig.* **6**, 29 (2022).
143. Engal, E. *et al.* The spectrum of pre-mRNA splicing in autism. *WIREs RNA* **15**, e1838 (2024).
144. Smith, R. M. & Sadee, W. Synaptic Signaling and Aberrant RNA Splicing in Autism Spectrum Disorders. *Front. Synaptic Neurosci.* **3**, (2011).
145. Douaud, M. *et al.* Epilepsy Caused by an Abnormal Alternative Splicing with Dosage Effect of the SV2A Gene in a Chicken Model. *PLOS ONE* **6**, e26932 (2011).
146. Heinzen, E. L. *et al.* Alternative ion channel splicing in mesial temporal lobe epilepsy and Alzheimer's disease. *Genome Biol.* **8**, R32 (2007).
147. Rusconi, F. *et al.* LSD1 Neurospecific Alternative Splicing Controls Neuronal Excitability in Mouse Models of Epilepsy. *Cereb. Cortex* **25**, 2729–2740 (2015).
148. Chung, Y. *et al.* Altered Rbfox1-Vamp1 pathway and prefrontal cortical dysfunction in schizophrenia. *Mol. Psychiatry* 1–10 (2024) doi:10.1038/s41380-024-02417-8.
149. Morikawa, T. & Manabe, T. Aberrant regulation of alternative pre-mRNA splicing in schizophrenia. *Neurochem. Int.* **57**, 691–704 (2010).
150. Sanders, B. *et al.* Transcriptional programs regulating neuronal differentiation are disrupted in DLG2 knockout human embryonic stem cells and enriched for schizophrenia and related disorders risk variants. *Nat. Commun.* **13**, 27 (2022).
151. Zhang, C.-Y., Xiao, X., Zhang, Z., Hu, Z. & Li, M. An alternative splicing hypothesis for neuropathology of schizophrenia: evidence from studies on historical candidate genes and multi-omics data. *Mol. Psychiatry* **27**, 95–112 (2022).
152. Gao, C. *et al.* RBFox1-mediated RNA splicing regulates cardiac hypertrophy and heart failure. *J. Clin. Invest.* **126**, 195–206 (2016).
153. Bonnal, S. C., López-Oreja, I. & Valcárcel, J. Roles and mechanisms of alternative splicing in cancer — implications for care. *Nat. Rev. Clin. Oncol.* **17**, 457–474 (2020).
154. El Marabti, E. & Younis, I. The Cancer Spliceome: Reprograming of Alternative Splicing in Cancer. *Front. Mol. Biosci.* **5**, (2018).
155. Venables, J. P. *et al.* RBFOX2 Is an Important Regulator of Mesenchymal Tissue-Specific Splicing in both Normal and Cancer Tissues. *Mol. Cell. Biol.* **33**, 396–405 (2013).
156. Zhang, Y., Qian, J., Gu, C. & Yang, Y. Alternative splicing and cancer: a systematic review. *Signal Transduct. Target. Ther.* **6**, 1–14 (2021).
157. Tazi, J., Bakkour, N. & Stamm, S. Alternative splicing and disease. *Biochim. Biophys. Acta BBA - Mol. Basis Dis.* **1792**, 14–26 (2009).
158. Croce, C. M. Causes and consequences of microRNA dysregulation in cancer. *Nat. Rev. Genet.* **10**, 704–714 (2009).
159. Sessa, F., Salerno, M., Esposito, M., Cocimano, G. & Pomara, C. miRNA Dysregulation in Cardiovascular Diseases: Current Opinion and Future Perspectives. *Int. J. Mol. Sci.* **24**, 5192 (2023).
160. Jauhari, A., Singh, T. & Yadav, S. Neurodevelopmental disorders and neurotoxicity: MicroRNA in focus. *J. Chem. Neuroanat.* **120**, 102072 (2022).
161. Juźwik, C. A. *et al.* microRNA dysregulation in neurodegenerative diseases: A systematic review. *Prog. Neurobiol.* **182**, 101664 (2019).
162. Witwer, K. W. Circulating MicroRNA Biomarker Studies: Pitfalls and Potential Solutions. *Clin. Chem.* **61**, 56–63 (2015).

163. Diener, C., Keller, A. & Meese, E. Emerging concepts of miRNA therapeutics: from cells to clinic. *Trends Genet.* **38**, 613–626 (2022).
164. Marwaha, S., Knowles, J. W. & Ashley, E. A. A guide for the diagnosis of rare and undiagnosed disease: beyond the exome. *Genome Med.* **14**, 23 (2022).
165. Barbieri, I. & Kouzarides, T. Role of RNA modifications in cancer. *Nat. Rev. Cancer* **20**, 303–322 (2020).
166. Motorin, Y. & Helm, M. RNA nucleotide methylation. *WIREs RNA* **2**, 611–631 (2011).
167. Adhikari, S., Xiao, W., Zhao, Y.-L. & Yang, Y.-G. m6A: Signaling for mRNA splicing. *RNA Biol.* **13**, 756–759 (2016).
168. Xiao, W. *et al.* Nuclear m6A Reader YTHDC1 Regulates mRNA Splicing. *Mol. Cell* **61**, 507–519 (2016).
169. Gilbert, W. V., Bell, T. A. & Schaening, C. Messenger RNA modifications: Form, distribution, and function. *Science* **352**, 1408–1412 (2016).
170. Martinez, N. M. *et al.* Pseudouridine synthases modify human pre-mRNA co-transcriptionally and affect pre-mRNA processing. *Mol. Cell* **82**, 645-659.e9 (2022).
171. Siletti, K. *et al.* Transcriptomic diversity of cell types across the adult human brain. *Science* **382**, eadd7046 (2023).
172. Yao, Z. *et al.* A high-resolution transcriptomic and spatial atlas of cell types in the whole mouse brain. *Nature* **624**, 317–332 (2023).
173. Yao, Z. *et al.* A transcriptomic and epigenomic cell atlas of the mouse primary motor cortex. *Nature* **598**, 103–110 (2021).
174. Lake, B. B. *et al.* Integrative single-cell analysis of transcriptional and epigenetic states in the human adult brain. *Nat. Biotechnol.* **36**, 70–80 (2018).
175. Trevino, A. E. *et al.* Chromatin and gene-regulatory dynamics of the developing human cerebral cortex at single-cell resolution. *Cell* **184**, 5053-5069.e23 (2021).
176. Zhu, K. *et al.* Multi-omic profiling of the developing human cerebral cortex at the single-cell level. *Sci. Adv.* **9**, eadg3754 (2023).
177. Ziffra, R. S. *et al.* Single-cell epigenomics reveals mechanisms of human cortical development. *Nature* **598**, 205–213 (2021).
178. Takei, Y. *et al.* High-resolution spatial multi-omics reveals cell-type specific nuclear compartments. 2023.05.07.539762 Preprint at https://doi.org/10.1101/2023.05.07.539762 (2023).
179. Wadden, J. *et al.* Ultra-rapid somatic variant detection via real-time targeted amplicon sequencing. *Commun. Biol.* **5**, 1–12 (2022).
180. Wierczeiko, A. *et al.* NanopoReaTA: a user-friendly tool for nanopore-seq real-time transcriptional analysis. *Bioinformatics* **39**, btad492 (2023).
181. Butto, T. *et al.* Real-time transcriptomic profiling in distinct experimental conditions. *eLife* **13**, (2024).

# 6 Appendix

## 6.1 Contribution to individual publications

**Table 1** Contributor role according to CRediT Taxonomy: an overview of the contributions to case studies 1-5.

| **Scientific publication** | Premature upregulation of miR-92a' s target RBFOX2 hijacks PTBP splicing and impairs cortical neuronal differentiation. **1** | Stage-specific expression patterns and cotargeting relationships among miRNAs in the developing mouse cerebral cortex. **2** | Cortexa: a comprehensive resource for studying gene expression and alternative splicing in the murine brain. **3** | More than a pore: How voltage-gated calcium channels act on different levels of neuronal communication regulation **4** | Neuroimage Denoiser - a Deep Learning Framework for Removing Noise from Transient Fluorescent Signals in Functional Imaging. **5** |
|---|---|---|---|---|---|
| **Conceptualization** Ideas, formulation or evolution of overarching research goals and aims | 40 % | 20 % | 100 % | 10 % | 100 % |
| **Methodology** Development or design of methodology; creation of models | 50 % | 40 % | 100 % | 40 % | 100 % |
| **Software** Programming, software development; designing computer programs; implementation of the computer code and supporting algorithms; testing of existing code components | 90 % | 30 % | 50 % | 100 % | 95 % |
| **Validation** Verification, whether as a part of the activity or separate, of the overall replication, reproducibility of results, or experiments and other research outputs | 30 % | 20 % | 100 % | 0 % | 100 % |

| | | | | | |
|---|---|---|---|---|---|
| **Formal analysis**<br>Application of statistical, mathematical, computational, or other formal techniques to analyze or synthesize study data | 80 % | 40 % | 100 % | 100 % | 100 % |
| **Investigation**<br>Conducting a research and investigation process, specifically performing the experiments, or data/evidence collection | 20 % | 20 % | 100 % | 10 % | 50 % |
| **Resources**<br>Provision of study materials, reagents, materials, patients, laboratory samples, animals, instrumentation, computing resources, or other analysis tools | 0 % | 0 % | 0 % | 0 % | 0 % |
| **Data Curation**<br>Management activities to annotate (produce metadata), scrub data and maintain research data (including software code, where it is necessary for interpreting the data itself) for initial use and later reuse | 80 % | 40 % | 100 % | 100 % | 100 % |
| **Writing – Original Draft**<br>Preparation, creation and/or presentation of the published work, specifically writing the initial draft (including substantive translation) | 80 % | 40 % | 100 % | 10 % | 100 % |
| **Writing – Review & Editing**<br>Preparation, creation and/or presentation of the published work by those from the original research group, specifically critical review, commentary or revision including pre or post publication stages | 20 % | 60 % | 30 % | 20 % | 30 % |

| | | | | | |
|---|---|---|---|---|---|
| **Visualization**<br>Preparation, creation and/or presentation of the published work, especially visualization or data presentation | 100 % | 40 % | 100 % | 25 % | 100 % |
| **Supervision**<br>Oversight and leadership responsibility for the research activity planning and execution, including mentorship external to the core team | 0 % | 0 % | 80 % | 0 % | 80 % |
| **Project administration**<br>Management and coordination responsibility for the research activity planning and execution | 0 % | 0 % | 80 % | 0% | 0 % |

## 6.2 Curriculum Vitae